

---

# Improvements in the Manufacturing of Pharmaceutical Dry Powder Formulations

*A Novel Method of Blend Analysis Using a Coloured Tracer*

---

By

DAVID K BARLING



Department of Chemical Engineering

MONASH UNIVERSITY

A dissertation submitted in Monash University in accordance with the requirements of the degree of DOCTOR OF PHILOSOPHY in the Faculty of Engineering

23-July-2014



*“Colour does not add a pleasant quality to design – it reinforces it”*

Pierre Bonnard (1867-1947)

French Artist, Founding Member of Les Nabis



## Table of Contents

Summary .....	xi
Copyright Notices .....	xiii
General Declaration .....	xv
Acknowledgements .....	xvii
1. Introduction.....	1
2. Background of powder blending and pharmaceutical dry powder inhaler (DPI) formulations.....	5
2.1 Dry Powder Inhalers (DPIs).....	7
2.1.1 DPI Formulation.....	8
2.1.2 DPI Device.....	13
2.1.3 Process of DPI aerolisation and drug delivery .....	14
2.1.4 Key criteria for success of DPI formulations.....	17
2.2 Characterisation of Dry Powder Inhaler Products.....	19
2.2.1 Content uniformity of dose .....	19
2.2.2 Inhalation property measurements .....	20
2.2.3 Difficulties with current testing methods.....	23
2.3 Powder blending .....	25
2.3.1 Mixture structure .....	26
2.3.2 Intrinsic Particle Properties .....	29
2.3.3 Particle Interactions .....	30
2.3.4 Blending kinetics.....	32
2.3.5 Mixing technologies for DPI formulations.....	35

---

2.3.6	Selection of operating conditions.....	40
2.3.7	Scale-up and blend optimisation .....	43
2.3.8	Monitoring of mixing conditions .....	46
2.4	Use of a coloured tracer to assess blending.....	47
2.4.1	Use of coloured tracers in blending .....	48
2.4.2	Colour theory.....	48
2.4.3	Previous work with iron oxide colour tracer .....	51
2.4.4	Mechanism of tracer blending .....	54
2.5	Concluding remarks.....	55
3.	Pigment characteristics and approach to blend analysis .....	57
3.1	Introduction to the use and properties of pigments.....	58
3.1.1	Preliminary studies and basis for this work.....	58
3.1.2	Background in pigments and iron oxide.....	59
3.1.3	Colour changes in iron oxide pigment.....	61
3.1.4	Characterisation of iron oxides.....	65
3.1.5	Properties of tracer used in studies .....	66
3.1.6	Stability of iron oxide pigments.....	70
3.2	Analysis of tracer colour changes during blending.....	71
3.2.1	Justification of using $C^*$ and $h$ for assessing dispersion and de-agglomeration .....	71
3.2.2	Methodology for colour measurements .....	72
3.2.3	First principle changes in CIE (1976) colour space during blending.....	74
3.2.4	Colour space considerations for particle damage and unintentional milling.....	76

---

---

3.2.5	Formulation curves.....	77
3.2.6	Benefits of tracer method and outline of studies .....	79
3.2.7	Comments on comparing tracer blends to drug blending .....	79
3.3	Concluding remarks on tracer .....	81
4.	Analysis and control of dry powder mixing using a coloured tracer.....	83
4.1	Introduction.....	84
4.2	Materials and Method.....	84
4.2.1	Powder selection and properties .....	85
4.2.2	Mixers and experimental scheme .....	86
4.3	Results .....	90
4.4	Discussion .....	96
4.4.1	Proposed mechanisms.....	97
4.4.2	Limits of analysis of colour change using blend lightness ( $L^*$ ) alone .....	98
4.4.3	Common plane in data .....	100
4.4.4	Industrial application of tracer blending .....	101
4.5	Conclusion .....	103
5.	Effect of tracer concentration on resulting colour curves .....	105
5.1	Introduction.....	106
5.1.1	Influence of tracer concentration on optical properties.....	106
5.1.2	Surface packing of particles.....	107
5.2	Materials and Method.....	109
5.3	Results .....	109

---

5.4	Discussion .....	114
5.4.1	Calculation of maximum surface coverage using first principles .....	114
5.4.2	Tracer coating of particles .....	119
5.4.3	Validation of the term 'Formulation curve' through comparison to initial data .....	123
5.4.4	Comments on previous work in literature .....	124
5.5	Conclusion .....	125
6.	Using formulation curves to assess content uniformity, energy input and blending dynamics	127
6.1	Introduction.....	128
6.1.1	Causes of poor blend uniformity .....	128
6.1.2	Assessment of blend uniformity.....	129
6.1.3	Powder flow and the rate of mixing .....	134
6.1.4	Positron Emission Particle Tracking (PEPT) .....	137
6.1.5	Energy input.....	141
6.1.6	Use of iron oxide to measure uniformity and predict mixing kinetics .....	143
6.2	Materials and Method .....	145
6.2.1	PEPT experiments.....	146
6.2.2	Colour measurements .....	147
6.2.3	Power and energy input measurements .....	147
6.3	Results .....	149
6.3.1	Visual observations in powder flow for each impeller type and speed .....	149
6.3.2	Colour tracer results .....	151
6.3.3	Power and energy input measurements .....	171

---

---

6.3.4	PEPT flow analysis .....	174
6.4	Discussion .....	187
6.4.1	Analysing uniformity from the shape of blend curves .....	187
6.4.2	Quantification of energy input with colour change .....	188
6.4.3	Coupling of flow analysis and colour data.....	190
6.4.4	Comments on the effect of impeller types on formulation curves.....	192
6.4.5	Benefits and limitations in use of iron oxide tracer .....	193
6.5	Conclusion .....	194
7.	The effect of fines on the shape of formulation curves in nominal and extreme blending conditions.....	195
7.1	Introduction.....	196
7.1.1	Milling and milling mechanisms .....	197
7.1.2	Issues associated with milling during blending .....	198
7.1.3	Current methods of detection.....	200
7.1.4	Effect of level of fines on DPI performance.....	201
7.1.5	Previous work in level of fines on DPIs.....	203
7.1.6	Use of iron oxide to detect milling and batch variation.....	204
7.2	Materials and Method.....	205
7.2.1	Powder selection and powder properties.....	205
7.2.2	Experimental scheme .....	206
7.3	Results .....	206
7.3.1	CIELCH formulation curves .....	207

---

---

7.3.2	Particle size data.....	211
7.4	Discussion .....	218
7.4.1	Correlation of level of fines and position in CIE colour space .....	218
7.4.2	Quantification of milling.....	221
7.4.3	Proposed tool for calculation of fines in milled formulation based on colour values	223
7.4.4	Comments on pre-milling behaviour and proposed mechanisms .....	225
7.4.5	Ability of method to detect batch-to-batch variation in formulation .....	228
7.5	Conclusion .....	229
8.	Review and application of colour tracer method in industrial blend analysis .....	231
8.1	Introduction.....	232
8.2	Review of formulations used in this thesis.....	233
8.2.1	Flooding fractions for each formulation.....	236
8.2.2	Similarity in mechanism between formulations.....	237
8.3	Review of colour tracer method results .....	238
8.3.1	Analysis of common plane/surface in colour space .....	238
8.3.2	Predicting the location and shape of formulation curves in CIELCH colour space.....	242
8.3.3	Description of all colour space regions.....	243
8.4	Proposed method for industrial application .....	245
8.4.1	Pre-blending procedures .....	245
8.4.2	Colour blending procedures and analysis.....	247
8.4.3	Comments on drug blending .....	257
8.5	Application of colour tracer method to previous work.....	257

---

8.6	Limitations of method and recommendations for future work.....	261
9.	Conclusion .....	265
	Nomenclature and glossary of abbreviations .....	269
	References.....	277

## Summary

The optimisation of dry powder pharmaceutical blending is very challenging, and often relies on costly and time consuming trial-and-error approaches which waste a lot of material. A novel method has been developed which can be used in place of the drug to quickly and effectively evaluate the progression of a dry powder mixing. By blending a small amount of colour tracer with the pharmaceutical formulation bulk, a vast amount of information on blend kinetics and behaviour can be extracted. Information on the degree of tracer spread and breakup can be obtained from measurement of the blend's colour, as well as providing quantitative insight into the energy input to the blend and its uniformity. It can also be used to identify conditions which may cause unintentional and undesirable particle damage during blending. By reducing the amount of drug required in preliminary testing, the colour tracer method provides a cost effective means of ensuring equivalent blending conditions between mixer types, scales and operating conditions.

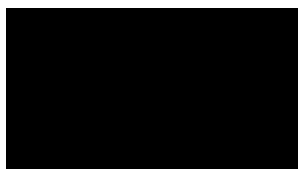


## Copyright Notices

Under the Copyright Act 1968, this thesis must be used only under the normal conditions of scholarly fair dealing. In particular no results or conclusions should be extracted from it, nor should it be copied or closely paraphrased in whole or in part without the written consent of the author. Proper written acknowledgement should be made for any assistance obtained from this thesis.

I certify that I have made all reasonable efforts to secure copyright permissions for third-party content included in this thesis and have not knowingly added copyright content to my work without the owner's permission.

David Barling



17-Mar-2015

---

Candidate's name (Printed)

---

Candidate's signature

---

Date



## General Declaration

### Monash University

#### Declaration for thesis based or partially based on conjointly published or unpublished work

In accordance with Monash University Doctorate Regulation 17.2 Doctor of Philosophy and Research Master's regulations the following declarations are made:

I hereby declare that this thesis contains no material which has been accepted for the award of any other degree or diploma at any university or equivalent institution and that, to the best of my knowledge and belief, this thesis contains no material previously published or written by another person, except where due reference is made in the text of the thesis.

This thesis includes 1 original paper published in a peer reviewed journal and a book chapter. The core theme of the thesis is to improve the optimisation of dry powder mixing processes. The ideas, development and writing up of all the papers in the thesis were the principal responsibility of myself, the candidate, working within the Doctorate of Philosophy under the supervision of Prof. Karen Hapgood and A/Prof. David Morton.

Thesis chapter	Publication title	Publication status*	Nature and extent of candidate's contribution
3, 4	Barling, D., Morton, D.A.V., Hapgood, K. (2014). "Pharmaceutical dry powder blending and scale-up: maintaining equivalent mixing conditions using a coloured tracer powder." Powder Technology. <a href="http://dx.doi.org/10.1016/j.powtec.2014.04.069">http://dx.doi.org/10.1016/j.powtec.2014.04.069</a>	In press	Designed and conducted experiments, wrote publication.
3, 4, 5, 6, 7	Barling, D., Morton, D., Hapgood, K. (2014), "Defining and Controlling Blend Evolution in Inhalation Powder Formulations Using a Novel Colourimetric Method". in: <u>Current Pharmaceutical Design - Pulmonary Drug Delivery</u> , Wiley <b>Chapter 10</b> .	Accepted	Wrote chapter

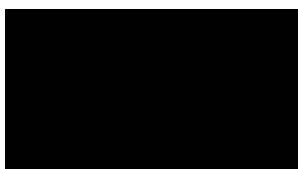
In the case of Chapter 6 my contribution to the work involved the following:

Nature of contribution	Extent of contribution (%)
Designing, preparing and conducting experiments as well as writing the thesis chapter. Help was sought when preparing and conducting half of the experiments, which related to the use of complex radiology equipment.	80

Assistance was provided by Prof. David Parker, Dr. Thomas Leadbeater and Dr. Joseph Gargiuli (Positron Imaging Centre, School of Physics and Astronomy, University of Birmingham) for the preparation and operation of the complex radiology equipment (including the preparation of the radioactive tracers as well as the Positron Emission Particle Tracker (PEPT). Dr. Thomas Leadbeater also built a measurement apparatus for subsequent experiments. Supervision for the work in Chapter 6 was extended to Dr. Andy Ingram (School of Chemical Engineering, University of Birmingham) and Prof. Jonathan Seville (Department of Chemical and Process Engineering, University of Surrey).

I **have not** renumbered sections of submitted or published papers in order to generate a consistent presentation within the thesis

David Barling



17-Mar-2015

---

Candidate's name (Printed)

---

Candidate's signature

---

Date

## Acknowledgements

This work would not have been possible without the combined efforts and supports of several individuals, corporations and research groups both locally and globally. It is therefore my pleasure to acknowledge and thank the following for their contributions to this thesis.

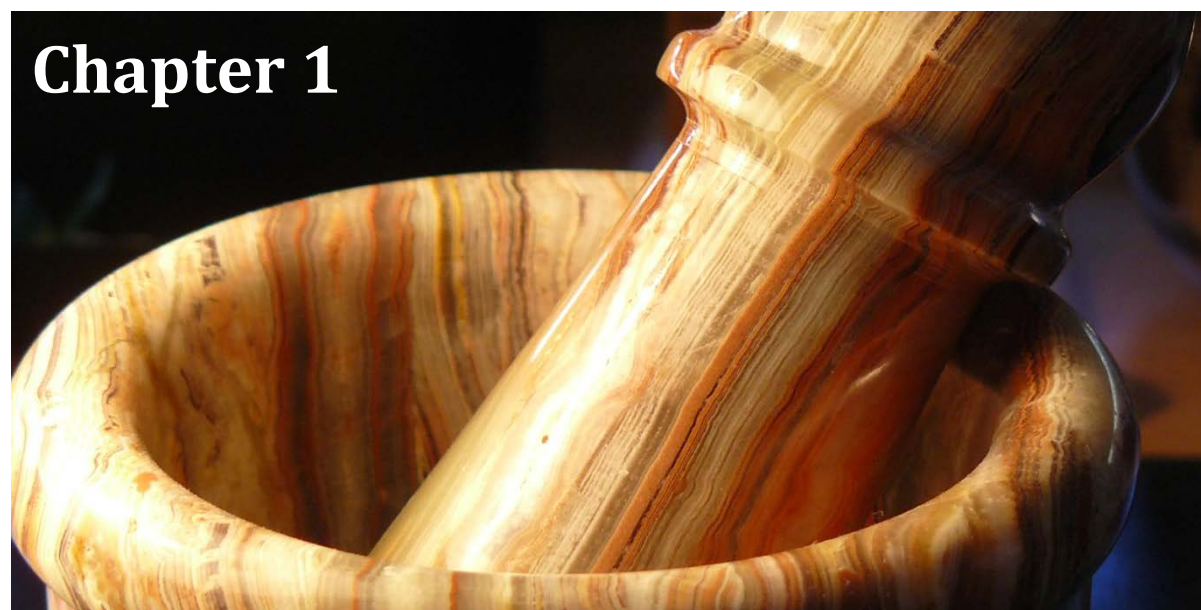
My co-supervisors Karen Hapgood (Department of Chemical Engineering) and David Morton (Monash Institute of Pharmaceutical Sciences, MIPS) for their guidance throughout this work. They have also provided many amazing and invaluable opportunities to me beyond this thesis for which I am extremely grateful.

GlaxoSmithKline Australia and the MIPS/GSK collaboration for their financial support, resources and guidance. Particular mention goes to Philip Leslie, Jonathan Parks and Ruth Howell. I would also like to thank them for the amazing opportunities they have provided me with during my studies.

The team at the University of Birmingham, U.K., for their assistance and guidance in the work of Chapter 6. Particular mention goes to Thomas Leadbeater, David Parker and Joseph Gargiuli (Positron Imaging Centre) as well as Andy Ingram (School of Chemical Engineering) and Jonathan Seville (Department of Chemical and Process Engineering, University of Surrey). I would also like to thank DFE Pharma for their generous contribution of materials towards the work.

I would like to dedicate this work to my father, Christina and our two boys Liam and Ryan.





# Chapter 1

## Introduction

**T**he mixing of dry powders dates back thousands of years and is a critical processing step in the manufacturing of a multitude of products including detergents, pigments, catalysts, fuels, fertilisers, foodstuffs and pharmaceuticals (*Rhodes, 2008*). It is often employed to ensure two or more materials are effectively distributed amongst one another in a homogenous state, but is also used to achieve desired powder structures and enhanced properties. In the pharmaceutical industry product homogeneity is an extremely important factor in powder mixing due to the small scale of powder used per dose (*Muzzio et al., 1997*). To increase product safety and consistency, a very fine degree of mixing is desired which can often be very difficult to achieve. This is due to the size, density and physical property differences of the powders used to create desired pharmaceutical formulations (*Kaye, 1997a*), and is particularly apparent in dry powder inhalation (DPI) formulations. An extra dimension of intricacy is also required for DPI formulations as a certain particle structure is desired to achieve effective drug delivery upon inhalation.

Current technologies employed in the pharmaceutical industry have historically been chosen based on an organisation's general validation experience base and availability of commercial equipment rather than their bespoke design and suitability to a specific task. This method of selection does not realise the true potential of some formulations, nor does it allow for the efficient production of novel and often intricate 'designer' drugs. There is also demand on pharmaceutical companies to adjust their production volumes based on consumer requirements. In such instances it may be desirable for a company to employ other mixing technologies or scales.

Unfortunately many of these desirable product attributes are very difficult to achieve, as powder flow throughout many powder mixing technologies and resultant mixing is not well understood (*Knight, 2004*). As such, the determination of the best mixing conditions in a given vessel, including operating conditions and mixing time are a purely trial-and-error approach and can be a time and financially costly process. Much of the determination for appropriate conditions comes from empirical data, based on the amount of shear dispersion energy applied during the blending process.

It would be beneficial for industry to have a means of gaining a better understanding of the influence of operating conditions on powder mixing in different mixing processes. This would allow for better predictions about the extent of mixing (both required intensity and mixing time). It could shift determination of the best operating conditions from the traditional haphazard trial-and-error approach to a more holistic and accurate process that has flexibility to be applied to a variety of situations rather than being product specific. It may also assist in scale-up and transfer between blender types.

Given the current state of technology in controlling and monitoring powder mixing, it is natural to raise the question:

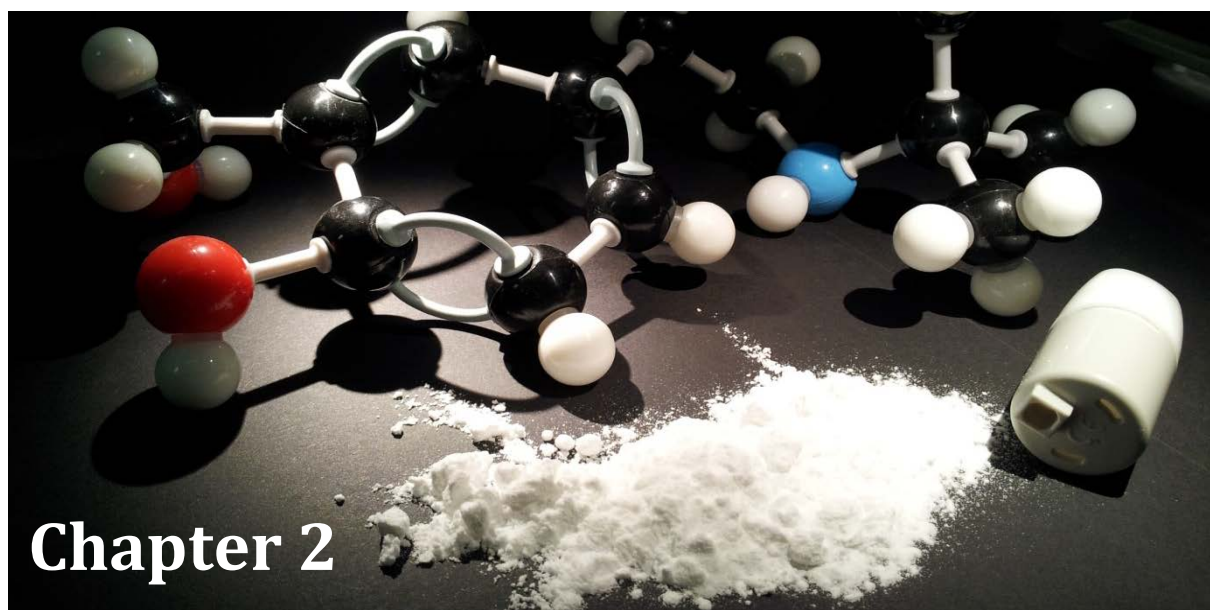
***“Is there a means of making blend analysis simpler and cheaper to improve process optimisation and/or scale-up?”***

Whilst easy to pose the question, finding a simpler and cheaper method is challenging. Any new means of assessing the blending of pharmaceutical formulations needs to provide information on several key blending aspects, namely:

- ***The degree of drug breakup and spread during mixing***
- ***The homogeneity of the blend/ability to assess total blend energy input***
- ***The degree of particle damage during blending (due to excess applied forces and unintentional milling)***

This thesis addresses these criteria and outlines a potential procedure by which, industries will be able to better determine mixing conditions for a given process. Ultimately, this could save significant time and cost in establishing effective scale-up or technology transfer conditions. The method proposed is cost effective, non-hazardous and involves the use of a sub-micron colour tracer to monitor the extent of mixing. The use of a coloured pigment as a preliminary testing method, and when used as a substitute for the pharmaceutical active in preliminary testing, may hold benefits in allowing an entire blend to be quickly and simply analysed through the blend's colour change as the level of mixing increases. The method outlined in this thesis also appears to be able to quantify content uniformity, energy input to the blend and the level of both pigment breakup and spread. It can also detect batch-to-batch variations in the level of fine particles and the generation of fines whilst mixing due to milling, and also provide a means of predicting the performance of DPI blends.





## Background of powder blending and pharmaceutical dry powder inhaler (DPI) formulations

***P**owder blending, and in particular the blending of DPI formulations, is extremely challenging. Its success relies on a strong understanding of the desired characteristics and aerolisation performance, as well as powder characteristics and behaviour in different mixing technologies and conditions. This chapter provides background into the general underlying topics of the thesis, providing information and context on the various challenges addressed and their significance to the field. Overviews are given for what constitutes a dry powder inhaler formulation and the key factors in ensuring effective drug delivery, the nature and difficulties of powder blending and specifically DPI formulating, as well as the methods for assessing blending behaviours. In addition, inspiration and background into the approaches in this thesis to simplify and improve the development stage of DPI manufacturing are provided. Some key terminologies and principles are also included in this chapter which are used throughout subsequent chapters.*

A pharmaceutical is defined by the Federal Food, Drug and Cosmetic Act (FFDCA, in America) as an “Article intended for use in the diagnosis, cure, mitigation, treatment or prevention of disease” and/or “intended to affect the structure or any function of the body”. Dry powder inhaler (DPI) formulations are no different (*Campbell, 2008a*). The use of the lungs as a route of drug administration is very effective and is relied on for the treatment of diseases such as asthma, chronic obstructive pulmonary disease (COPD), emphysema, cystic fibrosis, cancer, diabetes, osteoporosis, as well as general pain management (*Hickey and Crowder, 2007*).

DPIs have been in use since the 1960’s and through various developments and improved technologies have superseded Metered Dose Inhalers (MDIs) in terms of sales (but not volumes). Because of this they now dominate the inhaled drug market, with Advair Diskus the leading inhalation medicine and the only one in the top 30 medicines based on sales in the U.S. in 2013 (*Drugs.com, 2014*). Four of the top five inhaler-based medicines are either entirely DPI based, or offer both MDI and DPI systems (Advair/Seretide, Tamiflu/Relenza, Budesonide and Flovent). Drivers for their success include additional formulation stability in solid state form rather than involving liquid phase, as well as the banning of Chlorofluorocarbons (CFCs) and the major carbon footprint associated with HFA propellants (used in traditional MDI technologies (*Behara et al., 2011b*)). Another driver is the difficulty in effective drug delivery in MDI systems due to patient operation issues (such as coordination of inhalation and actuation) that are not present with DPI technologies (*Crompton, 1982, Newman and Busse, 2002*). This can be a problem with some patients, particularly the young and elderly (*Crompton et al., 2006*). DPIs also do not produce a cold sensation on inhalation (*Lavorini et al., 2008*). DPIs combine powder technology with device design to disperse dry particles in an aerosol for patient inhalation, and have four basic features: (1) a dose-metering mechanism, (2) an aerolisation mechanism, (3) a de-agglomeration mechanism and (4) an adaptor to direct entrained particles into the patient’s mouth (*Dalby et al., 2007*). They are typically breath actuated, re-loadable, and can be used for high and low-dose formulations as well as for peptide and protein drugs (*Wall, 1995*).

To create a final pharmaceutical product, several manufacturing steps need to be accomplished. Initially there is a research and development phase, whereby a drug is discovered that meets specific therapeutic needs, and developed into a product that can gain regulatory approval and be mass produced. Once the means of its manufacture are determined, the product can be made and distributed for therapy. A wide range of operations are involved in the manufacturing process, ranging from the manufacture of raw materials to the packaging of the final formulation (Figure 2.1).

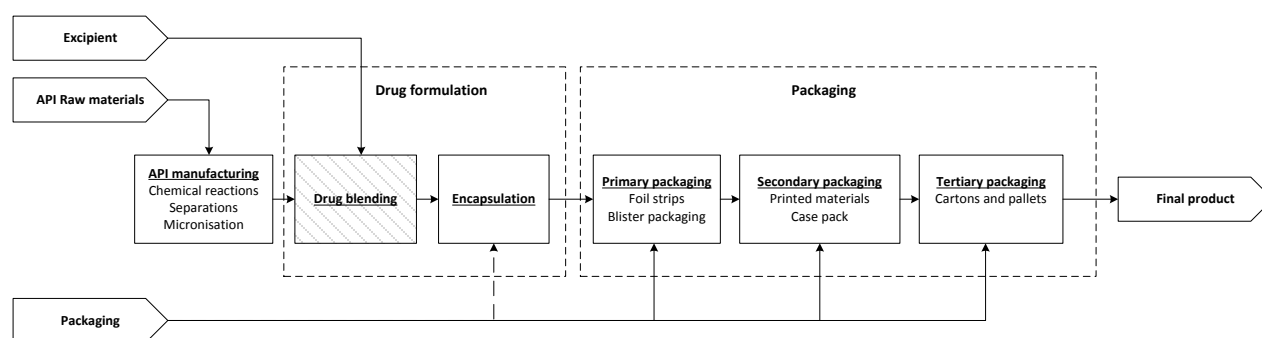


Figure 2.1: Schematic of key steps in the typical manufacturing of a pharmaceutical product

The formulation of the drug into a final product accounts for only one step of the manufacturing process, and whilst typically trivialised as “fairly straight forward [compared to the manufacturing of the API]” (Campbell, 2008a), it is an often an extremely difficult and challenging task. The formulation step may occur over several stages in which individual components or intermediates are created separately and then assembled. Also, processes are often designed to have discrete holding points at which process intermediates can be stored in a stable manner to allow for intermediate conditioning or the pooling of resources, particularly between the drug blending and encapsulation steps (Campbell, 2008a).

## 2.1 Dry Powder Inhalers (DPIs)

The development of a DPI typically covers the design of the device, process and powder formulation. Typically, development is heavily centred around the design of the device (Steckel et al., 2006),

however the key is in fact to match the device and formulation together with the patient's handling and compliance (*Harmer et al., 2004, Morton and Staniforth, Spring 2005*).

### 2.1.1 DPI Formulation

Dry Powder Inhaler (DPI) formulations are specifically structured pharmaceutical mixtures (*Hersey, 1975*), that can be either carrier based or carrier free. Carrier based systems dominate the current market however, and typically consist of ultrafine drug particles with an aerodynamic diameter in the range of 1-5 microns (*Telco and Hickey, 2005*) and a coarse carrier (*Malcolmson and Embleton, 1998*). Such systems are classed as binary, however ternary formulations also exist where a fine carrier of similar size to the drug particles is added to improve delivery performance (*Jones and Price, 2006*). The ternary component may also refer to additives such as magnesium stearate, which are becoming increasingly common in DPI formulations.

While most DPI formulations on the market consist of drug, carrier and sometimes an additive, other carrier free formulations exist, such as Turbohaler Pulmicort, where the formulation is drug only. Other formulations such as Oxis, add micronised lactose not as a carrier, but as diluent to enable reproducible powder metering.

The formulation step in the development of a DPI can be sub-divided into the development of micronised drug particles (such as milling (*Ticehurst et al., 2000*) or *in situ* micronisation (*Rasenack et al., 2003*)) and the development of a suitable carrier system (*Steckel et al., 2006*).

#### 2.1.1.1 Function of formulation

Whilst the lungs are an effective and quick route for drug administration, delivery is challenging due to the lung's evolved ability to filter particles and prevent foreign objects from entering and harming the lung and its function. Because of this physiological filtration system, formulations need to be designed in a particular way to 'cheat' the body's defences. To maximise drug delivery to the lower respiratory tract, particles need to be of a particular size to allow them to pass the various obstructions in the oropharyngeal region to reach the tracheobronchial region of the lung, and

ultimately transport to the surfaces of the bronchi or alveoli. For treatment of respiratory conditions such as asthma and COPD, drug deposition is primarily targeted to the bronchi for local deposition and topical treatment (Zeng *et al.*, 1999) (Figure 2.2).

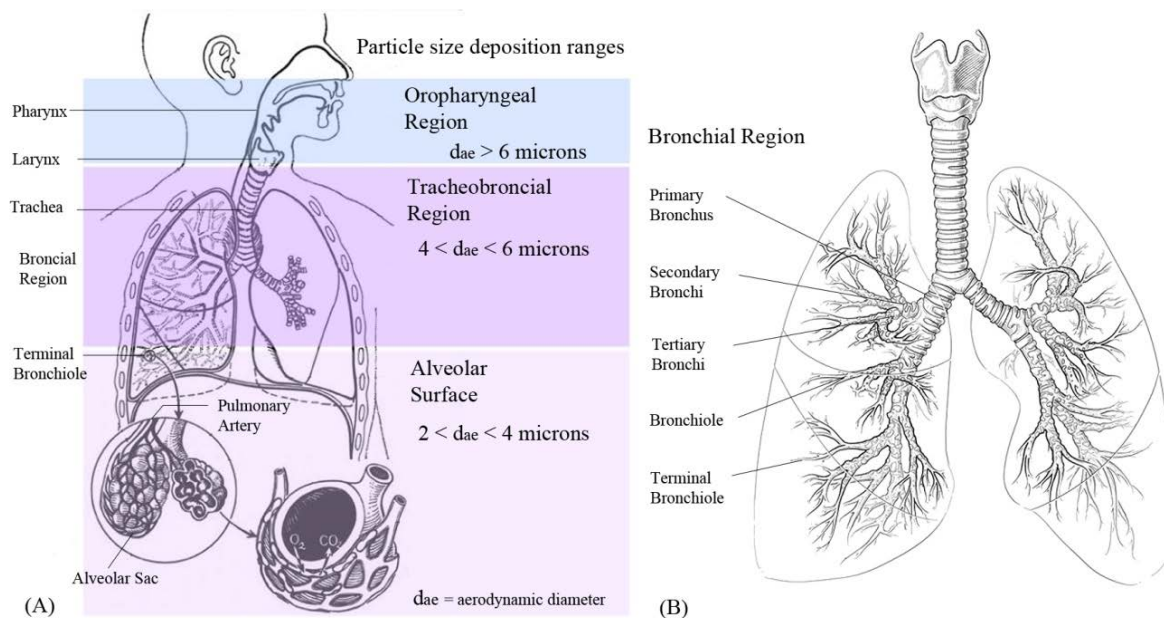


Figure 2.2: Diagram of human anatomy showing areas of interest and regions of inhaled particle deposition (A). Key points have been highlighted, including those in the bronchial region (B). Particle sizes for each respiratory region are adapted from research into the deposition of spherical particles of unit density for slow, oral tidal-breathing by an adult patient (Heyder and Svartengren, 2001).

From previous models and data for a tidally breathing adult (Heyder and Svartengren, 2001, Rudolph *et al.*), particles with an aerodynamic diameter larger than approximately  $6 \mu\text{m}$  are deposited mainly in the oropharyngeal region beyond the mouth and above the larynx. Beyond the larynx in the trachea and bronchial region (tracheobronchial region), particles having an aerodynamic diameter between  $4$  and  $6 \mu\text{m}$  are deposited. A peak deposition in the lung reaches a maximum for particles between  $2$  and  $4 \mu\text{m}$ .

However, in contrast to tidal breathing, with the deeper respiration used by a patient in activating an inhaler, smaller particles can be transported and retained in the bronchial/alveoli region. Deposition is not only dependent on particle aerodynamic size, but also velocity of inhaled breath.

It is now generally accepted that particles larger than 5 microns have a high probability of impact in the oropharyngeal region are swallowed. Hence, 5 microns is the widely used cut point for aerosol characterisation in defining a lung dose. Particles less than 1 micron have a reduced efficiency of deep lung deposition in tidal breathing due to lack of deposition mechanisms - and their exhalation is often assumed for inhalers. (Copley, 2010, Dunbar and Hickey, 2000, Gonda, 1990, Newman and Clarke, 1983). However, with correct patient inhalation and breath hold manoeuvre, such exhalation is over-estimated (Heyder and Svartengren, 2001).

#### *2.1.1.2 Components of formulation*

Obtaining drug particles in the desired size range is achieved through milling prior to formulation (Hickey, 1993, Price and Young, 2005) or through spray drying (Sou et al., 2011). Milling of the drug particles is typically required as their high purity and manufacturing techniques often creates crystals which are not of the desired particle size range for effective drug delivery (Price and Young, 2005). Particles of this appropriate size are cohesive since the magnitude of the interactive forces is greater than the gravitational detachment force (Visser, 1989). This makes them very sticky and so very challenging to re-suspend and aerosolise without them remaining heavily agglomerated and trapping in the device or the oropharyngeal region.

For this reason, a 'carrier' is introduced. Traditionally  $\alpha$ -lactose monohydrate has been used (Byron and Jashnani, 1990, Rowe et al., 2003b), which is blended with the cohesive drug particles to enhance flow, uniformity and aerolisation (Telco and Hickey, 2005). To date, lactose monohydrate remains the excipient of choice due to it being inert, cheap, relatively low in hygroscopicity, broadly available and the wide experience of its use and safety profile across the industry (teWierik and Diepenmaat, 2002). The performance of the formulation however is highly dependent on the lactose quality and source (Steckel et al., 2004), the size distribution of the lactose (Zeng et al., 1999) and the amount of fine particles in formulation (Lucas et al., 1998b). There are four solid forms of lactose:  $\alpha$ -lactose (both monohydrate and anhydrous), anhydrous  $\beta$ -lactose and amorphous lactose

(Vromans *et al.*, 1985, Vromans *et al.*, 1986). The physico-mechanical properties of lactose can be found in the literature (Angberg, 1995, Briggner *et al.*, 1994, Hogan and Buckton, 2001, Sebatua *et al.*, 1994, Wade, 2003, Young *et al.*, 2003).

A number of other excipients are available for use in inhalers, but those suitable for the multiple requirements of DPI formulations is limited (Hickey and Crowder, 2007). Excipients can serve several different purposes in the formulation, acting as diluents, dispersing agents, matrices, formulation aids and stabilizers. They act in reducing drug particle aggregation, and aid both re-suspension/fluidisation of the formulation as well as enhancing effective separation of the drug particles so they can be transported more efficiently to bronchi and alveoli surfaces. They can also aid in the metering of often highly cohesive drug particles (Frijlink and de Boer, 2004). Other formulation aids such as a force control agent may also be used to improve the dispersion properties, bioavailability of the drug and stability of formulation (Shur *et al.*, 2008, Zhou and Morton, 2012).

### **2.1.1.3 Structure of formulation**

To achieve a balance of good bulk flow properties and effective drug delivery to the bronchial/alveoli region of the lung, specific particle assemblies are required. To achieve this, a blending process is employed to adhere the fine drug particles to the high energy active sites on the carrier particles. The carrier particles are considerably larger, with a size range of typically between 50 and 300  $\mu\text{m}$  (Donovan and Smyth, 2010) (Figure 2.3).

Due to the chaotic and unpredictable nature of powder blending, it is very difficult to achieve an intimately homogeneous and structured blend. Whilst particular particle assemblies are desired, the final formulation in reality consists of lactose, fine lactose and drug in every imaginable combination from sticky drug clumps to drug and fine-lactose coated coarse lactose. Manufacturers of DPI formulations may endeavour to eliminate drug clumps as undesired structures to improve consistency and efficiency of the final product through a more robust understanding of the powders and mixing process. Further discussion of mixture types and analysis can be found in Section 2.3.

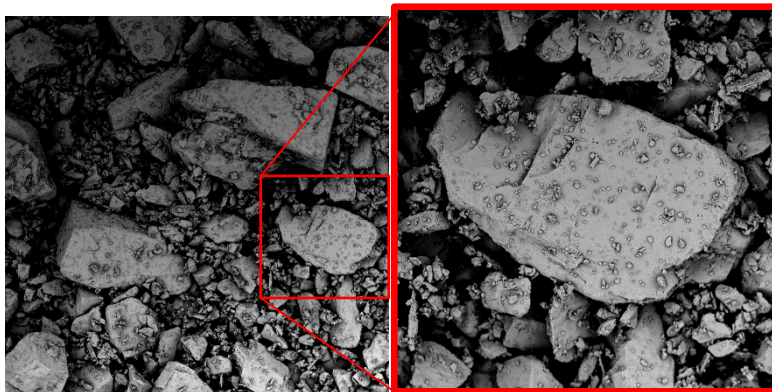


Figure 2.3: Scanning Electron Microscope images of a typical DPI ternary formulation, showing drug and fine lactose particles adhered to active sites of carrier lactose.

DPIs can vary dramatically in the loading of drug in their composition. The drug loading in a DPI formulation can be classed as dilute (less than 2% by weight), intermediate (between 2 and 15%) or high (greater than 15%) (*Thalberg et al., 2012*). The majority of DPI formulations lie within the dilute loading class (*Wagner et al., 2009*). In dilute systems the surface properties of the carrier tend to dominate the behaviour of the formulation (*Heng et al., 2000, Louey and Stewart, 2002, Young et al., 2005*), which is further explained in Section 2.1.4. The performance of dilute systems is often poor, with low drug delivery efficiencies ranging from single digit up to around 20%, which often correlate to a high variation in the lung dose to the patient (*Borgström et al., 2006*). Intermediate formulations often have higher delivery efficiencies to dilute formulations, however high drug loading often leads to a collapse in efficiency (*Louey et al., 2003*). This is often due to the physico-chemical properties of the formulation being outside the working range of the device, and can also lead to high variability in drug delivery. Devices such as the Turbuhaler are designed to overcome some of these effects of high loading and rely on carrier-free, soft pelletised micronised material.

Many studies have investigated the influence of carrier properties on product performance and have been summarised in literature (*Jones and Price, 2006, Thalberg et al., 2012*). Properties such as size, size distribution and shape affect powder dispersibility. Other properties such as the carrier rugosity, purity and crystallinity can also influence performance. As mentioned earlier, the addition of a ternary agent of the same fine-size range of the active ingredient influences (and often enhances)

the amount of active that reaches the lower airways (Curry *et al.*, 1974). Several theories as to how fine lactose influences the delivery of the active have been developed:

- The fine lactose competes with the active for “high energy” attachment sites on the carrier lactose (Hersey, 1975, Staniforth, 1996).
- Fine lactose forms easily dispersible multiplets with drug particles (Lucas *et al.*, 1998a).
- Fine lactose creates mono or multilayers between the larger carrier particles and the drug, reducing van der Waals forces of attraction between drug and carrier (Zeng *et al.*, 1998). This allows the drug particles to be dislodged from the carrier more easily.

The majority of research in this area has focussed on the addition of lactose fines (typically below 15  $\mu\text{m}$ ) to coarse lactose (typically above 50  $\mu\text{m}$ ) and drug (Donovan and Smyth, 2010, Guenette *et al.*, 2009, Jones and Price, 2006). These studies have found, predominantly through *in vitro* testing, that the addition of fines increases the delivered dose of the drug to the lung. Further discussion can be found in Chapter 7.

### 2.1.2 DPI Device

Beyond design of the formulation, the device itself is a critical component in effective drug delivery. Devices consist of a drug reservoir or pre-metered individual doses, the body of the device and a cover to prevent the ingress of dust and/or moisture (Dalby *et al.*, 2007). There are a multitude of DPI devices in use such as the Spinhaler<sup>®</sup> (Fisons), Rotahaler<sup>®</sup> (GlaxoSmithKline, U.S.A), Diskhaler<sup>®</sup> (GlaxoSmithKline), Accuhaler<sup>®</sup> (GlaxoSmithKline, U.K.) and Turbuhaler<sup>®</sup> (Astra Zeneca Lund) (Dalby *et al.*, 2007) (Figure 2.4). Current devices typically rely on prefilled doses of powder in foil blisters or gelatin capsules due to the difficulty in reproducible dose metering from an in-device reservoir. As well as dose metering, they differ based on different powder aerolisation mechanisms.

The internal geometry of the device is pivotal to the generation of the aerosol (Dalby *et al.*, 2007).

The dimensions of the channels that the airflow passes through determines the pressure drop across

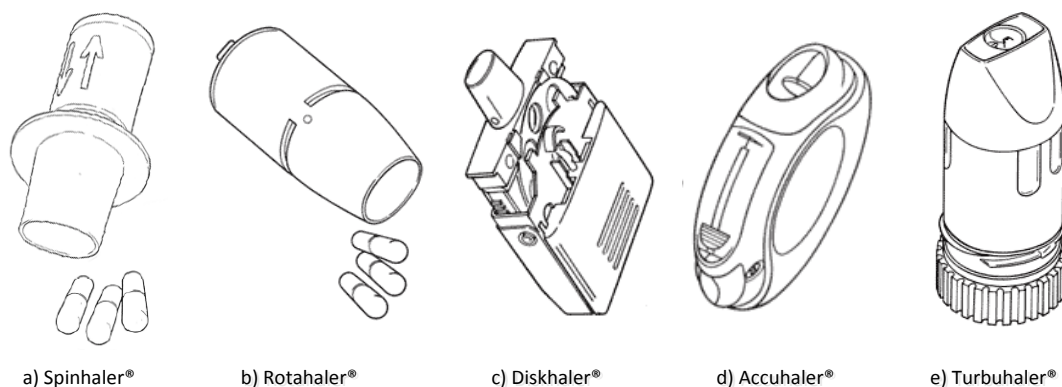


Figure 2.4: Examples of dry powder inhalation devices including Spinhaler® a), Rotahaler® b), Diskhaler® c), Accuhaler® d) and Turbuhaler® e) ([saglikpark.com](http://saglikpark.com), 2014).

the device, and local air velocities generated. The local air flows, coupled with the powder metering design determines how the powder is released. For example, release can be fast, with dense or dilute plumes, in stochastic boluses or a continuous stream. Air flows also determine whether accumulation occurs (due to severe changes in the direction of airflow). The rate and type of powder release has a great effect on the drug deposition within the lung and subsequently the *in vivo* drug profile in the patient. Also, the material that the device is made of can affect the behaviour of the formulation (Jones and Price, 2006). The materials that drug particles come into contact with during processing have a significant impact on the formulation's electrostatic properties of the formulation (Staniforth, 1994), which in turn can have effects on the amount of material that leaves the device during inhalation. Good release of powder from the device can be achieved through creating tortuous airflow paths through the use of either impactor grids and/or increasing the airflow resistance across the device (Ganderton, 1997, Nichols and Wynn, 2008).

The device can be modified to improve powder fluidisation, entrainment and dispersion by increasing the Reynolds Number and the number of impaction events within the device during inhalation (Telco and Hickey, 2005).

### 2.1.3 Process of DPI aerolisation and drug delivery

There are two types of aerolisation mechanisms in DPIs; passive systems and active systems (Tobyn *et al.*, 2004). Passive systems rely solely on the energy imparted by the airflow during inhalation to

aerolise the powder (Srichana *et al.*, 1998), whilst active systems also have additional methods of adding energy to the powder mass to facilitate fluidisation, and rely on mechanical mechanisms such as vibration, impact force, compressed air and impellers (Crowder *et al.*, 2001). Active systems potentially reduce patient-variability effects in drug delivery relative to passive systems (Louey *et al.*, 2006). Both types of system rely on the energy applied by the patient during inhalation and inherent pressure drops forming across the device (Pedersen and Steffenson, 1986).

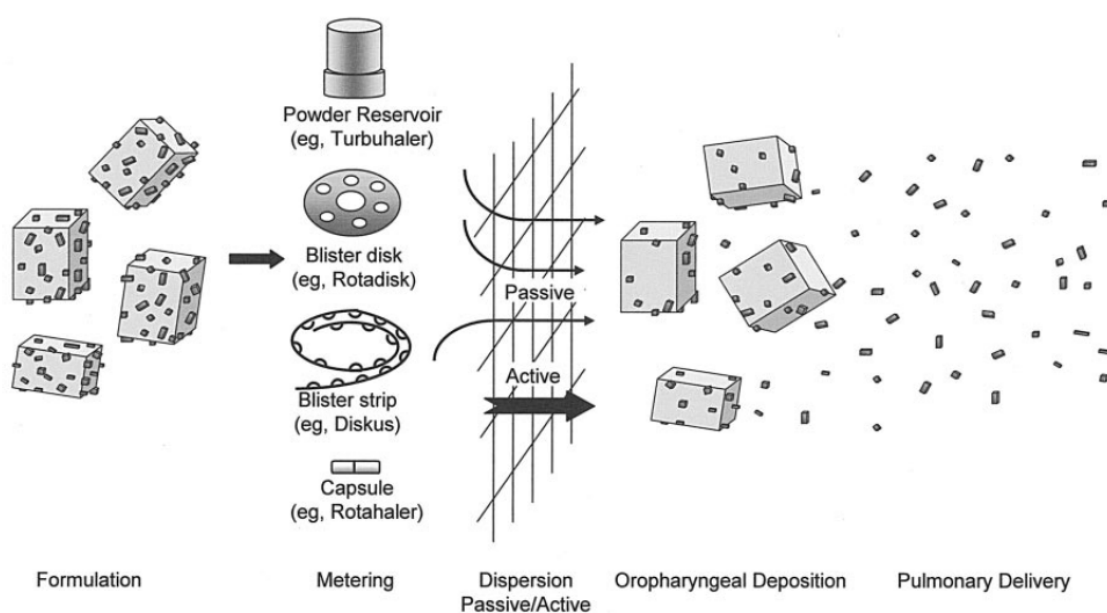


Figure 2.5: Schematic of aerolisation mechanisms of powder (Telco and Hickey, 2005).

The general principles of aerolisation remain constant for either system (Figure 2.5). During inhalation, a pressure drop is generated across the device (Howard, 1989) which is affected by the breathing cycle of the patient. Initially, when the patient begins breathing in and the airflow increases (i.e. when the pressure drop across the device is increasing), the blister powder mass or open capsule remains largely undisturbed. This behaviour can be described by Carman's Law (Carman, 1937). Once the airflow is accelerated to a threshold value, there is a sufficient pressure differential across the device to initialise powder fluidisation or capsule movement. At the critical, or minimum fluidisation velocity (MFV) (Castellanos, 2005), the pressure drop across the powder bed is equal to the weight of the powder or the capsule (Castellanos *et al.*, 1999). For capsule-based

systems, as the pressure drop continues to increase beyond the MFV, the capsule is lifted and begins to rattle around the device chamber, releasing powder on impact with the walls of the device. On impact, powder is ejected from the open capsule. Drug particles are then dispersed as an aerosol through mechanisms such as the Bernoulli or Venturi effect (*Cheng et al., 1989*). The increase in the pressure drop above the MFV influences the entrainment and aerolisation efficiency of the formulation within a DPI device, and is dependent on the inhalation profile of the patient.

Once aerolised, drug particles are ejected from the carrier particles to which they are loosely attached during the formulation process (*Concessio et al., 1999, Ganderton, 1992*). This occurs via the particle-particle or wall-particle collisions within the device (*Castellanos et al., 1999, Nichols and Wynn, 2008, Zeng et al., 2001*). The large carrier particles are used to aid fluidisation and dispersion to allow for the separation of individual particles into the aerosol. The process of detachment encompass aerodynamic, centrifugal, inertial, shear and frictional forces, which attempt to overcome the inter-particulate forces that bind components in the formulation (*Ganderton, 1997*). After a certain degree of entrainment, powder then exits the device, typically through a grid, and down a mouthpiece to the patient's throat. Due to their large size, carrier particles are typically deposited in the oropharyngeal region (back of the throat) (*Zeng et al., 1999*) or remain within the device.

There are four major mechanisms of deposition of drug within the lungs; inertial impaction, interception, sedimentation and diffusion (*Dalby et al., 2007*). Drug particles in DPI formulations are predominantly subject to inertial and sedimentary mechanisms, whereby small drug particles are separated from the lactose through differences in momentum and migration through voids respectively (*Figure 2.6*). This is due to the drug particles not being sub-micron in size and often being uniformly shaped.

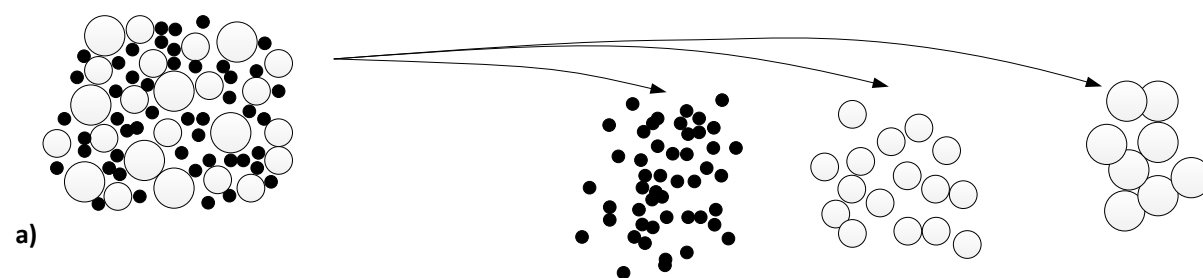
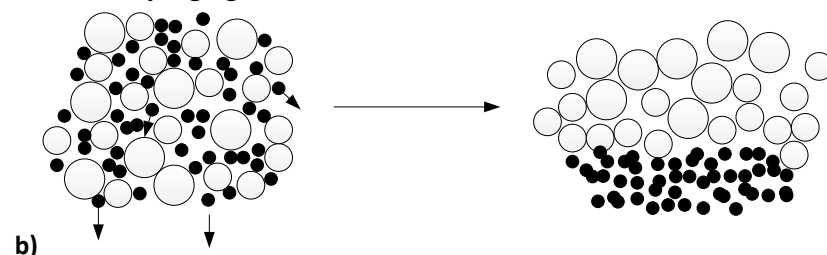
**Inertial segregation mechanism****Sedimentary segregation mechanism**

Figure 2.6: Schematic of inertial a) and sedimentary b) segregation mechanisms which are dominant in the de-agglomeration of drug particles from coarse carriers during aerolisation.

The combination of device and formulation can be considered to have a ‘working range’ in which drug delivery meets specifications and outside of which the product performance collapses. This range relates to the combination of formulation properties and device geometry/design (*Thalberg et al., 2012*). It is important therefore that formulation and device are well matched to create a broad and robust working range (*Harmer et al., 2004, Morton and Staniforth, Spring 2005*).

#### 2.1.4 Key criteria for success of DPI formulations

Beyond the device, the success of the formulation comes down to its consistency of dose and efficiency in aerolisation and drug delivery. Of these, consistency is more important than efficiency.

For most powder blends across all industries, including pharmaceuticals, arguably the most important criteria is blend homogeneity (*Kaye, 1997a*). It is important to ensure that each dose contains the same amount of drug, to ensure effective therapeutic treatment and to prevent adverse health effects from an overdose. DPI formulations have an additional requirement beyond blend homogeneity – particles must also be structured in a particular way to facilitate effective and consistent blend aerolisation and drug deposition in the lung over the life of the inhaler, from first to last dose. This adds extra complexity to blending and also ensuring product quality.

The fluidisation and entrainment behaviour of the DPI formulation within the device has a profound impact on its aerolisation ability (Telco and Hickey, 2005). The fluidisation properties of the powder are primarily governed by its packing properties, which relate to the physicochemical properties of particles and particle interactions (Geldart *et al.*, 2009, Geldart *et al.*, 1984, Valverde *et al.*, 1998). The fine lactose in formulation ensures that the drug particles are effectively delivered to the useful region of the lungs. Drug particles that bind to the carrier particle surfaces do not come off easily, however the strength of attachment decreases with decreasing carrier size. Because of this, it is desirable for the drug particles to adhere preferentially to the fine lactose rather than the coarse lactose (Jones and Price, 2006). This allows the drug particles to be transported deeper into the lung and increases their chances of being absorbed by the patient or being applied directly to the required regions. If engineered properly this can serve to improve the efficiency of the product, requiring less drug per dose and lowering the cost of production. Such structures are further discussed in Section 2.3.1. Dispersion and effective delivery of drug particles also relies on other factors such as rugosity (Dalby *et al.*, 2007), shape (Mullins *et al.*, 1992, Visser, 1989), moisture content (Konzny *et al.*, 1994), surface chemical composition (Al-Chalabi *et al.*, 1990) and charge (Hickey and Concessio, 1994). Particle morphology and density are also important for reproducible aerodynamic behaviour and lung deposition (Weers *et al.*, 2010).

The success of a DPI formulation lies not only with the formulation step but also with upstream raw material manufacturing and downstream packaging and storage conditions. Other effects such as environmental conditions and lengths of time until use, as well as the patient's loading and operation of device can affect product performance. These are typically ignored in process development as the manufacturer can only be expected to go so far in ensuring good performance.

## 2.2 Characterisation of Dry Powder Inhaler Products

Before a drug product can be commercialised, the process used to manufacture the formulation must be validated. Selected tests are also employed, although the number of required tests reduces once the product has been approved by the regulatory bodies meeting batch specifications. Typical tests are required to ensure the product's quality (such as appearance, content uniformity), chemical identity, potency, purity and safety (such as sterility or presence of contaminants) (*Campbell, 2008b*).

There are two standard types of tests for DPI formulations; consistency of drug content in dose and inhalation properties of the blend (*Byron, 1994, Jashnani et al., 1995*). Conventional methods for verification of powder-blend uniformity are based on invasive sampling and off-line destructive analysis with HPLC or UV/Vis Spectroscopy (*FDA, 2004*). Whilst testing drug content in a given mass of formulation is a relatively straight forward process, the characterisation of aerosols has always been challenging due to their dynamic and heterogeneous nature (*Hickey and Crowder, 2007*). The conventional methods of product performance focus on the aerodynamic behaviour, which is significant for the entry of particles to the lungs. These methods include dynamic particle size analysis, emitted dose, inertial impinger and impactor methods (*Hickey, 2004*). Other tests such as laser diffraction and velocimetry can also be conducted, however they are not standard regulatory tests for performance.

### 2.2.1 Content uniformity of dose

A simple test in determining the consistency of metered dose systems is to measure the content uniformity of the formulation. Whilst not testing the performance of the blend upon inhalation, it is an important test in consistency of drug content. The standard method of assessment is to take blend samples from a pre-defined mass of formulation (typically the mixed batch in pharmaceutical formulations) to the order of one to three doses worth of material (i.e. capsules or boluses) (*Muzzio et al., 1997*). Conventional methods for the verification of powder-blend uniformity are based on invasive sampling and off-line destructive analysis with HPLC or UV/Vis Spectroscopy (*FDA, 2004*).

Further discussion on methods of powder sampling for content uniformity measurements are provided in Chapter 6.

### 2.2.2 Inhalation property measurements

There are two basic categories for testing of inhalation properties, namely *in vitro* (from Latin: *in glass*) and *in vivo* (*within the living*). The latter is not associated with quality control for product release and is used predominantly in the clinical trials phase of product development until a product is registered (Campbell, 2008a). The registration process of a product involves a series of hurdles, which increase in length and cost as the product comes closer to gaining regulatory approval as a commercial product (Rowe et al., 2003b) (Figure 2.7).

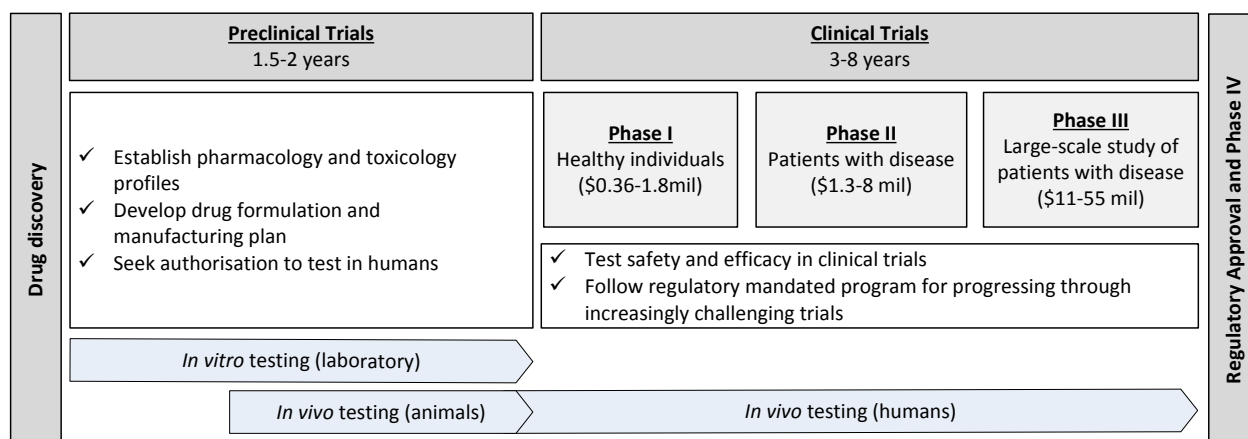


Figure 2.7: Structure and time scales for research and development of formulation pre-approval and the placement of *in vitro* and *in vivo* testing.

On average the development of a drug from discovery to manufacturing, including capital costs, is approximately \$1.24 billion USD (CISCRP, 2014). Also, the cost of *in vivo* testing is particularly costly. Understandably, most of the fundamental and academic research in drug performance has been made with *in vitro* measurements, due to high cost and labour demands associated with *in vivo* testing. Typical tests that assess inhalation performance include the emitted/delivered dose (ED/DD, amount of drug that leaves the inhalation device), the fine particle mass (FPM, amount of inhaled product of a size capable of penetrating the lung during inhalation) and fine particle fraction (FPF, the weight fraction of drug with an aerodynamic diameter of less than 5 µm compared to the total

drug content of the dose). These tests can be achieved on basic systems such as Twin Impingers (TIs), which had been commonly used due to their simplicity and ease of use (*Jashnani et al., 1995, Steckel and Muller, 1997*). More sophisticated technologies now exist however that have largely replaced TIs (termed cascade impactors, CIs). These provide more information on the Aerodynamic Particle Size Distribution of the drug (APSD) which is widely recognised as a Critical Quality Attribute (CQA) and not obtainable from TI testing. CIs allow for the measurement of other metrics such as the mass median aerodynamic diameter (MMAD) and geometric standard deviation (GSD) of drug in the deposition profile (*Copley, 2010*). Cascade Impactors are precision instruments that separate a sample on the basis of particle inertia without requiring information on particle density or shapes. Of these, Andersen Cascade Impactors (ACIs) are arguably the most commonly used impactor within the pharmaceutical industry for the testing of inhaled products (*Copley, 2010*), and are recommended by both the US and European Pharmacopoeia. Most new products however are tested via the Next Generation Cascade Impactor (NGI) (*Marple et al., 2003*), which relies on the same principles of characterisation. Only existing products tend to retain the use of ACI, as this allows comparison with previous data. Inhaler particle sizing systems are typically assembled in a simple configuration incorporating a mouthpiece, induction port (throat), impactor stack and vacuum pump. The cascade impactor itself consists of one or more stages, arranged in a vertical stack (*Figure 2.8*).

For most systems, the entrance to the impactor is fitted with a right angled induction port which is engineered according to the various Pharmacopoeias to ensure the aerosol cloud produced can be sampled reproducibly. The inhaler is connected to the throat using a mouthpiece adapter. For analysis of DPIs a pre-separator is also often fitted between the induction port and the impactor stack to collect the large mass of non-inhalable excipient (carrier). A vacuum pump operates at the base of the impactor to draw the aerosol cloud through the stack and a filter placed below the final stage to collect all material that passes through the entire stack.

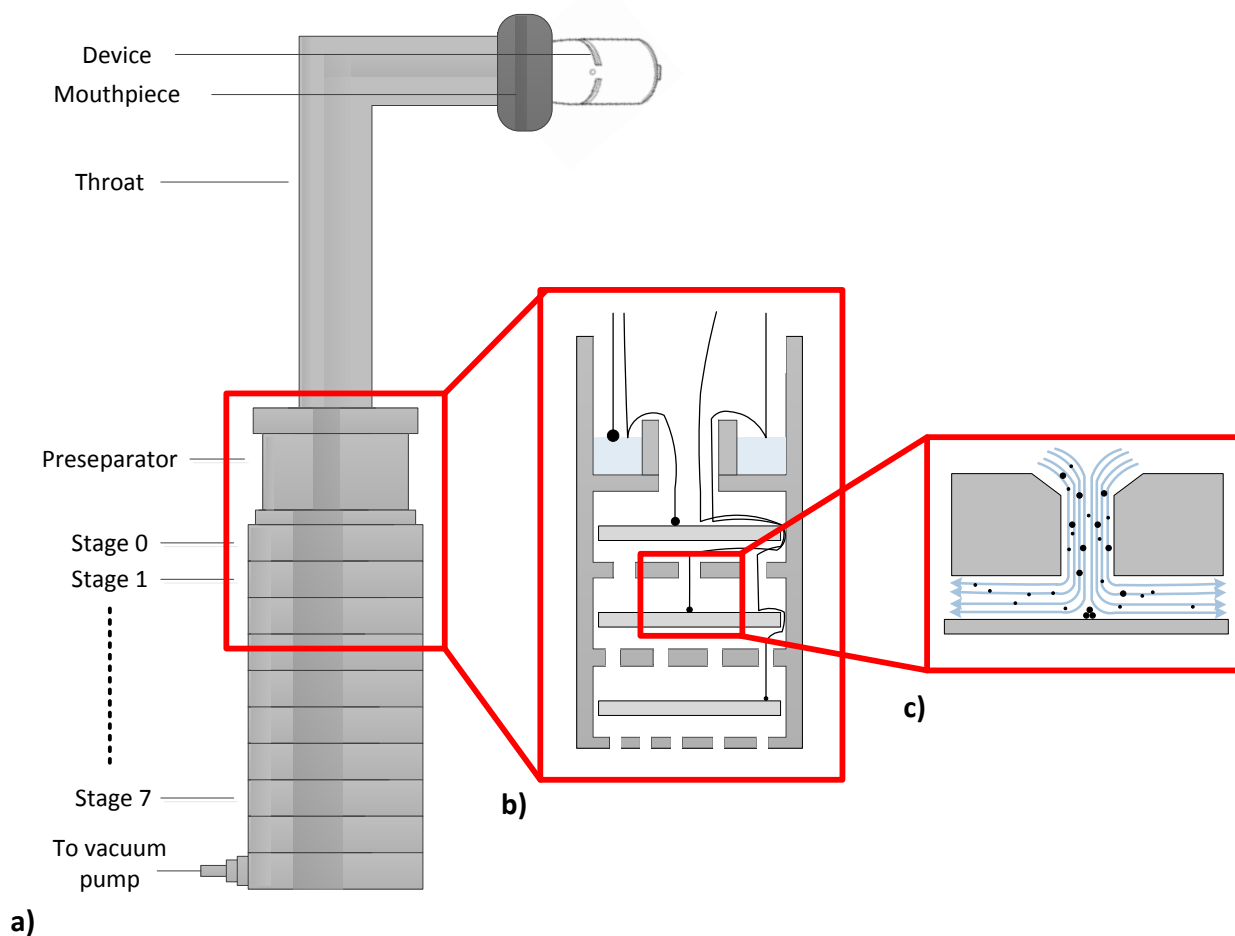


Figure 2.8: Schematic of Andersen Cascade Impaction (ACI) apparatus. A typical arrangement incorporates a mouthpiece, induction port (throat), cascade stack and vacuum pump a). Aerolised powder is forced through the impactor with the pump driven airflow and impacts/collects at various stages b). Inertial effects draw small particles deeper through the stack c).

As the entrained particles are drawn through the impactor by the airflow, they impact on plates at each stage. Initially, large particles and particle agglomerates (typically with an aerodynamic diameter greater than  $10\ \mu\text{m}$ ) become trapped in the pre-separator. The remaining aerosol travels down the stages and impacts on each plate, collecting on certain stages based on the particle's inertia and aerodynamic particle size. Air holes at the base of each plate, which decrease in size with progression down the stack, allow particles of a certain aerodynamic size to progress to the next stage. After firing several doses through the stack, the drug from each stage is collected to provide a drug deposition profile.

The ACI unit is not as simple to operate as the Twin Impinger and requires full disassembly between tests and consistency by the operator in ensuring even coating on each impactor stage plate and adequate rinsing to collect the drug. The NGI has been developed in recent years to tackle some of the challenges in ACI testing from manual handling and issues with complete disassembly between tests. It relies on identical principles however the 'stack' is horizontal and a tray of plates can be simultaneously collected for automated drug collection.

It is important to note that the pharmaceutical aerosol in Cascade Impactors does not reach equilibrium during sampling, and the resulting data must be interpreted in the context of the design of the experiments (i.e. particle size ranges for each stage are a function of the air flow rate through the impactor) (*Mitchell and Nagel, 2003*). This is done through mathematical correlations between the selected flow rate and a calibration flow rate (*Copley and McDonald, 2009*).

### 2.2.3 Difficulties with current testing methods

There are a multitude of means by which these technologies can give misleading information when testing and validating the performance of DPI formulations.

In respect to content uniformity tests, it is very difficult to obtain a representative sample of the powder, and often sampling leads to segregation and sample bias. Weight variability of the sample or metered dose, particle segregation, particle agglomeration, poor sampling strategies and a low sample size can give uniformity measurements with high variability (*Muzzio, 2006*). Outliers are often a product of agglomeration or segregation (*Bellamy et al., 2008*) of the pharmaceutical active in the powder mass. Further discussion on sampling issues in content uniformity measurements is provided in Chapter 6.

Successful and consistent measurement of inhalation performance is dependent on a wide range of variables. Particle momentum within impaction testing apparatus can lead to bounce and entrainment (in the case of solid particles), which can distort the measured aerodynamic particle size distribution (*Hickey, 1988*). Other effects of porous, hollow or elongated particles can also

augment results (Fults *et al.*, 1997), and in such cases results can be regarded as approximations. One frequently discussed issue with assessing the clinical performance of DPI formulations is the selection of appropriate volumetric flow rates in inhalation testing (Dalby *et al.*, 2007). To evaluate performance adequately, more than one flow rate is required (Byron, 1994, Byron *et al.*, 1994, Hindle and Byron, 1993), and should be determined based on the resistance of the device.

Environmental effects can also influence the result of impactor tests and powder sampling for content uniformity, in particular the aerolisation properties of the formulation within the device, which are heavily affected by relative humidity (Podczeczek *et al.*, 1997). For relative humidities above 65-75%, condensation of moisture between gaps can lead to the formation of strong capillary forces that can dominate adhesive/auto-adhesive interactions (Podczeczek *et al.*, 1996, Seville *et al.*, 1997) and long-term can lead to the formation of crystal bridges. Once a material has absorbed atmospheric moisture, the evaporation of the condensed water from the surface can also increase adhesive forces due to the formation of solid bridges of material previously dissolved in liquid bridges (Padmadisastra *et al.*, 1994). Relative humidity can also have a complex effect on the electrostatic charge of particles. At high relative humidity particles receive a negative charge, whereas at low humidity levels fine particles receive negative charge whilst large particles receive positive charge (Sutton, 1976). This can affect both aerolisation characteristics and segregation in the powder mass.

In summary, traditional methods are time consuming and reflect only a snapshot of the actual blend quality. Sampling methods are often error-prone and may include artefacts (Bodson *et al.*, 2006), since segregation and contaminations may be introduced (Muzzio *et al.*, 1997). To avoid misrepresentation of data, other techniques such as microscopy and laser diffraction can be coupled with impaction results. These however add to the labour demand of testing. In the process development stage where commercial product is not being manufactured it would be desirable to

have a simpler and more cost effective means of assessing blend performance either without, or with a reduction in, the use of the analytical systems outlined in this section.

## 2.3 Powder blending

It is relatively easy to question the validity of test results when a product fails to meet specifications. The fundamental issue however often lies not with the testing but with the mixing process itself and its inherent inadequacies in creating a homogenous, mixture with desired structure (Adam *et al.*, 2011). The homogeneity and structure of a mixture are dependent on several factors which relate to the particles and mixing system (Ngai, 2005) (Figure 2.9).

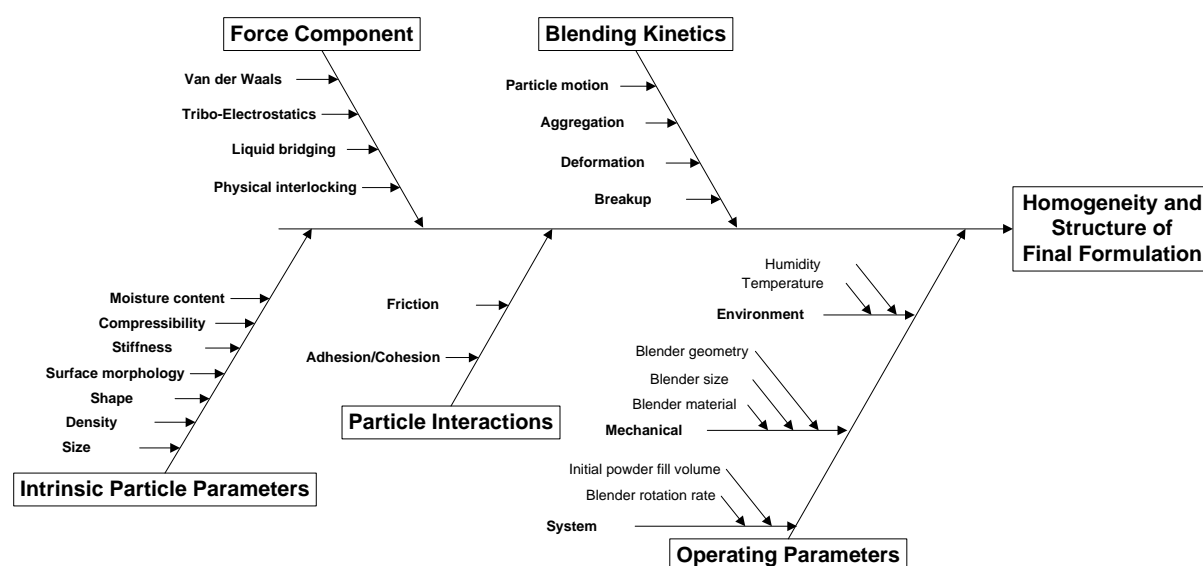


Figure 2.9: Layered factors in the homogeneity and structure of the final formulation. Factors adapted from Ngai (2005).

From the above diagram, the magnitude of the number of degrees of freedom in achieving good blending can be comprehended, as well as the inherent difficulty in understanding a given mixing system. The vast majority of formulations are manufactured in industry without a solid understanding of almost all the factors mentioned. Quite often the individual properties of each powder are well understood from the rigorous research and development programs which are part of the registration process for the product. Little else is understood on a scientific level however, particularly in relation to the mixing behaviour of the powder mixtures, and because of this,

decisions are often made with on a trail-and-error basis. For instance, mixing technologies are often selected based on a risk-adverse approach, with little regard taken for alternatives in other industries, whether it is fit for purpose, or the optimum operating conditions. Decisions for mixer selection and operating conditions are usually based on existing techniques that are either validated, or can be GMP validated based on historic experience. The pharmaceutical industry as a whole is hesitant on using new technologies because of their risk adverse nature, and as such its technologies have been said in the past to “lag far behind those of potato-chip and laundry-soap makers” (Abboud and Hensley, 2003).

Typically under this approach, conditions are selected from historical experience for a mixing technology of the appropriate scale, and batch after batch is processed empirically (and wasted) until a set of operating conditions passes the appropriate tests. Such selection of equipment and operating conditions often leads to batch failures as a fundamental mechanistic understanding of the process, and how to account for process deviations, does not exist. Ideally, an understanding of how to manipulate operating conditions to suit certain formulations should be made to allow for flexibility in manufacturing, and to lower the amount of batch failures that do and can occur. This section outlines some of the key factors above that can influence the quality of the final formulation.

### 2.3.1 Mixture structure

Before discussing some of the main influencers in powder blending, it is important to give mention to the different types of blend structure that exist, and to define their terminology. Over the years, mixtures have been given various labels such as ideal, random or perfect to describe a generated system or to specify a desirable mixing ‘end-point’ (Kaye, 1997a).

Initially in the mixing process, component-rich pockets exist where the concentration of certain components are very high. As mixing progresses, and material is displaced through shear-mixing and random tumbling (Kaye, 1997a), these pockets are broken up and components are intermingled with

one another. The intermingling of components within the powder mass, whilst driven by an ordered force (such as an impeller or through rotation of the mixing vessel) appears chaotic in nature.

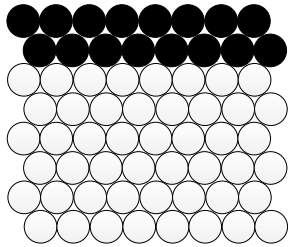
In a perfect system, components are eventually broken into individual particles that do not come into contact with one another (i.e. no agglomerates are present). Such a system is defined as 'ideal mixing' (Figure 2.10a) and represents the ultimate and practically unobtainable end-point of mixing, which has no objective meaning in the discussion of mixture structure. In a real process however, the components are randomly (or chaotically) arranged and as such never obtain ideal mixing. Such mixing is termed as 'random mixing' (Figure 2.10a). The equal separation and isolation of each component in the mixture, such as in an ideal mixture, is impossible in real situations. As such, there are inevitably small pockets of each component within the mixture which may represent incomplete mixing, as shown in Figure 2.10. With increased mixing however, these pockets are broken up and others are formed in their place. Because of their unavoidable nature in a real system, such agglomerates are termed as stochastic clusters (McCauley, 1993).

Despite the various terminologies for mixture structure, it is more meaningful in real situations to talk about the *operationally achievable structure* and what constitutes a satisfactory mixture, where the mixture is described in terms of the upper limits of the process and intended specifications of the blend respectively (Kaye, 1997a).

When making a composite material where a powdered ingredient is dispersed in a matrix, the clustering of fine particles can be an important factor (Kaye, 1997a). For example, in paints, the clustering of pigment may lead to a drop in the hiding and scattering power of the paint. A homogenous mix in which a large amount of stochastic clusters exists may be referred to as having low blend intimacy. One means of lowering the stochastic clustering of drug particles in a formulation is to create ordered structures. The concept of 'ordered mixing' has been proposed (Hersey, 1975), in which fine particles adhere to larger carrier particles to form structured agglomerates (Figure 2.10b). The work of Hersey initially created ordered structures to develop

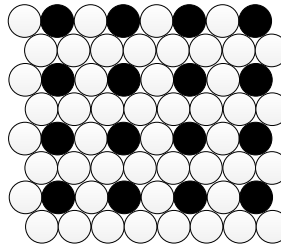
**Conceptual systems**

Active Pharmaceutical Ingredient

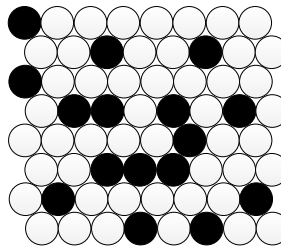


a)

Excipient

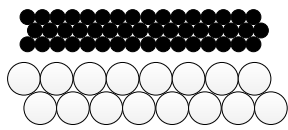


Perfect or ideal mix



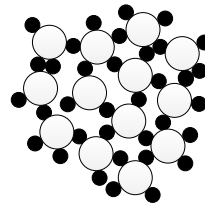
Random mix

Active Pharmaceutical Ingredient

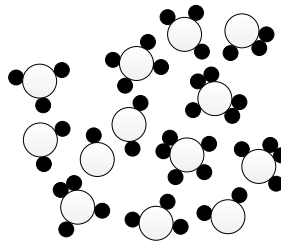


b)

Excipient



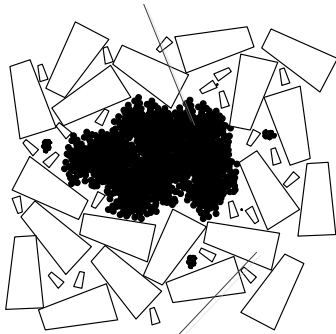
Ordered mix (Structured)



Ordered mix (Freely moving)

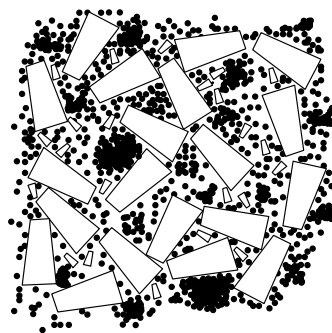
**Realistic system**

Active Pharmaceutical Ingredient



c)

Excipient



Incomplete Ordered mix

Figure 2.10: Schematic of various types of conceptual mixtures such as random and perfect/ideal (a) or ordered (b). A realistic mixture is also shown for the blending of small and large particles, generating an incomplete ordered mixture (c).

pharmaceutical formulations for drug delivery in which the variation of active was minimised (Hersey, 1981, Hersey and Cook, 1974, Hersey et al., 1974). This type of mixing also goes by other names, including regimented, structured and interactive. The strength of these ordered structures is affected by the morphology, size difference and the adhesion/cohesion force balances between the fine and coarse particles. Orr defines an ordered structure as one in which a coated particle is agglomerated to others by the same material to which it is coated. Incomplete ordered mixing has also been defined, where full dispersion of agglomerates of coating have not been achieved. Other terms such as total mixing, pseudo-random and imperfect mixing have also been introduced (Staniforth, 1994, Staniforth, 1996, Staniforth and Morton, 2005).

As mentioned in Section 2.1.1, the real structure of a ternary DPI formulation contains all possible combinations of drug, fine excipient and coarse excipient. Some structures can be classed as ordered, as shown in Figure 2.3, whilst others are pure clumps of drug or fine excipient. Such systems can be classed as ‘incomplete ordered mixtures’ (Figure 2.10c) (Orr, 1974). A good explanation of various types of structures in incomplete ordered mixtures can be found in “*Dry powder inhaler formulations-simple two component powder mixtures or a multi-particulate nightmare*” (Stewart et al., 2005).

A comprehensive assessment of mixing in the pharmaceutical industry have been compiled by Orr (Orr, 1974, Orr and Shotton, 1973) and Fan (Fan et al., 1990). Three-dimensional descriptions and depictions of powder structure also exist (Kaye, 1997a).

### 2.3.2 Intrinsic Particle Properties

Whilst particles are solid, collectively in a powder they exhibit the combined properties of solids (particle rigidity), liquids (bulk flow characteristics) and gases (compressibility), making their behaviour very complex (Rhodes, 2008). The behaviour of the bulk powder is dependent on how particles interact with one another, with various physical and chemical properties affecting mixture behaviour. Properties such as particle size, size distribution, shape, surface texture, surface area,

density, elasticity, porosity, hygroscopicity, electrostatic propensity, hardness, amorphous content and adhesion/cohesion balances can all influence the type of interactions that particles undergo.

Ultimately, the flow and manoeuvrability of individual particles within the bulk flow during mixing determines whether drug can be sufficiently de-agglomerated and attached to the active sites of the carrier lactose (i.e. the sites of high surface energy) to create ordered structures (*Hersey, 1975, Young et al., 2005*). Other effects on the powder also come into play whilst it is being blended, such as the degree of consolidation, aeration, surrounding humidity levels and the extent of shear/strain applied to the powder (*Freeman, 2012*). Due to the nature of DPI formulations, all of the above mentioned factors can influence blending as particles vary significantly in size, flow properties and surface chemistry.

When discussing the issues associated with powder mixing, it is important to identify the two main classes of powder (*Kaye, 1997a*). The first class, described as free flowing powders, are relatively easy to mix but are prone to segregation and handling issues. The second class, called cohesive powders, are bound together by a range of forces such as electrostatic and van der Waals. They are relatively difficult to mix effectively but are less prone to segregation. Powders with different properties (size, density, shape, etc.), such as in a typical DPI formulation, tend to exhibit segregation and collect together in a mixture. This can occur both during blending and post blending through moving, pouring, conveying or further processing the formulation. The particle properties also define the likelihood of certain types of particle-particle interactions that are likely to occur during chaotic blending, and whether desired ordered structures are likely to be achieved with a given powder mix. This not only depends on the geometric and density properties of the particles, but also their binding affinities for one another.

### 2.3.3 Particle Interactions

An important inter-particle factor in the blending of pharmaceutical excipients and drug particles is the adhesion/cohesion forces between each component and their affinities to one another (*Begat*

*et al.*, 2004, *Behara et al.*, 2011a). These forces describe the bonding properties of each particle and give insight into whether particles are likely to stick to ones of the same type or others within the blend, as well as whether a powder is cohesive or free-flowing in nature. This in turn can affect aerosolisation properties and the fine particle drug deposition in the lung. The cohesive powder tensile strength is defined by the particle size, packing fraction and work of adhesion/cohesion (*Kendall and Stainton*, 2001), and is related to the complex surface nature of particles which have a non-homogenous surface morphology and composition, with variable crystallinity and impurities (*de Boer et al.*, 2003). For DPI formulations this can be a complex mixture of particle interactions ranging from loosely adhered, open packed particles which readily aerosolise to closely packed agglomerates that are unlikely to aerosolise under standard DPI conditions (*Behara et al.*, 2011c). Effects such as mechanical interlocking of particles can also influence their adhesion/cohesion properties. Interlocking is dependent on the particle shape and stiffness of the material. Particles that have rough or jagged surfaces lock whilst moving past each other, encouraging surface interactions and binding (*Freeman*, 2012).

Due to the cohesive nature and size of drug particles and strong adhesion forces to each other or the carrier, their delivery to the lungs is generally inefficient. Surprisingly (and disappointingly), most commercial devices deliver less than 20% of the emitted dose (i.e. having a Fine Particle Fraction, FPF, of 20%) (*Smyth and Truman*, 2007). The main cause being the processing of the formulation, as processing has a large influence on the extent to which drug particles adhere to one another and the carrier (*Thalberg et al.*, 2012). A decrease in FPF with mixing time has been observed for the blending of lactose and salbutamol sulphate in a high-shear mixer (*Steckel*, 2007) and for budesonide and lactose in a Turbula mixer (*Jones et al.*, 2010), suggesting that with too much processing, drug particles are adhered too strongly to the high-energy active sites of the carrier and do not dislodge during inhalation. A fine balance of blending is needed therefore to ensure that drug material is sufficiently de-agglomerated but not strongly adhered to the carrier. To do this, knowledge of the

adhesion/cohesion balance between the materials in formulation is required (Begat et al., 2004, Behara et al., 2011a).

Attempts to measure the cohesive forces between particles have been made previously using Atomic Force Microscopy (AFM) and a colloid probe (Louey and Stewart, 2002, Young et al., 2006). Whilst these works have been useful in understanding particle interactions, they do not accurately represent the effects of particles in a powder bed, or account for the variability in packing. They do go some of the way however to understanding the propensity of a particular drug to adhere to itself or the carrier. This can provide insight into how to blend them effectively to create a higher yield of desired structures throughout the blend.

#### 2.3.4 Blending kinetics

The flow of powder in a mixer influences the type and frequency of inter-particle interactions, and affects the properties of the final blend and the mixing kinetics. Several mechanisms occur during the mixing of powders and are caused by convective (bulk), diffusive (relative) and frictional (shearing) motions (Rhodes, 2008) (Figure 2.11).

Convective mixing (Figure 2.11a) relates to the bulk motion of the particles, and is introduced to the powder through the motion of impeller blades and the effect of gravitational and centripetal forces on the moving mass of particles (Ramaker, 2001). This can have a profound influence on the homogeneity of the mixture. Diffusive mixing (Figure 2.11b), which relates to a particle's relative motion to the bulk, occurs when a powder mass is sufficiently aerated to facilitate the random particle migration. Frictional or shear mixing (Figure 2.11c) describes the moving of layers of particles relative to one another. This can occur when powder undergoes a sudden compression, and fail zones within the bed force layers of particles to slip across one another. Inter-particle frictional forces are required in the blending of cohesive and/or partially cohesive powder systems to de-agglomerate small cohesive particular aggregates into smaller aggregates or primary particles. In doing so, and through the aid of bulk material movement, cohesive components are able to

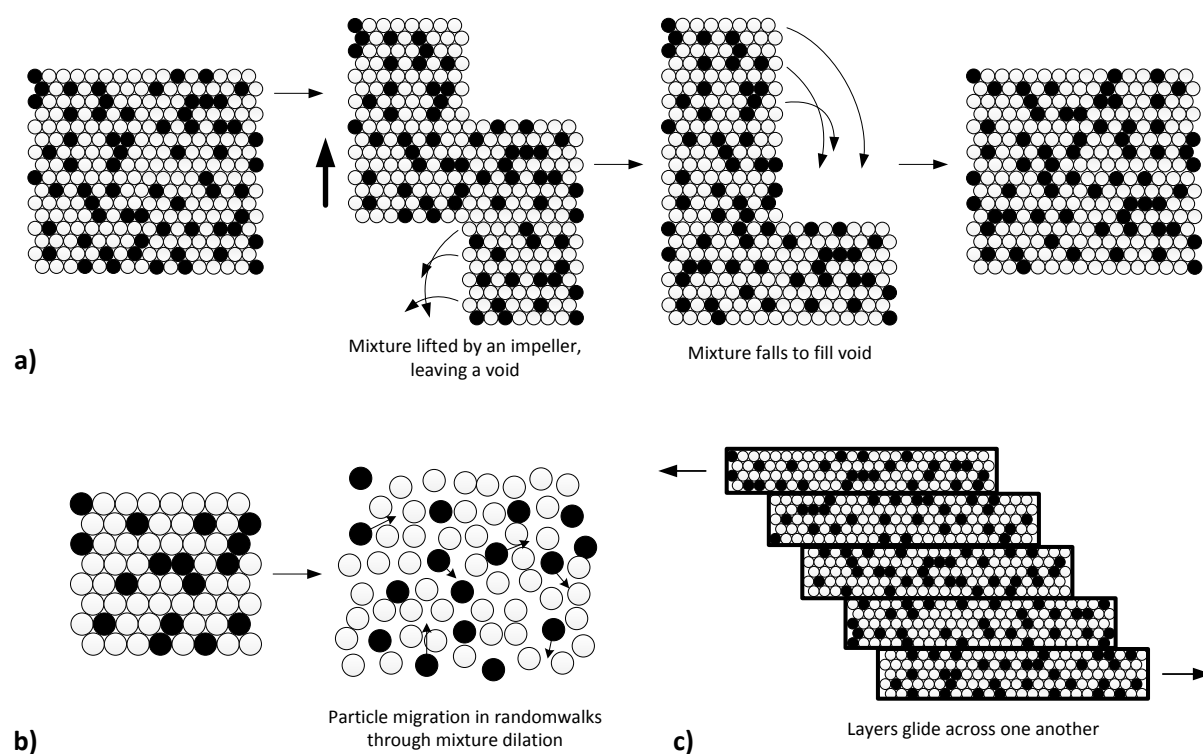


Figure 2.11: Schematic of the fundamental mechanisms in powder mixing; convective (a), diffusive (b) and frictional (c). distribute themselves more evenly through the blended powder mass, thereby increasing the degree of mixing and improving blend homogeneity. For pharmaceutical formulations, this ensures that the final product provides a reproducible dose and increases uptake into the patient respectively.

In a real process, such as in an impeller mixer, all of these mechanisms can occur simultaneously. As the impeller moves through the powder mass it exerts compressive and shearing forces on the powder through direct contact. In the region ahead of the impeller, material is forced forward and impacts on material further upstream, subjecting it to compressive forces. As the blade passes underneath the powder is forced up and over the impeller, subjecting it to frictional mixing (*Knight, 2004*). During this process a void is created below the impeller which powder falls in to, creating a region where the bulk density is relatively low and dispersive mixing can occur. Repeated impeller impacts result in convective mixing as bulk powder swirls around the mixer.

Whilst helpful in explaining the behaviour of powder motion, the use of such terms is not strictly correct. These terms were originally used to describe fluid mixing and do not necessarily correlate to

the mixing of solids as there is no true equivalent for Brownian motion within a powder unless the powder is diluted by vibration or fluidisation (Kaye, 1997b). In a powder mixer, true continuous diffusion does not exist; instead there is small-scale chaotic dispersion from the agitation of the powder bed, which is one or two orders of magnitude different from the gross displacements created by the motion of rotating paddles and diversionary baffles. It has been proposed instead that the diffusional movement and convective displacement of powder during mixing can be better applied to a randomwalk theory of dispersion, in which the distribution of probable steps during mixing are a culmination of many small probable steps (diffusional dispersion) and large rare event leaps (convective displacement) (Kaye, 1997b). This approach is argued to give more meaningful communication of powder motion and is the basis for the Levy flight theory, which is discussed further in Chapter 6.

When discussing powder mixing, particularly in DPI formulations, it is important to distinguish between the ability of the powder to create chaotic conditions within the mixer and the ability of the mixer to de-agglomerate material and create an intimate mixture. Another way of viewing mixing therefore is to shift focus to the movement of the minor component in a blend rather than the bulk motion, which is often rate limiting for mixing and in the case of most DPI formulations, where the minor component is the drug (Thalberg *et al.*, 2012). As both the breakup and spread of drug are important to the success and reproducibility of many pharmaceutical dry powder formulations, the dispersion (spread) and de-agglomeration (breakup) of the often cohesive drug component can be used to assess chaotic conditions and intimacy of the blend respectively, and convey more meaningful information on the quality and characteristics of the mixture (Figure 2.12).

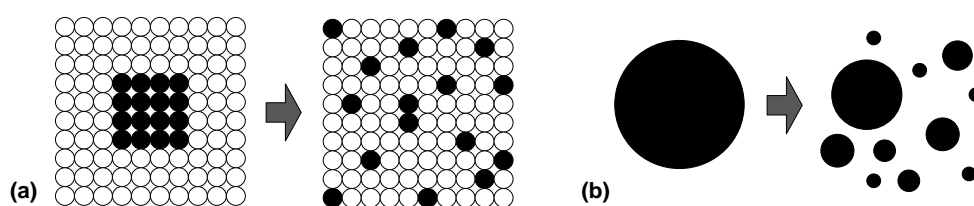


Figure 2.12: Schematic of mixing mechanisms of interest: dispersion (a) and de-agglomeration (b).

In the past, these two mechanisms have been monitored together, and it has been suggested that the 'fail' of many batches comes from the lack of shear zone de-agglomeration in the mixer, despite efficient chaotic mixing (Kaye, 1997b). It would therefore be recommended that the performance of a system be monitored in regards to both mechanisms.

As well as understanding the mechanisms behind creating a homogenous and structured mixture, there are mechanisms that also antagonise blending - causing the segregation of components. Several mechanisms can lead to the segregation of powder formulations, both during and post-blending, and are based predominantly on differences in particle size and density.

During mixing, inertial and percolation effects can cause the segregation of carrier and drug. These effects are analogous with the effects which cause the dispersion of drug particles from carrier particles during inhalation, and are outlined in Section 2.1.4. Because of this, care must be taken to select a mixing technology which promotes good mixing kinetics but minimises the likelihood of segregation occurring.

### 2.3.5 Mixing technologies for DPI formulations

A variety of different types of mixing technologies are employed in industry for the commercial production of DPI formulations. When classing different mixing technologies it is useful to refer to their degree of 'shear dispersion' (Kaye, 1997a), which describes the degree of frictional mixing (described in Section 2.3.4). Shear forces are required in the blending of cohesive and/or partially cohesive powder systems to de-agglomerate small cohesive particular aggregates into smaller aggregates or primary particles. In doing so, cohesive components are able to distribute themselves more evenly through the blended powder mass, thereby increasing the degree of mixing. Some mixers lack shearing mechanisms in their operation, which eliminates their ability to de-agglomerate cohesive material. Other mixers provide shear force to the powder mass unevenly through localised regions of high shear located around a moving blade. As DPI formulations depend on drug de-

agglomeration, the level of shear dispersion in a given mixing technology can be a useful means of comparison.

### 2.3.5.1 Rotating or Tumbling mixers

The simplest type of mixer employed in the pharmaceutical industry is the horizontal rotating drum (Kaye and Sparrow, 1964). A wide variety of drum mixers exist, abiding by the same principles where the powders are mixed through tumbling as the entire vessel is rotated by a shaft. Vessels vary in geometry, including the familiar V, Y and double cone types (Kaye, 1997d) (Figure 2.13). Other tumbler designs include inclined drum, twin shell, cube and mushroom shapes (Sastry *et al.*, 1997).

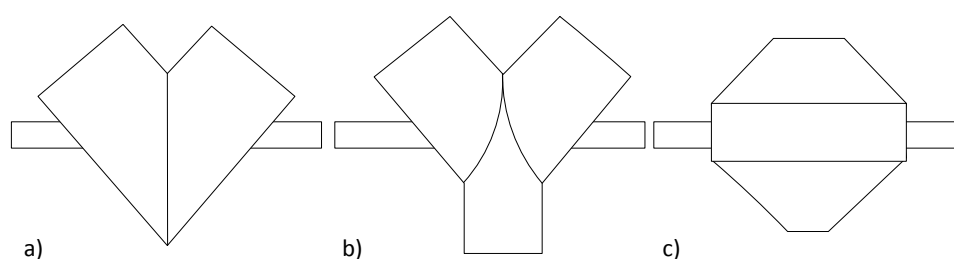


Figure 2.13: Diagrams of typical tumbling mixers including V a), Y b) and double cone configurations c).

In these mixers a volume percentage of the vessel is filled with powder, referred to as the ‘powder charge’ (Kaye, 1997a), and is rotated at a pre-determined speed on a shaft. The charge of the vessel can affect powder flow, with large charges suppressing freedom of motion of the powder and low charges reducing the momentum of material inside during rotation. The rotation of the drum also affects powder flow, with high speeds centrifuging the powder to the walls and lowering the amount of tumbling and powder intermingling. Tumblers are suitable for gentle blending and are capable of handling large volumes of material, and may or may not include baffles to facilitate the mixing of powders. Whilst considered to not have sufficient shear dispersion forces to ensure de-agglomeration of the drug particles on their own, the movement of large carrier particles in a tumbling process has been reported to provide sufficient impacting and abrasive collisions to facilitate de-agglomeration (de Villers, 1997).

### 2.3.5.2 High-shear mixers

Of all powder mixing technologies, the vertical high-shear mixer is of particular interest due to its common use across the pharmaceutical industry. These mixers are flexible in design and are used in wet granulation (Faure et al., 2001, Gottfries et al., 1996, Litster, 2003), agitated drying (Lee and Lee, 2003, Lekhal et al., 2003, Lekhal et al., 2004), tablet press operations (Conway et al., 2005) and dry powder blending (Telco and Hickey, 2005). High-shear mixers can be used to mix materials with a wide range of properties including cohesive powders (Muzzio et al., 2004). Material containment is also good, making it possible to process hazardous materials and minimise potential contamination. For these reasons, mechanical type mixers are widely used in pharmaceutical, chemical, metallurgical and food processing industries (Knight, 2004).

Through rotation of the impeller, shearing and compaction forces are exerted on the powder mass. The extent of these depends on the desired product attributes and the raw material properties (Figure 2.14).

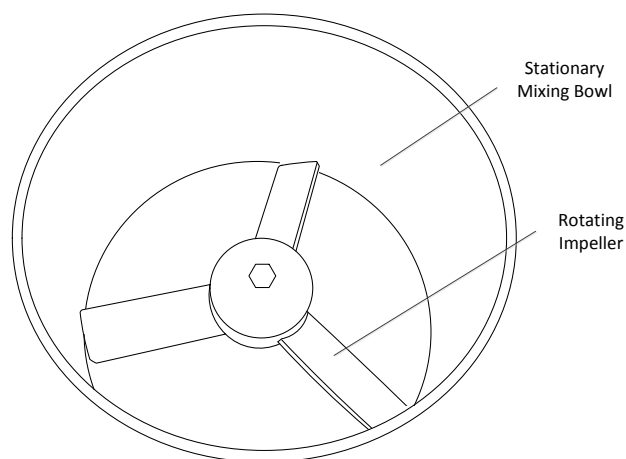


Figure 2.14: Diagram of typical high-shear mixer showing mixing vessel and impeller. Powder is agitated by the rotating impeller.

Shear dispersion forces in these technologies are considerably higher than in tumbling mixers, making complete drug de-agglomeration possible. Undesirable effects can occur as a by-product of ensuring complete de-agglomeration through the entire powder mass however, due to the shear dispersion being applied in localised regions surrounding the impeller blade. Different powder flow

regimes can be generated in this type of mixer based on impeller size, shape and rotation speed and can affect the rate and effectiveness of mixing. Further discussion on high-shear mixers and powder flow regimes is provided in Chapter 6.

### 2.3.5.3 Other mixing technologies

Beyond the standard technologies of tumbling and high-shearing, others exist which facilitate strong convective mixing with ultra-high levels of shear dispersion. One such technology is referred to as dry impact blending or Mechanofusion<sup>®</sup> (a trade name for the process invented at Hosokawa Micron Ltd. (Yokoyama *et al.*, 1987)). This system was developed in the mid-1980s and used a high-powered mechanical energy device to dry coat powders without using binding liquids (Yokoyama *et al.*, 1983). It is used for coating fine particles onto coarse particles, creating value-added composite particular materials and making it particularly useful in creating ordered structures of drug and carrier.

In mechanofusion, the host and guest particles are brought together through mechanical forces generated by powder impaction on a surface. Traditional dry impact systems consist of a rotating cylindrical chamber, with an inner rounded piece (compaction arm) and scraper blade on a stationary shaft (Figure 2.15).

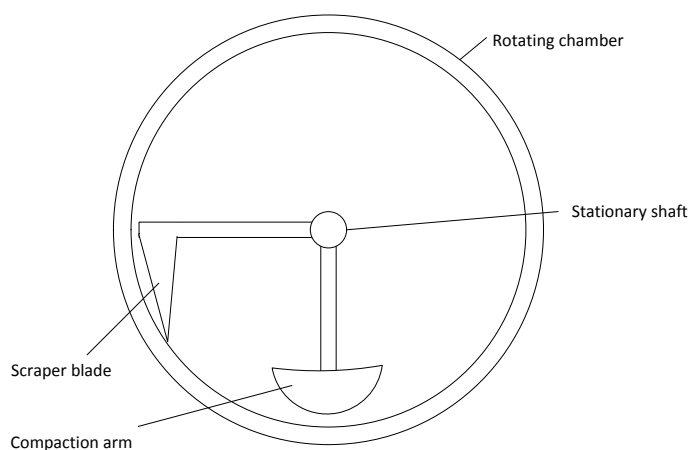


Figure 2.15: Schematic of dry impact or mechanofusion system with scraper and compaction arm.

The radius of the inner piece is less than that of the chamber and the clearance space is adjustable (typically between 2 and 5 mm) and the clearance between the scraper blade and the wall is usually

0.5 mm. The clearances influence powder properties, particle size and desired product properties. When the chamber rotates, powder is forced to the chamber wall by centrifugal motion. As the powder is forced into the converging space between the chamber wall and the rounded-inner piece it is acted on by severe compressive, shearing and attrition forces, thereby modifying the particle's surface texture. Small particles are not only de-aggregated and coated on the surface of larger carrier particles, but are fused to their surface and can even penetrate into the body of the larger particles (Alonso *et al.*, 1989a), generating hybrid particles. One can also achieve filming, whereby the coating material shear-smears over the surface of the larger particles under grinding forces (Kaye, 1997a).

Modified mechanofusion mixers also exist, which use variation of this mechanism to achieve the same outcome, whereby an impeller rotates within a stationary-walled vessel. The modified systems are closer in design to a high-shear mixer, however it is designed to operate with a very high rotational speed (500-7000 rpm) and the impeller has a clearance from the vessel walls for high-shear impaction of the powder to the wall surface and with other particles. During operation powder is not only forced to the walls of the mixer where it is compressed and undergoes shearing, but powder is also lifted from system walls through intense oscillating convective mixing over and under the impeller blades. A modified mechanofusion system is used in various studies throughout this thesis and shown in Chapter 4.

Each mixing system outlined in this section differs substantially in the nature of powder mixing and the intensity of shear dispersion that the powder undergoes. Whilst there are many other technologies that are employed in pharmaceutical powder blending, including continuous mixing systems, these are considered beyond the scope of this thesis and are not included. A good reference of powder mixing technologies can be found in "*Perry's Chemical Engineer's Handbook*" (Sastry *et al.*, 1997). Ultimately, the selection of which mixing equipment is right for the task is

determined by the desired outcome for the formulation, and can be fine-tuned by varying the operating conditions within the chosen technology.

### 2.3.6 Selection of operating conditions

To achieve good powder mixing, the operating parameters need to be chosen carefully to influence the powder kinetics and flow in the desired manner. During blending, the type of blender and mixing principles will determine the magnitude of the shear, inertial and compression forces that act on the powder during blending, which can influence the bulk powder properties (*Shur et al., 2008*). For example triboelectric charging of the lactose can occur, which has been shown to decrease the performance of DPI formulations (*Mackin et al., 1997*). Due to the complexity of particle interactions and adhesion/cohesion balances, the properties of a powder blend are susceptible to changes in the level and nature of energy applied to them. Changes in the level and intensity of energy can be caused by a multitude of factors, and can give rise to problems with formulation.

It is important therefore to ensure that a sufficient degree of blending is reached and that the final formulation is not over or under-blended. To achieve good homogeneity and structure in the blend, sufficient de-agglomeration and distribution of the drug must occur. Small particles such as those required for DPI formulations are notoriously difficult to disperse due to their high cohesivity (*Hickey et al., 1994*). This is attributed mainly to electrostatic, Van der Waals and capillary forces (*Dalby et al., 2007*). High levels of shear mixing are required to overcome the cohesive forces between the drug particles. An excess of energy is also required to ensure de-agglomeration throughout the entire batch. Applying too little energy to the blend can result in under-blending, where insufficient de-agglomeration of raw material occurs, creating drug and lactose-rich pockets in the blend. Applying too much energy can have a similar effect on the final blend, potentially re-agglomerating material and causing blend segregation. Over-blending can also damage primary particles in the blend, affecting inter-particle adhesion, blend homogeneity, inhalation performance and chemical stability of the formulation. Also, with some blenders there are regions where powder can sit or cake, often

below the impeller or on the vessel walls. This causes a form of powder segregation which affects the mixing of the powders as a whole and can result in drug rich pockets or heel residues. If high in size or quantity they can affect the drug concentration in the entire batch, and if they dislodge during mixing can affect the blend homogeneity. Such segregation is caused by systems that contain powders with significantly different sizes and/or densities. The caking and heel residue often forms during initial mixing where fine material is not sufficiently blended with the large particles and separates. This can also occur if a powder mixture is over blended.

A challenge identified by Knight (*Knight, 2004*) in powder mixing technology is that there is little knowledge into how to design mixers and mixing conditions to inherently give better control over mixing end-point. Unfortunately to date there is still a lot that is not known, and the issue of being unable to accurately predict effective mixing conditions is still present in industry. Common practice in the pharmaceutical industry is to determine the appropriate mixing conditions for a given mixer and formulation using a trial-and-error approach, typically adjusting the process intensity (impeller speed, drum rotation rate), mixing time and loading (amount of material per batch). Once the desired conditions are determined they are used continuously, without further improvements. Trial-and-error approaches such as these are often time consuming and require a large amount of material and labour for testing. This can prove to be very costly, particularly in the trialling of large mixers or products that contain expensive components.

Various studies have been conducted on the behaviour of free-flowing and cohesive materials in batch blenders, although cohesive studies are more recent (*Sarkar, 2010*). A study into the effect of high-shear batch blending on  $\alpha$ -lactose monohydrate showed that several process parameters had a significant effect on the final product (*Bridson et al., 2007*). Relative humidity, energy input, temperature, mixer blade design and mixer headspace humidity were all tested to determine their significance on particle size and surface properties. The following conclusions were drawn from the study:

- The storage of powders prior to blending is important and should be considered part of the manufacturing process, with careful monitoring and control due to formulation sensitivity to relative humidity.
- The total energy input should be monitored during blending in order to control particle size distribution. The bowl temperature, power number and humidity of the blending environment are secondary and may be unimportant to input energy.
- Attention should be paid to the mixer blade design to ensure that powders are well mixed and the effects on primary particle interactions are fully understood.

Other studies have given insight into the influence of adjusting operating parameters in systems with different levels of cohesion, such as how blender loading can affect blending rates (*Sudah et al., 2005*). In free-flowing materials, mixing becomes more effective when a larger number of smaller blades are used compared to few larger blades (*Laurent and Bridgwater, 2002b, Laurent and Bridgwater, 2002c, Malhotra and Mujumdar, 1990, Malhotra et al., 1988*) and that for certain ranges of impeller speed, fill height is more influential on mixing than the impeller speed itself (*Laurent and Bridgwater, 2000, Laurent and Bridgwater, 2002a*).

It has been found with cohesive systems that mixing rate improves with a low level of cohesion, but decreases as cohesion increases (*Chaudhuri et al., 2006, McCarthy, 2003*). This is believed to be caused by the emergence of spontaneous chaotic flow when fine cohesive powders are introduced, thereby enhancing mixing compared to non-cohesive, free flowing materials (*Shinbrot et al., 1999*). Whilst there are several studies that investigate the influence of operating conditions on blending kinetics and even particle attrition, there is a lack of data and reviews on the influence of blending processes on the physicochemical properties of the bulk powder formulation, or the resultant effect on powder fluidisation and DPI performance (*Shur et al., 2008*).

### 2.3.7 Scale-up and blend optimisation

The trial-and-error approach in determining mixing conditions outlined in the previous section also offers little flexibility in production, both through formulation and volumes. This can cause significant development or ongoing manufacturing delays for companies as process scaling is often required due to the volume demand for a particular product fluctuating with market interest and medical needs. Due to the importance of the role of excipients in DPI formulations it is also necessary to ensure consistent uniformity and interchangeability that may arise from batch-to-batch variations, or in the event that excipient type or supplier need to be changed (*Gamble et al., 2010*). To create a robust process that can tolerate such changes, a solid working understanding of the system is required.

Product scaling, both up and down, is an inevitable task with the lifetime of a product. To get to manufacturing operations from drug discovery, companies need to go through several scale-up processes as clinical development progresses. Manufacturing processes created during preclinical development are gradually scaled up to commercial levels as clinical development progresses (*Figure 2.16*).

Pharmaceutical industries constantly also require the upscale or resizing of manufacturing processes once a product is being commercially manufactured. This can be done to suit varying demands for their products and to cope with limitations in the availability of process equipment on site. Typical pharmaceutical batch mixing systems, such as high-shear mixers, are difficult to scale due to their geometries and the nature of the impeller (*Timko et al., 1990*). Process optimisation also plays a part in the resizing of equipment, as well as continuing over the life cycle of the product, particularly when changes in technology, regulatory requirements and/or product quality issues occur. It is therefore important that process optimisation is an integral part of process scaling.

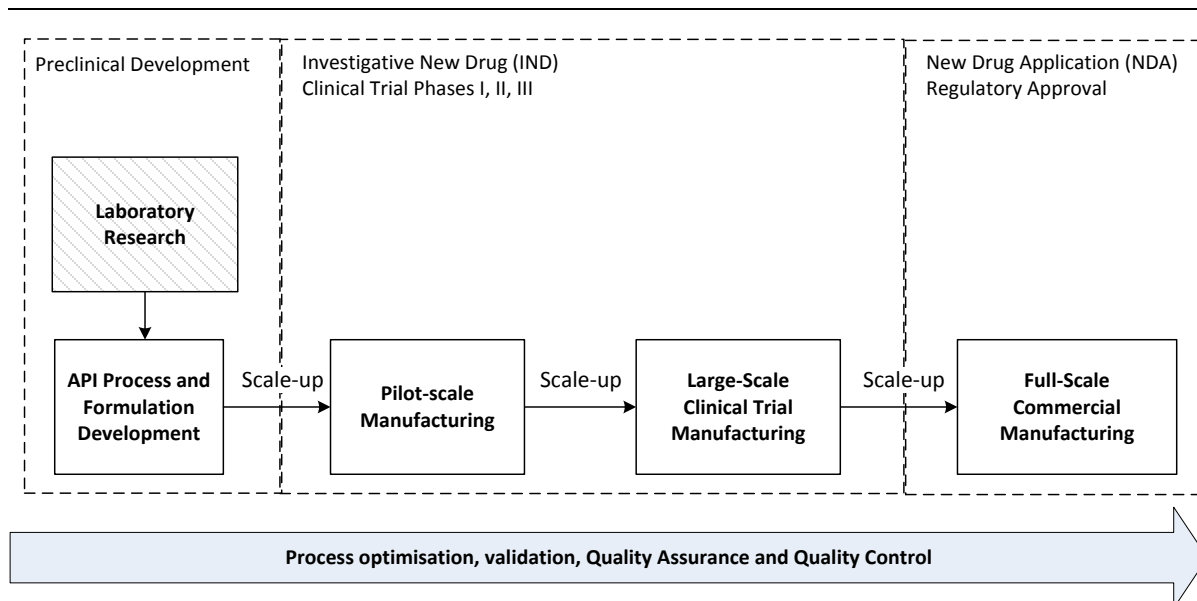


Figure 2.16: Development of scale-up operations leading to commercial production of a formulation.

The scale-up of formulations in processes such as high-shear mixers poses many problems, with little accuracy and science behind keeping the shear forces and total energy applied to the powder constant. Due to the lack of understanding of scale-up, there is often a high risk of over or under-blending, resulting in poor blend quality (Landin *et al.*, 1996b). Knight (2004) suggested that the key to obtaining better control over the extent of mixing is an understanding of material motion within the mixer and how the mixer interacts with the material during the mixing process. Many methods have been developed based on macro- and micro- scale approaches to try and tackle the issue of determining end point conditions empirically (such as input time, tip speed, power, energy consumption, torque, etc.), but each suffer from their own flaws (Faure *et al.*, 1998, Ogawa *et al.*, 1994, Zega *et al.*, 1995). Comprehensive reviews of such scaling methods can be found in “Granulation” (Mort, 2007) or the “Encyclopedia of Pharmaceutical Technology” (Levin, 2007).

Arguably the most successful method for up scaling equipment is to use a dimensionless correlation, in which a series of dimensionless variables are created that can explain all relevant elements of the process that need to be scaled. Dimensionless correlations such as the swept volume ratio (Schaefer, 1988, Schaefer *et al.*, 1986, Schaefer *et al.*, 1987), constant dimensionless impeller tip speed (Schaefer *et al.*, 1992), Froude number (Horsthuis *et al.*, 1993, Litster *et al.*, 2002, Nilpawar *et al.*,

2006, Ruegger *et al.*, 2006, Tardos *et al.*, 2004) and a constant dimensionless bed height (Litster *et al.*, 2002) have all been proposed for effective upscale, but have shown limitations and inadequacies in their use. Other correlations such as the Scaling index (Tardos *et al.*, 2004) and combinations of dimensionless groups (Cliff and Parker, 1990, Landin *et al.*, 1999, Landin *et al.*, 1996a, Landin *et al.*, 1996b) have also been proposed.

One of the most successful and widely applicable correlations is the one developed by Landin *et al.* (1996), which focusses on modelling the flow within a high-shear mixer using a modified Reynolds number, Power number and Froude number. This correlation was later expanded to accommodate large, industrial mixers and slightly modified further to gain a better fit to experimental data.

Unfortunately, the dimensionless correlations provide information on instantaneous properties of the mixer and give no information about how long powders need to be mixed for at different scales to achieve the same extent of mixing. They are also generally highly limited in their use and do not account for changes in flow profile within a given mixing technology.

Various mathematical models exist for the mixing of powders based on fundamental and often a large number of parameters (Mort, 2007). Computational methods for the modelling of powder flow within mixers, such as Discrete Element Modelling (DEM) and Computational Fluid Dynamics (CFD) are beginning to gain popularity (Langston *et al.*, 2004, Ng *et al.*, 2009, Radeke *et al.*, 2009) However, to date they are computationally expensive and not readily available to industry. Many of these methods are deterministic or microscopic. Others resort to stochastic approaches (Kaye, 1997a). Many of the computational and experimental methods simplify the mixing process by using free flowing or spherical powders which do not correlate to systems that contain cohesive materials and/or powders with a wide size distribution. Also, due to current limitations in computer processing capabilities, simulations are heavily simplified by containing considerably less particles than a real system, and coefficients that are based on the simplification of experimental data (Niklasson Bjorn *et*

al., 2005). Because of these limitations, their use is limited to providing a better understanding of the process kinetics but not necessary in determining appropriate mixing conditions.

In short, dimensionless correlations and scaling factors are complex and their practical value and validity highly questionable (Zlokarnik, 1998). Because of this, the scaling of mixers remains a predominantly “dark art”, and ultimately relies on the use of empirical blend assessment and trial-and-error approaches to determine adequate mixing conditions.

### 2.3.8 Monitoring of mixing conditions

There are several different ways in which mixing characteristics can be monitored or predicted to provide information on powder flow and the extent of mixing in a given system, and are based on the use of tracers and trackers to monitor mixing. A *tracer* is defined as a material that is able to assess the generation of chaotic conditions within the mixer, with no discrimination of flow, such as with coloured or fluorescent particles. Such systems can be used to assess the rate of mixing and the homogeneity of the blend over time. The use of colourants is described in Section 2.4. Unlike tracers, a *tracker* as an additive that is able to be distinguished from the blend through some property such as radioactivity or magnetism, and as able to trace out directions and pathways within a powder mixer.

For example, in the case of Positron Emission Particle Tracking (PEPT), the location of the single radioactive tracker particle is recorded over time through detection of its positron emissions to provide information on flow within the mixer. The information is cumulatively collected to provide residence time distributions of the tracker in the powder mass. The concepts and previously relevant work using this technique are discussed in Chapter 6.

## 2.4 Use of a coloured tracer to assess blending

As outlined in Section 2.2, current methods for assessing the extent of blending and appropriate mixer settings for a given formulation are laborious, time consuming and costly. They also do not allow for assessment of the entire blend, but rather provide representations through several small samples. In the development phase of commissioning a new piece of equipment, implementing scale-up or developing a new formulation, countless batches of material can be consumed until satisfactory blending conditions are determined. In the case of new drugs or large batches, this can become very costly and in some cases may even discourage rigorous testing, validation and process understanding. Alleviations to lab time and costs can be made in the development phase through elimination of analytical assays and the removal of the pharmaceutical active, which is often the costly component of a formulation. A general assessment of operating conditions for a given mixing system can be made through analysis of the excipient's mixing characteristics alone. One such means is to analyse the colour of pigmented excipient in the chosen mixing technology. Quick assessment of blend progression can be done visually by the operator, thereby minimising or eliminating analytical demand and allowing for a broader analysis of the entire powder mass, as well as eliminating the wastages associated with drug blends.

The definition of a pigment, as given by the Colour Pigments Manufacturers Association (CPMA) (Lewis, 1998) is that:

*“Pigments are coloured, black, white or fluorescent particulate organic and inorganic solids which usually are insoluble in, and essentially physically and chemically unaffected by, the vehicle or substrate in which they are incorporated. They alter appearance by selective absorption and/or by scattering of light... Pigments retain a crystal or particulate structure throughout the coloration process. When a pigment is used to colour or opacify a substrate, the finely divided insoluble solid remains throughout the colouration process”.*

Pigments are different to dyestuffs (or dyes), which “penetrate the substrate in a soluble form”. As pigments are being used to mark and assess the characteristics of powder blending in this work, they are primarily referred to as ‘tracers’.

### 2.4.1 Use of coloured tracers in blending

Colour has been used extensively to monitor the progress of mixing processes and operating conditions in the pigment, paint and plastics industries, where the consistent mixing of two or more different coloured powders is required and monitored (Kaye, 1997b). Their mixing is dependent on the cohesivity and fineness of each colour component. The first noted example of this (Gray, 1957) as cited by Kaye (1997) is where an optical probe was used to investigate the internal structure of a mixer and its performance in a mixer. Another study (Ashton et al., 1966) used a similar probe to explore mixing structures in a variety of tumblers as well as a ribbon blender, fluidised bed mixer and orbiting screw mixer.

### 2.4.2 Colour theory

The colour of a substance relies on its emitted spectrum of electromagnetic radiation within the visible range of the electromagnetic spectrum (400-750 nm) (Figure 2.17):

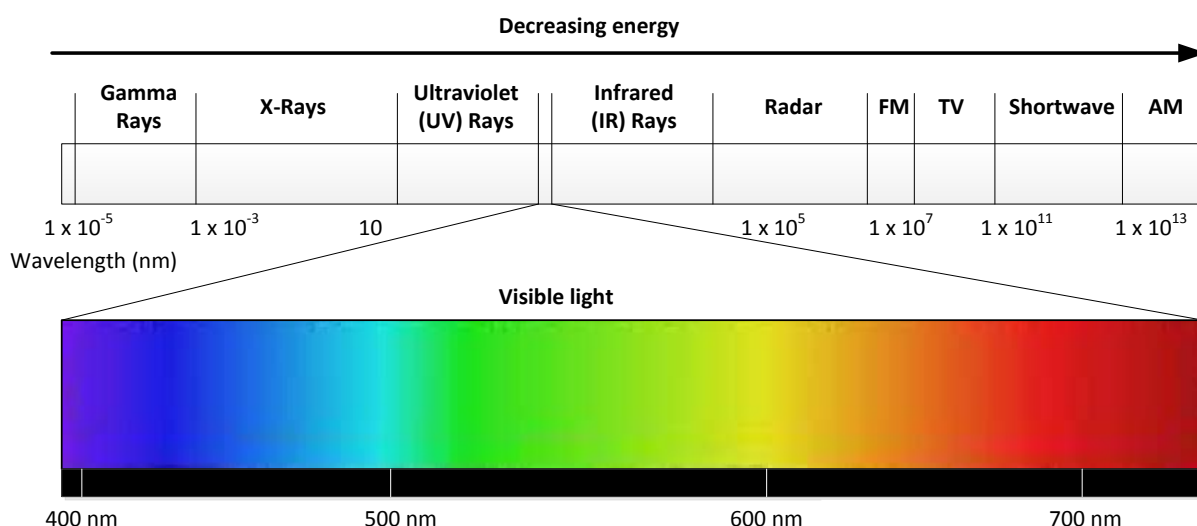


Figure 2.17: Electromagnetic spectrum showing the visible range of light.

For a given electromagnetic source impacting on a material, various wavelengths of light are absorbed and others reflected, giving rise to a particular colour which can be measured and quantified. Colour analysis of powder blends can be conducted through several methods including by eye (Völz, 2001). The most accurate and simple to employ 'in the field' is the use of a spectrophotometer (Chong, 1988), which measures the reflectance pattern of electromagnetic radiation emanating from the powder sample using a particular light source. The reflectance pattern can then be interpreted to enable evaluation and comparison of the sample in a 3-dimensional colour space. Colour information can be acquired and conveyed in several different ways. Detailed fundamental concepts of colour science, types of illuminants and types of instruments for colour measurement are described in other sources (Billmeyer, 1987, Billmeyer and Alessi, 1981, Billmeyer and Saltzman, 1981, Chong, 1988, Hunter and Harold, 1987a, Hunter and Harold, 1987b). Of the many colour spaces defined in literature (Billmeyer, 1987), two are most prominent; the tristimulus and CIELAB spaces.

The CIE (1976)  $L^*a^*b^*$  (CIELAB) colour space is used most commonly and obtained through mathematical manipulation of the tristimulus values (Billmeyer and Saltzman, 1981). It is widely used in colour analysis, including pharmaceuticals (Subert and Cizmarik, 2008) due to its ability to *quantitatively* compare colours, and has been included in the *US Pharmacopeia* since 1985. Each particular colour has a unique position in the 3-dimensional CIELAB colour space (Figure 2.18).

The CIE colour space is intuitive to use and is modelled on human perception of colour. In the CIE colour space,  $L^*$  values serve as the degree of tint (white) and shade (black) in a colour, with values ranging from purely white ( $L^* = 100$ ) to purely black ( $L^* = 0$ ). Values along the  $L^*$ -axis are termed as achromatic (without hue).  $a^*$  and  $b^*$  values denote a colour's comparative position in terms of red-versus-green (positive and negative  $a^*$  respectively) and yellow-versus-blue (positive and negative  $b^*$  respectively). In addition, the Cartesian coordinate system can be converted to cylindrical coordinates (i.e. the CIELCH space) to analyse the blends hue (h) and hue

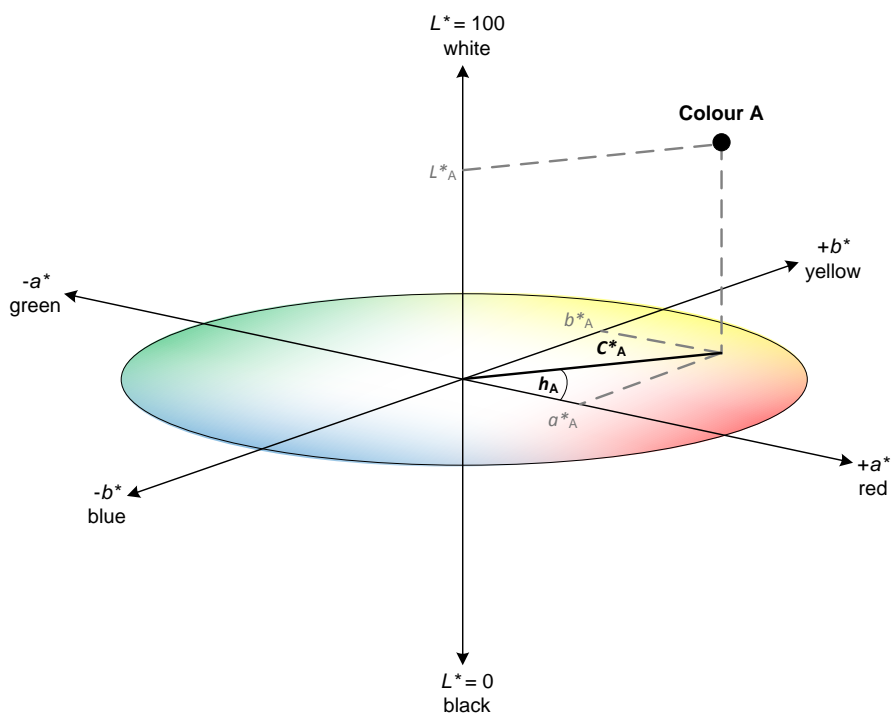


Figure 2.18: CIELAB (1976) colour space showing colour values obtained from a single measurement (a) and those obtained from the comparison of two measured samples (b). Further information can also be gained from a sample through representation in polar coordinates.

saturation ( $C^*$ ). A mathematical interpretation of the colour perceived by a human eye is defined by the hue, which in CIELCH space is termed the hue angle ( $h$ ) (Eqn. 2.1).

$$h = \tan^{-1} \left( \frac{b^*}{a^*} \right) \quad (\text{Equation 2.1})$$

The degree of a colour's hue saturation (or hue intensity) which is termed by CIE (1976) as Chroma ( $C^*$ ), is defined as the length of a line perpendicular to the  $L^*$ -axis to the colour's value in the CIE colour space (Eqn. 2.2).

$$C^* = \sqrt{a^{*2} + b^{*2}} \quad (\text{Equation 2.2})$$

Both  $C^*$  and  $h$  are useful quantities but traditionally the CIELAB Cartesian space is preferred for simplicity of comparing colours through calculating  $\Delta E^*$ . Shifts in the hue can be influenced by the Chroma of the sample. An improved colour difference formula can be used to mitigate this (Völz, 2001). Also within this space, for a given perceived difference between two arbitrary colours by eye,

there is a chord in the CIE colour space ( $\Delta E^*$ ) which can be used to quantify the difference between two colours (Eqn. 2.3):

$$\begin{aligned}\Delta E_{AB}^* &= \sqrt{(L_B^* - L_A^*)^2 + (a_B^* - a_A^*)^2 + (b_B^* - b_A^*)^2} \\ &= \sqrt{(\Delta L_{AB}^*)^2 + (\Delta a_{AB}^*)^2 + (\Delta b_{AB}^*)^2} \quad (\text{Equation 2.3})\end{aligned}$$

This property of the CIE colour space is what makes it widely used by a range of industries for the conveying and comparison of colour information.

### 2.4.3 Previous work with iron oxide colour tracer

A proposed means of analysing blend progression by coloured tracer is to use a known amount of iron oxide in replacement of the cohesive pharmaceutical active in a typical DPI formulation. Iron oxide is a pharmaceutical excipient and is commonly used as a colouring agent in tablet manufacturing (Chan, 2006), as well as in the plastic industry to colour calcium carbonate fillers (Kaye, 1997b). It is available in a variety of colours, depending on the iron oxidation state and degree of hydration (Cornell and Schwertmann, 1996, Rowe et al., 2003a). Whilst comments were made on changes to  $a^*$  and  $b^*$  or  $\Delta E^*$  in previous work (Lim, 2003, Satoh et al., 1993), when data is interpreted appropriately, 'orange' or more aptly named 'yellow-shaded' red iron oxide can be seen to change hue when sufficient energy is applied during mixing. In the case of a mimic pharmaceutical formulation, the iron oxide replaces the active ingredient (typically 1-2 wt%) and is blended with lactose. In such a system it is believed that dispersion of the relatively small amount of red pigment in the white lactose can give a broader colour spectrum than with a high percentage of iron oxide as the formulation can change from pink (little mixing) to deep red (good mixing) as the pigment is dispersed throughout the lactose powder and lactose surfaces. Further discussion on the types of iron oxide and physical causes of colour differences are discussed in Chapter 3, and the effect of concentration of pigment in Chapter 5.

Previous works by Satoh and others have extensively investigated the change in colour of iron oxide pigment in a white bulk powder (calcium carbonate) in different mixers and mixing conditions (Iwasaki and Satoh, 2002, Iwasaki et al., 2003, Satoh et al., 1993, Satoh et al., 1994, Satoh et al., 1998, Sugai et al., 1997). Satoh and co-workers began with an initial study to characterise mixer types based on process intensity (Satoh et al., 1993). In this study Satoh et al. tested the novel method of adding red iron oxide powder (5 wt%) to white calcium carbonate and measuring the colour change during mixing in various processes. The colour change was primarily compared by a “degree of dispersion” (*DoD*) scale, which was the ratio of various powder and blend’s *L*-values and directly proportional to measured voltages (*V*) of the photometer used (Eqn. 2.4):

$$DoD = \eta = \frac{L_{max} - L_{sample}}{L_{max} - L_{eq.}} = \frac{V_{max} - V_{sample}}{V_{max} - V_{eq.}} ; \quad 0 < \eta \leq 1 \quad (\text{Equation 2.4})$$

Where  $L_{max}$  corresponds to the lightness of the white component (calcium carbonate) and  $L_{eq}$  relates to the equilibrium value when the iron oxide is completely dispersed amongst the powder. It was found that as mixing time increased, lightness decreased. Results from this work also show that a change in hue occurred at high levels of mixing. However, this was not considered worth discussion. Using the “degree of dispersion” (*DoD*) factor, Satoh et al. (1993) were able to classify blenders based on the shape of curves generated when plotted against mixing time. For each process type, a distinct series of curves was observed. Among the Satoh works, one particular study investigated the link between iron oxide colour change and mixing conditions in a high-shear mixer (Sugai et al., 1997). In the work by Sugai et al. (1997), *DoD* was linked to blade speed, chopper speed, mixing time and fill level (Figure 2.19).

In this work, they measured blend colour values at high intensities and found that a mixing end-point could be reached (i.e. the *DoD* factor remained constant with further mixing) and that the equilibrium point could be increased with a more intense mixing process. Through two separate studies (Iwasaki and Satoh, 2002, Satoh et al., 1998), a quantitative link was made between the

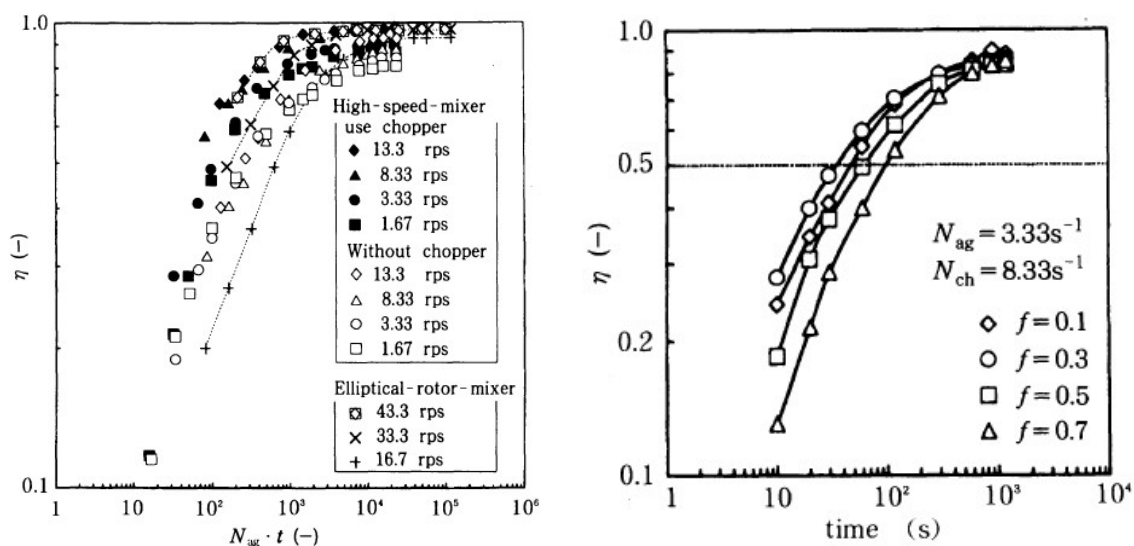


Figure 2.19: Relationships between total number of revolutions of the agitator ( $N.t$ ) (left), and fill fraction ( $f$ ) (right) on DoD ( $\eta$ ) in a high-shear mixer (Sugai et al., 1997).

energy input to the blend over time using iron oxide and calcium carbonate. A model for the de-agglomeration of the iron oxide was proposed, involving the step-wise de-agglomeration of initial clumps. With a few assumptions the energy required to break each size of agglomerate was derived and with experimental data, a correlation between energy added to the blend and mean particle diameter ( $d_{50}$ ) was determined. This in turn was used to create a correlation between energy input and DoD, as DoD was found to be proportional to  $d_{50}$  in previous work (Sugai et al., 1997). With this correlation, the DoD-time curves from the work of Sugai et al. (1997) were converted to energy input-time curves and conclusions about dominating mechanisms in each mixer type were made. Iwasaki and Satoh (2002) proposed that on an energy-time curve, regions with low gradient suggested that convective mixing was dominant and regions of large gradient (linear behaviour on a log-log plot) suggested dominance of shearing (and hence de-agglomeration) mechanism. Iwasaki and Satoh proposed that within the range of 0.1-100 MJ/m<sup>3</sup>, all mixer types exhibit shear-dominant mixing.

Lim (2003) used 'orange' iron oxide in dry powder mixing to determine an appropriate mixing time in experimental work. A lactose blend containing 2 wt% iron oxide was mixed in a vortex mixer. Samples of powder were collected at set time intervals and analysed in a tristimulus colorimeter,

and the average colour difference ( $\Delta E^*$ ) and Chroma ( $C^*$ ) plotted against mixing time. It was observed that an initial increase in colour intensity (decrease in lightness) occurred as mixing time increased, eventually reaching a steady colour. Lim also proposed that in the initial stages of the mixing process, lumps of pigment were quickly and evenly distributed in the powder mixture. It was also proposed that once the blend colour was observed to be fairly stable, de-agglomeration of the pigment occurred and primary particles distributed on the lactose particle surface.

#### 2.4.4 Mechanism of tracer blending

Other studies involving iron oxides have been conducted. Black magnetite was used by Alonso to assess and propose blending mechanisms during mixing in a low shear rotary-type mixer with rocking motion (Alonso *et al.*, 1989b) and combined high-shear mixing with mechanofusion (Alonso *et al.*, 1989a). In these studies the influence of tracer concentration, impeller speed and mixing time on the mixture properties and rate of mixing were discussed. Again, blend lightness ( $L^*$ ) was used to assess the degree of mixing. The flow properties and packing characteristics of blends were found to be affected by the surface roughness of non-coated particles, and the degree of tracer de-agglomeration. A mechanism for the blending of fine colour tracer in coarse material was proposed (Alonso *et al.*, 1989a) (Figure 2.20):

1. At the beginning of mixing, or for low intensity processes, the aggregates of tracer adhere to the large particles in their immediate vicinity.
2. When the coarse particles carrying tracer impact on those that do not, they transfer a portion of tracer. In the study, this step was envisaged as a second-order reaction between coated and non-coated particles.
3. For high intensity mixing, such as that which occurs in a mechanofusion process, the agglomerates of tracer are gradually dispersed across the surface of carrier particles through friction and collisions between particles. The mechanical energy input, which can be altered

by mixer rotational speed, was also proposed to affect the rate and maximum amount of de-agglomeration.

4. In a mechanofusion process, due to its special design, the carrier surfaces are highly modified and a partial penetration of the tracer into the carrier particles was observed.

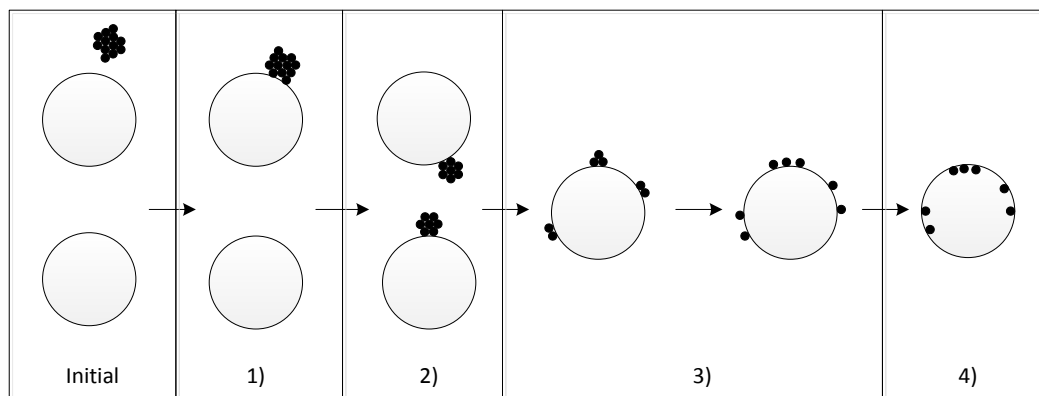
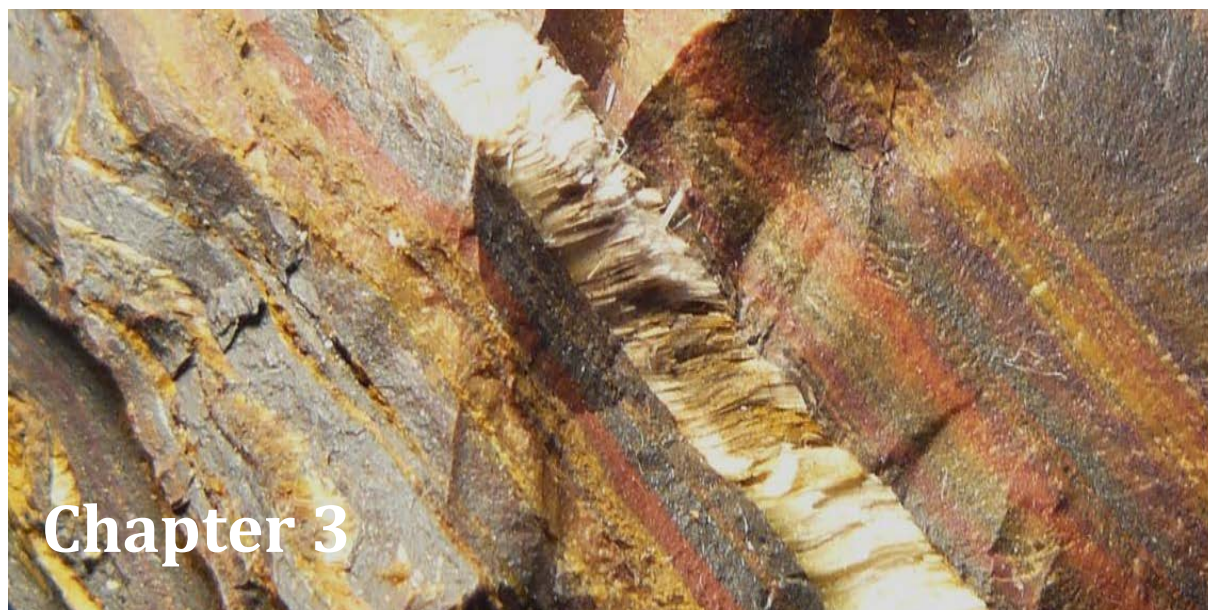


Figure 2.20: Mechanism of tracer coating as proposed by Alonso et al. (1989)

## 2.5 Concluding remarks

The pharmaceutical industry is currently undergoing a dramatic change in the way their formulations are manufactured, moving away from the traditional trial-and-error approach and moving towards science- and risk-based development of products and processes (Burcham and Roginski, 2009, Garcia-Munoz and Gierer, 2009, Klinzing et al., 2009, Muteki et al., 2009). This new concept is being driven under the concept of “Quality by Design” (QbD) which is described by several ICH (International Conference on Harmonisation of Technical Requirements for Registration of Pharmaceuticals for Human Use) guidelines including ICH Q8 (R2), ICH Q9 and ICH Q10 (Adam et al., 2011). The crux of the QbD focuses on science-based design and development of formulations and manufacturing processes to ensure good product quality. This current reform in the pharmaceutical industry has created an opening for the implementation of new blending strategies and technologies.

It would be beneficial for a novel analytical method to be developed that could provide a greater amount of information on how a formulation behaves in different operating conditions. This should help reduce time and costs associated with scaling and/or process optimisation. This should also help steer industry away from the traditional trial-and-error approach, towards the increasingly favoured and accepted Quality by Design method, and allow for a more robust method of manufacturing which was less prone to unpredictable and unavoidable batch failures. In line with this, there are also demands for greater control and process understanding, particularly as the industry moves from batch to continuous manufacturing. Currently, the best candidate appears to be the use of a colour tracer as it can be assessed by simple analytical means and can provide information on the blend as a whole (compared to the use of a radioactive tracker). The use of colour tracers is explored further in Chapter 3.



## Pigment characteristics and approach to blend analysis

**I**n this chapter, a novel and robust colourimetric method is proposed with which the extent and type of powder mixing can be assessed, based on the physical appearance of an iron oxide tracer. When the tracer is added in small amounts to a bulk powder, the blend exhibits two types of colour changes (increase in hue intensity or change in hue from red to orange) based on the level of tracer dispersion and de-agglomeration respectively. These changes are recorded at different mixing times over the duration of mixing, and plotted in the CIELCH colour space to create 'formulation curves'. Such curves can aid in the assessment of the level of tracer dispersion and de-agglomeration and can ultimately be used to assess various and multiple blend qualities, showing equivalent mixing and simplifying process optimisation in the manufacturing of pharmaceutical formulations. This chapter describes the preliminary work in developing the colour method, providing a background into iron oxides and the physical explanations of the observed colour changes. Justifications for the use of this method to interpret blending characteristics are also included.

### 3.1 Introduction to the use and properties of pigments

As mentioned in Chapter 2, the approach for this thesis is to use a coloured tracer (a.k.a. pigment) to monitor the blending of dry powders in different mixers as a function of “energy” applied and ultimately enable effective and efficient process optimisation and scaling. The terms tracer and pigment are interchangeable in this thesis, however the term ‘tracer’ is typically used when describing it as a component in the blend, and ‘pigment’ is used when describing it as a raw material. The definition of a pigment is provided in Section 2.4.

#### 3.1.1 Preliminary studies and basis for this work

The tracer used in this study was also used in a previous study (*Schultz, 2011*), in which it was mixed with lactose in industrial scale high-shear mixers to quickly and simply verify that the blend was uniform and that no white patches of powder were present which indicated dead zones. It was observed over the course of mixing that the 0.3 wt% pigmented blend not only changed colour from light pink to a dark pink as pigment spread through the lactose, but that it also became slightly orange. This change in hue from red to orange was re-affirmed in preliminary lab-scale experiments, in which the tracer blend was passed through a high-intensity milling process (spiral air jet mill) and blended in an ultra-high shear mechanofusion mixer (*Figure 3.1b* and *c* respectively). The change in hue can also be observed when raw pigment (i.e. 100% iron oxide) is smeared by hand (*Figure 3.1a*). The spread of pigment and the resulting increase in hue intensity can be emphasised in low intensity processes such as a tumbler mixer (*Figure 3.1d*). When pure pigment is dispersed and sheared in an intense environment such as an air jet mill, it exhibits a bright orange hue, but reverts back to red-brown when agitated due to its re-agglomeration (as described in *Section 3.2*). This was observed when material was collected for sampling. However in the presence of a dispersant such as lactose, the change in hue was observed to be permanent.

To better explain the physical nature of the pigment and the causes of its colour changes, a summary of the properties of pigments and iron oxides is provided in the remainder of Section 3.1. This is

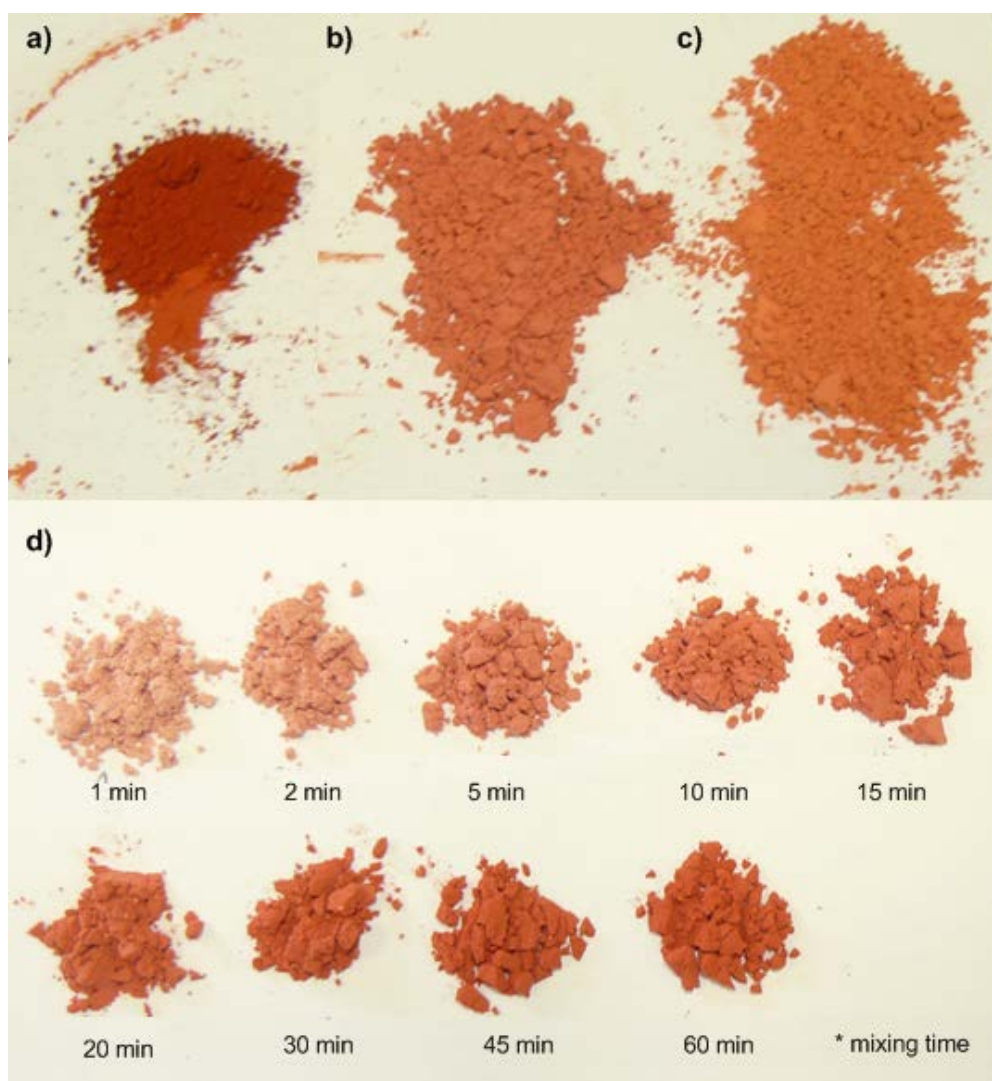


Figure 3.1: Demonstrations of pigment de-agglomeration (a-c) and dispersion (d) where pure iron oxide pigment is smeared by hand (a), mechanofused with lactose (b) and jet milled with lactose (c). When mixed in a low intensity process (such as a tumbler), the hue intensity can be seen to increase as the pigment disperses through the lactose (d).

followed by an outline of the approach taken in the subsequent chapters to explain and interpret the measured colours of pigmented blends (Section 3.2).

### 3.1.2 Background in pigments and iron oxide

Pigments can be classed as either organic or inorganic (Lewis, 1998). Inorganic pigments primarily consist of oxides, sulphides, oxide hydroxides, silicates, sulfates and carbonates, and normally consist of single-component particles with well-defined crystal structures (Völz *et al.*, 2006). Many of these can be found in nature but are also synthesised, depending on application, to ensure consistency and quality. Iron oxides are one such example of an inorganic pigment. They can be

found abundantly in nature within rocks, soil and water systems, and can be extracted or synthesised for industrial applications as catalysts and colourants (Cornell and Schwertmann, 1996). They offer many desirable properties as pigments - with low solubilities (i.e. high stability), low toxicity, brilliant colours and the ability to substitute cations in their structure (and thereby change material properties) with ease.

Sixteen different polymorphs of 'iron oxide' exist, composed of Fe (iron, typically in a trivalent state) together with O (oxides) and/or OH (oxide hydroxides or hydroxides respectively) (Table 3.1).

Table 3.1: List of iron oxides (Cornell and Schwertmann, 1996)

Oxide hydroxides and hydroxides	Oxides
Goethite $\alpha$ -FeOOH	Hematite $\alpha$ -Fe <sub>2</sub> O <sub>3</sub>
Lepidocrocite $\gamma$ -FeOOH	Magnetite Fe <sub>3</sub> O <sub>4</sub>
Akaganéite $\beta$ -FeOOH	Maghemite $\gamma$ -Fe <sub>2</sub> O <sub>3</sub>
Schwertmannite Fe <sub>16</sub> O <sub>16</sub> (OH) <sub>y</sub> (SO <sub>4</sub> ) <sub>z</sub> .nH <sub>2</sub> O	$\beta$ -Fe <sub>2</sub> O <sub>3</sub>
$\delta$ -FeOOH	$\epsilon$ -Fe <sub>2</sub> O <sub>3</sub>
Feroxyhyte $\delta'$ -FeOOH	Wüstite FeO
High pressure FeOOH	
Ferrihydrite Fe <sub>5</sub> HO <sub>8</sub> .4H <sub>2</sub> O	
Bernalite Fe(OH) <sub>3</sub>	
Fe(OH) <sub>2</sub>	

The iron oxides differ mainly in the way their basic structural units are arranged in the crystal lattice. These differences affect the material properties of each polymorph, such as colour, magnetism and stability. In some cases, other anions such as Cl<sup>-</sup> or SO<sub>4</sub><sup>2-</sup> are also present in the structure.

All iron oxides exhibit several common properties. Due to their high energy of crystallisation, iron oxides often form minute crystals both in nature and in industrial synthesis and therefore have high surface areas, typically >100 m<sup>2</sup>/g (Cornell and Schwertmann, 1996). This allows for vivid, transparent colours, as high surface areas give rise to low opacity of colour. Most pigments in general are colloidal in nature and have a typical particle size in the range of 0.03-0.15  $\mu$ m, with surface areas in the order of 70-90 m<sup>2</sup>/g. Opaque grades of pigments have considerably smaller

surface areas (often 18-24 m<sup>2</sup>/g). The most common colour shades of iron oxide are red, brown and yellow, however other colours such as purple, black and greenish-blue also exist. The colour of an iron oxide powder depends mainly on its crystal structure (*Schwertmann and Cornell, 1991*), with principle electronic transitions such as charge-transfer, and to a lesser extent *d-d* transitions, responsible for its observed colour.

### 3.1.3 Colour changes in iron oxide pigment

Charge transfer involves the absorption of electromagnetic radiation (light) (*Section 2.4.2*), which excites and transfers an electron from a ligand of a metal complex to a molecular orbital on the central metal ion (*Nassau, 1998a*). As the distance travelled by these electrons is relatively large, intense colours are viewed. This transition is responsible for the observed colour in many of the trivalent (Fe<sup>3+</sup>) iron oxides. The colours displayed through charge transfer however are less brilliant (or electric) than those of other pigments, which are caused by *d-d* transitions (*Schwertmann and Cornell, 1991*). *d-d* transitions involve an electronic orbital transition from the ground state to an excited state (often the first excited state) through absorption of electromagnetic radiation, and occur for ions with *d*-orbital vacancies. For instance, the dark colour of a mixed valence compound such as magnetite arises from an electronic transition from divalent (Fe<sup>2+</sup>) to trivalent (Fe<sup>3+</sup>) ions.

Photons can interact with a material in several different ways as depicted for a semi-transparent material (*Figure 3.2*). When a photon impinges on a pigment mass, a small fraction is specularly reflected. The remainder is either absorbed by the pigment particle, scattered or may simply pass through the mass (shown in bold in *Figure 3.2*) (*Torrent and Barron, 2002, Völz et al., 2006*).

The physical-optical properties of the pigment are therefore affected mainly by the absorption and scattering of light. A pigment for instance will appear white if the vast majority of light is scattered and black if the vast majority absorbed. The scattering and absorption in a coloured pigment depend on the wavelengths of light, and relate to the possible electron excitation levels. For this reason, pigments can be characterised by their spectral reflectance curves, with the spectrum (and hence

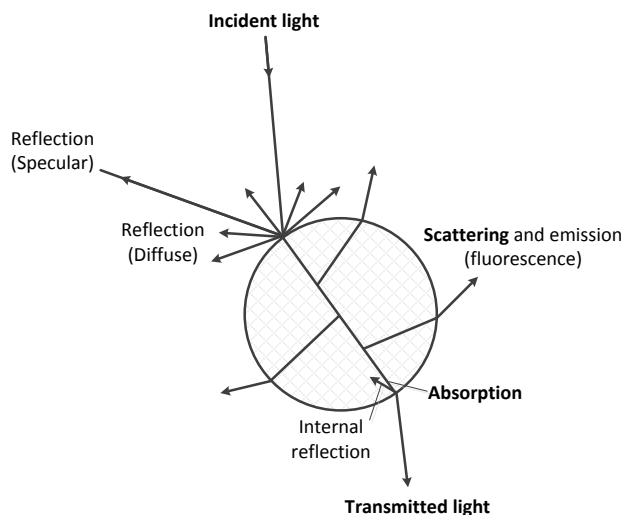


Figure 3.2: Interactions of light with a semi-transparent material. The main interactions for iron oxide pigments are the absorption, scattering and transmittance of light.

colour properties) almost completely derivable from physical quantities (Völz, 1975).

Whilst not responsible for the fundamental colour of iron oxides, variations in geometric properties of the pigment such as particle size, particle size distribution and shape can alter the perceived colour (Völz et al., 2006). Particle size distribution is affected by the relative populations of isolated (primary particles), agglomerated or aggregated particles (Honingmann and Stabenow, 1962) (Figure 3.3). These definitions are used in subsequent chapters when describing the breakup of pigment.

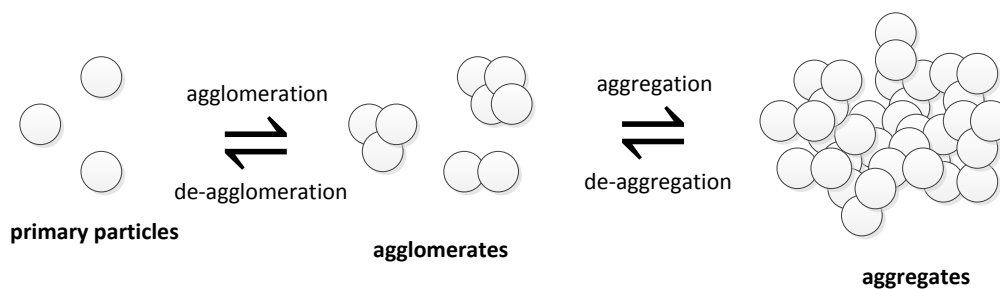


Figure 3.3: Dry pigment particles can take the form of primary particles, agglomerates and aggregates. These forms affect the size distribution and optical properties of the pigment.

For pigments, changes in the primary particle size or particle size distribution can lead to slight shifts in the observed colour (Winter, 1979). Coloured solids show one or more absorption bands in the visible spectrum and the width, profile and position of absorption bands affects the observed colour. With decreasing particle size (higher surface area) of a coloured powder, the position and profile of

absorption bands can shift, thereby changing the observed colour. Mie's theory (*Mie, 1908*), which relates the proportion of absorption and scattering to the geometric diameter of a particle, states that for a given particle size, there must be a particular wavelength of maximum light scattering. As the particle size decreases, the absorption of light increases and the uniformity of scattering decreases. This can influence overall UV attenuation (*Kobo Products Inc., 2014*), and can result in a yellowing of the observed hue for a pigment. This is observed for the iron oxide tracer in this thesis, which changes from red to orange as the particle size distribution decreases (*Figure 3.4*).

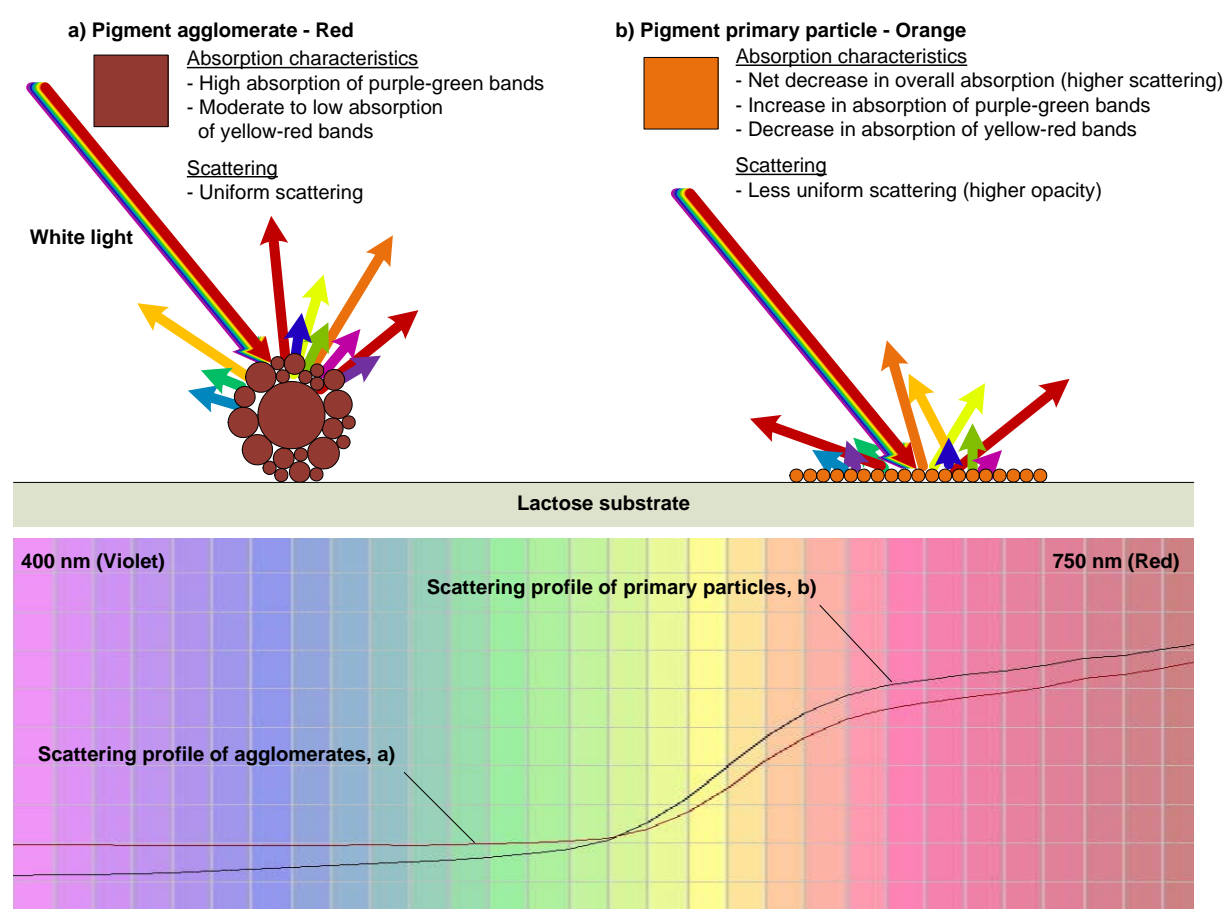


Figure 3.4: Effect of particle size on pigment hue. As the particle size decreases, the scattering of light becomes more dominant and a shift in the absorbed wavelengths of light is observed.

Whilst particle size can affect the hue of the pigment, there is a lower limit for particle size (in the nano-scale, around 20 nm), below which the absorption becomes independent of the particle size. Any further reduction in the particle size beyond the lower limit does not produce additional net absorption of light by the pigment (*Völz et al., 2006*).

In addition, the effective reflectance and colour of a powder mixture is highly complex and can relate to the packing of particles, their size and shape and agglomeration/structure (Figure 3.5). Consideration for these phenomenon is also required, particularly when using colour to assess blend progression and characteristics.

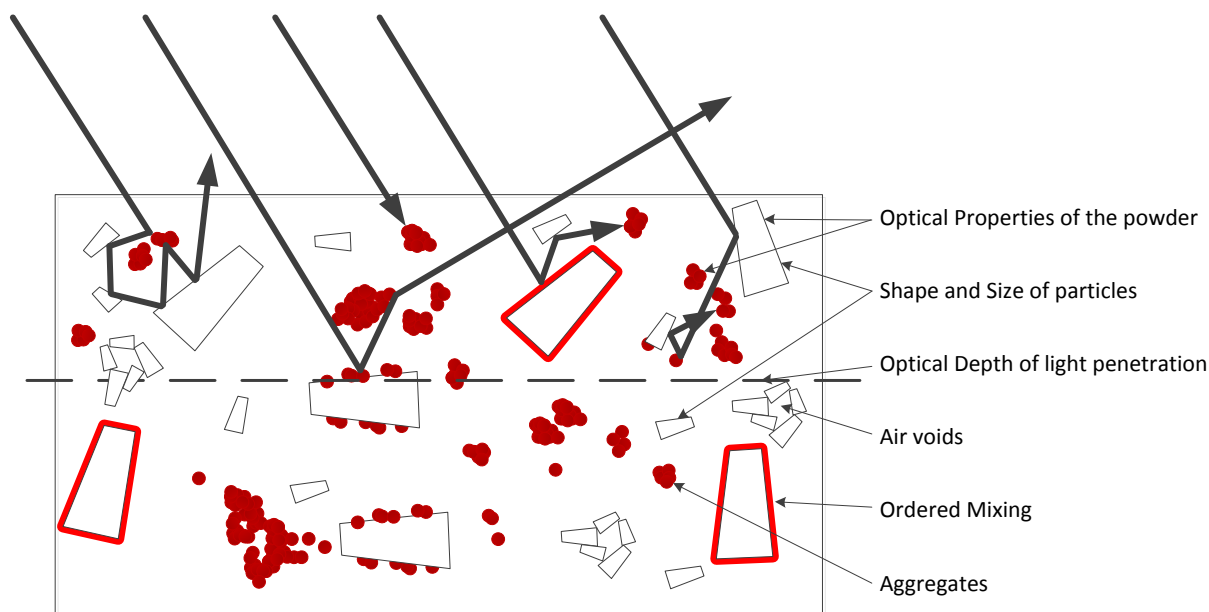


Figure 3.5: Factors influencing the effective reflectance of a powder mixture containing coloured material.

A pigment's properties can also be expressed by several other quantities beyond its colour. In particular it can be expressed in terms of its tinting strength, lightening power, scattering power, hiding power and transparency (Völz *et al.*, 2006).

- The *tinting strength* is a measure of a colourant's ability to confer colour to a light-scattering material through its absorption properties. Within certain limits, the relative tinting strength can be interpreted as a ratio of absorption coefficients of equal masses of test and reference pigment. The measurement of tinting strength is highly dependent on the criteria used for measurement.
- The *lightening power* of a pigment is similar to tinting strength but refers to the ability of a pigment to improve a material's light-scattering properties. Both of these parameters are

classified as yield properties. For instance, if the tinting strength is doubled, only half the weight of pigment is required. Scattering power is often used to compare white pigments.

- The definition of *hiding power* is based on a black and white contrasting support on which the pigment is applied. The hiding thickness  $h$  (in mm) is determined at the point at which the contrasting surface is observed, by eye, to disappear. The reciprocal of this, the *hiding power*, is an indicator of pigment yield.
- The *transparency* of a pigmented system denotes its ability to scatter light as little as possible.

The most important of these quantities to the works presented is the pigment's hiding power, and is explored in depth in *Chapter 5*.

### 3.1.4 Characterisation of iron oxides

Colour differences have been used extensively to distinguish between various iron oxides and particle sizes, and rely on various colour interpretation methods such as Kubella-Munk theory, Munsell and the CIE colour space (Scheinost and Schwertmann, 1999, Torrent and Barron, 2002). Much of the work on colour values of iron oxides are in the Munsell colour space, which has been traditionally used in geology and mineral studies (Cornell and Schwertmann, 1996). Whilst similar to the CIE colour space described in *Chapter 2*, it does not enable quantitative comparison between different colours.

In addition to colour analysis, several methods have been recommended in the literature for the characterisation of iron oxide (Wilson, 1987), the most important of which are X-ray Diffraction (XRD) and electron microscopy. In addition, Mossbauer spectroscopy, infrared spectroscopy and thermal analysis give useful information (Kosmas et al., 1986, Schwertmann and Cornell, 1991, Vandenberghe et al., 2000). X-ray diffraction (XRD) is critical in identifying the type and purity of iron oxide powders (Schwertmann and Cornell, 1991). It can also provide information about crystal size and disorder, structural parameters (unit cell lengths), degree of isomorphous substitution and surface area. Each

crystalline phase has a set of characteristic peaks in XRD which can be found in the JCPDS mineral powder diffraction file (Smith *et al.*, 1999). Peak locations can characterise the material and peak properties (such as height, width or area) can be used to quantify the amount of material present. The intensity of a peak can be used to estimate the relative proportion of a compound in a mixture. The principles of X-ray diffraction can be found in the literature (Skoog *et al.*, 1998). Infrared (IR) Spectroscopy can help to identify the presence of certain bonds in the crystal lattice (such as distinguishing between the presence of OH- and O- groups). In this technique infrared radiation passes through the sample and is absorbed at different wavelengths based on the composition and structure of the material (Skoog *et al.*, 1998). Infrared analysis provides a rapid means of identifying if the sample is crystalline. It is also useful for detecting trace amounts of one iron oxide in the preparation of another, such as determining the presence of goethite in hematite (Schwertmann and Cornell, 1991). These methods have been used in this chapter to confirm the type and purity of iron oxide present in the tracer.

### 3.1.5 Properties of tracer used in studies

The iron oxide tracer used in this work was manufactured by Rockwood Pigments, U.S.A.. The pigment is a precipitated, ultra-high purity yellow-shaded iron oxide of the general class *Pigment Red 101* (Colour index no. 77491, CAS 1309-37-1). Pigment Red 101 (Synthetic  $\text{Fe}_2 \cdot x\text{H}_2\text{O}$ ) is also known as Hematite, Mars Red, Ferrite Red, Rouge, Turkey Red and Persian Gulf Oxide (Lewis, 1998). The wide range of colour shades, acid and alkali resistance and economy of production account for hematite's extensive use in construction materials, paints and coatings, plastics, paper, cosmetics and even some pharmaceutical solid dosage forms (Capel *et al.*, 2006, Cornell and Schwertmann, 1996, Garetto, 2012, Subert and Cizmarik, 2008). Hematite is also known for its use as a catalyst in such processes as the conversion of ethylbenzene to styrene and the controlled combustion of rocket fuel. For many of these applications, hematite crystals with a particle size of around 0.1-3  $\mu\text{m}$  are typically used (Garetto, 2012). Hematite has a corundum crystal structure; with colour varying from light red to dark violet with increasing particle size. A yellow tinge in red iron oxide can be

observed for particles with a diameter of around 0.1  $\mu\text{m}$  (Völz *et al.*, 2006), and violet at around 1.0  $\mu\text{m}$  as per the effects of particle size described in Section 3.1.3.

The industrial synthesis of pigments is strictly controlled by qualitative and quantitative chemical and x-ray analysis on the raw materials, intermediates and products (Gall, 1975, Rechmann and Sutter, 1976). This serves to ensure reproducibility of colour in pigment between batches. There are many routes to the synthesis of red iron oxide pigments (Garetto, 2012). The 'Pigment Handbook' (Patton, 1973) states that red iron oxides can be synthesised through the roasting of ferrous sulphate, dehydration of yellow iron oxide (goethite), direct precipitation or by oxidation of black iron oxide (maghemite). All these methods can also be used to produce clean colour yellow-shaded red iron oxide.

The typical precipitation of red iron oxide is relatively costly compared to the other methods since it requires an acidic or neutral medium and results in low space or time yields (Oehlert *et al.*, 1997), however it is especially suitable for producing soft pigments with a pure, bright hue (Völz *et al.*, 2006). Precipitated iron oxides often contain larger amounts of arsenic and antimony compared to other synthesis routes (Oehlert *et al.*, 1997), and have larger losses upon ignition due to trapped water during crystal nucleation and growth in the medium. The loss of trapped water (typically 2 wt% of pigment) upon heating (between 400°-1000°C) also results in the loss of the clean colour shade (red) and yellow tinge. Interestingly, precipitated red iron oxides are very sensitive to grinding, which can lead to changes in the pigment shade when processed (Oehlert *et al.*, 1997). This property is exploited in this work. The specific pigment used in this study ("Ferroxide®" High-Purity Synthetic Iron Oxide Red 212P, Rockwood Pigments, U.S.A.) has been produced using the precipitation route, however it has been produced with ultra-purity and has the following specifications as provided by the supplier (Rockwood Pigments, 2009) (Table 3.2). This pigment is a member of the general class Pigment Red 101 previously described.

Table 3.2: General and batch-specific properties of iron oxide pigment used in study (Ferroxide® High-Purity Synthetic Iron Oxide Red 212P, Rockwood Pigments, U.S.A.)

Fe <sub>2</sub> O <sub>3</sub> content (%)	>97
SiO <sub>2</sub> + Al <sub>2</sub> O <sub>3</sub> content (%)	0.5
Specific Gravity (g/cm <sup>3</sup> )	5.0
Surface Area (m <sup>2</sup> /g, m <sup>2</sup> /mol) (Assuming atomic weight of Fe <sub>2</sub> O <sub>3</sub> = 159.7g.mol <sup>-1</sup> )	14, 2236
Tap Density (g/cm <sup>3</sup> )	0.7
325 Mesh Retention (%)	0.1
Water Soluble Salts (%)	0.3
Ignition loss (%)	1.0
Moisture content (%)	<1
pH	6
Particle Shape	Spherical
Predominant Particle Size (µm)	0.10
Batch Specific L*/C*/h (ColorFlexEZ 45/0)	29.6 / 44.5 / 39.0

The pigment is also claimed to have trace amounts of several transitional metals, all of which are lower than levels traditionally found in precipitated red iron oxide. The purity of the pigment was confirmed through infrared spectrometry and x-ray powder diffraction, and is expected to be made up of approximately 99 wt% hematite with 1 wt% water, with no other iron oxides or hydroxides present. In relation to pigment stability, the supplier states that Ferroxxide® 212P is colour-stable in processing temperatures below 400°C and does not undergo chemical changes below 1000°C. It is also stable under exposure to sunlight and UV radiation, and is alkali, chemical and weather resistant.

Due to the small primary particle size of the pigment (0.1 µm), the powder is expected to be cohesive and hence agglomerates and aggregates will always be present. The size and types of agglomerates and aggregates that form within the pigment were identified using laser diffraction (*Malvern Mastersizer Scirocco 2000, Malvern Instruments Ltd, UK*) (*Figure 3.6*) and scanning electron microscopy (SEM) (*Figure 3.7*).

Laser diffraction identified three main forms that the primary particles assume in the pigment powder mass, which for this work have been defined as agglomerates, small aggregates and large aggregates (*Figure 3.6*). Pigment was also observed to form 'clumps' in the order of 1-10 mm,

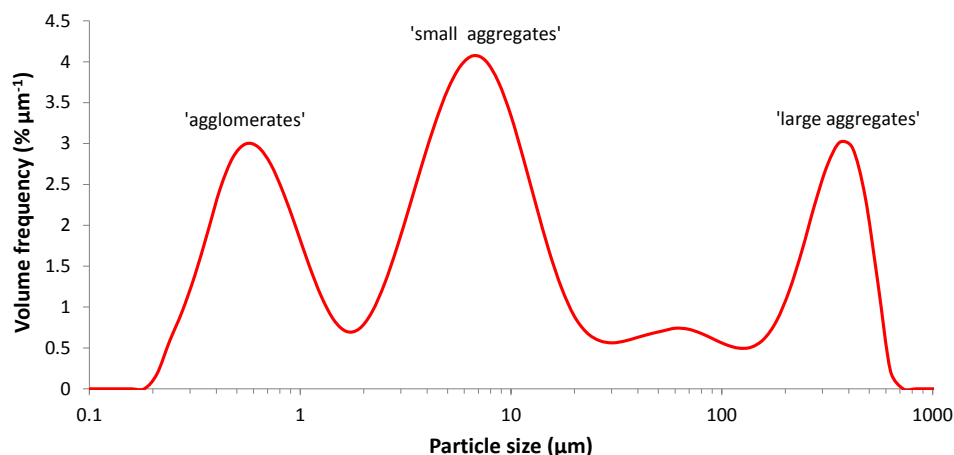


Figure 3.6: Particle size distribution of Rockwood Ferroside 212P showing size distribution of agglomerates and small and large aggregates.

however these were broken up to enable Malvern analysis and would have no bearing on actual blending as they were easy to de-clump. Figure 3.6 is intended to show the relative sizes and distributions of particle agglomerates and aggregates. The air dispersion system for Figure 3.6 (at 3.2 bar) was not strong enough to de-agglomerate the pigment and show the primary particle size distribution.

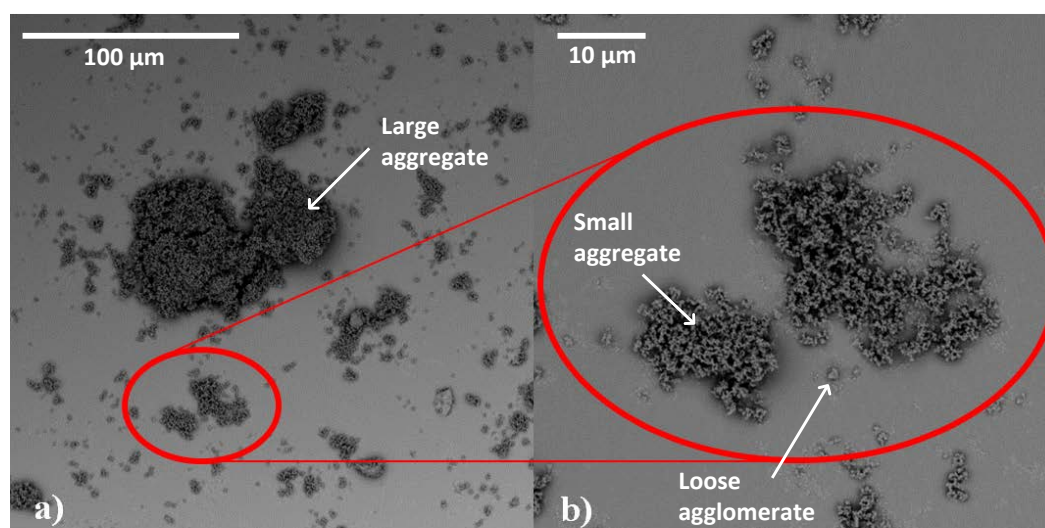


Figure 3.7: SEM images of (a) large and (b) small aggregates, as well as loose agglomerates. Spherical primary particles can also be identified in the images.

Primary particle size and spherical shape were confirmed from SEM images (Figure 3.7). Primary particles can be seen to form agglomerates, large aggregates (Figure 3.7a) and small aggregates (Figure 3.7b).

### 3.1.6 Stability of iron oxide pigments

The stability claims of the pigment given by the manufacturer are consistent with literature (Navrotsky *et al.*, 2008, Völz *et al.*, 2006). Pigments can deteriorate and lose (or change) their colour by reacting with each other, the medium, other components or impurities present in the atmosphere, or through various effects of light (Nassau, 1998b). The best known structural changes to pigments are yellowing (Epple and Englisch, 1975), chalking and loss of gloss (Völz *et al.*, 2006). Inorganic pigments are chemically very stable and are classed as one of the most stable colouring matters. Oxides are especially stable as they have a highly protective effect on the substrate (Kampf and Papenroth, 1977). The physical properties of pigments are often a function of exposed surface. The smaller the pigment particles, the higher the surface area and the more susceptible the material is to degradation by UV radiation, environmental factors and chemicals (Lewis, 1998). The heat and chemical resistance of oxide pigments are generally very high (Kresse, 1977).

In relation to the thermodynamic stability of the pigment, hematite has the lowest Gibbs free energy (i.e. highest thermodynamic stability) of all polymorphs of iron oxide/hydroxide. At the surface area of the hematite pigment calculated from manufacturer's specifications (2236 m<sup>2</sup>/mol, Table 3.2), the hydrated form is also highly stable, and considered unable to convert to another polymorph (Navrotsky *et al.*, 2008) (Figure 3.8).

Unlike hematite, other polymorphs of iron oxide are known to convert to more stable configurations, such as the conversion of ferrihydrite to hematite when kept in contact with the atmosphere for long periods of time (Schwertmann and Cornell, 1991). This is believed to be caused by adsorption of non-stoichiometric water. Hematite is stable on heating up to 1200°C in air (Völz *et al.*, 2006), whilst others such as black and yellow iron oxide (maghemite and goethite respectively) revert to hematite at 350°C and 180°C respectively.

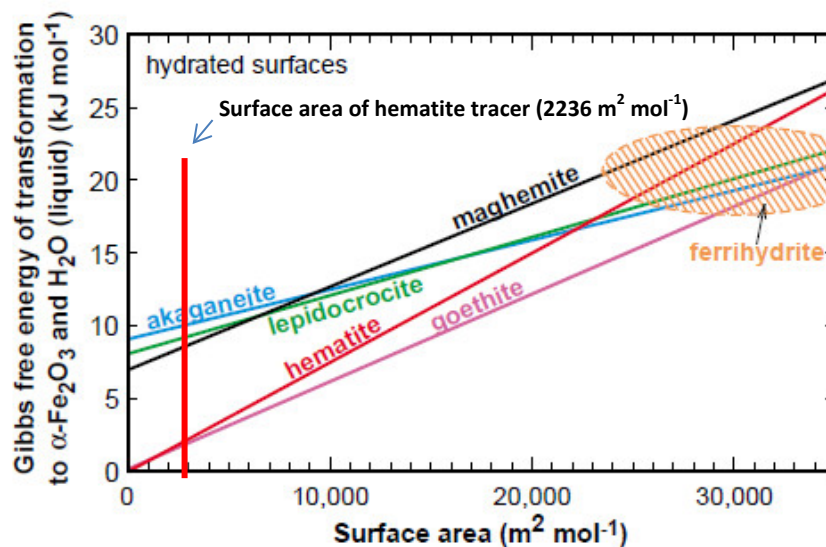


Figure 3.8: Gibbs free energy map for various hydrated iron oxides as a function of surface area (Navrotsky *et al.*, 2008), showing that hematite is highly stable in its form as provided in this study.

## 3.2 Analysis of tracer colour changes during blending

As discussed in Section 2.4.3, previous work in analysing powder mixing using red iron oxide focussed on the change in blend lightness ( $L^*$ ). From the use of this particular tracer, and exploitation of the yellow-shade that is generated when primary pigment particles are isolated, it is believed that an additional and previously unpublished dimension can be added to blend analysis, which enables the measurement of both the spread and breakup of tracer. This section outlines the colour changes of focus and their interpretations in the CIE colour space to build a robust means of assessing blend progression.

### 3.2.1 Justification of using $C^*$ and $h$ for assessing dispersion and de-agglomeration

As mentioned in Section 2.1.4, the main indicators of good mixing for DPI formulations are the spread and breakup of the drug through the carrier excipient. These two mixing mechanisms can be individually and simultaneously observed through characteristic colour changes in the blend (Figure 3.9).

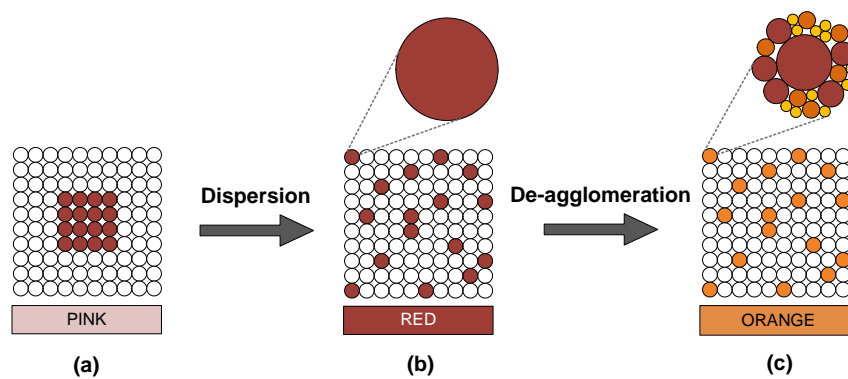


Figure 3.9: Schematic of sub-micronised hematite tracer dispersion (a-b) and de-agglomeration (b-c).

As the pigment, by definition, does not penetrate the medium in which it is being used, the strength of colour (i.e. hue intensity) depends on the tracer particles being spread in a stable, homogenous manner. Because of this, it is proposed that the hue intensity (Chroma,  $C^*$ ) can be used exclusively to measure and quantify the degree of dispersion of tracer within the blend (Figure 3.9a-b). Similarly the visual change in the hue of the blend ( $h$ ) from red to orange is solely due to a physical effect caused by the de-agglomeration of the tracer into primary particles (Völz *et al.*, 2006, Winter, 1979), and as such can be used to measure and quantify tracer de-agglomeration (Figure 3.9b-c). Information about both the hue and hue intensity of tracer in the blend is best conveyed through use of the CIELCH colour space as the hue and hue intensity are represented independently. The CIELAB space and  $\Delta E$  values (described in Section 2.4.2) are not used in these studies as the  $a^*$  and  $b^*$  values are a function of both the tracer dispersion and de-agglomeration, and are not independent of each other.

### 3.2.2 Methodology for colour measurements

There are two methods used for the measurement of colour: the tristimulus method using a three-filter colorimeter and the spectral method using a reflectance spectrometer (Völz *et al.*, 2006). The latter is used in this study, with colour changes in the powder blend recorded using a bench-top spectrophotometer (ColorFlex EZ 45/0, HunterLab Inc., U.S.A.) (Figure 3.10).

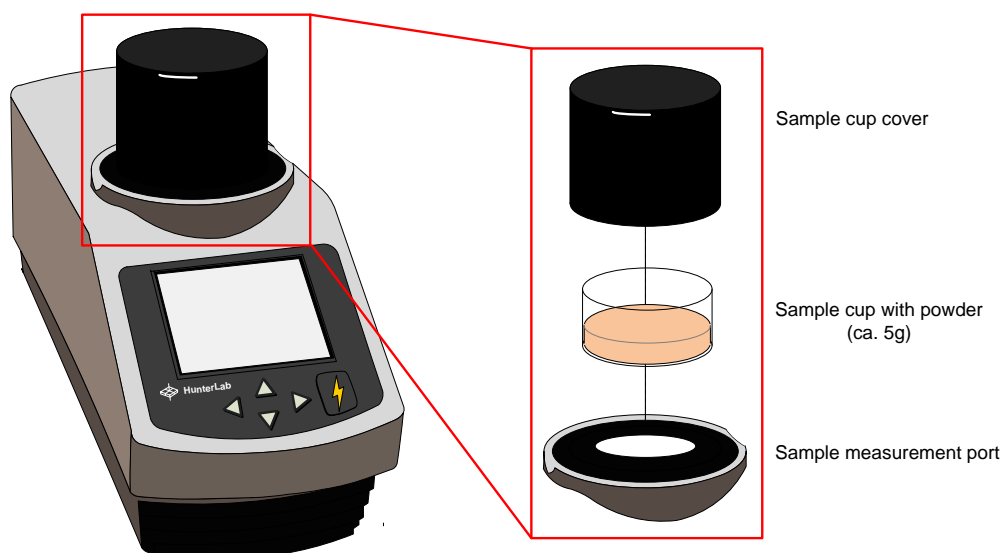


Figure 3.10: Hunterlab colourimeter and schematic of powder loading and sampling.

Several key properties of the spectrophotometer are highlighted in Table 3.3. In the spectrophotometer, colour samples are evaluated in almost the same way as in visual evaluation by excluding gloss effects (Völz *et al.*, 2006).

Samples of each powder blend were taken at set time intervals of mixing in each mixing system and recorded using a large transparent sampling cup (approx. 6 cm in diameter and 3.5 cm high). The collected powder was tapped to ensure that the surface created was as even as possible. Average values were recorded from four readings taken through 90° rotations of the sampling cup over the measurement port. Powder samples were returned to the bulk blend after measurement.

Table 3.3: Key properties of ColorFlex EZ 45/0 colourimeter (Hunterlab, 2014)

Measurement Principle	Port up and port forward dual-beam spectrophotometer
Geometry	45° illumination / 0° viewing
Port diameter	31.8 mm illuminated
View diameter	25.4 mm measured
Spectral range	400-700 nm
Spectral resolution	<3 nm
Light source	Pulsed Xenon Lamp
Flashes per measurement	1
Colourimetric repeatability	$\Delta E^* \leq 0.05$ CIE L*a*b* on white tile
Illuminant used	D65
Calibration method	Calibrated instrument white and black tiles

For all mixers, small samples (approx. 5 g) of the blends were sampled as a function of mixing time and the colour of the blends analysed. Climate factors (temperature, relative humidity) were recorded for each experiment and relative humidity (RH) was kept within the acceptable range of 35-60% (which mitigates against electrostatic and particle autoadhesion effects (*Bridson et al., 2007, Podczeck et al., 1997, Podczeck et al., 1996*)). Un-pigmented lactose was used as a 'control' reference for each formulation prior to analysis, and sample measurements were compared to these to give relative values in the CIECLH colour space.

### 3.2.3 First principle changes in CIE (1976) colour space during blending

The dispersion and de-agglomeration of tracer affect the CIE colour space differently, with dispersion affecting the hue intensity ( $C^*$ ) and de-agglomeration affecting the hue ( $h$ ) independently. Both however affect the blend lightness ( $L^*$ ), and in contradictory manners. This section outlines the proposed shifts in the CIE colour space resulting from the dispersion and de-agglomeration of tracer and their anticipated effects on blend lightness. The shape of 'blend curves', which are assembled from tracer blend data over the course of mixing, are also discussed.

#### 3.2.3.1 Colour change from tracer dispersion

As the iron oxide tracer disperses throughout the white lactose it retains its hue (i.e. level of red) but the blend increases in hue intensity ( $C^*$ ) and decreases in lightness ( $L^*$ ) (i.e. the blend becomes a darker red colour as white surfaces are covered) (*Figure 3.11*).

As shown in *Figure 3.6*, the tracer can be in the form of primary particles, agglomerates, small aggregates and large aggregates. As a change in hue is only associated with the isolation of primary particles, a change in hue intensity ( $C^*$ ) alone implies that the iron oxide has retained its *total* amount of agglomerates and aggregates before and after migration within the lactose matrix. In a low-intensity real mixing system, it is anticipated that the weak forces that hold large aggregates together are overcome by the bulk motion of the blend and are reduced to agglomerates and small aggregates, but are not strong enough to cause substantial de-agglomeration of the tracer. This

effect of mixing is not expected to affect the hue and does not affect meaningful interpretation of the change in hue.

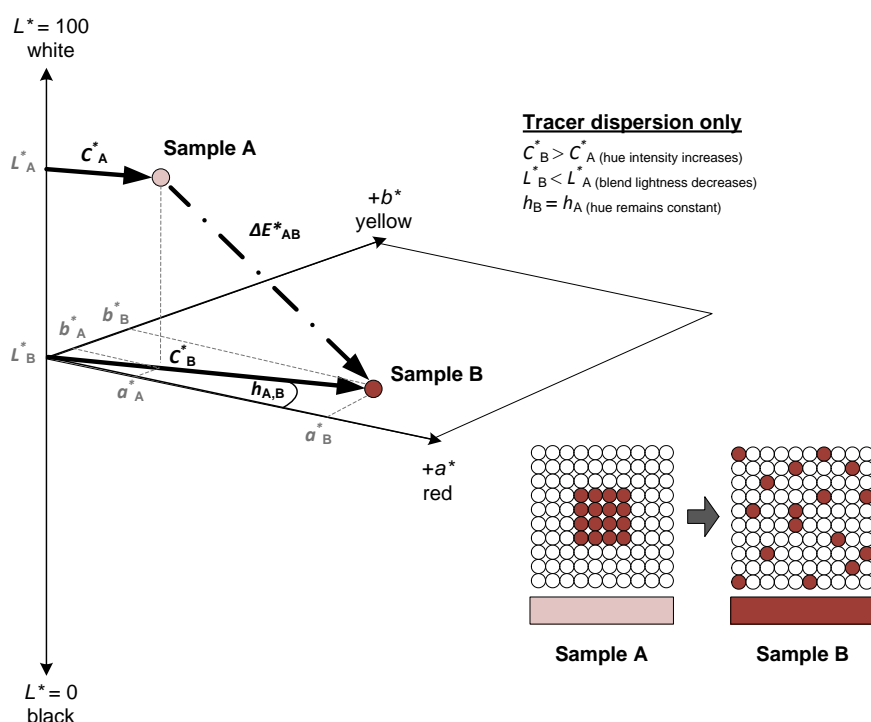


Figure 3.11: Shift in CIE colour space due to tracer dispersion. As the tracer spreads throughout the lactose bulk the hue does not change, but the intensity of the hue increases and blend lightness decreases. Colour changes from light pink (Sample A) to dark red (Sample B).

### 3.2.3.2 Colour change from tracer de-agglomeration

As the tracer breaks up within the lactose the blend hue ( $h$ ) increases (Figure 3.12). As the tracer is mixed in a sufficiently intense process, the population of agglomerates and ultimately primary particles increases, thereby increasing the 'yellowness' of the blend. In a pure de-agglomeration process with no dispersion it would be expected that there would be no change in the colour intensity ( $C^*$ ) but there would be an increase in the hue angle ( $h$ ) and the lightness ( $L^*$ ) of the powder. At the concentrations of tracer in lactose typically used in this thesis there is insufficient tracer to fully coat each lactose particle. Such a system is referred to as a *mass tone* (Völz et al., 2006), where the tracer is applied as a layer and does not hide the substrate (i.e. lactose) completely. Because there is no competition between particles for substrate surfaces, the lactose also creates a

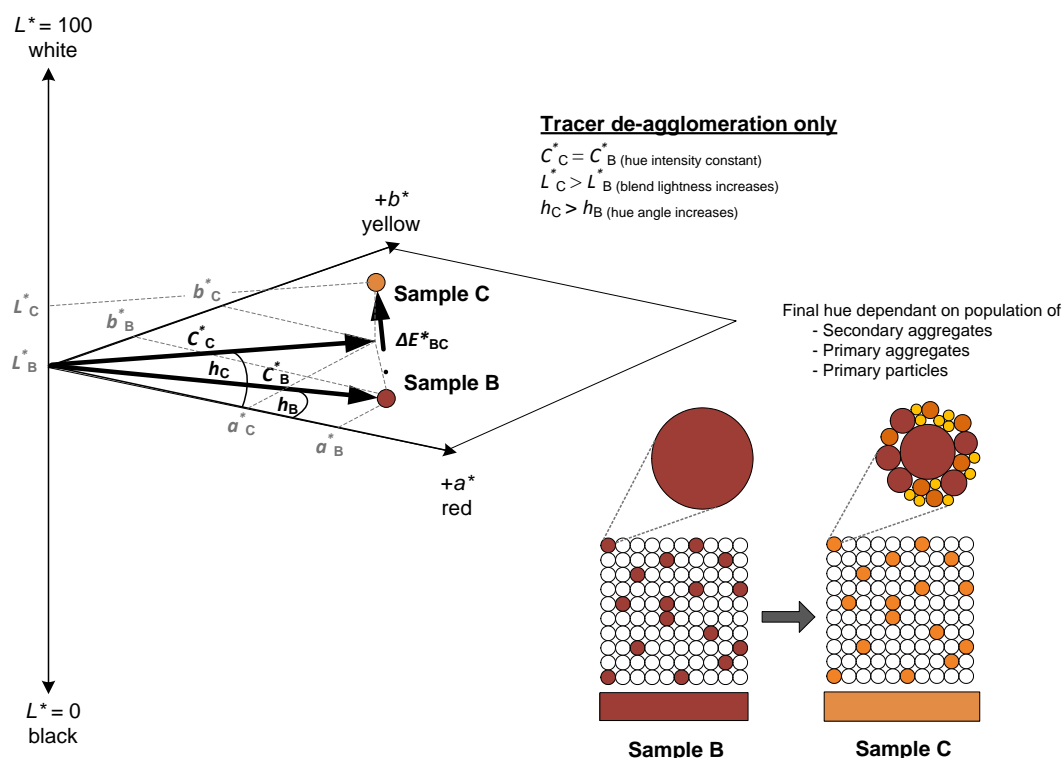


Figure 3.12: Shift in CIE colour space due to tracer de-agglomeration. As the iron oxide (red) tracer de-agglomerates in the lactose matrix (without dispersion), the hue of the sample changes from red (Sample B) to orange (Sample C). In doing so the hue angle and blend lightness increase, but the hue intensity is theorised to remain constant.

matrix in which the de-agglomeration of tracer is irreversible and highly stable. Because of this it is expected that blends retain their initially recorded colour indefinitely and can be remeasured at a later date. This stable structure is known as an ‘ordered mixture’ (Section 2.3.1) and is well known in the pharmaceutical and toner industries.

### 3.2.4 Colour space considerations for particle damage and unintentional milling

For extremely intense mixing it is expected that the milling of lactose particles may occur. In such a system, sufficient energy is applied to the blend to guarantee that the tracer is well dispersed and highly de-agglomerated, however it is also intense enough to fracture lactose particles. As fresh lactose surfaces are produced during fracture, the whiteness of the blend increases, thereby increasing the blend lightness ( $L^*$ ) and decreasing hue intensity ( $C^*$ ) whilst retaining hue ( $h$ ) (Figure 3.13).

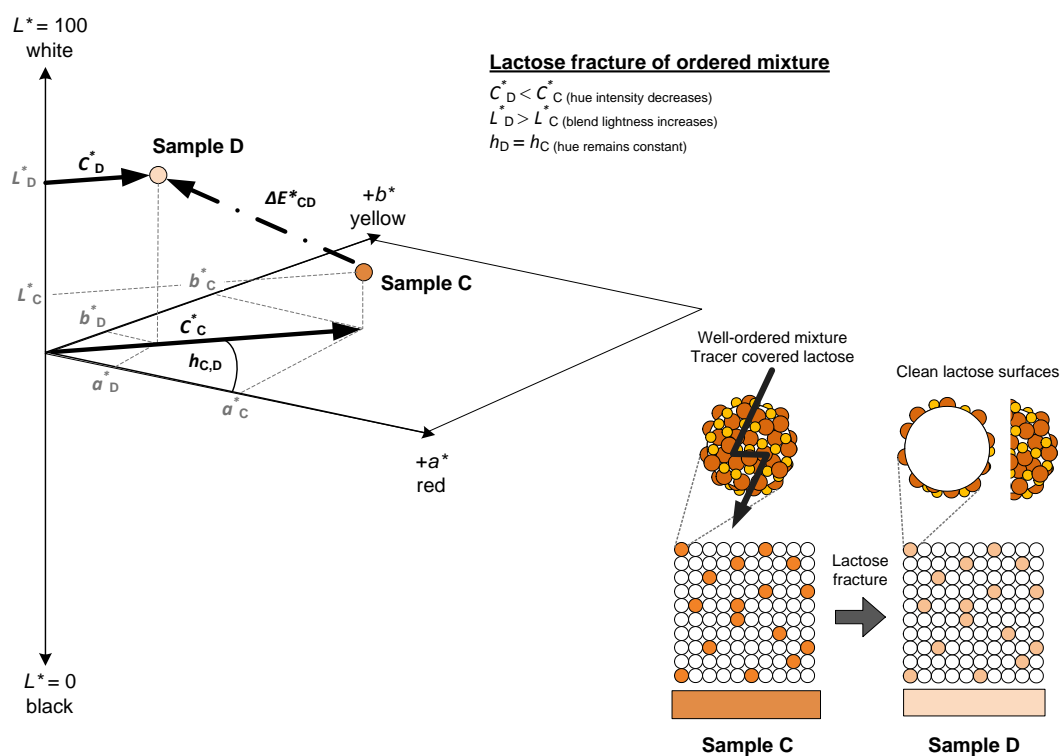


Figure 3.13: Shift in CIE colour space from excipient milling when there is sufficient process intensity to fracture well coated lactose particles, exposing clean white surfaces. Fracture of coated lactose particles would result in an increase blend lightness and decrease in the hue saturation at constant hue (Sample D).

In essence, the changes seen in the processes are the opposite of those observed during tracer dispersion. Whilst not included in Figure 3.13, such shifts in the CIE colour space may also occur with intense localised mixing, where a large level of tracer de-agglomeration occurs with little dispersion. Detection of this phenomenon however is beyond the scope of this thesis.

### 3.2.5 Formulation curves

In a real mixing process, it is expected that both dispersion and de-agglomeration of tracer occur. Initially, energy applied to the blend would be transferred to the dispersion of tracer. Once the tracer agglomerates and aggregates are fully dispersed, and sufficient intensity exists in the system (i.e. rate of energy input, power) to overcome the inter-particle forces between primary tracer particles, de-agglomeration is anticipated to occur. During de-agglomeration of tracer there is inherent further dispersion as the primary particles are spread over the substrate surface (Figure 3.14).

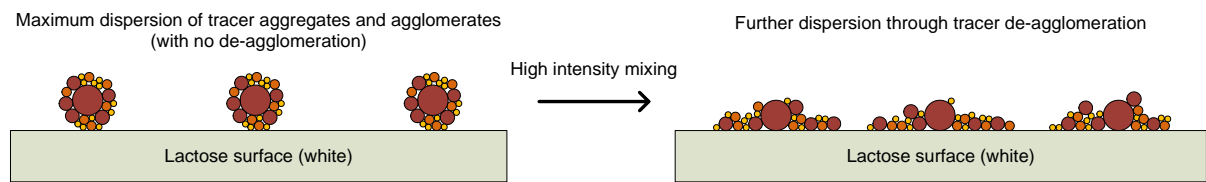


Figure 3.14: Predicted behaviour of tracer clumps on lactose surfaces showing further dispersion of tracer from its de-agglomeration under high intensity mixing.

In an ideal dispersion-only system, measurement of the blend over increasing mixing time would generate a straight line in the CIE colour space with decreasing  $L^*$ , increasing  $C^*$  and constant  $h$  (Figure 3.15).

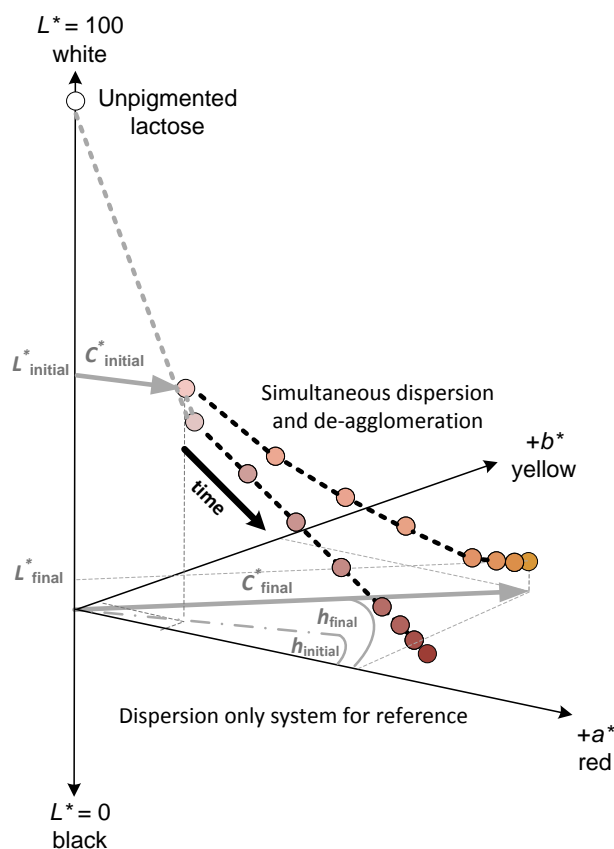


Figure 3.15: Expected shape of blend colour curves as a blend’s colour values are measured over time for a dispersion-only system, and a system in which simultaneous dispersion and de-agglomeration occurs.

In a realistic system however where both dispersion and de-agglomeration of tracer are occurring simultaneously, a curve is generated in the colour space over time with increasing  $h$ . With simultaneous dispersion and de-agglomeration of tracer the blend lightness ( $L^*$ ) is expected to remain fairly constant due to its simultaneous increase and decrease. A realistic curve is expected to

therefore have a straight region for low mixing times when tracer is initially dispersed, which then curls in the  $C^*-h$  plane with fairly constant  $L^*$ .

### 3.2.6 Benefits of tracer method and outline of studies

Generating colour curves with this method for different mixing systems and operating conditions can give insight into the behaviour of different mixers and enable prediction of the best operating conditions. To give a broad validation to the industrial use of colour tracers for process optimisation, the experimental studies in this thesis depict its use in:

- Assessing the behaviour of different mixing systems and operating conditions and predicting process end-points and equivalent mixing between systems (*Chapter 4*).
- Determining the robustness of method in regards to tracer concentration (*Chapter 5*).
- Measuring the content uniformity of a mixture and linking the colour changes to energy input and powder flows within the mixer (*Chapter 6*).
- Detecting and quantifying unintentional milling during mixing (*Chapter 7*).

Finally, a step-by-step method is proposed for its industrial use (*Chapter 8*). It is hoped that the use of the iron oxide tracer can quickly and simply determine best operating conditions in the scale-up or blend optimisation of pharmaceutical DPI formulation manufacturing.

### 3.2.7 Comments on comparing tracer blends to drug blending

A number of questions arise in regards to the robustness, suitability and significance of the use of iron oxide as an analytical tool for powder blending. Of particular interest are the ability of the tracer to predict the blending of a real drug formulation and the reproducibility and reliability of colour data collected. It is important to note that the agglomerate strength and cohesion/adhesion properties of the tracer will not match those of any particular drug. For the purposes of this new approach it is important to appreciate that the properties of the tracer are not intended to match those of any drug.

The method outlined in this work does not provide direct information about how any specific drug would spread and de-agglomerate in a mixing system. Instead the approach is proposed to be used as a cost and time effective preliminary tool for showing equivalent blending conditions between two or more systems, or in enabling process optimisation. In addition the flow and flow modifying behaviour of the tracer blend is almost certainly different to that of any drug blend due to the different adhesion/cohesion properties of the tracer and APIs. Also, the tracer used in these studies is spherical and smaller in equivalent diameter than DPI drugs; which are often acicular, shard-like or plate-like due to their crystal habit as well as pre-blending micronisation (*Section 2.1.1*).

The studies described in this work are based on a pre-manufacturing process, in which the mechanics of the *bulk excipient* are assessed in a quick and simple manner. It is not intended in these works for the tracer to be included in future drug blends to assess the quality of each batch. Such a system would create a multitude of complexities to formulation, with the tracer having a potential influence on drug delivery and blending, as well as the associated regulatory concerns and revisions with altering the formulation. It should also be stressed that this method is a bulk analysis method. The scale of scrutiny in this method is not of the order of a pharmaceutical dose (i.e. milligrams) but considerably larger (i.e. in the order of ~5 grams). In addition, the method does not indicate whether tracer has coated the fine or coarse lactose in a given sample, which for a drug in a DPI formulation dictates the inhalation performance. These factors make the use of a colour tracer a preliminary method for process benchmarking, optimisation, scale-up and transfer. Hence it may have significant value in reducing time and costs in process development. Ideally, pre-manufacturing colour data would be coupled with drug blend data under the same mixing conditions and compared to enable educated estimates of drug performance for a certain colour blend, particularly where specific powder structures are desired. This method provides an excellent tool by which many different properties of a given mixer type and set of operating conditions can be quickly and simply assessed. It also allows for rapid identification of potential heel residue, and dead-zones in a blender, which are very significant causes of batch failures.

### **3.3 Concluding remarks on tracer**

A novel and robust method of assessing the characteristics and behaviour of various blending systems is proposed through use of a colour tracer. As the tracer is blended it can undergo two different types of colour change, either increasing in intensity (from pink to red), or changing hue (from red to orange). These changes can be quantitatively measured in the CIECLH colour space and used to characterise and compare blends, as well as identify specific stages in blend progression.





## Analysis and control of dry powder mixing using a coloured tracer

**T**he current means in industry of selecting the best operating conditions and appropriate mixers for the manufacturing of pharmaceutical dry powders relies largely on the use of empirical trial-and-error approaches. The inherent flaws in this approach create very challenging and costly issues. In this chapter, the viability of the iron oxide tracer (specified in Chapter 3) to assess and compare the extent of blending between different operating conditions and mixers is investigated. Using a series of predominantly inhalation grade lactose blends, formulation-specific colour curves are generated which are able to clearly distinguish and group mixers into low and high intensity given their range of values along the curve. These initial results suggest that the iron oxide tracer method could provide the basis for a more robust new quantitative approach to blend optimisation, the production of equivalent blends between mixer types, scales and operating condition. It may also be able to identify specific phases during process evolution such as milling during powder blending and so be used for blend optimisation.

## 4.1 Introduction

As discussed in Chapter 2, obtaining a homogenous pharmaceutical blend or ensuring blend equivalence in process scale-up and technology transfer is a very challenging task, particularly for pharmaceutical formulations where the scale of scrutiny is very small. Traditional methods for determination of the best mixing conditions in a given vessel, including fill height, operating speed and mixing time is a purely trial-and-error approach and can be a time and financially costly process for industry. It would therefore be beneficial for such industry needs to gain a better quantitative understanding of the influence of operating conditions on powder mixing in different mixing processes. This would allow for better predictions about the extent of mixing (both required intensity and mixing time) and shift determination of the best operating conditions from the traditional haphazard trial-and-error approach to a more holistic and accurate process that can improve blend homogeneity and other desirable blend properties, and also has flexibility to be applied to a variety of situations rather than being product specific. It may also assist in scale-up and transfer between blender types.

The use of the coloured tracer specified in Chapter 3 as a preliminary testing method, and when used without the presence of pharmaceutical active, may hold benefits in allowing an entire blend to be quickly and simply analysed through the blend's colour change as the level of mixing increases. The multi-dimensional colour change of the hematite tracer may also provide key information on mixing mechanisms such as the extent of de-agglomeration and dispersion, and serve as a more rigorous analytical method to those discussed in Section 2.2.

## 4.2 Materials and Method

Two main experimental sets were constructed for this general viability study; a comparison of formulations between different mixer designs, and a comparison of operating conditions for a given formulation in selected mixers.

Many of the materials and mixers outlined in this chapter are general across all other studies. For this reason, detailed descriptions of each material and mixer are provided to allow for cross referencing in subsequent chapters.

#### 4.2.1 Powder selection and properties

The **standard tracer concentration** across all studies in this thesis is 1 weight percent (wt%), which was selected based on obtaining good colour change information across a wide range of powders and operating conditions. Justifications for this concentration are outlined in Chapter 5. The **standard lactose** used in this thesis is Lactohale LH200, which was selected based on its commercial availability and model broad (bimodal) size distribution. This is often employed in DPI formulations and so allows for the analysis of general DPI powder blending behaviour. All lactoses were sourced from DFE-Pharma, Germany.

In this study, the standard lactose was complimented by a series of other lactose and lactose blends which varied in size distribution (*Figure 4.1*). Two inhalation grade lactose blends with different levels of fine material and cohesivity were made from the combination of commercial coarse-fraction lactose (Respitose SV003) and fine lactose (either Pharmatose 450M or Lactohale LH230). In addition to the inhalation grade formulations, a sieved lactose (Pharmatose 200M) was added to generalise the study (and extend it to non-inhalation pharmaceutical formulations).

For simplicity each lactose is numbered from “*Lactose 1*” through to “*Lactose 4*” in order of increasing ultrafines and fines content (i.e. particles less than 4 and 15  $\mu\text{m}$  respectively) as shown in Table 4.1. Formulation 5, which was blended in large scale mixers (i.e. > 25 litres), uses Lactose 1 at a lower than standard concentration of tracer (0.3 wt%) due to limitations in tracer availability. Particle size distributions in this study were collected using dry powder laser diffraction (*Malvern Mastersizer Scirocco 2000, Malvern Instruments Ltd, UK*) at a dispersion pressure of 3.2 bar (which allowed for good particle dispersion without particle attrition).

A full range of lactose and lactose blend properties across all studies in this thesis can be found in Chapter 8.

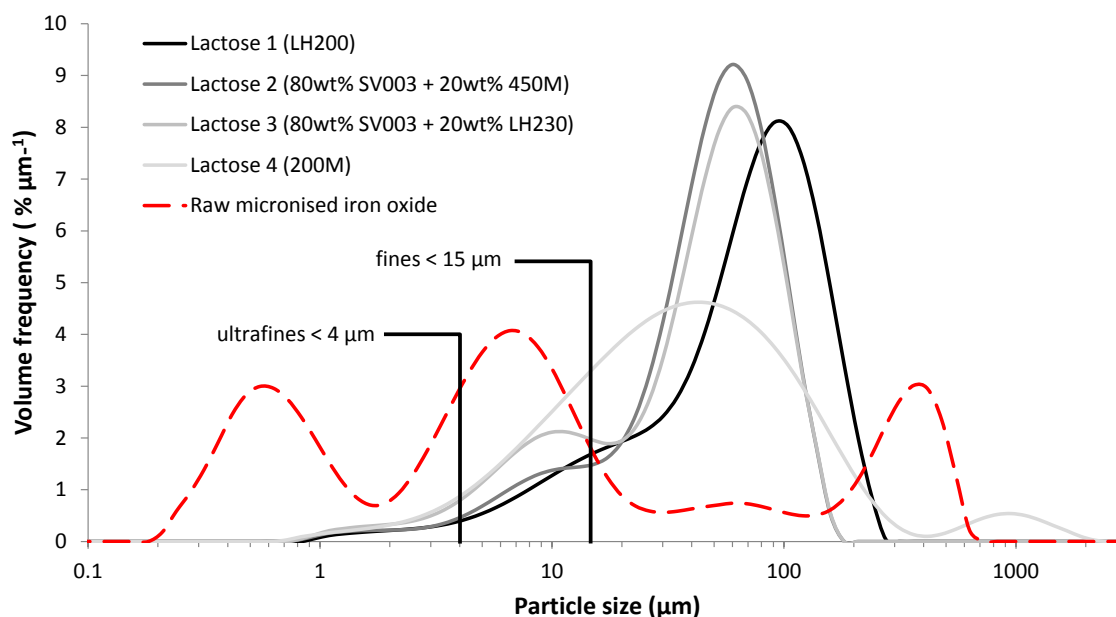


Figure 4.1: Particle size distributions of lactose mixtures used in this study (*Malvern Mastersizer Scirocco 2000, Malvern Instruments Ltd, UK*). Lactoses are numbered in order of increasing ultrafines and fines (i.e. particles less than 4 or 15  $\mu\text{m}$  respectively, *Table 4.1*). Size ranges of tracer agglomerates and aggregates are also shown for comparison.

Table 4.1: Volume percentage of fine (<15  $\mu\text{m}$ ) and ultrafine (<4  $\mu\text{m}$ ) lactose particles for each lactose blend. (*Malvern Mastersizer Scirocco 2000, Malvern Instruments Ltd, UK*). Formulations were observed to have the same particle size distribution as the lactose grades without tracer, given the very low concentration of tracer used by volume.

Formulation #	Tracer concentration	Lactose Grade	vol.% < 4 $\mu\text{m}$	vol.% < 15 $\mu\text{m}$
1	1 wt%	Lactose 1 (LH200)	2.4%	12.8%
2	1 wt%	Lactose 2 (80wt% SV003 + 20wt% 450M)	2.6%	13.9%
3	1 wt%	Lactose 3 (80wt% SV003 + 20wt% LH230)	4.1%	21.3%
4	1 wt%	Lactose 4 (200M)	4.2%	25.4%
5	0.3 wt%	Lactose 1 (LH200)	2.4%	12.8%

#### 4.2.2 Mixers and experimental scheme

Tracer blends were mixed in three different mixer types, a low intensity tumbling mixer (0.3L, *Turbula T2F, Willy A. Bachofen, Switzerland*), a vertical-axis high-shear mixer (KG5, *Key International, U.S.A.*) with two bowl sizes (1-litre and 5-litres) and a modified ultra-high shear mechanofusion mixer (AMS-MINI, *Hosokawa Micron Ltd., Japan*). General mixing principles for each of these mixer types can be found in Section 2.2.3.

The tumbler mixer used in this study has two arms which rotate and invert a small cylindrical drum of powder (0.3 litres) in a “figure-eight” motion to enhance overall mixing and minimise the formation of dead zones in the powder (Figure 4.2). The rotation speed can be varied between 34 and 101 rpm.



Figure 4.2: Turbula T2F tumbler (Willy A. Bachofen, Switzerland). Rotating arms hold each end of the drum with one arm (shown with red pin) mechanically driven. When operating drum is inverted and rotated in a “figure-eight” motion.

The vertical-axis high-shear mixer (HSM) in this study uses a three blade impeller at a variety of rotation speeds (with the aid of a variable speed drive) to impart shear on the powder and induce different types of powder flow within the mixer (Figure 4.3). Speeds were varied between 100 and 450 rpm, and discussion on powder flow regimes in high-shear mixers can be found in Chapter 6.



Figure 4.3: KG5 Laboratory scale mixer (Key International, U.S.A.). Mixer contains a variable speed motor with touch screen interface (a) and a standard 3-bladed inclined impeller within mixing bowl (b).

The ultra-high shear mechanofusion process used in this thesis is different to traditional mechanofusion processes (Section 2.2.3). A Nobilta configuration was employed (Hosokawa Micron Ltd.) which is not dissimilar to a standard high-shear impeller mixer (Figure 4.4). The key difference is that the mechanofusion impeller rotates at up to 3000 rpm, which is significantly faster than a high-shear mixer. The impeller compresses and shears powder in the 1 mm gap between the impeller and mixer walls in a similar manner to other mechanofusion systems. During operation powder is forced to the walls of the mixer where it is compressed and sheared, and is also lifted from the walls through the oscillating pathway of the bulk powder and under the impeller blades.

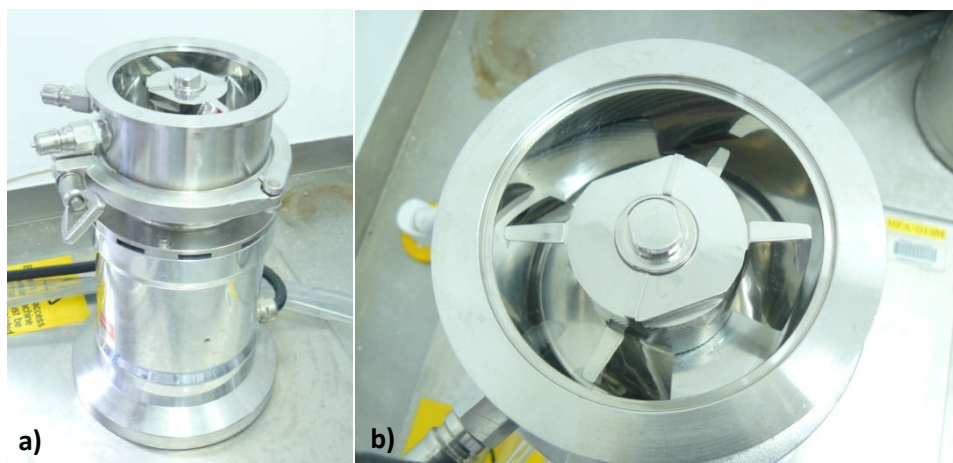


Figure 4.4: Modified mechanofusion mill (AMS-MINI) developed by Hosokawa Micron Corp. Images show a) electric motor with exposed mixing chamber and b) close-up of impeller in mixing chamber.

Using these three mixer types, a set of 36 blending experiments was created using the four lactose types at a variety of operating conditions and scale (Table 4.2).

Standard lactose and tracer concentrations were used in all mixer types, scales and operating conditions to assess the tracer method's sensitivity and viability. Other lactose blends were manufactured at a single operating condition in a particular mixing system (often at best mixing) to observe the effect of varying the level of fines on colour changes. Additional experiments were conducted at 3000 rpm in the mechanofusion mixer to observe the effect of milling during blending. In addition, a fifth formulation comprising of 0.3 wt% tracer in LH200 was used with a series of industrial-scale vertical-axis high-shear mixers (25-litre mixer at 600 rpm, (T.K. Fielder TRV25,

Table 4.2: Blending experiments conducted using different types of lactose, mixers and processing conditions.

Experiments conducted		Formulation 1 LH200	Formulation 2 SV003 + 450M	Formulation 3 SV003 + LH230	Formulation 4 200M
HSM KG5-1L	100 rpm	✓			
	185 rpm	✓	✓	✓	✓
	300 rpm	✓			
	400 rpm	✓			
HSM KG5-5L	150 rpm	✓			
	235 rpm	✓			✓
	350 rpm	✓			
	450 rpm	✓			
Tumbler Turbula T2	34 rpm	✓	✓		
	49 rpm	✓	✓		
	72 rpm	✓	✓	✓	✓
	101 rpm	✓	✓		
Mechanofusion AMS-MINI	600 rpm	✓	✓	✓	✓
	1000 rpm	✓			
	2000 rpm	✓			
	3000 rpm	✓	✓	✓	✓
‡Industrial-scale HSMs (various scales)	-	✓ (4 blends)			

‡Lower iron oxide concentration (0.3 wt%) compared to standard concentration (1.0 wt%). Labelled as Formulation 5.

Table 4.3: Scale and simple dimensions of mixers used in this study.

Formulations	Ref#	Mixer	Mixer type	Mixer scale (vol, L)	Mixer fill (kg)	Mixer vessel dimensions (m)		
						A	B	C
Formulations 1-4	1)	Turbula T2F	Figure-eight tumbler	0.3	0.05	0.06	0.12	-
	2)	Key International KG5 1L	High shear mixer	1	0.3	0.14	0.035	0.08
	3)	Key International KG5 5L	High shear mixer	5	1.5	0.205	0.05	0.12
	4)	Hosokawa AMS-MINI	Mechanofusion	0.1	0.03	0.1	0.1	0.05
Formulation 5	5)	T.K. Fielder TRV25	High shear mixer	25	12	0.325	0.125	0.31
	6)	T.K. Fielder PMA65	High shear mixer	65	30	0.51	0.105	0.32
	7)	Diosna P100	High shear mixer	100	65	0.7	0.085	0.4

Aeromatic-Fielder, Switzerland), 65-litre mixer at 200 and 400 rpm (Fielder PMA65C, Aeromatic-Fielder, Switzerland) and a 100-litre mixer at 200 rpm (Diosna P100, Diosna, Germany)). Simple scales and mixer dimensions are included in Table 4.3.

All blends in this study were manufactured within a 35% to 60% relative humidity range. Colour data was collected as specified in Section 3.2.2 using the standard time points up to 60 min. Blend samples were returned to the bulk after measurement.

### 4.3 Results

When the CIELCH values for all blends are compiled, they form a series of colour curves, which overlap and conform for a given formulation, regardless of the mixer used, process scale or operating conditions. These overlapping ‘blend curves’ create a series of ‘formulation curves’. An example of this overlapping is shown for Formulation 1 at low values of  $C^*$  and  $h$  in the  $C^*$ - $h$  plane (Figure 4.5).

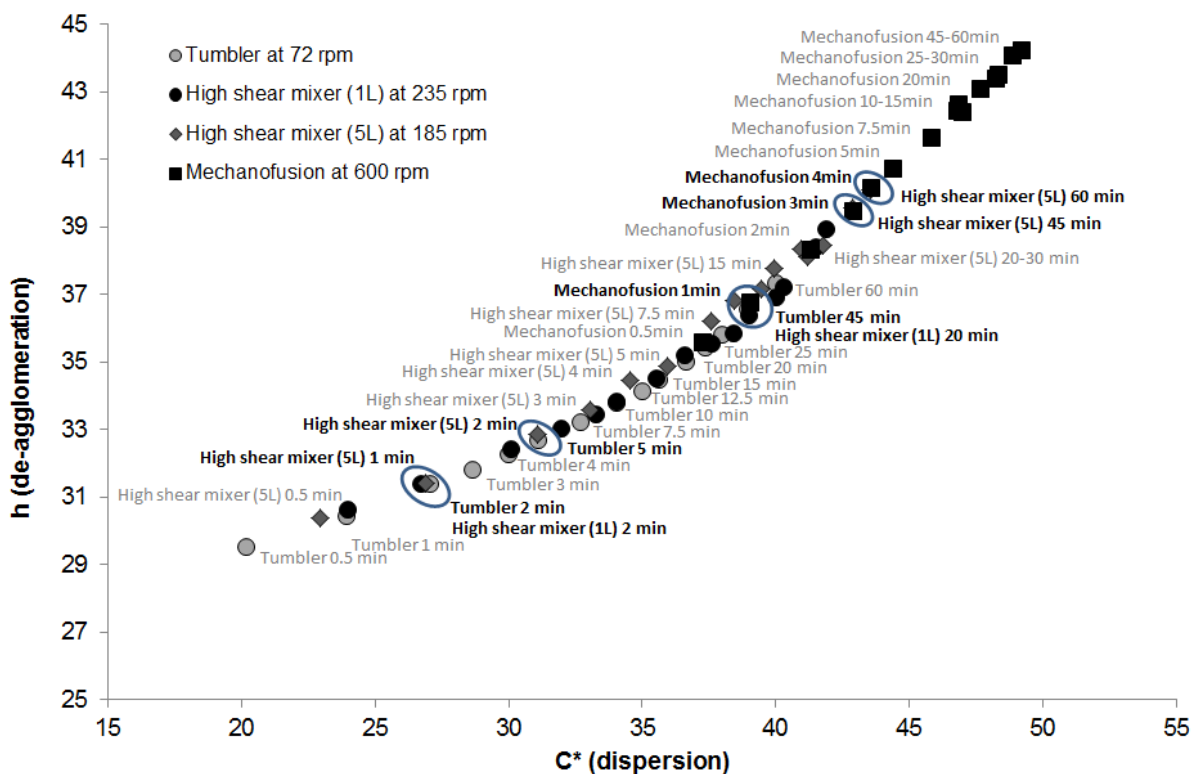


Figure 4.5: Section of the colour curve for Formulation 1 in the  $C^*$ - $h$  plane showing the overlap of blend curves in different mixers and scales.

Whilst blend curves overlap onto a single formulation curve, the points at which they start and finish depend on the process and process intensity. As blend curves for different mixers often partially overlap along the formulation curve, points at which colour data points align are often easy to collect. The circled points indicate that blend equivalence is achievable. For instance, the circle at lowest  $C^*$  shows the blend colour achieved in a 5L high-shear mixer after 1 minute of mixing at 185 rpm can also be achieved in a 1L high-shear mixer after 2 minutes of mixing at 235rpm, or by using a tumbling mixer for 2 minutes at 72 rpm.

Whilst blend curves all overlap with one another for a given formulation, different formulations can be seen to create separate formulation curves in the CIELCH colour space (Figure 4.6).

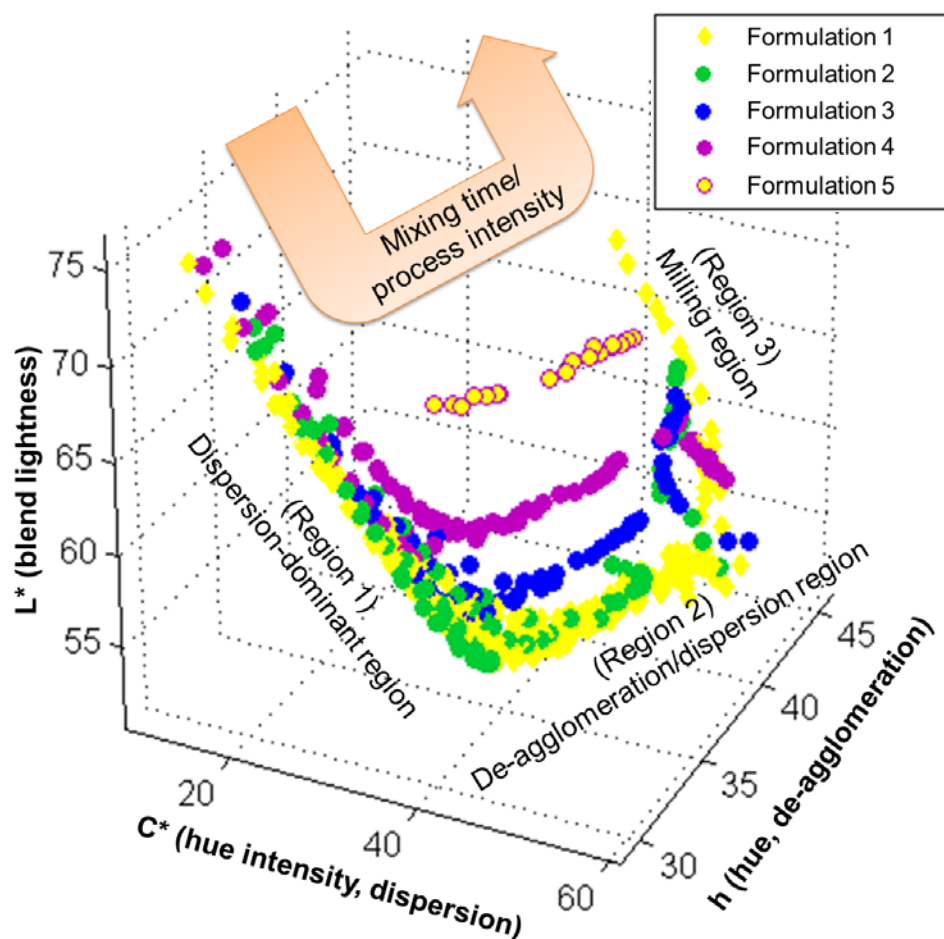


Figure 4.6: Colour curves generated for each formulation in the CIELCH colour space.

Formulation curves appear to follow the same line in the CIECLH colour space at low levels of  $C^*$  and  $h$ , and separate from each other as  $C^*$  and  $h$  increase. With constant tracer concentration, the values at which a formulation curve is likely to deviate from the others depends on the level of fine material (in this case lactose). Increased levels of fines create a deviation from the other process curves at lower values of  $C^*$  and  $h$ . Tracer concentration also appears to affect the nature of the process curves generated, with weaker concentrations of tracer in the same lactose type generating a curve with the same shape in the  $L^*C^*h$  colour space, but at a higher blend lightness. Formulation curves are therefore sensitive to both the type of lactose used and the concentration of tracer.

From the colour curves three clear regions of tracer mixing can be identified (*Figure 4.6*):

*Region 1: Dispersion-dominant mixing*, where tracer spreads throughout the bulk material actioned by bulk motion.

*Region 2: De-agglomeration/dispersion mixing*, where further energy input to the well dispersed blend results in aggregate breakup into agglomerates and primary particles. Further dispersion is seen in this region as the agglomerates are broken up and re-dispersed.

*Region 3: Particle damage/milling*, where energy input is sufficiently high to damage and break large bulk particles, thereby generating more white surfaces and lowering the intensity of colour in the blend (i.e. decreasing  $C^*$ ).

These different regions of mixing can also be seen in a projection on the  $C^*-h$  plane, in which the degrees of tracer dispersion and de-agglomeration can also be simply quantified and compared for all blending systems and formulations (*Figure 4.7*).

As mentioned previously, *Figure 4.7* shows that the blend curves start and finish at different points along a formulation curve based on the mixing time and mixing intensity (i.e. operating speed and mixer type). Blends manufactured in the tumbler sit entirely within the dispersion-dominant region, regardless of mixing speed. High-shear mixer blends appear to be largely within the de-

agglomeration/dispersion region, as with low speed (600 rpm) mechanofusion blends. Higher speed mechanofusion blends (i.e. at speeds greater than 600 rpm) produce colour measurements that fall into the milling region, suggesting that milling or another high intensity powder blending phenomenon is occurring. The observation that blend curves for different mixers occur in different regions of their respective formulation curves is consistent with the theory that the tracer will experience different forces and mixing dynamics within each mixer.

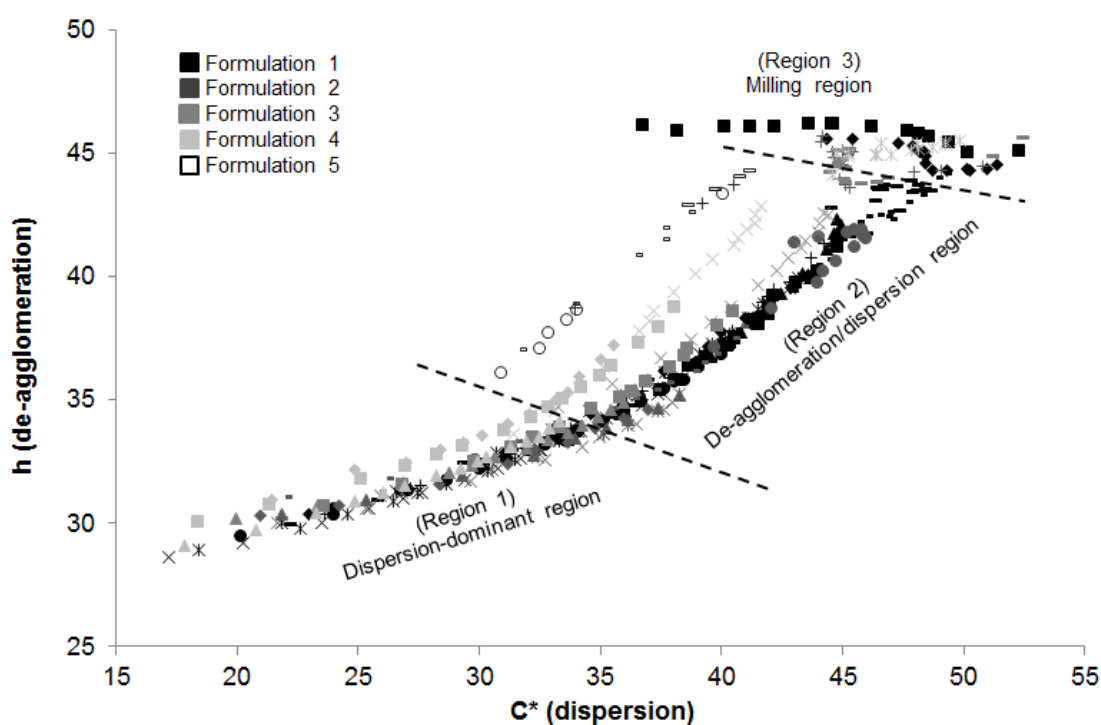


Figure 4.7: Degrees of dispersion ( $C^*$ ) and de-agglomeration ( $h$ ) for all blends tested. Formulations are as shown in legend. Different symbols indicate different mixers and/or operating conditions, and dashed lines show approximate points at which different mixing regions start and finish.

Blend curves overlap with one another for a given formulation in the dispersion-dominant and de-agglomeration/dispersion regions. However, blend curves in the milling region are highly variable, suggesting a fairly stochastic and/or chaotic process in this high-intensity blending/milling region. This may be caused by a competition between lactose milling and tracer re-dispersion/re-agglomeration, as well as effects previously observed in other studies such as tracer particles imbedding into the bulk powder particles (Alonso *et al.*, 1989a). It appears that for blends manufactured in the mechanofusion mixer at 3000 rpm (i.e. in an ultra high-shear environment),

there is an initial and maximum degree of dispersion and de-agglomeration. The values associated with this initial point vary with the level of fines in formulation, with an increase in fines increasing the value of  $L^*$  and decreasing the initial value of  $C^*$  (Figure 4.8). Further discussion of possible mechanisms within the milling region are provided in Section 4.4.1 and Chapter 7.

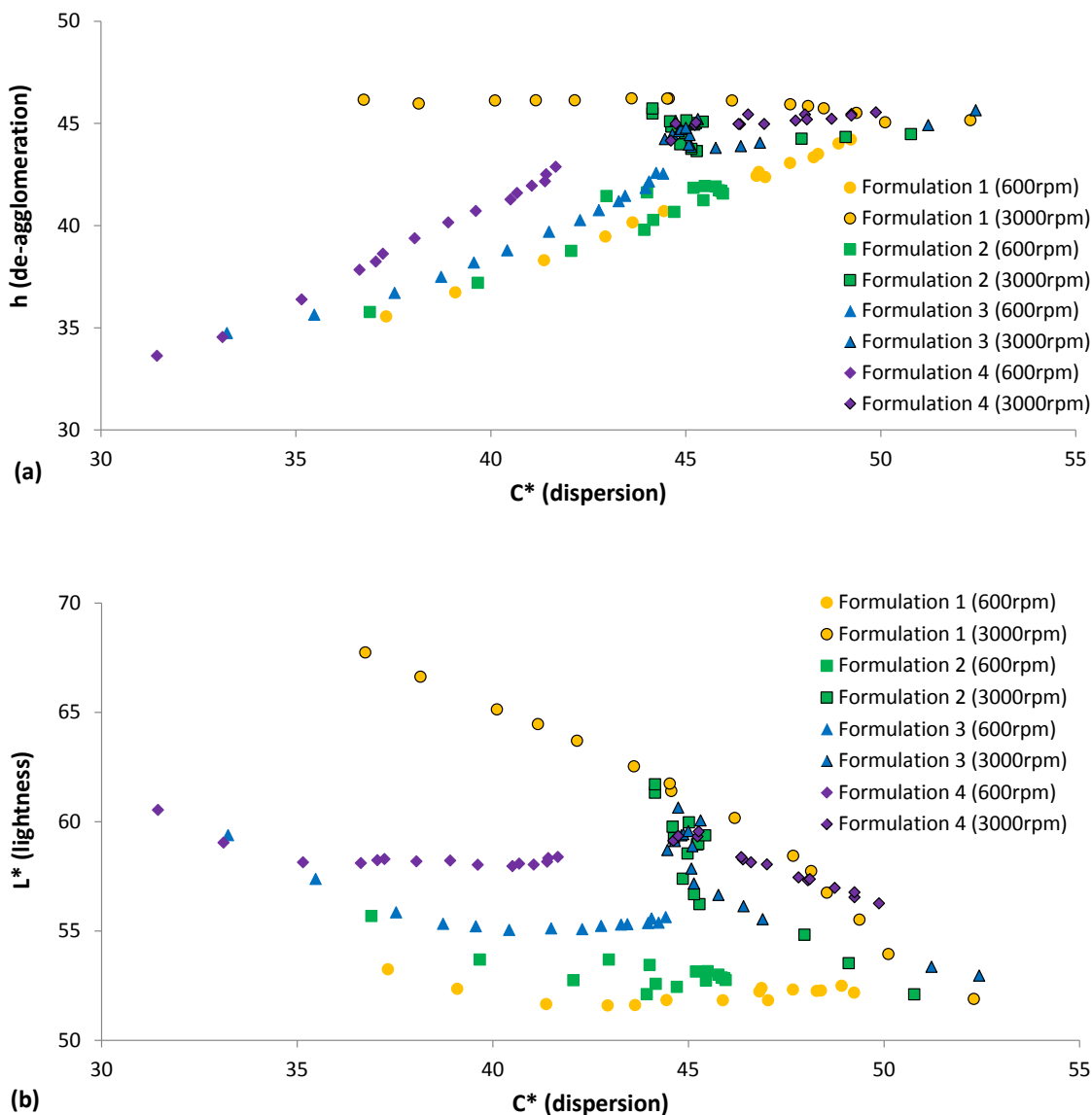


Figure 4.8: Mechanofusion data for each formulation at 600 and 3000rpm in the a)  $C^*$ - $h$  and b)  $L^*$ - $C^*$  planes. Blend curves for a given formulation show no overlap.

As blend hue ( $h$ ) remains fairly constant throughout the milling region (Figure 4.8a), it is proposed that the increase in blend lightness ( $L^*$ ) and decrease in degree of dispersion ( $C^*$ ) (Figure 4.8b) are attributed to the generation of additional white surfaces within the blend. An excess of energy and

power is applied to the blend during high-speed mechanofusion mixing, which is sufficiently high to both entirely disperse and de-agglomerate tracer in a very short period of time, resulting in an initial value at high  $C^*$  and  $h$ . Additional blending appears to result in the fracture of lactose particles, and the generation of further white surfaces which aid in increasing blend lightness and lowering hue saturation ( $C^*$ ). Particle milling was assessed for each formulation using laser diffraction, with the effect of milling most observable in Formulation 1, which had the lowest initial level of fines (*Figure 4.9*).

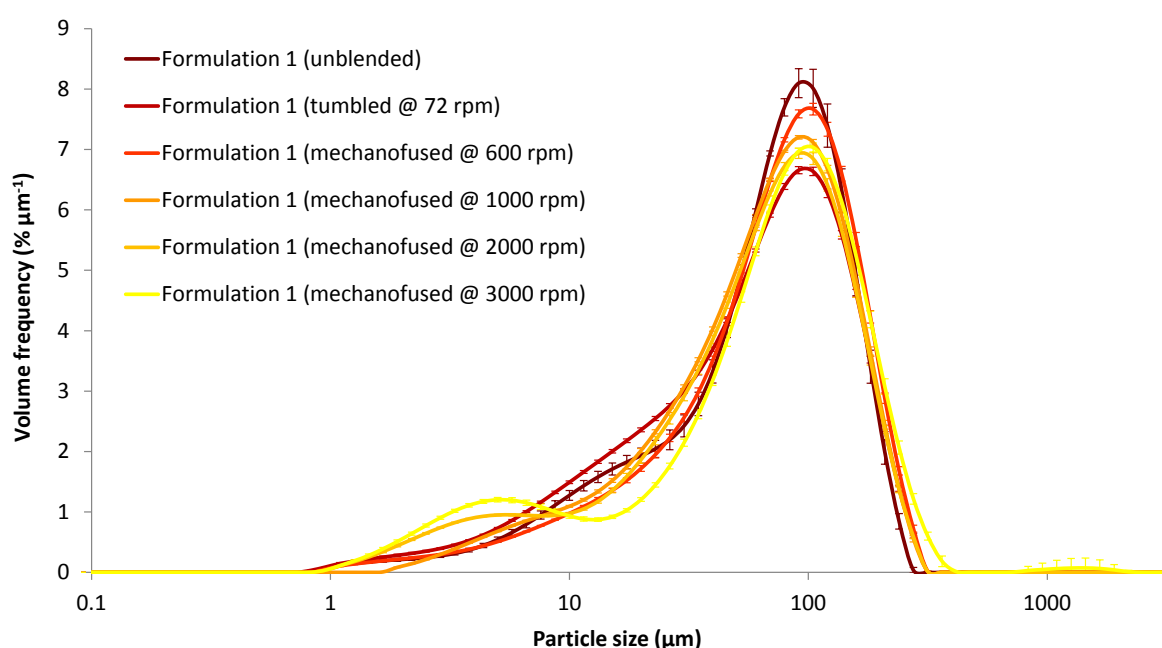


Figure 4.9: Particle size distributions for Lactohale LH200 formulations containing 1 wt% iron oxide tracer (*Formulation 1*) after 60 minutes of mixing. Distributions show a clear generation of fine particles when mechanofused at speeds greater than 1000 rpm.

A clear increase in the volume percentage of fine particles when mechanofused at speeds of 2000 and 3000 rpm indicate that milling of large lactose particles is indeed occurring, and that values along curves within the milling region can be used to provide information about the extent of over-mixing and milling.

In addition to particle size analysis, scanning electron microscopic (SEM) images for several blends were recorded and compared to see if the effects of mixing time and mixer on particle interactions and behaviours could be observed (*Figure 4.10*). No clear change between SEM images is observed

across the conditions shown. This may be a function of image resolution and the practicalities of subjective image analysis on such tracer clumps, and the spread of individual tracer particles on lactose surfaces.

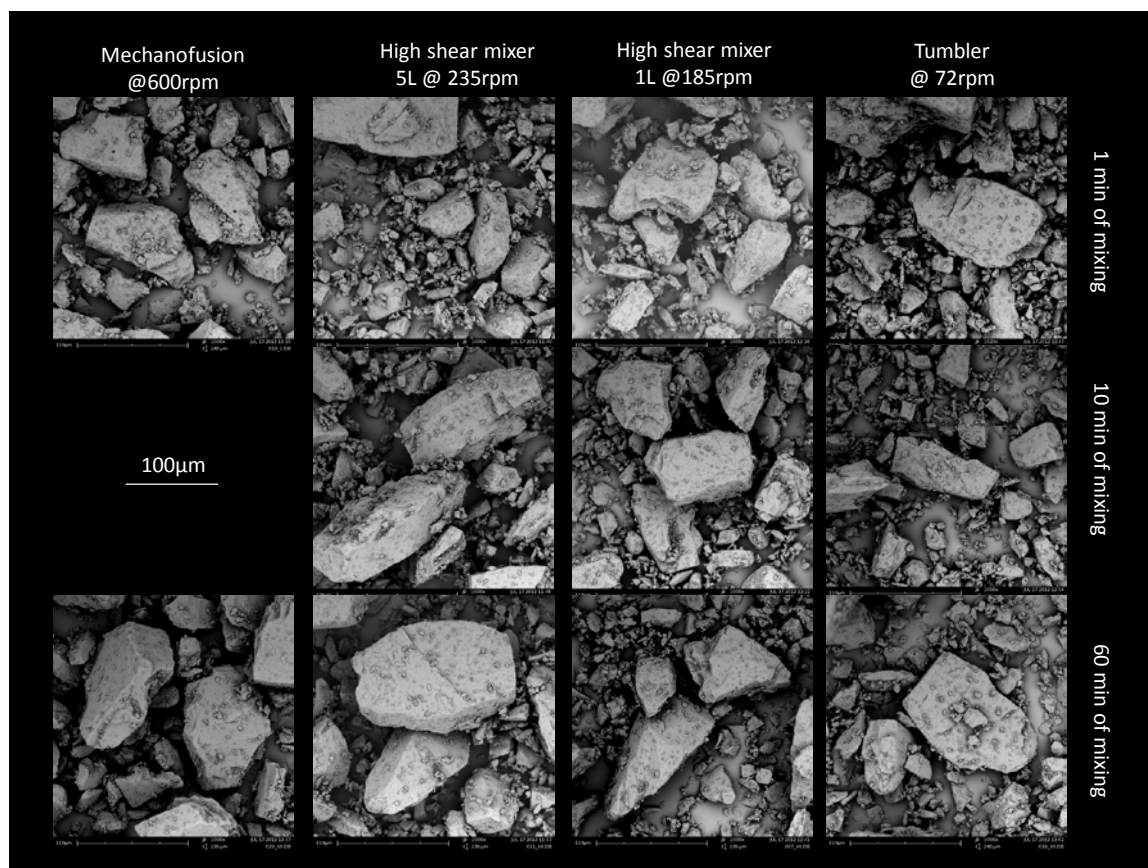


Figure 4.10: Scanning electron microscopy (SEM) images for Formulation 1 blends manufactured in each lab-scale mixer.

#### 4.4 Discussion

Results show promise for the ability of the iron oxide tracer to assess blending in a wide variety of different mixers and mixing conditions. Several aspects to the use of the colour tracer, and colour analysis however require further discussion, including possible mechanisms of tracer coating within each region of the formulation curve, limitations of using a single colour value in blend analysis, the 3-dimensional plane on which all formulation curves appear to align, and the application of the tracer in industrial blend analysis.

#### 4.4.1 Proposed mechanisms

Results from this study agree with previously proposed mechanisms for the coating of large carrier particles with iron oxide (Section 2.4.4). Based on the shape of formulation curves in the CIELCH colour space, the following mechanism is proposed for the progression of powder mixing from unblended to milled material (Figure 4.11):

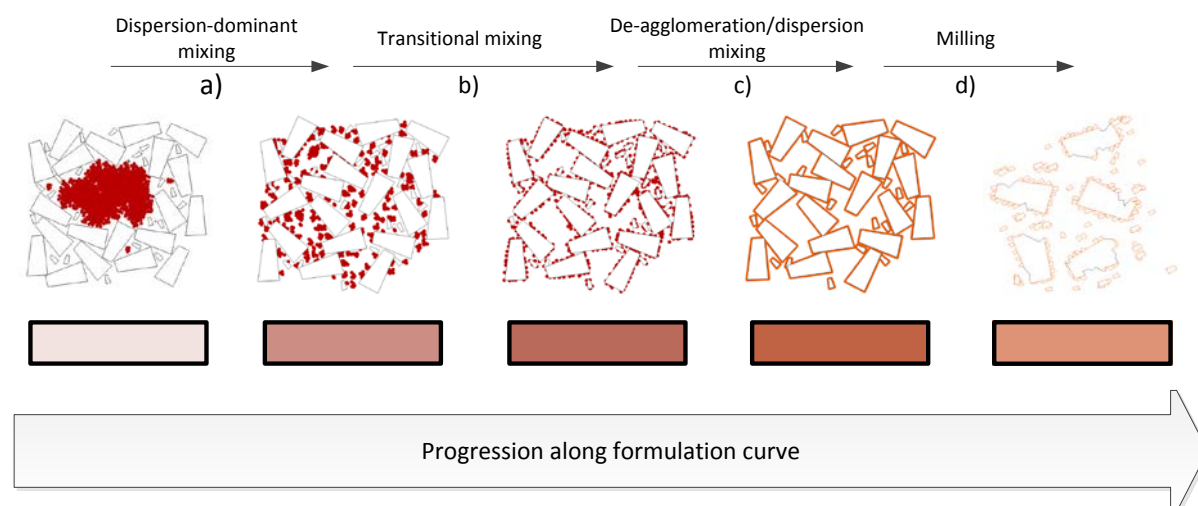


Figure 4.11: Proposed mechanism for the coating of lactose particles by tracer during blend progression from the dispersion-dominant region to the milling region along a given formulation curve. Typical colour swatches for blends in these regions are also provided.

- Dispersion-dominant mixing.* Tracer aggregates and agglomerates disperse through the bulk lactose and adhere to lactose surfaces in their immediate vicinity. De-aggregation also occurs.
- Transitional mixing between dispersion-dominant and de-agglomeration/dispersion mixing.* Inter-particle collisions between lactose particles occur, forcing those with tracer aggregates and agglomerates to share tracer with non-coated particles, inherently causing de-agglomeration. Initially the population of aggregates adhered to the lactose is large and the rate of de-agglomeration is low due to the size-driven preferential de-aggregation of tracer with inter-particle collisions.
- De-agglomeration/dispersion mixing.* As the population of aggregates decreases, the rate of de-agglomeration increases and eventually becomes greater than that of de-aggregation.

Tracer agglomerates are de-agglomerated and dispersed across the surface of carrier particles through friction and collisions between particles.

- d) *Milling*. If there is sufficient intensity in the process to ensure full de-agglomeration of the tracer on the lactose surfaces, lactose particles are also likely to fracture when colliding with one another and the vessel. In this mechanism coated lactose particles are fractured, exposing new uncoated surfaces and lowering the hue intensity. As all tracer particles are already attached to the lactose surfaces, these new surfaces are unlikely to be coated to the same extent as initial ones (*Milling region mechanism*). Based on previous work by Alonso *et al.* (Section 2.4.4), it is possible that the tracer may be imbedded into the surface of the lactose particles. Due to the relative hardness of iron oxide compared to lactose it is proposed that the embedding of tracer may enhance surface modification (or roughening), and facilitate/enhance the attrition of lactose.

The coating and distribution mechanisms of iron oxide proposed above could not be observed in SEM images (Figure 4.10) and are based on physical hypotheses based on the properties of the tracer and particle size distribution data. The effects of mechanofusion on milling and colour changes in the milling region are investigated further in Chapter 7.

#### 4.4.2 Limits of analysis of colour change using blend lightness ( $L^*$ ) alone

Satoh and Iwasaki (Section 2.4.3) studied the blending of various metal oxides in a variety of mixers and looked at the blend lightness ( $L^*$ ) alone. This limitation ignores a significant amount of information contained by the blend colour. It may also give a false indication of the true level of mixing that is occurring in the blend. As dispersion of iron oxide decreases lightness and de-agglomeration slightly increases it, the competition between the two mechanisms can result in constant  $L^*$  (Figure 4.12). From this study it would appear that blend lightness is a function of *both* dispersion and deagglomeration, and as such cannot be used exclusively to evaluate blend quality and the extent of mixing (Eqn. 4.1).

$$L^* = f(C^*, h) \quad (\text{Equation 4.1})$$

This finding is evident in inspection the the  $L^*-C^*$  and  $L^*-h$  planes (Figure 4.12a and b respectively), in which large regions exist where  $L^*$  remains constant whilst  $C^*$  and  $h$  increase respectively. This phenomenon is attributed to a balance between dispersion and de-agglomeration mechanisms in the dispersion/de-agglomeration region.

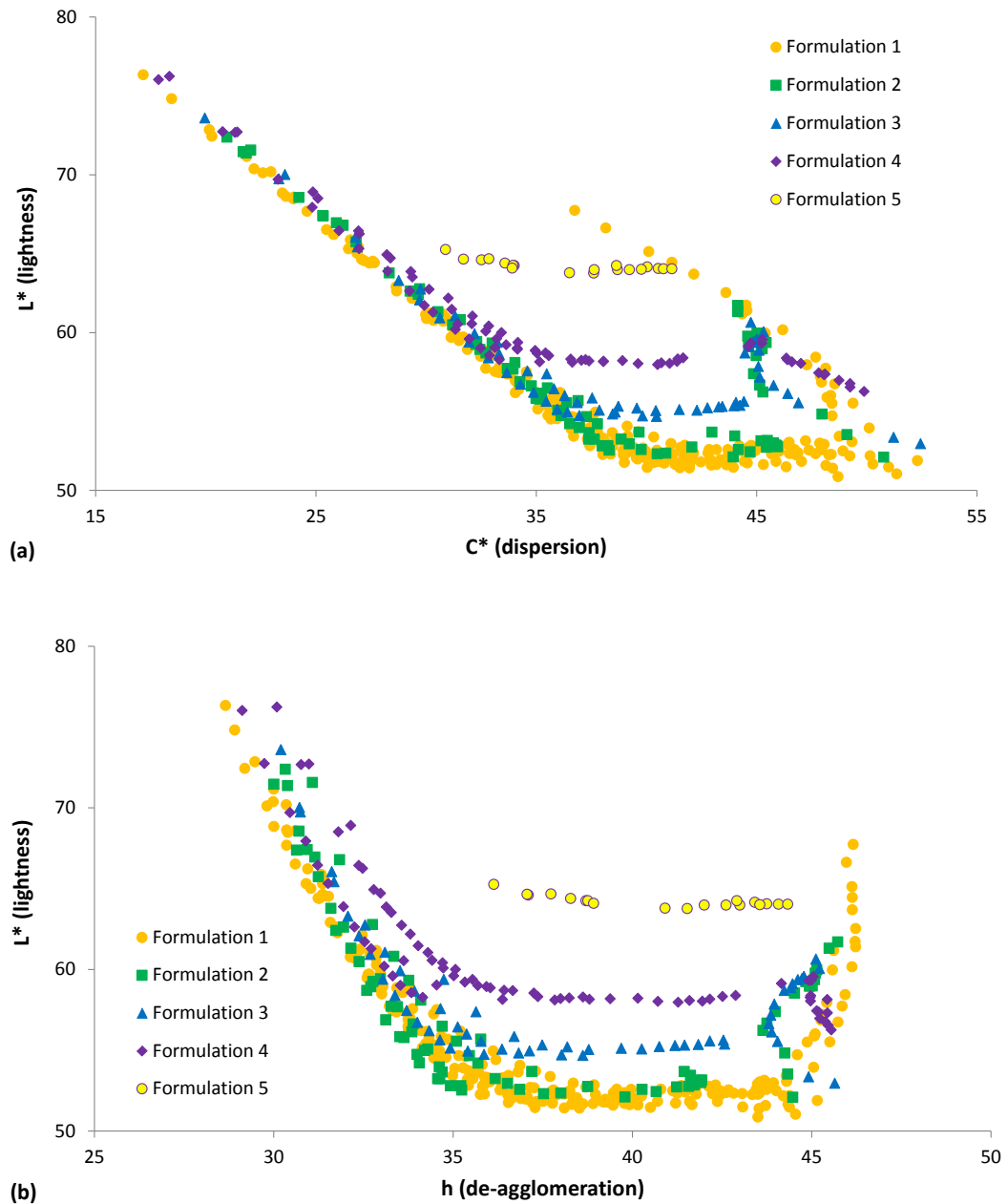


Figure 4.12: Comparisons of blend lightness ( $L^*$ ) to the (a) degree of tracer dispersion ( $C^*$ ) and (b) de-agglomeration ( $h$ ). Both the degree of dispersion and de-agglomeration continue to increase when a limiting value of blend lightness is reached.

The use of blend lightness alone appears to only hold valid within the dispersion-dominant region, and as such is not particularly useful in blending analysis on most mixing systems. Blend lightness is influenced by tracer dispersion, de-agglomeration, and milling, and as such cannot be used exclusively to evaluate blend quality and extent of mixing.

#### 4.4.3 Common plane in data

When plotted in a three-dimensional space it is clear that all data points in the  $L^*C^*h$  colour space align on a simple surface, across all formulations, processes, processing conditions, process scales, blend times and with milling. This phenomenon can be approximated with a simple (or ‘common’) plane ( $R^2 = 0.9544$ , Figure 4.13), which is arranged below to appear as a straight line. This can be better represented by a more complex 3<sup>rd</sup>-order polynomial (in respects to  $C^*$  and  $h$  in Equation 4.1) surface that accomodates for the shape of the milling region ( $R^2 = 0.990$ , Figure 4.14). Such surfaces that all formulation curves align on are termed ‘common planes’, and are mentioned in subsequent chapters. These 3-dimensional surfaces are a function of the material colours in the formulation, with white from the lactose and red/orange from the hematite tracer. It is expected that different tracers or bulk powder colours would result in a different surface in the CIELCH colour space.

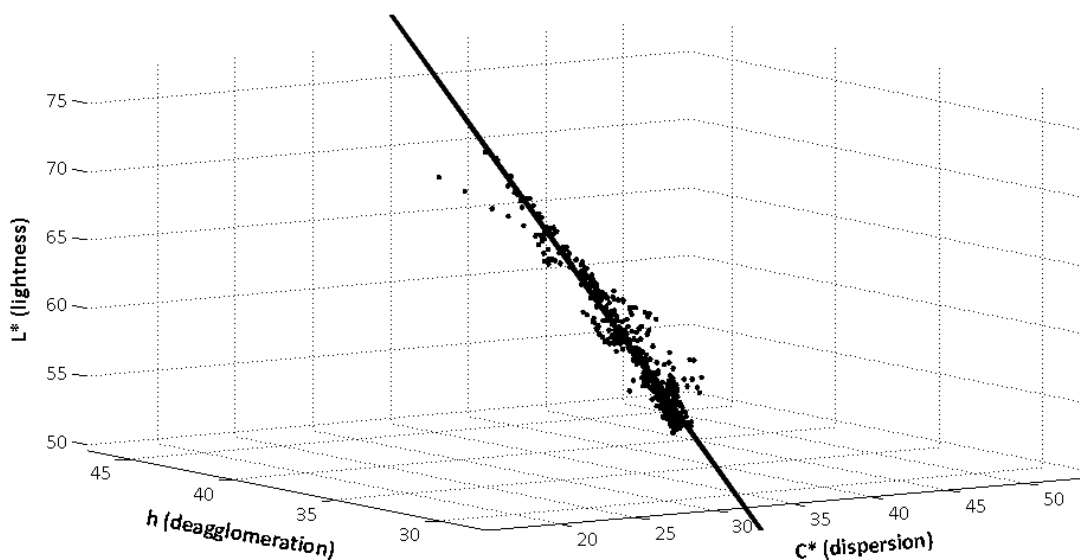


Figure 4.13: Plane of best fit for all colour data obtained in this study using MATLAB.

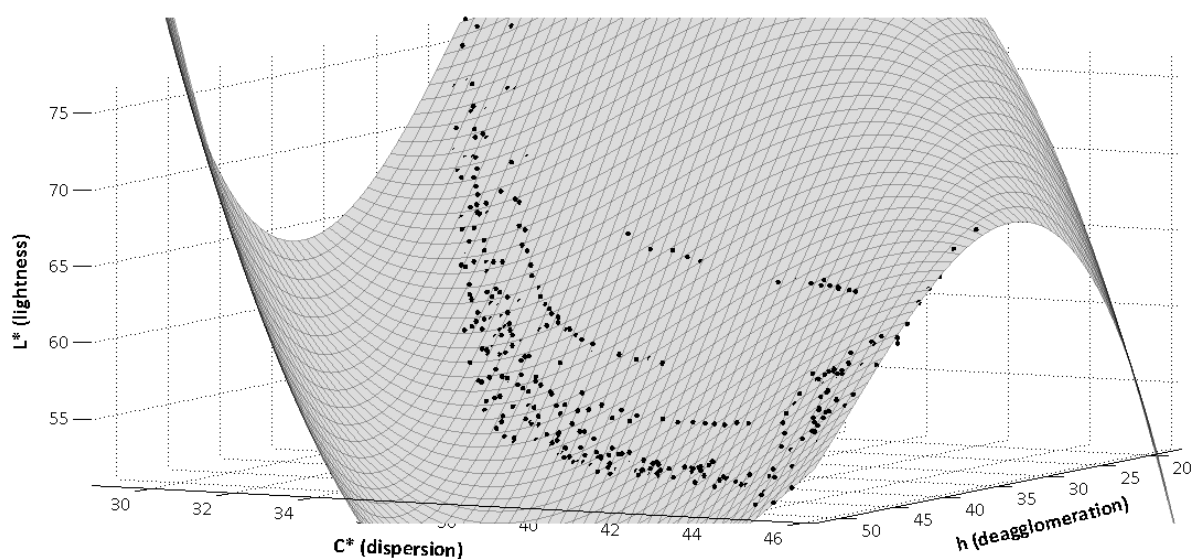


Figure 4.14: Cubic surface plot modelled to all colour data using *MATLAB*.

Further discussion of the equations and fits of these common planes is given in Chapter 8.

#### 4.4.4 Industrial application of tracer blending

The use of this sub-micronised hematite for a quick and simple analysis of blending and blend mechanics has broad and high impact potential, as changes in the blend can be quickly analysed and do not require the use of lengthy analytical methods. When coupled with drug release data, this method may be used to prove equivalent mixing between two different mixing systems or conditions, and/or be used for process validation, qualification and optimisation. For a given formulation, a tracer blend with a particular colour will have particular degree of dispersion and deagglomeration ( $C^*$  and  $h$  respectively), which suggests that it has been subjected to a certain level of total mixing energy and/or shear during mixing. It is therefore likely that placing the tracer blend in a new mixer and identifying the new mixing conditions that produce an identical blend colour would mean that an equivalent amount of total energy and shear has been applied to the blend in the new mixer and hence demonstrate blend equivalence.

The lab scale experiments conducted indicate that this method can be applied effectively to a wide range of different mixers, operating conditions and scales to determine what settings are required to achieve an equivalent blend for a given composition. If the pharmaceutical drug blend is then

manufactured at the same conditions as the colour blend (but with the tracer now replaced with the drug), and if the drug uniformity and product performance data is correlated with the blend colour data, then the formulation blending curve can lead to fine tuning of real pharmaceutical manufacturing, and potentially create a means of rapid, robust and simple blend optimisation.

As mentioned in Section 3.1.4, the tracer is stable to atmospheric moisture and temperatures of up to 1100°C. This implies that any changes in the measured colour are attributed to physical changes in the clumping and spread of tracer exclusively, and not through thermal and chemical degradation. We have found that a blend's initially recorded colour remains stable for weeks after blending, suggesting it can be remeasured at a later date. Whilst the tracer is unaffected by relative humidity (RH) during storage, it has been observed in some preliminary experiments that the RH of the surrounding environment can influence the starting and finishing values of a blend curve along its respective formulation curve during blending, with an increase in RH resulting in lower initial and final values of  $C^*$  and  $h$ . This suggests the blend material becomes 'stickier' at higher RHs and therefore requires a more intense process to de-agglomerate to the same extent. This observation may provide another benefit for the use of submicronised iron oxide tracer in monitoring powder mixing. It must be stressed however that these observations are preliminary and require further testing and validation.

Overall, this blend tracer approach appears to provide a robust and simple means of blend analysis and provides information about multiple aspects of blending. It enables the simultaneous quantitative analysis of tracer dispersion and deagglomeration, which when compared to drug blends under the same mixing conditions, provide a tool for blend optimisation or scale-up. Additional benefits of formulation curves, such as their ability to quantitatively assess blend homogeneity and milling are covered in subsequent chapters of this thesis.

## 4.5 Conclusion

Several blends of sub-micronised iron oxide tracer and different types of pharmaceutical grade lactose were manufactured in tumbler, vertical-axis high-shear and mechanofusion mixers in a variety of different scales and operating conditions to analyse the mixing behaviour and mixture quality over time. From analysis of the CIELCH (1976) colour values, formulation-specific curves were generated which appear to be independent of process type, intensity and scale, with different processes lying on different regions of the curve. Along these formulation curves, three distinct regions corresponding to tracer blending mechanisms were observed (dispersion-dominant, de-agglomeration/dispersion and milling), and allowed for a thorough analysis and comparison of mixers. Formulation curves could also measure the quality of the blend both in terms of the degree of tracer dispersion and de-agglomeration. The curves could further detect the presence of unintentional particle damage and milling. The findings of this study highlight the benefits of assessing the CIELCH values of the formulation and the limitations in the comparison of blend lightness ( $L^*$ ) values alone. This method of colour analysis ultimately has the potential to be used as a time and cost effective means of assessing a given process and set of operating conditions to ensure the desired degree of mixing and enable effective process scaling or technology transfer.





## Effect of tracer concentration on resulting colour curves

**T**he iron oxide tracer used in this thesis is environmentally, thermodynamically and thermally stable for use as an analytical tool in dry powder blending. However the robustness, reliability and significance of colour measurements across various tracer concentrations needs to be investigated and demonstrated. In this chapter, the effects of blend tracer concentration on formulation curves are studied. A new region of the formulation curves, the 'saturated' region, is identified for formulations that contain an excess of tracer (as determined from first principles), and recommendations are provided for the design space of operation (the upper and lower limits of tracer) as well as a means of calculating the optimal amount of tracer given a specific bulk powder.

## 5.1 Introduction

It has already been determined that the tracer itself is colour stable to environmental effects and temperatures of up to 400°C; however it is anticipated the significance of blend colour measurements should be sensitive to concentration effects. The tracer method in this thesis relies on the spectrophotometric measurement of both hue and hue intensity, which are attributed to tracer dispersion and de-agglomeration respectively (*Section 3.2.1*), and as such it can be surmised that there are upper and lower limits for their detection.

As specified in *Section 3.2.2*, spectrophotometric measurements in this work rely on bulk analysis of the blend. Because of this, there is a point at which the measured change in colour would be below the sensitivity of the spectrophotometer (*Nippolainen et al., 2010*), and no meaningful assessment could be made. Conversely at high concentrations of tracer, in which lactose particles have the potential to be saturated with tracer particles, there would be a point at which any further mixing would show no further change in dispersion, and it would be impossible for primary particles to be isolated, hindering any changes in hue.

The aim of this chapter therefore, is to test and provide insight into the concentration limits at which changes in the system are likely to either be undetectable or "drowned-out" due to saturation.

### 5.1.1 Influence of tracer concentration on optical properties

As outlined in *Section 3.1.3*, the hiding power of a tracer refers to how well it can conceal the substrate to which it is adhered to. The standard test is to determine the thickness of tracer required to conceal, by eye, the interface between a white and black tile. The hiding power is calculated from the inverse of this thickness. Iron oxides, including hematite, have excellent hiding power (*Cornell and Schwertmann, 1996*), and as such require only small amounts to optically obscure the substrate. In systems involving white and coloured materials, such as lactose and hematite tracer, segregation effects can occur that change the optical appearance of the blend. Such effects can occur with increasing tracer concentration. With a high tracer concentration, the distance between tracer

particles on the substrate surface decreases and consequently there is interaction and hindrance between the light scattered by each individual particle. This usually results in an overall failure of scattering power (Völz *et al.*, 2006). This phenomenon is termed as *flooding* (Völz *et al.*, 2006), and in the case of the hematite tracer used in this work, would result in an increase in absorption and negate any hue change from the de-agglomeration of tracer particles.

The upper and lower limits for good colour measurement of iron oxide tracer in a white blend have been suggested in literature (Kaye, 1997b). Previous work, using yellow iron oxide tracer with calcium carbonate, stated that the colour change up to concentrations of 10% gave excellent information on assessing mixture progression to within 1% of the nominal value (Kaye, 1997b). Less precise measurements were made with up to 40% tracer. However above this concentration, the colour change provided no information at all. This suggested that flooding had occurred.

### 5.1.2 Surface packing of particles

The coverage of tracer on a surface is analogous with the mathematical problem of packing shapes within a given space and can be used to predict concentrations at which flooding may occur. In the case of spherical mono-sized particles such as those of the colour tracer used in this work (Section 3.1.5), and due to their relatively small shape compared to the carrier particles (Figure 4.1), the coverage of tracer on carrier can be simulated through the packing of discs in a 2-dimensional Euclidean space. For such problems, a term defined as the packing density ( $\eta$ ) is used to describe the fraction of 2-dimensional space taken up by the disc compared to the total space per particle, inclusive of gaps between discs. With increasing voidage between discs, the packing density decreases. There are many different ways in which mono-sized discs can be packed onto a plane, with a total of 11 different circle packings based on uniform tilings with lines of symmetry by reflection or rotation (Williams, 1979). In this chapter, the spread of tracer particles is calculated from first principles based on two uniform packings as well as a computer generated random packing (Figure 5.1).

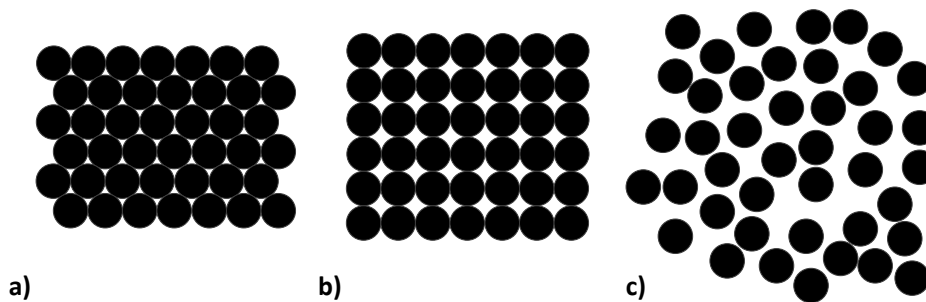


Figure 5.1: Three examples of disc packing; a) hexagonal, b) square and c) random.

The maximum packing density possible for discs can be achieved through hexagonal packing (Steinhaus, 1999) (Figure 5.1a), in which each circle is surrounded by 6 others and the gaps between each disc is minimised. The packing density for this configuration is greater than 90% (Eqn. 5.1).

$$\eta_{hex} = \frac{\pi}{2\sqrt{3}} \approx 0.9069 \quad (\text{Equation 5.1})$$

Another uniform packing that is tested in this chapter is square packing (Figure 5.1b), in which each disc is surrounded by eight others and the packing density is reduced (Eqn. 5.2).

$$\eta_{square} = \frac{\pi}{4} \approx 0.7854 \quad (\text{Equation 5.2})$$

Finally, in the realistic case of tracer coating due to particle interactions, particle packing is expected to be random (Figure 5.1c). With random packing, the packing density is determined from the random placement of discs in a predefined, very large 2-dimensional space. Discs are randomly allocated a position in the space, and are placed if their boundary does not overlap with any discs already laid. The software continues to run until no further discs can be placed in the predefined space given the condition of no overlap. The packing density is then calculated from several thousand simulations. In such a case computer simulations have approximated the packing density to be approximately 55% (Hinrichsen et al., 1986) (Eqn. 5.3).

$$\eta_{random} \approx 0.547 \pm 0.003 \quad (\text{Equation 5.3})$$

By using each of these packing densities and knowing properties of the tracer and carrier, theoretical coverage can be calculated for different types of packing that may occur. These predictions will be compared to experimental tracer concentrations in Section 5.4 to help justify experimental observations on the shape of formulation curves.

## 5.2 Materials and Method

Blends with varying levels of colour tracer (0.3, 1, 2, 5 and 10 wt%) were mixed in two different types of mixer that varied in mixing nature and intensity; namely the mechanofusion and tumbler mixer outlined in Section 4.2.2 at 600 rpm and 72 rpm respectively. In line with previous studies, the standard lactose (Lactohale LH200) was used and blends were mixed for 60 min. Data and particle size distributions for both tracer and lactose can be found in Sections 3.1.5 and 4.2.1 respectively. Colour measurements were conducted as outlined in Section 3.2.2 at the standard time points of 0.5, 1, 2, 3, 4, 5, 7.5, 10, 12.5, 15, 20, 25, 30, 45 and 60 minutes.

Brunauer Emmet Teller (BET) analysis was conducted on the lactose to obtain a surface area for calculations. In the BET analysis, 4 grams of lactose was degassed at 40°C for 1 hour, followed by the use of nitrogen as a probe molecule. The partial pressure was then ramped from 0 to 96% in 3% increments and this procedure was repeated three consecutive times on each sample. The temperature throughout was  $25 \pm 0.1$  °C. The sample was allowed to reach a near equilibrium state ( $\%dm/dt = 0.0002\%/min$ ) at each humidity stage before progressing to the next.

## 5.3 Results

As with previous work, blend colour values were recorded over mixing time in the two different mixers used, and overlapped to generate a series of formulation curves (*Figure 5.2*). The results show that tracer concentration affects the shape of formulation curves in the colour space.

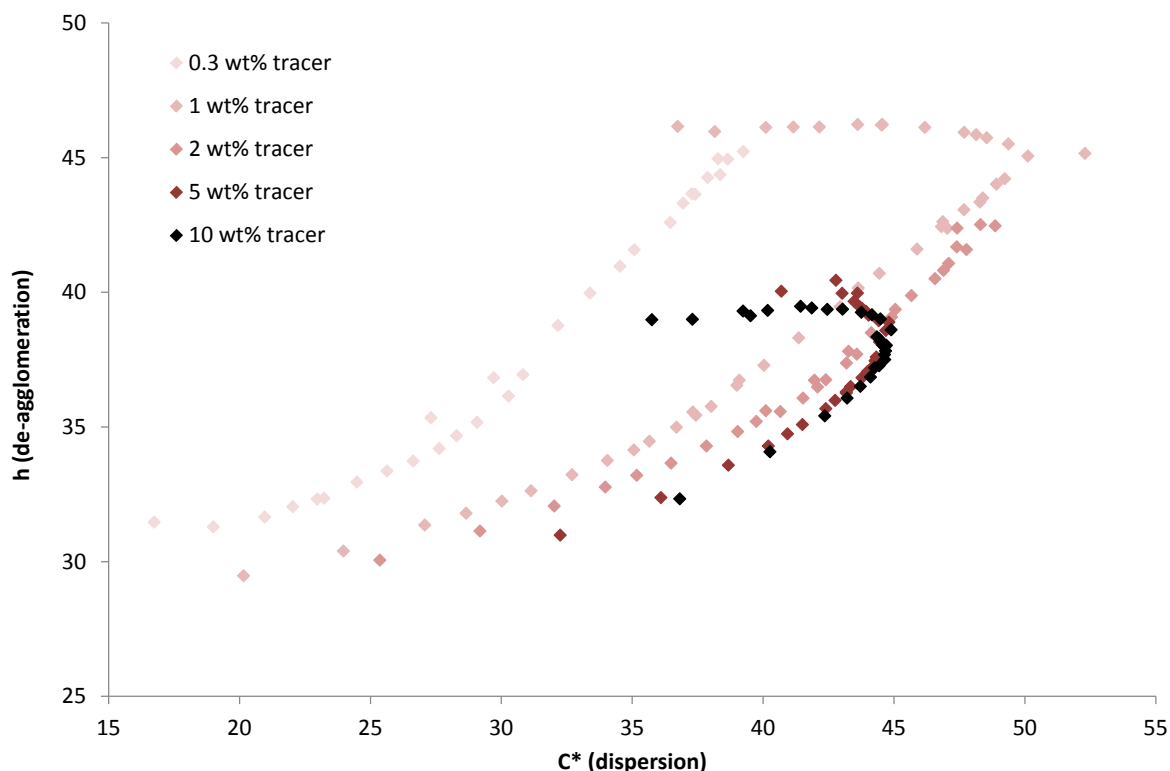


Figure 5.2:  $C^*$ - $h$  plots of formulations varying in tracer concentration.

For 0.3 and 1 wt% tracer formulations, formulation curves assume a similar shape to those obtained in Chapter 4 in the  $C^*$ - $h$  plane, beginning with a straight line at low  $C^*$  and  $h$ , which deviates to another straight line at a certain value of  $C^*$ . These two straight lines are indicative of dispersion-dominant and de-agglomeration/dispersion mixing.

Formulation curves generated at higher tracer concentrations yield different shaped curves in the CIE colour space. For higher tracer concentrations, formulation curves 'double-back' beyond the dispersion-dominant region in a similar manner in the  $C^*$ - $h$  plane as observed previously for the milling region (Chapter 4). This phenomenon becomes visible in the 2 wt% tracer formulation curve, where at high  $C^*$  it can be seen to curl back into the 1 wt% tracer curve. This 'doubling-back' is more obvious in the 5 and 10 wt% tracer curves, which almost entirely overlap with one-another. In this region, and similar to the change due to milling, hue intensity decreases at constant hue over mixing time. Unlike the curves observed in Chapter 4, which all overlapped in the dispersion-dominant region, it would appear that formulation curves that vary in tracer concentration do not overlap.

Instead they are observed to lie upon and shift downward along the common 3-dimensional plane discussed in Section 4.4.3 with increasing tracer concentration.

When the curling behaviour of the 5 and 10 wt% tracer curves appeared similar in the  $C^*-h$  plane (Figure 5.2) however when viewing them in respect to blend lightness ( $L^*$ ) a difference between the two can be seen (Figure 5.3).

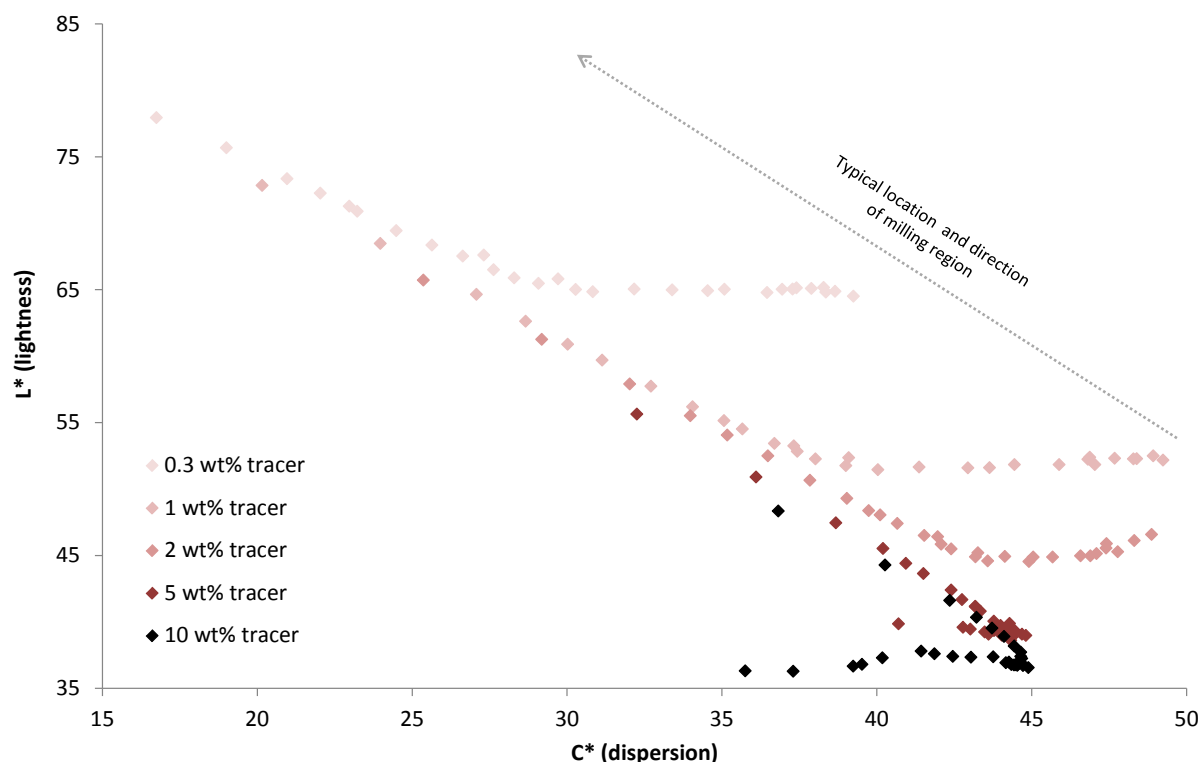


Figure 5.3:  $L^*-C^*$  plane of the CIELCH colour space for formulation curves of different tracer concentration. The new region caused by an excess of tracer is clearly visible.

As previously discussed, formulation curves typically progress linearly downwards in the  $L^*-C^*$  plane in the dispersion-dominant region, deviate to constant  $L^*$  in the de-agglomeration/dispersion region, and then rise linearly in the milling region. Both the 0.3 and 1 wt% tracer curves follow this trend in the dispersion-dominant and de-agglomeration/dispersion regions, however the typical trend in the de-agglomeration/dispersion region is lost at higher tracer concentrations. In the de-agglomeration/dispersion region, the 2 wt% tracer formulation curve shows slight deviation by not progressing with constant blend lightness ( $L^*$ ), and the 5 and 10 wt% tracer curves deviate at fairly

constant blend lightness but with decreasing hue intensity ( $C^*$ ). This ‘fold-back’ region observed for the 5 and 10 wt% tracer formulations are very different in nature to the milling region previously observed (*Chapter 4*) and are therefore believed to be caused by an effect of tracer saturation and not milling. In this ‘saturated’ region, formulation curves of different tracer concentration overlap in the  $C^*-h$  plane, but not in the  $L^*-C^*$  plane, with lower tracer concentrations having a higher blend lightness ( $L^*$ ). When formulation curves are observed in the  $L^*-h$  plane, they all exhibit similar characteristics to one-another (*Figure 5.4*):

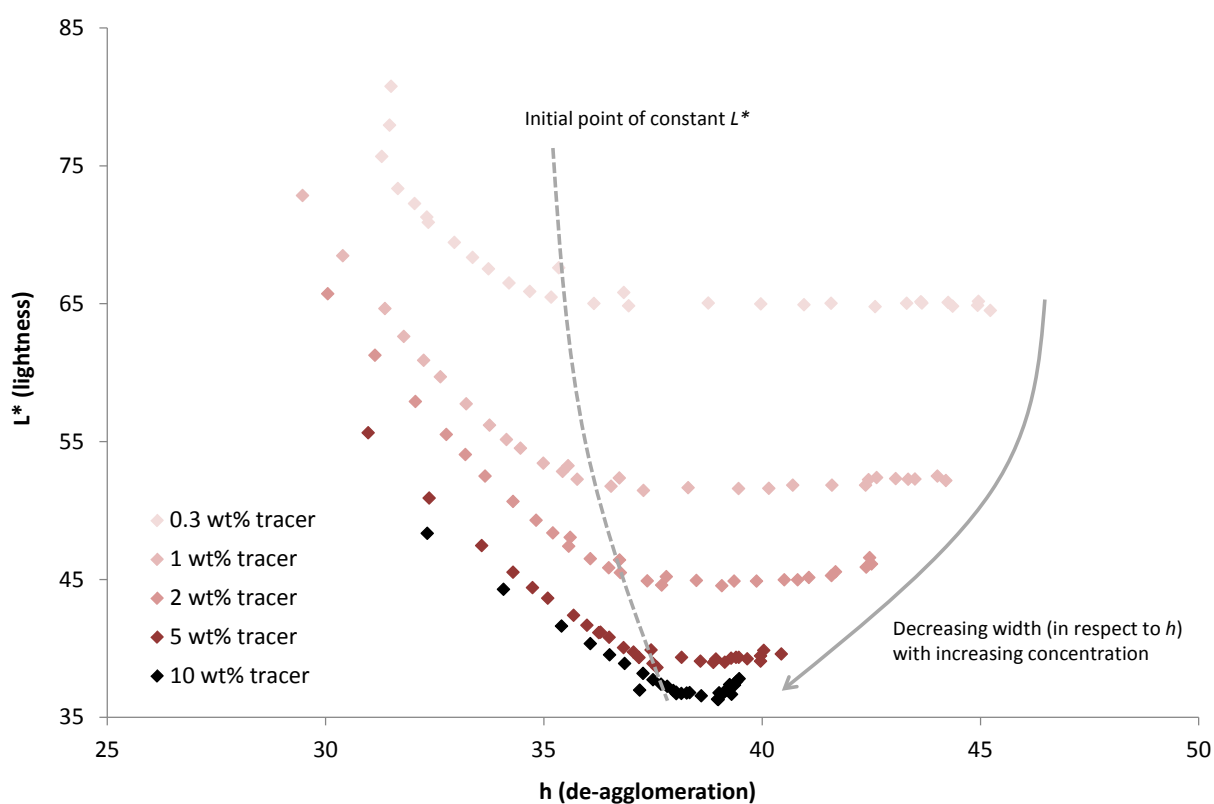


Figure 5.4:  $L^*-h$  plane in the CIELCH colour space showing change in width of formulation curve with respect to tracer concentration.

In the  $L^*-h$  plane, the width (or span) of formulation curves (in respect to  $h$ ) decreases with increasing tracer concentration and the initial point of constant  $L^*$  in the de-agglomeration/dispersion region occur at higher  $h$ . The 3-dimensional length of the de-agglomeration/dispersion and saturated regions however are fairly constant between concentrations as the saturated region ‘folds back’ at constant  $h$  (*Figure 5.5*).

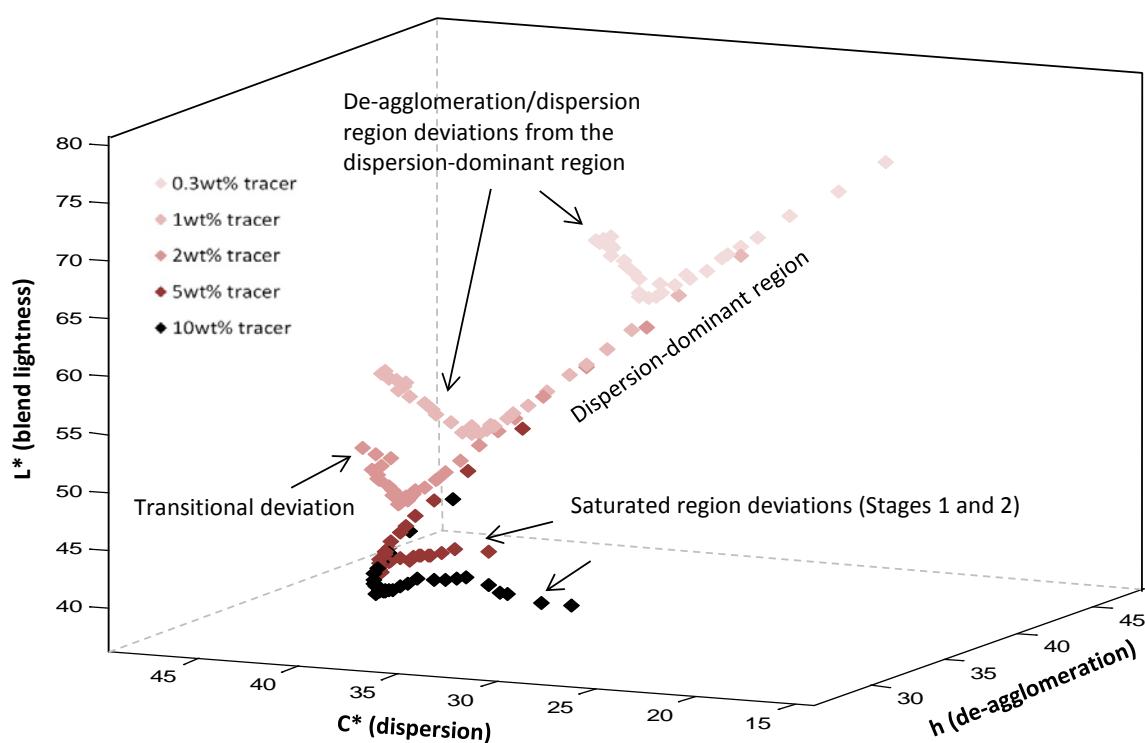


Figure 5.5: 3-dimensional view of formulation curves in the CIELCH colour space showing the deviations of the de-agglomeration/dispersion and saturated regions from the dispersion-dominant region.

When viewing in the 3-dimensional space, the deviation of the saturated region from the common plane in Chapter 4 (Figure 4.13) can be seen. The deviations of the de-agglomeration/dispersion and saturated regions from the dispersion-dominant region are observed to go in separate directions in the CIELCH colour space (Figure 5.5). The formulations curve for 2 wt% tracer deviates from the dispersion-dominant region in the CIELCH space at an angle between that of the de-agglomeration/dispersion and saturated regions, suggesting that the formulation is beginning to be influenced by an excess of tracer at 2 wt%. The saturated region (from the 10 wt% tracer curve) has two stages. In the first stage, blend lightness increases with a very slight increase in  $h$ , followed by a second section in which the blend lightness and hue return to their original values. A proposed cause of this is outlined in Section 5.4.2. Discussion and validation of the saturated region being driven by an excess of tracer is provided in Sections 5.4.1 and 5.4.2.

## 5.4 Discussion

The formulation curves show that an excess of tracer is present at 5 and 10 wt% tracer. This drives the deviation of the saturated region from the de-agglomeration/dispersion region in the CIELCH colour space. As stated in Section 5.1, the theoretical percentage coverage of lactose surfaces by tracer can be calculated from first principles, and can be used to validate the hypothesis of the effects of excess tracer and propose mechanisms behind the colour changes in the saturated region.

### 5.4.1 Calculation of maximum surface coverage using first principles

The coverage area of a single spherical tracer particle ( $A_{tpc}$ ) can be equated to its projected area (i.e. area of a circle of equal diameter to the particle) (Eqn. 5.4):

$$A_{tpc} = \frac{\pi}{4} D_{tp}^2 \quad (\text{Equation 5.4})$$

Where  $D_{tp}$  is the diameter of a tracer particle. Factoring in a packing density,  $\eta$ , for the tracer particles as provided in Section 5.1.2 gives an expression for the total tracer particle coverage per particle ( $A_{ttpc}$ , Eqn. 5.5).

$$A_{ttpc} = \frac{A_{tpc}}{\eta} = \frac{\pi}{4\eta} D_{tp}^2 \quad (\text{Equation 5.5})$$

The mass of a single spherical tracer particle ( $m_{tp}$ ) can be calculated from the true density of the material ( $\rho_{tp}$ ). This equation assumes no porosity in the particle (Eqn. 5.6).

$$m_{tp} = \rho_{tp} V_{tp} = \frac{\pi}{6} \rho_{tp} D_{tp}^3 \quad (\text{Equation 5.6})$$

The area of total coverage per unit mass of tracer ( $\hat{A}_{tc}$ ) can therefore be expressed as:

$$\hat{A}_{tc} = \frac{A_{ttpc}}{m_{tp}} = \frac{(\pi/4\eta) D_{tp}^2}{(\pi/6) \rho_{tp} D_{tp}^3} = \frac{3}{2\eta \rho_{tp} D_{tp}} \quad (\text{Equation 5.7})$$

Given a formulation that contains a certain weight percentage of tracer ( $w$ ), the surface areas of tracer ( $\hat{A}_{tc}$ , Eqn. 5.8) and substrate ( $\hat{A}_{fs}$ , Eqn. 5.9) per unit mass of formulation can be expressed as:

$$\hat{A}_{ftc} = \hat{A}_{tc} \left( \frac{w}{100} \right) = \frac{0.03w}{2 \eta \rho_{tp} D_{tp}} \quad (\text{Equation 5.8})$$

$$\hat{A}_{fs} = \hat{A}_s \left( \frac{100 - w}{100} \right) \quad (\text{Equation 5.9})$$

Where  $\hat{A}_s$  is the specific surface area of the substrate. From these terms, the fraction of substrate surface covered by tracer given a certain weight percentage of tracer in formulation (i.e. the flooding fraction,  $f$ ) is therefore (Eqn. 5.10):

$$f = \frac{\hat{A}_{ftc}}{\hat{A}_{fs}} = \frac{\hat{A}_{tc} w}{\hat{A}_s (100 - w)} = \frac{\beta w}{\eta (100 - w)}; \quad \beta = \frac{3}{2 \rho_{tp} D_{tp} \hat{A}_s} \quad (\text{Equation 5.10})$$

This provides a general equation for the *maximum* coverage of any spherical, mono-sized tracer that is significantly smaller in size to the substrate materials (i.e.  $D_{tp} \ll D_s$ ). This equation also assumes complete de-agglomeration of tracer.

The properties of the tracer and substrate in this study are outlined below (Table 5.1). The assumption of complete de-agglomeration is realistic in this study as blending in the mechanofusion mixer at 600 rpm has been shown to provide enough mixing energy for complete de-agglomeration of tracer without imbedding it in the lactose particles (Alonso *et al.*, 1989a).

Table 5.1: Defined parameters of tracer and substrate (lactose) used in this study to specify the general equation for tracer coverage.

$\rho_{tp}$ (hematite)	5240 kg/m <sup>3</sup>	Literature (Cornell and Schwertmann, 1996)
$D_{tp}$ (tracer)	100 nm	Manufacturer specifications (Rockwood Pigments, 2009)
$\hat{A}_s$ (Lactohale LH200)	250.6 ± 3.0 m <sup>2</sup> /kg	BET analysis (outlined in Section 5.2)

Given the values for the tracer and substrate provided in Table 5.1, for the specific case of 1 wt% hematite in 99 wt% Lactohale LH200 in this study (Eqn. 5.11):

$$f = \frac{\beta w}{\eta(100 - w)}; \beta = 11.42 \pm 0.14 \quad (\text{Equation 5.11})$$

Using the three different packing densities for the tracer in Section 5.1.2, the total surface areas of tracer and carrier per unit mass of formulation can be compared at different concentrations of tracer using Equations 5.8 and 5.9 (Figure 5.6).

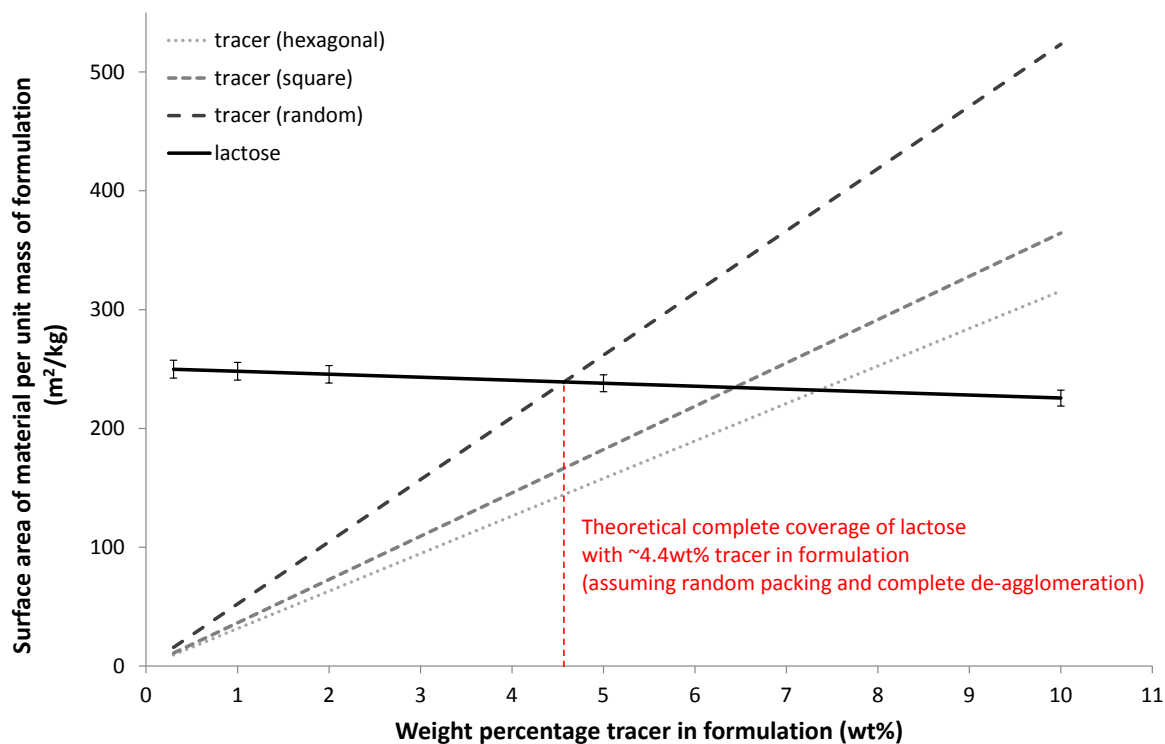


Figure 5.6: Surface areas for tracer and carrier per unit mass of formulation applying three different packing densities for the tracer.

From these results it is anticipated for all types of tracer packing on the lactose surface, complete coverage of all surfaces of the lactose is possible with less than 10 wt% Ferroside 212P tracer in formulation. This would therefore explain why the 10 wt% tracer curve behaves differently to those of lower tracer concentration. The most realistic scenario of tracer coverage utilises the random packing density of the tracer, particularly given the random collisional and frictional mechanisms required for tracer coating during mixing. In such a scenario approximately 4 wt% tracer in formulation can theoretically cover all available lactose surfaces (Figure 5.6).

These results also suggest that the first stage of the saturated region, which is observed for both the 5 and 10 wt% tracer formulations, is caused by complete coverage of substrate by tracer. The second stage, which was observed for the 10 wt% tracer and occurs at tracer levels which cause a flooding fraction greater than 1 (i.e.  $f > 1$ ), is driven by super-saturation of the substrate.

Based on the observation that the 2 wt% tracer curve (which has a flooding fraction of 0.43) began to show signs of tracer saturation and deviation from the 0.3 and 1 wt% tracer curves, it is recommended that the total amount of tracer in formulation should coat less than 40% of the available substrate surface (i.e.  $f$  should not be greater than 0.4). It is also recommended based on the 0.3 wt% tracer curve that the maximum tracer coverage should be more than 5% to ensure that adequate information can be gathered from measurements in colour change (i.e.  $f \geq 0.05$ ).

From the assumption of mono-sized, randomly-packed, spherical tracer particles, a general equation for the recommended tracer concentration in a formulation can be constructed from Equation 5.10 for any tracer and excipient (Eqn. 5.12).

$$w = \frac{100f}{(2.742/\rho_{tp}D_{tp}\hat{A}_s) + f}; \quad 0.05 \leq f \leq 0.4 \quad (\text{Equation 5.12})$$

And for the specific formulation used in this study (Eqn. 5.13):

$$w = \frac{100f}{20.88 + f}; \quad 0.05 \leq f \leq 0.4 \quad (\text{Equation 5.13})$$

So that the tracer is within the range of ( $0.3 \leq w \leq 2$ ). General expressions can also be constructed for the prediction of critical and optimal tracer concentrations in formulation. Theoretical flooding of the system occurs for  $f = 1$  as there is enough tracer in the formulation to completely cover the substrate. This value represents the theoretical upper limit of tracer (Eqn. 5.14).

$$w_{flooding} = \frac{1}{(0.02742/\rho_{tp}D_{tp}\hat{A}_s) + 0.01} \quad (\text{Equation 5.14})$$

The theoretical upper limit should not be confused with the practical upper limit. In a real system, flooding begins at lower concentrations of tracer than the theoretical flooding fraction of 1, hence the recommendation to remain below a maximum fraction coverage (i.e. flooding fraction) of 0.4. This may be due to the nature of tracer de-agglomeration, which relies on the impact of particles and agglomerates with one another as described in Section 5.4.2.

There is a balancing act between having sufficient tracer to increase sensitivity in colour change and not too much tracer as to hinder de-agglomeration on the carrier surface. Based on the results obtained, it is recommended that optimal information can be obtained when the maximum coverage possible is approximately 20% of the available excipient, which can be generalised by the following equation (Eqn. 5.15).

$$w_{optimal} \approx \frac{1}{(0.14/\rho_{tp}D_{tp}\hat{A}_s) + 0.01} \quad (\text{Equation 5.15})$$

This expression has the potential to be used as a means of determining tracer concentration prior to preliminary blending experiments.

Also, a general equation can be used to check whether flooding may affect measurements in a formulation using this specific tracer with any substrate (Eqn. 5.16).

$$f = \frac{5233.26 w}{\hat{A}_s(100 - w)} \quad (\text{Equation 5.16})$$

If the flooding fraction is above 0.4, then it is likely that the tracer will affect the colour change and formulation curves will enter the saturated region. Similarly, if the flooding fraction is below 0.05, the sensitivity of colour changes is likely to be too low to detect effectively. Further examples of this equation's use are provided in Chapter 8.

#### 5.4.2 Tracer coating of particles

The deviation of formulation curves from the dispersion-dominant region into the saturated region at high tracer concentrations is attributed to effects of an excess of tracer and not milling. Changes due to milling were observed in Chapter 4 for mechanofused blends at 2000 and 3000 rpm. Unlike the milling region, in which blend lightness increases and hue intensity decreases with mixing time, blend lightness in the saturated region does not increase. Instead, hue intensity decreases at relatively constant lightness and hue, suggesting that:

- Further de-agglomeration of tracer is insignificant (hue remains relatively constant).
- The total exposed lactose surface area (i.e. white surface area) remains constant (lightness remains largely unchanged).
- The total 'observed' tracer surface area decreases (hue intensity decreases).

The absence of milling with Lactohale 200 when tumbling or mechanofusing at 600 rpm was demonstrated with particle size distributions in Chapter 4. Both this and the prediction of substrate saturation outlined in Section 5.4.1 indicate that deviations in the formulation curves at high tracer concentration are most likely an effect of an excess of tracer in the blend. These conclusions imply that in the saturated region, the tracer was undergoing a multi-layering effect on the lactose surfaces; effectively 'soaking' up any loose agglomerates or aggregates of tracer. As commented on in Section 5.3, there appears to be two stages to the saturated region of the colour curves and therefore, two potential mechanisms.

Given the shape of the formulation curve at 10 wt% tracer, the following mixing mechanism is proposed when supersaturated coverage is possible. The mechanisms observed for the dispersion-dominant and de-agglomeration/dispersion regions in Chapter 4 for a non-saturated formulation were as follows (*Figure 5.7*):

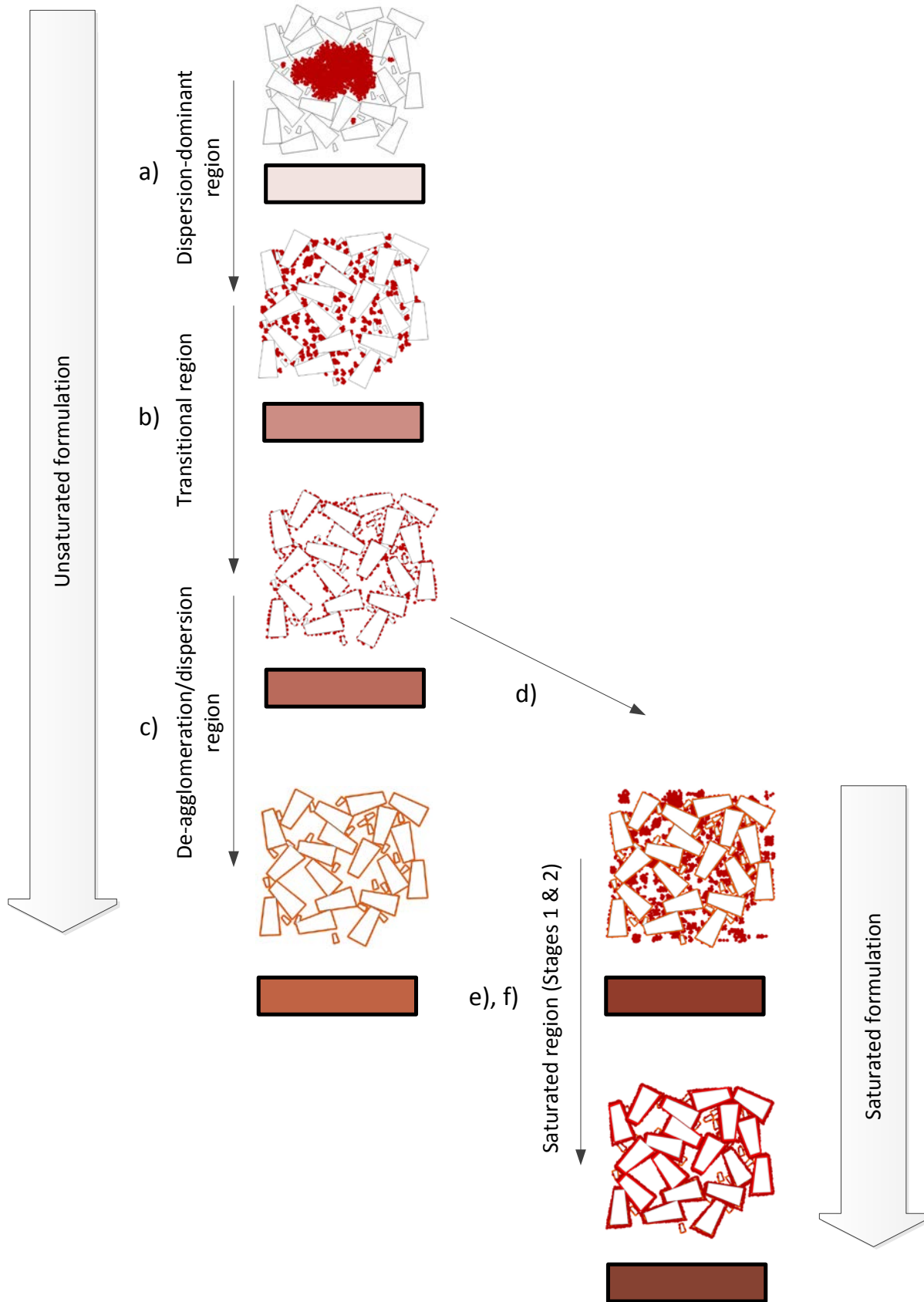


Figure 5.7: Proposed mechanisms and forms of tracer present at different points along the formulation curves for sub-saturated and saturated formulations.

- a) Tracer aggregates and agglomerates disperse through the bulk lactose and adhere to lactose surfaces in their immediate vicinity (*dispersion-dominant region mechanism*). De-aggregation of the tracer also occurs.
- b) Inter-particle collisions between lactose particles occur, forcing those with tracer aggregates and agglomerates to share tracer with non-coated particles, inherently causing de-agglomeration (*transitional region between the dispersion-dominant and de-agglomeration/dispersion regions*). Initially the population of aggregates adhered to the lactose is large and the rate of de-agglomeration is low due to the size-driven preferential de-aggregation of tracer.
- c) As the population of aggregates decreases, the rate of de-agglomeration increases and eventually becomes greater than that of de-aggregation. Agglomerates of tracer are de-agglomerated and dispersed across the surface of carrier particles through friction and collisions between particles (*de-agglomeration/dispersion region mechanism*).

Due to the adhesion properties of the tracer, tracer particles require a vacant space on a lactose particle surface to prevent re-agglomeration and maintain the orange hue (i.e. they need to be isolated single tracer particles). In a system with an excess of tracer aggregates, such as the formulation comprising of 10 wt% tracer in this study, there ends up being insufficient lactose surfaces to facilitate complete and stable de-agglomeration of the tracer. Instead, lactose particles experience an endless barrage of agglomerates, which suppress the isolation of tracer particles and hence the orange hue.

For a formulation with an excess of tracer, mechanisms a) and b) are identical to those of an unsaturated formulation. Deviations between saturated and unsaturated blends begin at mechanism b), and deviate from c) into d) (*Figure 5.7*):

- d) Agglomerates of tracer are de-agglomerated and dispersed across the surface of carrier particles through friction and collisions between particles. Surfaces become completely

covered in de-agglomerated tracer, and are also covered in agglomerates. Additional loose tracer aggregates and agglomerates in the formulation drown out the change in hue.

- e) The packing of tracer primary particles on the lactose surface is consolidated as agglomerates on saturated lactose particles collide with one-another (*the saturated region, Stage 1*).
- f) Once consolidated packing is achieved on the lactose surface, multi-layering of tracer on lactose particles occurs, driven by inertial effects of the lactose particles which are able to overcome inter-particle adhesion between tracer particles. The multi-layering causes tracer particles to no longer be isolated from one another and thus the hue reverts slightly (*saturated region, Stage 2*).

These proposed mechanisms for the saturated region are consistent with the calculated oversaturation of tracer in the formulation in Section 5.4.2, which suggest that there is enough tracer in formulation to coat the lactose 2.3 times over when 10 wt% tracer is used. If the system is saturated with tracer, any milling of particles would not be observed through measuring the colour change as fresh uncoated lactose surfaces that were generated through particle fracture would immediately be coated with tracer.

Chapter 3 described several different properties of the powder blend could affect the measured colour (*Section 3.1.4, Figure 3.5*). One factor was the optical depth, or depth of light penetration. Essentially, light will travel in a straight line until it interacts with a particle. Once it is intercepted it will react in a variety of ways, including absorption and scattering (*Section 3.1.4, Figure 3.3*). If the beam of light does not interact with any material at the sampling interface (i.e. directly at the base of the sample cup), it can enter the powder mass through the interstices between particles. If light manages to penetrate into the powder mass, it will be refracted, scattered or absorbed to various extents depending on the size, shape and type of particles it hits, and may or may not exit the powder mass again. The deeper the light penetrates into the powder mass (i.e. the larger the optical depth), the less likely the light is to be directed towards the detector, or escape at all. Essentially, the

hue intensity drops due to the increase in optical depth that arises from the multi-layering and consumption of loose tracer aggregates. As the loose aggregates of tracer (shown in *Figure 5.7*) are layered on to the already coated lactose particles, the interstices between the lactose particles increase. This in turn increases both the amount of light that penetrates into the powder mass and the optical depth. This phenomenon is not seen in unsaturated formulations because either all tracer aggregates are adhered to the abundant lactose surfaces, or they do not fill enough interstices to alter the bulk measurement of colour.

#### 5.4.3 Validation of the term 'Formulation curve' through comparison to initial data

Chapter 4 proposed that curves in the CIE colour space were formulation dependent, and relied on the type of lactose and quantity of tracer used. With formulations 1 and 5 in the previous chapter (*Section 4.2.1*), which both used the same lactose but varied in tracer concentration, different curves were observed. The curve using 0.3 wt% tracer (*Formulation 5*) was constructed entirely from industrial scale high-shear mixer blends, which were not reproduced in the lab-scale *Formulation 1* curve. It was not clear therefore if the difference between the formulation curves in the CIE colour space were an effect of mixer scale or tracer concentration. When the *Formulation 5* data from Chapter 4 is compared to the lab scale tumbler and mechanofusion data from this chapter, they align within reasonable limits (*Figure 5.8*).

Whilst there is a slight discontinuity between the mechanofusion and industrial-scale high-shear mixer data (shown in red), it still aligns with the tumbler data, suggesting the discrepancy may be attributed to the complex and intense nature of the mechanofusion process, or be an effect of too low a concentration of tracer particles in formulation or batch variations in the lactose used.

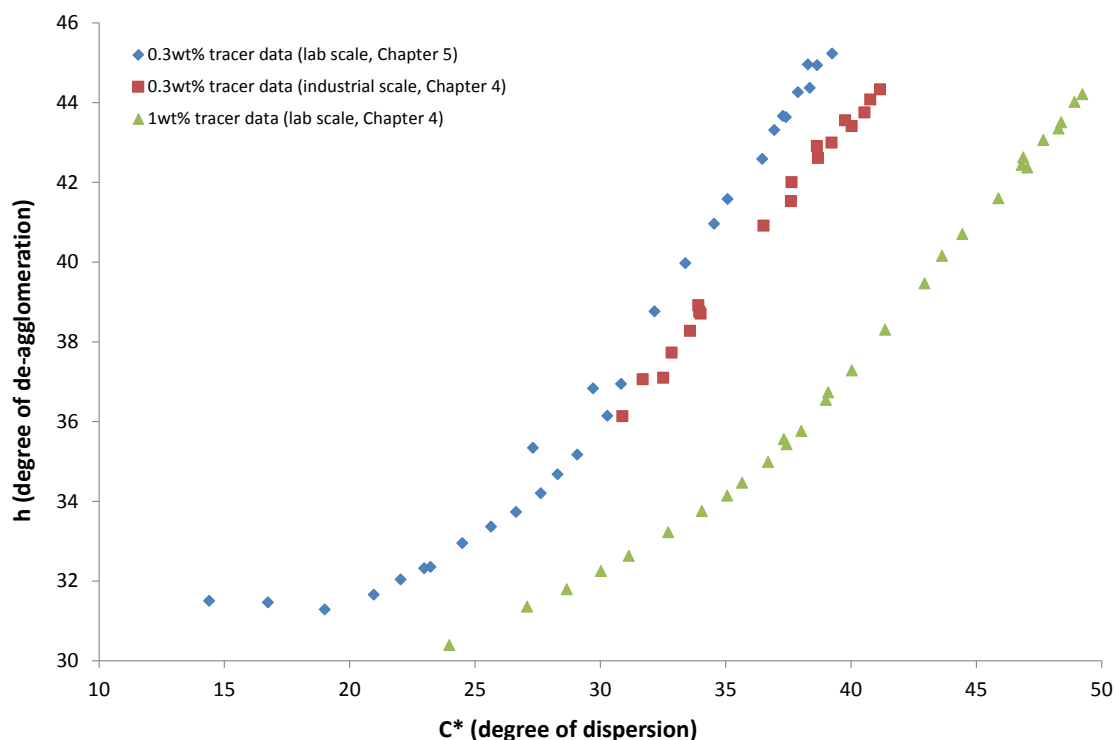


Figure 5.8: Comparison of blend curves obtained in Chapter 4 and 5 confirming that colour curves are dependent on formulation and not mixer type or scale.

#### 5.4.4 Comments on previous work in literature

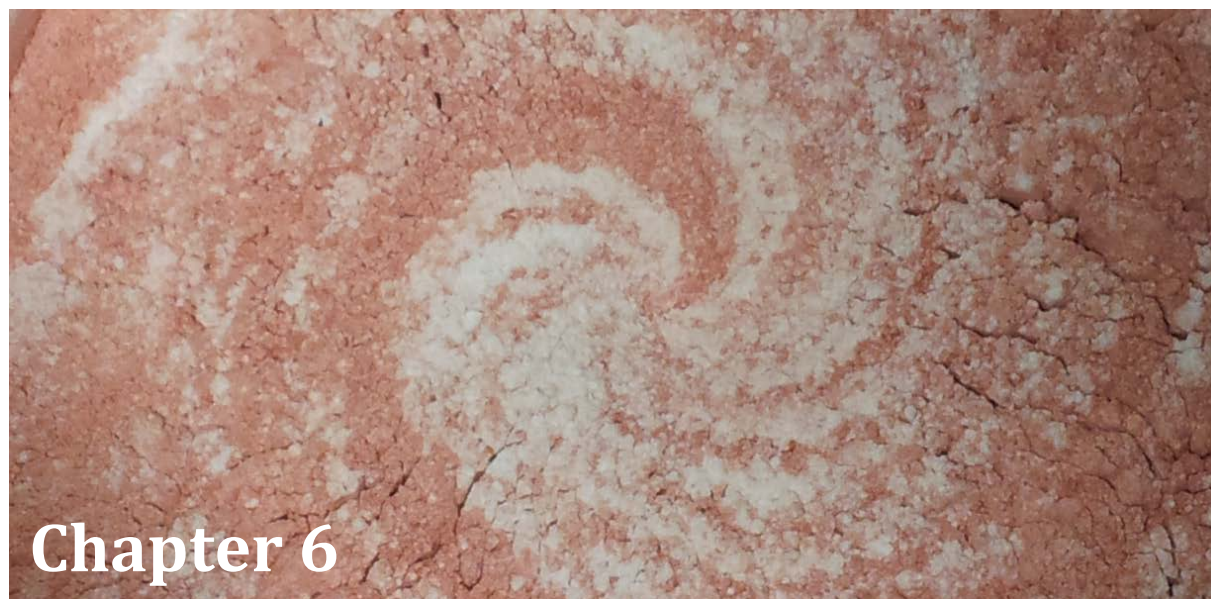
The previous work with yellow iron oxide from literature (*Kaye, 1997b*) found that tracer concentrations of up to 10% provided useful blend information. Beyond 40% flooding occurred. Similar behaviour was observed in this work, however flooding was observed to occur at concentrations of tracer below 5 wt%, particularly in relation to the measurement of changes in hue. This may explain why the previous work by *Satoh and co-workers (1993)*, who used 5% tracer in formulation (outlined in *Section 2.4.3*), relied heavily on the measurement of blend lightness and did not make comment on the change in hue during mixing. As shown in Figure 5.7, at an oversaturation of tracer, the system becomes predominantly linear in the  $L^*-C^*$  plane. This suggests that only the dispersion of tracer can be measured with confidence. Other effects, such as the type of tracer used may also affect the change in hue that can be observed during blending, particularly if the tracer is

above 100 nm in primary particle size. Further discussion and comparison of the method used in this thesis in reference to previous works such as Satoh's is provided in Chapter 8.

## 5.5 Conclusion

Results of this chapter demonstrated that the shape and location of formulation curves in the CIE colour space relies on the concentration of tracer. For formulations comprising of the same substrate (in this case the same type of lactose), significantly different curves were generated with different levels of tracer. The amount and significance of information obtained from measuring the colour change of a blend over mixing time was also dependant on the amount of tracer in formulation; with too little or too much tracer effectively invalidating the method. In this chapter a new colour curve region (the 'saturation' region) was identified, which is a product of excessive tracer in formulation. Through first principle analysis of the coating of substrate with tracer, an ideal design space was recommended for blending; such that between 5% and 40% coverage of the substrate can be achievable with the selected tracer. This allows for good sensitivity in measurement and prevents formulation curves deviating into the saturated region, which otherwise restricts insight into blending characteristics, limiting optimisation of pharmaceutical powder blending. Equations were also derived from first principles for the calculation of ideal tracer content of a given formulation to optimise blend analysis.





## Using formulation curves to assess content uniformity, energy input and blending dynamics

**C**ontent uniformity is an important key attribute in DPI formulations and often forms the basis for dictating the operating conditions in the early stages of process scale-up or optimisation. The rate and degree to which a blend reaches satisfactory uniformity ultimately depends on the process kinetics (i.e. powder flow and particle interactions), which are governed by the mixer geometry and the amount and rate of energy applied to the powder. Current industrial means of determining content uniformity are labourious and costly, and methods for assessing powder flow and energy input are not readily available and difficult to interpret. In this chapter, the colour tracer method is tested to determine whether it can be used to quantify blend homogeneity and identify regions of poor mixing, as well as potentially quantify energy input to the blend and give insight into powder flow. Such abilities would extend the benefits of using the colour tracer method and potentially simplify and accelerate early process development and validation.

## 6.1 Introduction

Whilst current drivers in the pharmaceutical industry are pushing for the implementation of continuous or semi-continuous powder mixing processes, many still employ traditional batch systems, in particular vertical-axis high-shear mixers. These mixers are often selected due to their ability to handle a wide variety of powders both cohesive and free-flowing. However, they produce complex heterogeneous powder flows and structures that are difficult to predict. These flows vary dramatically with powder properties as well as mixer and impeller geometries, making it very difficult to tune the process to ensure sufficient de-agglomeration and blend uniformity.

### 6.1.1 Causes of poor blend uniformity

As outlined in Section 2.1.4, the homogeneity of a pharmaceutical blend is arguably its most important attribute. Without good homogeneity, the drug content of doses would be highly variable and irregular. This is critical for DPI formulations where drug content needs to be the same for each metered dose. Four main factors lead to non-uniformity of API and excipient and changes in delivered dose; weight variability in final dose, drug segregation, drug agglomeration and poor equipment design/operation (*Muzzio, 2006*). Variability in dose metering can be detected and corrected during filling, however the other causes of poor uniformity are more complex and difficult to resolve.

The effects of blending can be reduced or even reversed depending on the flow of material during agitation and the powder properties themselves. These phenomena include powder segregation which occurs due to size and density differences in the particles and poor mixer design or operation. The segregation behaviour of a material can also be affected by variability in raw material quality (e.g. particle size or crystallinity) or environmental conditions (e.g. moisture, temperature). Very often a DPI blend is unable to meet product specifications despite good blend homogeneity due to an insufficient degree of de-agglomeration caused by a lack of shear dispersion zones within the mixer (*Kaye, 1997a*).

The shortcomings of a particular mixing technology are particularly noticeable when blending powders with small particle size and/or high cohesivity. Such properties can not only result in a poor blend intimacy but can lead to the formation of poorly mixed heel residue and vessel caking. These residues are often rich in the finer, more cohesive components, resulting in a form of segregation which can lower the effective yield of the process. The locations where these residues form in the mixer are termed 'dead zones', and arise from the geometry and operating conditions of mixing equipment. Sections of poorly mixed material prevent true blend uniformity, affect the nature of any subsequent mixing and can randomly dislodge at any time during the mixing process; affecting the rest of the batch. In a bladed mixer such as the traditional high-shear mixer, these regions typically occur where the impeller is either unable to reach, or unable to generate sufficient energy in neighbouring particles to cause agitation, which are typically in the region underneath the impeller or in the corner of the vessel where the base meets the walls (*Hare et al., 2011*). Some adherence to the lid and upper walls is also possible. Despite the significant influence of dead zones on the quality of the final product, there has been very little research into their presence and formation, much less how to minimise them. The iron oxide method in this thesis can be used to detect these dead-zones, as losses of tracer in heel residue could be detected by a corresponding shift in the formulation colour curve. Also, regions of poorly mixed material could be identified by eye due to their particular colour.

### 6.1.2 Assessment of blend uniformity

Methods of monitoring blend uniformity and the extent of de-agglomeration and segregation are critical for the production of a highly reproducible product. As mentioned in Section 2.2.1, the standard method for measuring content uniformity in industry is to collect several set quantities of powder from the blend drum or mixer at set positions and depths using a sample thief (*Muzzio et al., 2003, Muzzio et al., 1997*).

Thief probes are typically made of two concentric cylinders, in which the inner cylinder has one or more openings that can be exposed by rotating the outer cylinder. Two types of sample thief are commonly used; size- and end-loading probes (Berman *et al.*, 1996, Muzzio *et al.*, 2003). These differ by the location of the openings on the thief but use the same mechanism for sample collection. Other designs exist, such as core samplers (Susana *et al.*, 2011) and end-cup thieves (Muzzio *et al.*, 2003). These rely on a different mechanism for powder collection.

A typical end-loading sample thief consists of an outer hollow cylinder and an inner rod (Figure 6.1).

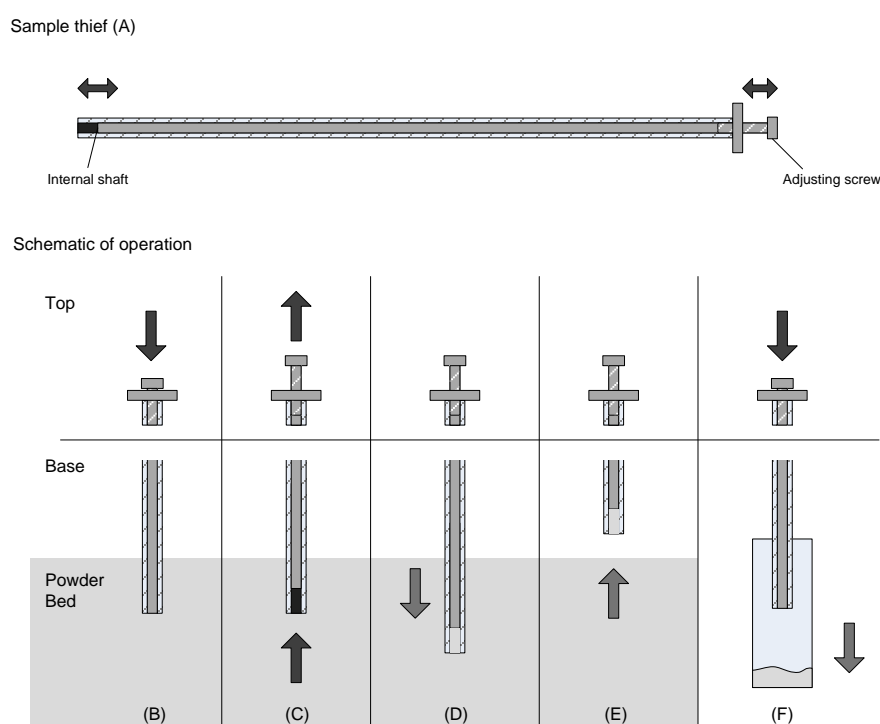


Figure 6.1: Schematic of powder thief (A) and powder sampling using the thief (B-F). Top button is pushed down to prevent powder entering inner chamber (B). Once at the desired height button is released (C) and thief thrust into powder bed to fill cavity (D). Thief is then extracted from bed (E) and powder collected for analytical testing (F).

A screw at the top of the thief can be turned to determine the empty volume achievable at the base (Figure 6.1A). When the thief is placed in the blend drum, the top button is pushed down to prevent entrainment of powder (Figure 6.1B). At the set position and depth of powder the top button is released (Figure 6.1C) and the opened thief thrust into the powder until such point as the cavity

within the outer tube at the base of the thief is filled with powder (Figure 6.1D). The thief is then removed from the blend drum (Figure 6.1E) and evacuated into a sample vial (Figure 6.1F).

Once a set number of samples are taken, the drug content of samples are then determined through chemical analysis such as High Performance Liquid Chromatography (HPLC) or UV/Vis spectroscopy. In the production of pharmaceutical formulations the blending end-point (i.e. the point at which satisfactory key attributes are achieved) is generally first established by setting an appropriate limit for the uniformity of the drug in a blend, usually through analysis of the relative standard deviation (*RSD*), which relates to the standard deviation and average value for drug content (Eqn. 6.1).

$$\%RSD = \frac{\textit{st. deviation}}{\textit{average}} \times 100 \quad (\textit{Equation 6.1})$$

Calculation of *%RSD* is applied across the series of samples collected at an appropriate scale of scrutiny (typically in the order of a unit dose). According to the FDA guidance document (FDA, 2003), a *%RSD* of  $\leq 5.0\%$  is recommended as a hurdle for assuring sufficient blend homogeneity.

The variation in sample drug content has been termed in literature as the legal variation (Kaye, 1997a), and is a function of the true variance in the blend and the variance caused by sampling error and measurement technique (Fan *et al.*, 1990). As mentioned in Section 2.2.3, due to the scale of scrutiny required in testing pharmaceutical blends (i.e. in the order of a single dose) it is very difficult to obtain a representative sample of the entire blend by sampling a handful of minute quantities. There is debate over the most appropriate location, number and size of samples that provide a representation of the entire batch (Berman *et al.*, 1996, Chang *et al.*, 1996, Kaye, 1997a, Muzzio *et al.*, 2003, Muzzio *et al.*, 1997).

When mixtures are created by chaotic mixing, as outlined in Chapter 2, a firm understanding of the variation in mixture structure is required, particularly when determining the sampling scheme (locations) for a powder mass and reducing bias (Brittain, 2002, Kaye, 1997a). One such means used

in the pharmaceutical industry is to sample the blend along three different planes to create a sampling map (Figure 6.2).

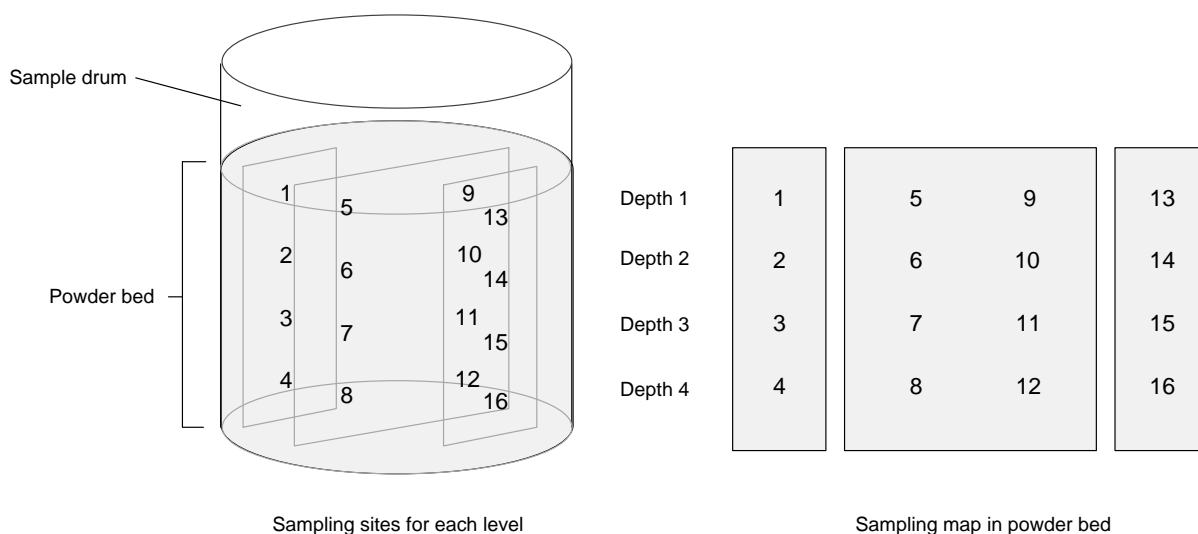


Figure 6.2: Systematic sampling of a powder mass to best obtain a representative sample.

The two widely known ‘golden rules’ of sampling are that powder should be sampled when in motion, and that the whole of the powder should be sampled over a series of small samples (*Allen, 1975*). Unfortunately, the use of industrial sampling tools such as a thief probe violates both of these rules, and in fact considerably increase the legal variation of the blend beyond the true blend variation (*Schofield, 1976, Yip and Hersey, 1977*). This is caused by bed disturbances when the thief enters the powder bed, and bias with particles of different sizes entering the thief unevenly (*Muzzio et al., 2003*). For these reasons it has been suggested by *Kaye (1997)* that sampling should be carried out immediately after the powder settles within the container or mixer.

Statistical guidelines for the number of samples recommend that at least 30 are required (*Devore, 1982*). In real situations however, this number of samples can be impractical due to physical constraints in the sampling mechanism, such as with a sample thief, where it is rarely practical to take more than 10-20 samples (*Muzzio et al., 1997*). In such instances, a minimum of 10 samples has been reported to provide adequate representation of the blend (*Zeng et al., 2000*).

In addition to the sampling locations, the sample size of a powder is difficult to design due to the size of individual particles. It is not enough to take as small a sample as physically possible. Most sample sizes are designed around the desired outcome (or scale of scrutiny), which in the case of pharmaceuticals is to ensure that the drug content between doses is consistent. Whilst indexes exist for determining sample size (such as the Buslik's Index (*Bulisk, 1950, Bulisk, 1973*) and the rationalised sampling efficiency factor (*Kaye, 1997a*), they are not relevant in the sampling of pharmaceutical powders due to the low scale of scrutiny required to ensure consistent drug content in each dose (*de Boer et al., 1991*). Sample sizes for content uniformity in pharmaceutical formulations are instead regulated by a published court ruling in the U.S.A., termed the 'Barr Decision' (*Muzzio et al., 1997*), which states that samples should not exceed more than 3 unit doses in size.

Other novel methods exist beyond the use of a sample thief for assessing content uniformity. These are currently more prevalent in academia; however through technological advances some of these methods are gaining favour with regulatory bodies, particularly when coupled with continuous mixing systems for real-time quality control. Particle size distribution has been reported to be able to assess the content of different components when they differ in particle size (*Kaye, 1997b*), and was recommended by the Barr Decision in ruling out concerns over handling issues and associated segregation. Mixtures can also be assessed through Infrared (IR) analysis (*Ciurczac, 1991, El-Hagrasy et al., 2001, Luypaert et al., 2007, Reich, 2005, Siesler et al., 2006*) and optical reflectance (*Alonso et al., 1988, Subert and Cizmarik, 2008*). Offline analysis of blending technologies can also be performed through the use of radioactive tracers (such as in Computerised Axial Tomography, CAT (*Moselman, 1987*)) and through Poisson tracking, where a set number of tracer particles are added to a system and counted from samples to form a probability distribution (*Moroney, 1953*). Such a method can be used to verify the presence of good mixing and shift focus of failed mixes to the inadequate de-agglomeration of material. It is also theoretically possible to assess a mixture by examining it under a microscope and carrying out a size distribution on the relative proportion of

components (Kaye, 1997b). Images can also be inspected in random lines through across the sample and counting the number of interactions with one component. Such methods are used in the concrete industry and geosciences (Chayes, 1956).

### 6.1.3 Powder flow and the rate of mixing

The particle flow within a given mixing technology dictates the frequency of inter-particle collisions (i.e. mixing rate) and also whether certain blend attributes (such as high intimacy) are achievable. A lack of understanding about the mixing mechanics and powder flow in a mixer can lead to problems during process design, operation and scale-up; including non-uniform flow, jamming, and segregation (Wibowo and Ng, 2001). An understanding of how to manipulate or optimise flow can assist in the rational and robust design of mixing processes, effectively determining mixing end-point, developing process models and increasing process reproducibility, as highlighted by several authors (Cameron et al., 2005, Faure et al., 2001, Niklasson Bjorn et al., 2005). Whilst appealing on paper, obtaining an understanding of the powder flow within a given mixing system is by no means an easy task. It is difficult to characterise powder flow due to the wide range of behaviours that it can exhibit, from solid-like quasi-static to rapid fluid-like flows (Campbell, 2006, Remy et al., 2010a).

For this reason, the flow of powder generally does not conform to the continuum models used in fluid mechanics. The complex nature of powder flow is also typically compounded in industrial processes due to the wide range of equipment selection, configurations, internals (such as impellers, choppers and baffles) and process scales. The properties of the powder also affects flow, with cohesive mixtures showing a higher level of spontaneous chaotic flow compared to free-flowing materials (Chaudhuri et al., 2006, McCarthy, 2003).

In a high-shear mixer, two distinct flow patterns (or regimes) can be observed which are classed as bumping and roping (Litster et al., 2002, Nilpawar et al., 2006, Remy et al., 2010a) (Figure 6.3).

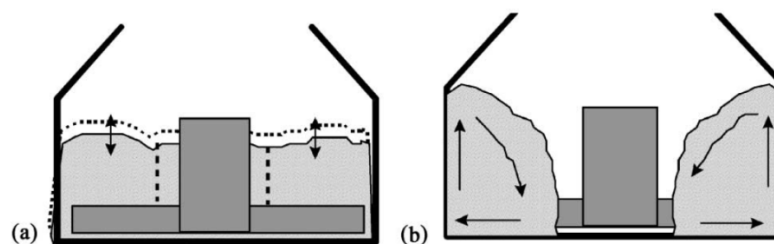


Figure 6.3: Schematic of bumping (a) and roping (b) powder flow regimes in a high-shear mixer (Litster *et al.*, 2002).

In bumping regime (Figure 6.3a) the powder surface remains horizontal and the powder bed oscillates laterally up and down as the impeller blade passes below.

As the impeller speed is increased to above a critical level (determined by mass of powder, powder properties and mixer geometry (Ramaker *et al.*, 1998)) centrifugal forces exceed the gravitational forces on the powder and the powder mass enters the roping regime. This critical transition point is suggested to be specific to the process equipment (Nilpawar *et al.*, 2006). At impeller speeds marginally below the transition point the flow pattern exhibits hybrid flow with characteristics of both bumping and roping regimes (termed the 'transitional regime') (Tran *et al.*, 2006).

In the roping regime (Figure 6.3b) powder from the top surface of the toroid tumbles down the powder surface into the centre of the vessel, where it is then forced up the vessel walls (through conservation of mass). As the powder bed gets lifted by the blade it is more resistant to falling back and as a consequence material is continuously pushed upwards at the mixer wall (Nilpawar *et al.*, 2006). In this regime the entire mass of powder is in motion and circulating, thus suggesting a more even distribution of components within the powder mass and inherent improvements in mixing capabilities. The torus that forms can be characterised by its helical shape (Holm *et al.*, 1996, Schaefer *et al.*, 1993) due to a combination of two independent powder trajectories caused by centrifugal forces, impact forces and gravity. At too high an impeller speed the centre of the torus can become unstable and the flow failure is reached (Litster *et al.*, 2002).

The conditions that trigger a change in flow regime are not well understood. Several attempts have been made to determine what criteria are responsible for the flow regime change (Litster *et al.*,

2002, Remy et al., 2010b). Litster et al. (2002) described the transition point as a deviation from proportionality between the surface powder velocity and the impeller tip speed. At higher impeller speeds the proportionality between the two quantities is lost (Litster et al., 2002, Remy et al., 2010b).

Several methods exist for the analysis of powder flow, and rely on experimental measurement of surface powder velocities, the use of radioactive trackers, and computer modelling. The types and limitations of computer simulations are outlined in Section 2.3.7.

Powder velocity has been measured by several techniques; the two most common being the use of high speed video camera or laser to measure the velocity of the powder surface (Conway et al., 2005, Darelius et al., 2007a, Darelius et al., 2007b, Hosikian et al., 2010, Litster et al., 2002, Muguruma et al., 2000, Plank et al., 2003, Ramaker et al., 1998, Russell et al., 2003) and the use of a radioactive tracker (Parker and Fan, 2008, Parker et al., 2002, Parker et al., 2008, Seville et al., 2005). According to the work of Litster et al. (2002), the velocity of the powder on the surface of the bed is a function of impeller speed, mixing scale and fill level and increases linearly with an increase in impeller speed in the bumping regime, but is largely independent of impeller speed in the roping regime. In addition, the critical impeller speed at which flow regimes change has been found to be dependent on fill height, mixer scale, and powder type (Hosikian et al., 2010, Plank et al., 2003). Whilst helpful in determining properties of the powder flow, the measurement of powder velocities on the surface of the bed are not representative of the entire powder mass and only provide a 2-dimensional field of analysis. Processes such as Positron Emission Particle Tracking (PEPT) can be used to obtain 3-dimensional flow information and powder velocity data throughout a mixer (Knight et al., 2001, Stewart et al., 2001a, Wellm, 1997), as well as being able to study material motion (Forster et al., 2000). Further discussion on PEPT is provided in Section 6.1.4.

One of the most interesting advancements in flow analysis to come out of PEPT studies is experimental validation of the Levy flight theory, which relates to the chaotic motion of a single particle through a powder bed whilst in motion. Computer simulations of powder mixing rely on

chaos theory, which in powder mixing is essentially deterministic, but so complex that the system as a whole appears to behave chaotically. Such systems have to be studied empirically to discover patterns and gain understanding of their behaviour (Kaye, 1997c), and parameters can be applied to computer models to better simulate a realistic mixing process. As described in Section 2.3.4, the diffusional movement and convectional displacement of powder during mixing can be applied to a randomwalk theory of dispersion, which forms the basis of the Levy flight theory. A levy flight relates to the path that a given particle makes through the other material, and tracks both small and large leaps in all directions based on probability distributions (Figure 6.4).

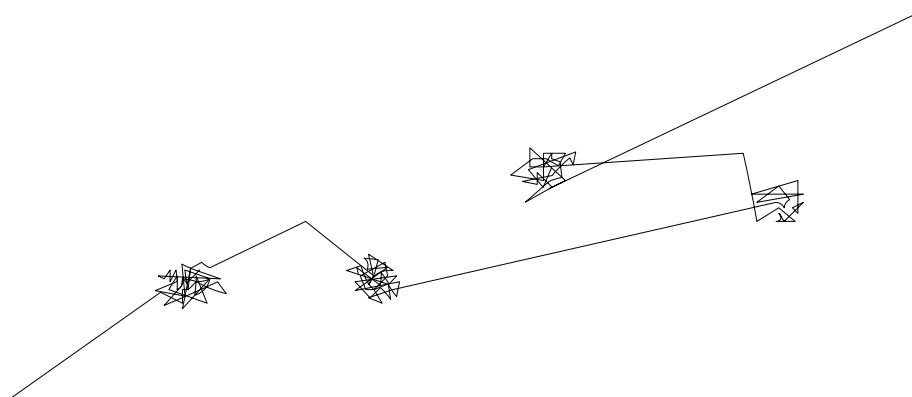


Figure 6.4: Schematic of Levy flight, which is a type of random walk in which large steps occasionally occur and is used in place of Brownian motion to explain the motion of particles within a powder bed.

For a randomwalk to be an exact Levy flight, the probability of steps of certain sizes should fit to a particular probability distribution (Mandelbrot, 1977). Techniques such as PEPT make it possible to identify probable Levy flights in a powder mixer and enable their use in predicting the overall intermingling of ingredients within the powder mixture (Kaye, 1993).

#### 6.1.4 Positron Emission Particle Tracking (PEPT)

As previously mentioned, Positron Emission Particle Tracking (PEPT) provides 3-dimensional information about powder flow throughout the entire mixing vessel and not just the powder surface, and allows for analysis of flow in non-transparent systems (Forrest *et al.*, 2003, Laurent, 2006, Lim *et al.*, 2003, Tran *et al.*, 2006). PEPT relies on the use of radioactive tracker particles (Parker and Fan, 2008) to map the 3-dimensional powder (or fluid) flow in a mixing process. The location of the

tracker particle is recorded at a series of time points by detecting its emissions using a positron camera and location algorithm. Tracker particles can be radioactively labelled by direct irradiation, ion-exchange or surface modification using  $^{18}\text{F}$ ,  $^{61}\text{Cu}$  or  $^{66}\text{Ga}$  radioisotopes. The most commonly used of these is Fluorine-18, which has a half-life of 109 min. It is produced from purified water via a reaction of  $^{16}\text{O}(^3\text{He},\text{p})^{18}\text{F}$  under direct bombardment using a 33 MeV  $^3\text{He}$  beam from a cyclotron (such as the one at the University of Birmingham, U.K.). Ideally for smooth tracking, the irradiated particles should be irradiated to between 300 and 1000  $\mu\text{Ci}$  (Parker and Fan, 2008). Their detection during powder blending relies on the generation of positrons ( $e^+$ ) through  $\beta^+$  decay of the radioisotope (Eqn. 6.2):



In this process, electron neutrino ( $\nu_e$ ) are also emitted. The positron then rapidly annihilates with an electron in the vicinity to give rise to a pair of 511 keV  $\gamma$ -rays emitted back-to-back (Eqn. 6.3):



The two gamma rays are simultaneously recorded in the two detectors and the trajectory of the two beams is determined through a location algorithm. From this the location of the tracker particle can be found to within the resolution of the camera (which is 0.6 mm at the University of Birmingham, U.K.) at the point in space where the two beams meet (Figure 6.5).

The location algorithm used to pinpoint the tracker calculates the point which minimises the sum of perpendicular distances to the various recorded trajectories (Parker and Fan, 2008), and discards all 'corrupt' recorded events which can provide a false location. Many of the corrupt recordings are only 'corrupt' in the sense that they relate to a future time step and are therefore involved in the determination of the next location. An explanation of the mechanics behind the location algorithm can be found in Parker and Fan (2008). The velocity of the tracker particle at any point in time is calculated from its location at over a series of weighted consecutive time periods. As the error

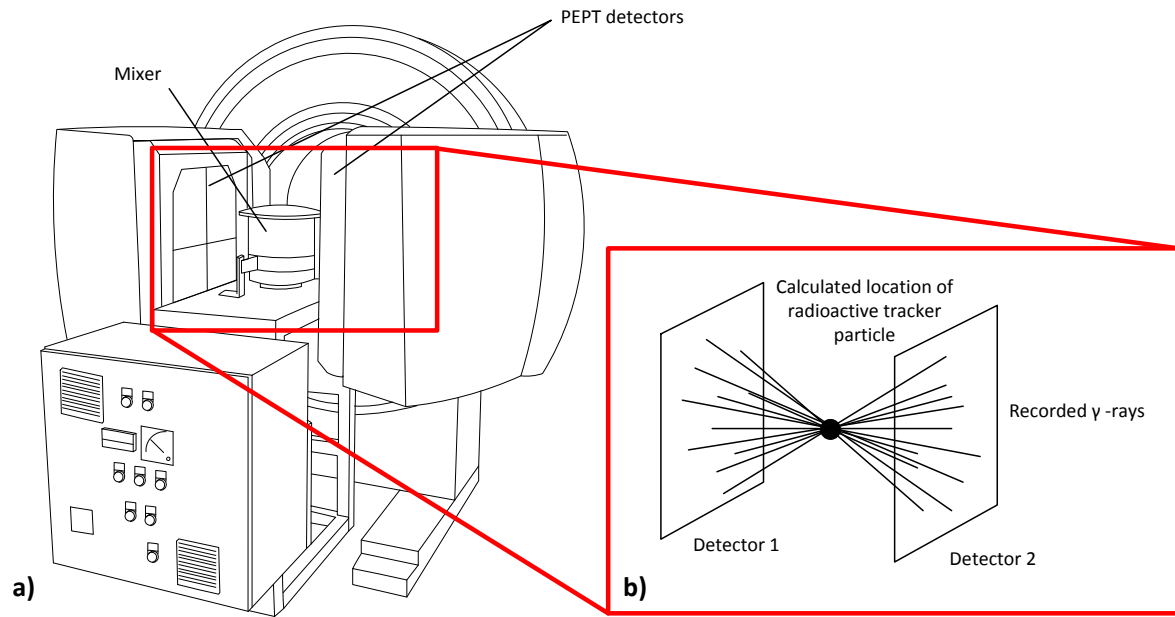


Figure 6.5: Diagram of Positron Emission Particle Tracker setup (a) and key principles in measurement (b).

associated with particle position measurement is significant, the velocity is not measured from only two points but rather 6 using the six-point method (Hare *et al.*, 2011) (Eqn. 6.4):

$$v_n = 0.1 \left( \frac{p_{n+5} - p_n}{t_{n+5} - t_n} \right) + 0.15 \left( \frac{p_{n+4} - p_{n-1}}{t_{n+4} - t_{n-1}} \right) + 0.25 \left( \frac{p_{n+3} - p_{n-2}}{t_{n+3} - t_{n-2}} \right) + 0.25 \left( \frac{p_{n+2} - p_{n-3}}{t_{n+2} - t_{n-3}} \right) + 0.15 \left( \frac{p_{n+1} - p_{n-4}}{t_{n+1} - t_{n-4}} \right) + 0.1 \left( \frac{p_n - p_{n-5}}{t_n - t_{n-5}} \right) \quad (\text{Equation 6.4})$$

Where  $v_n$  is the velocity at position  $p$  and time  $t$  for data point  $n$ . This method eliminates erratic results with large error that come from using two points only (Stewart *et al.*, 2001a). From this data the tangential velocity of the tracker particle can also be calculated (Eqn. 6.5):

$$v_\theta = v_x \sin(\psi_p) + v_y \cos(\psi_p) \quad (\text{Equation 6.5})$$

Where  $\psi_p$  is the angular location of the particle.

The ability of PEPT to assess the flow and velocity of powder during blending has been utilised in a variety of technologies such as:

- i. Fluidised beds (Chan *et al.*, 2010, Movahedirad *et al.*, 2014, Seiler *et al.*, 2008, Van de Velden *et al.*, 2008, Yang *et al.*, 2002).

- ii. Rotating drums (*Bbosa et al., 2011, Ding et al., 2002, Ding et al., 2001, Govender et al., 2011, Ingram et al., 2005, Kallon et al., 2011, Kuo et al., 2003, Lim et al., 2003, Malhotra et al., 1990, Sicalwe et al., 2011, van der Westhuizen et al., 2011, Volkwyn et al., 2011*).
- iii. Tumbling mixers (*Armstrong et al., 2010, Kuo et al., 2005*).
- iv. Stirred tanks (*Barigou, 2004, Stewart et al., 2001a, Stewart et al., 2001b, Wildman et al., 2000*).
- v. Cyclomix high-shear mixer (*Ng et al., 2007a, Ng et al., 2007b, Schutyser et al., 2003*).
- vi. Ploughshare mixers (*Forrest et al., 2003, Laurent, 2006, Laurent and Bridgwater, 2000, Laurent and Bridgwater, 2002a, Laurent and Bridgwater, 2002b, Laurent and Bridgwater, 2002c, Laurent et al., 2002d, Portillo et al., 2010*).
- vii. Vertical-axis high-shear mixers (*Knight et al., 2001, Saito et al., 2011a, Saito et al., 2011b, Saito et al., 2011c, Saito et al., 2011d, Tran et al., 2006*).

These results have provided insights into key flow mechanisms and types of mixing that can be achieved within mixers of various geometries and configurations. Of particular interest to this study however are the works that assess powder flow within vertical axis high-shear mixers. Within these studies, the two powder flow regimes (bumping and roping) have been shown to exist (*Knight et al., 2001*) and insights into their transitional criteria have been investigated (*Knight et al., 2001, Tran et al., 2006*). Also, the effects of different impellers on the powder flow profiles within a high-shear mixer have also been studied (*Saito et al., 2011a, Saito et al., 2011b, Saito et al., 2011d*). Average powder velocities within a high-shear mixer have been found to be within 10-30% of the impeller speed depending on the impeller geometry and powder fill in both dry powder (*Knight et al., 2001*) and wet granulation (*Plank et al., 2003*) mixing systems.

Whilst PEPT is a powerful tool for flow analysis, it is important to mention its limitations. One of the limitations of PEPT is that the flow profile of a very small number of particles is used to represent the flow profile of an entire powder mass. Due to the small number of particles used, PEPT analysis

needs to be conducted over a large time period to allow the tracker particles to be detected in every location of the mixer and enable analysis of the flow throughout the entire mixer. For this reason, only steady-state flow profiles can be effectively analysed. Typically with the use of a single tracker particle analysis needs to be conducted over at least 2 hours of mixing, and due to the half-life of the radioisotope, the frequency of events is considerably lower at the end of mixing compared to the start. Also, to obtain representative data points for the flow of all the powder, the tracker particle needs to be of the same size and density as the bulk of the powder. With current technology, up to three tracker particles can be measured simultaneously by giving each one significantly different radioactivity. This can allow for shorter mixing times and more thorough occupancy of the mixer by the particles but relies on the tracker particles remaining separated at all times (beyond the resolution of the camera) and is less precise than when using a single tracker. Also, current technology permits tracker particles down to 20  $\mu\text{m}$  to be detected however in practice (due to physical handling issues) they are limited to around 100  $\mu\text{m}$ .

### 6.1.5 Energy input

The shear dispersion force, which is described in Chapter 2, is process specific and affects the extent of drug de-agglomeration during blending. The level of shear dispersion applied to a blend is determined empirically and often applied violently and non-specifically in localised regions of the process vessel. Such uneven and intense local application of shear dispersion can damage and potentially “over-blend” particles, causing blend segregation and creating unstable surface regions (e.g. micro- and nano-fractures or amorphous domains) on particles, resulting in poor product performance. The effect of power and energy inputs to the blend on the dispersion and de-agglomeration of drug have been studied (*Adi et al., 2007, Hare et al., 2011, Kendall and Stainton, 2001, Knight et al., 2001*). In general, the power of the process dictates the degree of drug de-agglomeration and the energy input (which is a function of both the powder input and mixing time) dictates the degree of drug dispersion. This is due to the relatively low energy required to spread drug clumps through the bulk powder compared to the greater energy to overcome the cohesive

inter-particulate forces in an agglomerate. For this reason in weak mixing systems such as tumblers, it is possible to have a homogenous mixture with low intimacy (i.e. degree of de-agglomeration).

The power input to the powder can influence powder flow, blend kinetics and the rate of mixing. The power draw on the mixer (i.e. torque of the impeller) varies with both height and bevel angle of the impeller blades, and is approximately proportional to the mass fill and impeller speed (*Knight et al., 2001*). The power applied to the blend can be calculated through various means including measuring the mixer torque (*Bridson et al., 2007, Knight et al., 2001*) or power draw on the mixer (*Sirois and Craig, 2000*), or through first principles (*Iwasaki and Satoh, 2002, Knight et al., 2001*). In experimental studies using a high-shear mixer with a rotating impeller, the power input to the blend ( $P$ ) has been calculated from the measured torque with the following relationship (*Bridson et al., 2007, Knight et al., 2001*) (Eqn. 6.6):

$$P = \frac{2\pi FRN}{60} \quad (\text{Equation 6.6})$$

Where  $R$  is the inner radius of the mixer at the wall (meters),  $F$  is the measured force (Newtons) and  $N$  is the impeller rotation speed (rpm). Other techniques have been used to determine the power of a mixing system. This includes the derivation of torque from powder velocity and dimensionless parameters such as those in Section 2.3.7 (*Van den Ban, 2007*), and by measuring the difference in electrical current supplied to the mixer between being loaded and running empty (i.e. determining the power required to move the powder alone). The latter does not account for frictional losses and other factors that affect the blending outcome.

Once the power is determined, the total energy input to the blend can be calculated by integration over the mixing period (*Bridson et al., 2007*) (Eqn. 6.7):

$$E = \int_{t_1}^{t_2} P dt \quad (\text{Equation 6.7})$$

Equation 6.7 assumes that the power input is constant over the selected time period and start-up and shut down effects are negligible. This assumption is valid for dry, non-milling powder systems where mixing occurs over a large mixing time to establish steady-state.

Another useful term relating to the power of the impeller is its drag at a particular speed, which can be used to class and compare impellers with different geometries. The drag of an impeller as it rotates through a media (in this instance powder) can be represented by the dimensionless Power number (also known as the Newton Number), which relates resistance force to inertial force (Eqn. 6.8).

$$N_p = \frac{P}{\rho N^3 D_i^5} \quad (\text{Equation 6.8})$$

Where  $P$  is the power consumed in order to move the impeller at a set speed  $N$ ,  $\rho$  the density of the medium and  $D_i$  the impeller diameter. This equation is used in this study to categorise and distinguish impeller types.

#### 6.1.6 Use of iron oxide to measure uniformity and predict mixing kinetics

A thorough understanding of powder flow within a mixer can not only enable the right end point to be met consistently, but also improve the robustness of the process and prevent batch failures. Effective flow understanding not only relies on the velocity profiles within the mixer but also the energy applied to the powder during mixing and analysis of the extent of mixing.

Frequently, PEPT analysis is employed as a complimentary analysis tool, often utilising single values of an entire flow (such as the average velocity) coupled with an externally measured quantity such as impeller torque. Whilst mathematical means of predicting the extent of mixing have been proposed based on the instantaneous trajectory of the tracker particle (Jones *et al.*, 2007) and through 3-dimensional computer mixing simulations based on PEPT measurements (Kuo *et al.*, 2004, Seville *et al.*, 2005, Wildman *et al.*, 2008), they do not provide a simple and practical means for industry to assess blending ad-hoc. Also to date, no empirical comparison between content

uniformity and PEPT velocity profiles has been made in a high-shear mixer, nor is there any analysis of the degree of de-agglomeration based on powder flow.

Based on the findings from Chapter 4 it is proposed that the submicronised iron oxide tracer may not only be able to assess its degree and rate of dispersion and de-agglomeration through the bulk powder, but may also be able to assess and quantify content uniformity and energy input. As mentioned in Chapter 2, the rate of tracer mixing has already been investigated in a high-shear mixer (*Sugai et al., 1997*). The study found that each impeller speed and fill level showed similar rates of mixing but different end points. For impeller speeds up to 500 rpm, the mixing end points were found to be fairly similar, with a small increase in the extent of mixing with increasing blade speed. At 800 rpm a large increase in the extent of mixing was observed, suggesting that at very high speeds the degree of de-aggregation increases dramatically, as also observed in the studies of Chapters 4 and 8. A later study (*Iwasaki et al., 2006*) was also able to link the measured colour change to energy input, suggesting that perhaps it may also apply to the tracer used in this thesis.

Knowledge of levels and locations of energy and shear in a mixing system can not only improve mixer mechanistic understanding, but can also be utilised to refine current correlations used for process scale-up and improve knowledge of the location and severity of regions of little or no mixing (dead-zones) in a traditional batch bulk blending system. By coupling PEPT powder flow data with iron oxide tracer, it is thought that the tracer method can be extended and validated to include analysis of energy input and blend homogeneity, and provide basic flow kinetic understanding to systems without necessarily using PEPT.

## 6.2 Materials and Method

To test the use of the iron oxide tracer in quantitatively assessing content uniformity and energy input, as well as providing insight into powder flow; a variety of flow regimes, impeller speeds and impeller types were used. In total, a set of 12 experiments were constructed by altering the impeller types and speeds. Four impeller types were selected for this study; two bevelled edge impellers (duo-blade and tri-blade, both with a leading edge of  $11^\circ$ ), a flat-edge tri-blade impeller and a tri-blade impeller with raised and bent arms (*Figure 6.6*).

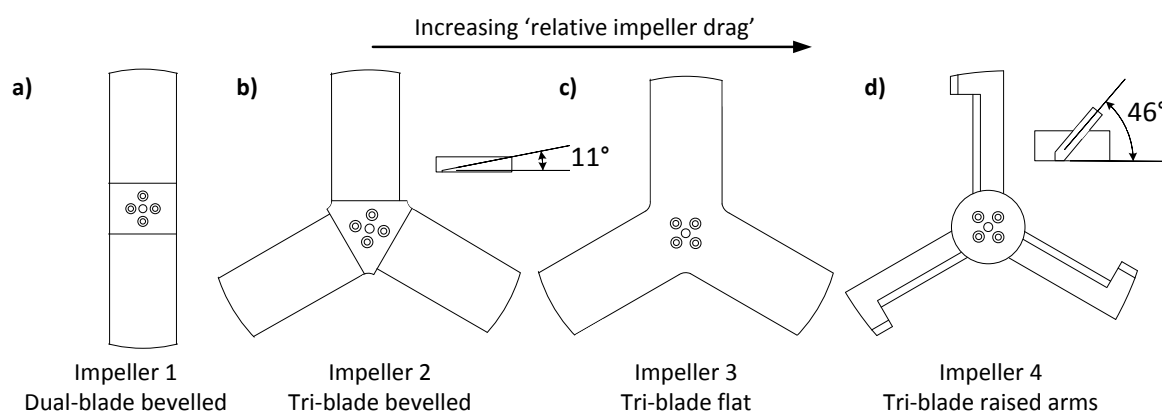


Figure 6.6: Diagram of Impellers used in this study: (a) dual-blade bevelled edge ( $11^\circ$ ), (b) tri-blade bevelled edge ( $11^\circ$ ), (c) tri-blade flat edge and (d) tri-blade raised and bent arms ( $46^\circ$ ).

Impellers are numbered 1-4 based on their increasing 'relative impeller drag' through the powder at a given speed. Using Equation 6.8, the following Newton (a.k.a. Power) numbers, which represent the drag coefficient of the impeller, have been calculated for each impeller type and speed (*Figure 6.7*). Calculations were made using cross-sectional areas from PEPT occupancy plots (*Section 6.3.4*) and power measurements from Section 6.3.3. For each impeller, the drag experienced at low speed (100 rpm) is an order of magnitude higher than at both 200 and 300 rpm, which is consistent with the resistance behaviour of powders (*Kaye, 1997a*).

A single scale 7 litre high-shear mixer was chosen (inner diameter 0.21m) to ensure that sufficient impeller arm length was achieved and radial effects of mixing could be observed. Each impeller type was mixed at 100, 200 and 300 rpm using 2kg of formulation comprising of standard lactose

(Lactohale LH200) with the standard tracer concentration (1 wt%). These powders were identical to those in previous chapters. The tracer was shipped to the U.K. for the experiments and the same grade of lactose (but a different batch number to the other studies) was supplied specifically for this study by DFE Pharma, Germany.

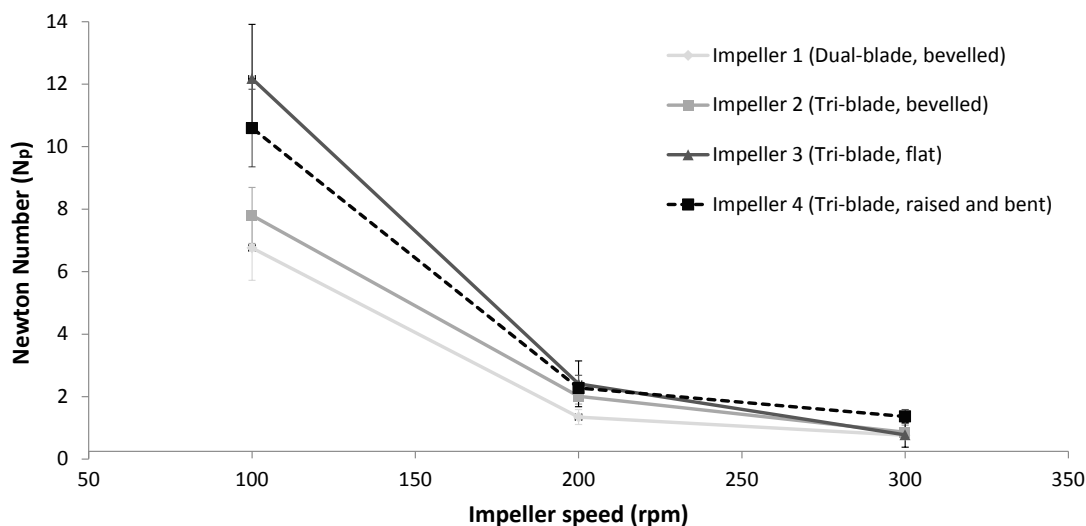


Figure 6.7: Newton number (impeller drag coefficient) for each impeller type at each mixing speed. Coefficients based on measurement of bed height and power from PEPT and torque data respectively.

### 6.2.1 PEPT experiments

PEPT tracker particles of 100  $\mu\text{m}$  were made by activating ion exchange resin beads (*DOWEX SBR ion exchanger, DOW Chemical Company, Belgium*), which reduced the risk of segregation with the bulk lactose (70  $\mu\text{m}$ ). De-ionised water was activated with  $^3\text{He}$  to generate  $^{18}\text{F}$ -isotopes from water molecules. A small amount of activated water (1-2 mL at 60-70 mCi) was transferred to a small glass vial and several resin beads placed in the water. The solution was then stirred with a centrifugal stirrer under a hot lamp until the water evaporated, leaving dry activated beads (150-300  $\mu\text{Ci}$ ). For each PEPT experiment a single labelled tracker bead was extracted. Measurements were recorded for each impeller type and speed within the PEPT for 120 minutes of continuous mixing to allow for the tracker particle to occupy all available spaces within the mixer. Results were analysed using "Track" (PEPT data analysis software developed at the University of Birmingham).

### 6.2.2 Colour measurements

An identical set of blends were made under the same conditions, but without the PEPT system, to analyse the change in blend colour over time; both in terms of different regions of the powder bed and the overall uniformity of the blend. The colour values of each blend were recorded in the CIE (1976) colour space using the spectrophotometer outlined in Chapter 3. Samples of blend were taken at sixteen cross-sectional regions of the powder (in accordance with the minimum number of sampling points outlined in Section 6.1.2) (*Figure 6.8*). Sampling was conducted by partitioning the powder bed between impeller blades with a metal partition and excavating the different regions in alphabetical order. The depth of sampling for each region was estimated by eye and coincided with a single scoop of the sampling ladle. Once colour data was obtained at a given time point, each sample was returned to the vessel gently to minimise mixing during sampling. Colour values were recorded at the time intervals used in Chapter 4 and using the method outlined in Section 3.2.2. Average values of  $L^*$ ,  $C^*$  and  $h$  at each time point were taken from all 64 measurements (i.e. from four measurements at each of the sixteen regions in the bed).

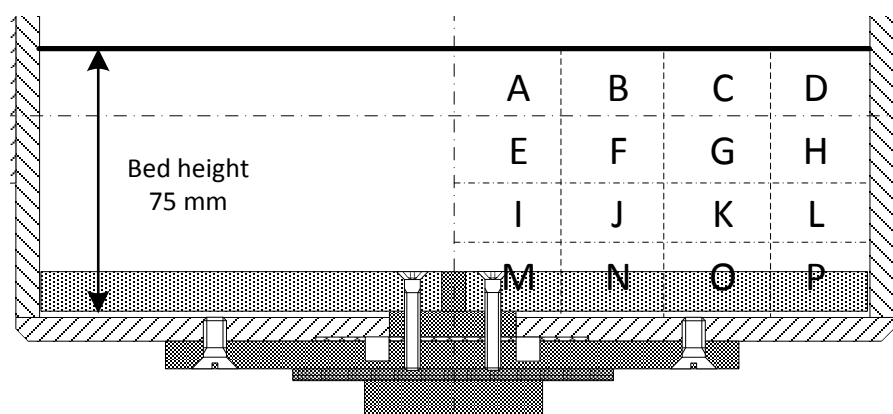


Figure 6.8: Sampling scheme for colorimeter measurements. 16 cross-sectional regions of powder (A-P) were sampled for blend colour at 15 set time intervals for each blend. A metal partition was used to enable sampling of a wedge of the powder.

### 6.2.3 Power and energy input measurements

Force (or torque) measurements were taken alongside colour measurements using a pressure transducer attached externally to the mixer frame. The mixing bowl was placed on a ring of bearings

and was free to rotate into the transducer as the powder resisted the impeller movement. A protruding arm on the mixer impacted with the transducer causing a voltage to be read (Figure 6.9).

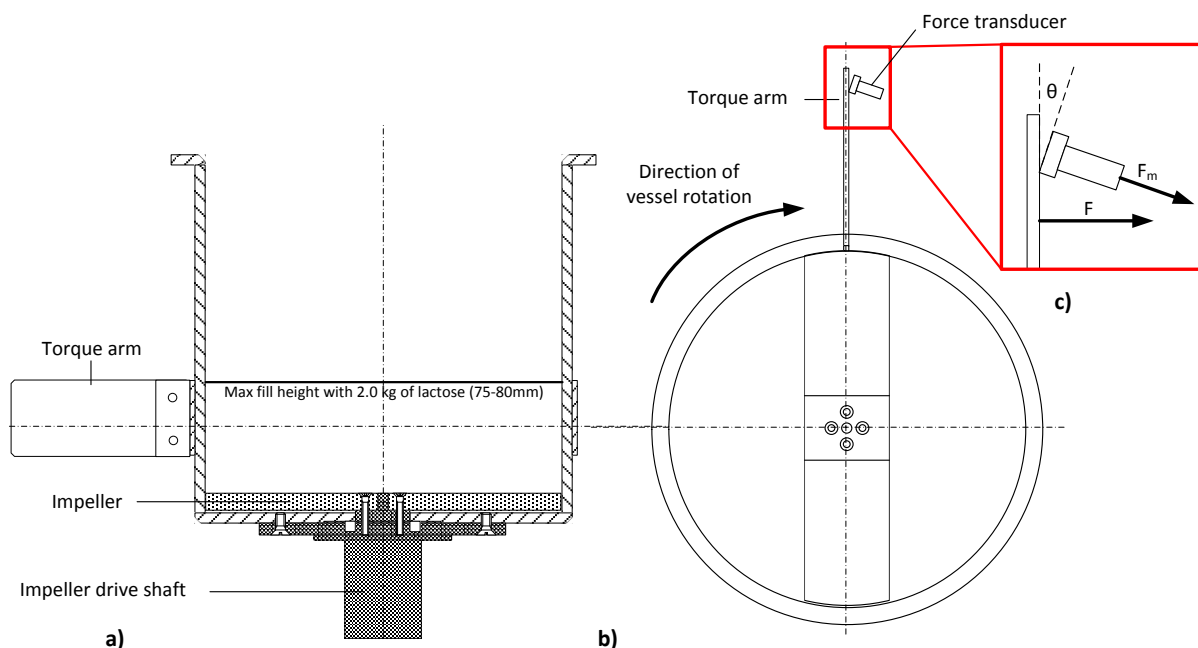


Figure 6.9: Schematic of mixing vessel showing torque arm a), rotation of vessel and interaction with force transducer b), and schematic showing key parameters for calculation of energy input to the blend c).

As the torque arm pushes on the transducer at a non-tangential angle ( $\vartheta$ ) (Figure 6.9c), a correction factor is required for the actual force applied by the arm ( $F$ ) versus the measured force on the transducer ( $F_m$ ) (Figure 6.9c) (Eqn. 6.9):

$$F = \frac{F_m}{\cos(\theta)} \quad (\text{Equation 6.9})$$

The reading of the force transducer ( $\gamma$ ), which is in arbitrary units, is linearly related to the measured force (Eqn. 6.10):

$$F_m = G[\gamma - \gamma_0] \quad (\text{Equation 6.10})$$

Where  $G$  is the transducer gain and  $\gamma_0$  is the baseline reading of the meter. The transducer gain was determined experimentally from calibration with weights of known mass. Incorporating Equations 6.5, 6.8 and 6.9 provides an equation for determining the power of the mixer (Eqn. 6.11).

$$P = \frac{2\pi G[\gamma - \gamma_0]}{60 \cos(\theta)} RN = \left( \frac{\pi RG}{30 \cos(\theta)} \right) [\gamma - \gamma_0]N = A[\gamma - \gamma_0]N \quad (\text{Equation 6.11})$$

Substituting coefficients for a transducer with a gain of 0.0464, angle from torque arm of 18.73°, and mixer radius of 0.21 m, provides the final equation for calculation of power transferred to powder (Eqn. 6.12):

$$P = \left( \frac{\pi \times 0.21 \times 0.0464}{30 \times 0.9470} \right) [\gamma - \gamma_0]N = 0.00108[\gamma - \gamma_0]N \quad (\text{Equation 6.12})$$

The energy input is then simply related to the time integration of power (Eqn. 6.6) (Bridson *et al.*, 2007). On the assumption that the power input is constant over a given time period and there are no start-up/shutdown effects, this equation can be further simplified (Eqn. 6.13):

$$E = \int_{t_1}^{t_2} P dt = P[t_2 - t_1] = 0.00108[\gamma - \gamma_0][t_2 - t_1]N \quad (\text{Equation 6.13})$$

For measurements of energy input, the gain (Eqn. 6.9) was calculated from the mean readings during and between mixing steps (i.e. for  $\gamma$  and  $\gamma_0$  respectively).

## 6.3 Results

A vast amount of information can be drawn from the complimenting colour and PEPT measurements that were taken in this study, and as such, require several sections. The results have been split into subsections that reflect the type of analysis; namely observational (Section 6.3.1), colour (Section 6.3.2), torque (Section 6.3.3) and PEPT (Section 6.3.4).

### 6.3.1 Visual observations in powder flow for each impeller type and speed

Prior to colour and PEPT analysis, each impeller was tested at impeller speeds varying from 40 rpm to 410 rpm to select suitable conditions for the main experimental set that would provide a wide

range of flow profiles, both in the bumping and roping regimes. Observed flow types were classed into four main categories and twelve sub-categories, which were based on the two fundamental flow regimes of bumping and roping (*Table 6.1*). Each type of powder flow regime is assigned a colour based on intensity, with yellow being the weakest and red the strongest.

**Table 6.1: Flow classifications used to assess impeller types and operating speed. Colours indicate the relative intensity of mixing, with yellow being the weakest flow regime and red the strongest.**

Flow class	Regime	Description
Bump 1	Bumping	Wave bumping (very slow almost see shape of impeller under powder)
Bump 2		Strong and quick waves, not quite established bumping
Bump 3		Clear bumping of powder, no observable rotation on surface
Trans 1	Transitional	Bumping with slight rotation
Trans 2		Half roping-half bumping transitional
Trans 3		Almost roping, little bit of bumping
Rope 1	Roping	Clear roping of powder
Rope 2		Strong roping flow, good solid vortex
Rope 3		Very strong roping, powder apex away from mixer walls
Unst. 1	Unstable	Violent roping, superimposed wave forming on surface near walls
Unst. 2		Unstable flow, centre of vortex continuously changing
Unst. 3		Ultra unstable flow, expulsion of powder from mixer

Using the flow classification system in *Table 6.1*, the flow types were observed by eye and recorded for each set of impellers and impeller speeds (*Table 6.2*). For impeller speeds below 140 rpm, flow patterns were observed to be independent of impeller type. At higher impeller speeds however, the comparative flow patterns for a given impeller speed became increasingly varied, with the raised and bent tri-blade impeller exhibiting a very narrow transitional flow band (not observed at the speeds selected) and reaching flow failure at speeds greater than 350 rpm. At this speed, large quantities of powder were been ejected from the vessel. Little difference was observed in flow patterns between the bevelled duo- and tri-blade impellers, suggesting that the inclusion of a third bevelled blade made little difference to the bulk flow of material in the vessel. When comparing the

Table 6.2: Observed flows for different impellers and impeller speeds. Selected speeds for main body of work are highlighted by boxes. Colours indicate the relative intensity of mixing, with yellow being the weakest flow regime and red the strongest.

Observed flow classes		Impellers			
		Dual-blade Bevelled, 11°	Tri-blade Bevelled, 11°	Tri-blade Flat	Tri-blade Raised and bent, 46°
Impeller speed (rpm)	40	Bump 1	Bump 1	Bump 1	Bump 1
	70	Bump 2	Bump 2	Bump 2	Bump 2
	<b>100</b>	<b>Bump 3</b>	<b>Bump 3</b>	<b>Bump 3</b>	<b>Bump 3</b>
	140	Tran 1	Tran 1	Tran 2	Rope 1
	170	Tran 2	Tran 2	Tran 3	Rope 2
	<b>200</b>	<b>Tran 3</b>	<b>Tran 3</b>	<b>Rope 1</b>	<b>Rope 3</b>
	240	Tran 3	Tran 3	Rope 2	Unst 1
	270	Rope 1	Rope 1	Rope 2	Unst 2
	<b>300</b>	<b>Rope 2</b>	<b>Rope 2</b>	<b>Rope 3</b>	<b>Unst 2</b>
	350	Rope 2	Rope 2	Rope 3	Unst 3
	380	Rope 3	Rope 3	Unst 1	-
	410	Unst 1	Rope 3	Unst 1	-

effect of a bevelled edge on flow profile (compared to flat blade), the flat tri-blade impeller exhibits more developed flow to its bevelled counterpart for a given impeller speed greater than 100 rpm.

### 6.3.2 Colour tracer results

The spread of colour tracer throughout the blend increases with increased mixing time. This corresponds to an increase in the measured hue ( $h$ ) and hue saturation ( $C^*$ ), and improved consistency of colour throughout the blend (*Figure 6.10*).

For low mixing times ( $\sim 0.5$ -1 min at 100 rpm) rich pockets of tracer can be found in a sample that is predominantly white (*Figure 6.10a*). At moderate mixing times ( $\sim <10$  min at 100 rpm) there are still tracer hotspots, however they are typically smaller and more spread through the collected sample (*Figure 6.10b*). At high mixing times ( $>10$  min) each and every sample appears by eye to be uniform in colour, and the blend as a whole is uniform (*Figure 6.10c*). As the colour measurement method outlined in Chapter 3 is a bulk analysis method, it is unable to identify tracer hotspots but rather records the sample as a single colour. Unevenness in the blend however can be detected by measuring the deviation between samples and is investigated in this section.

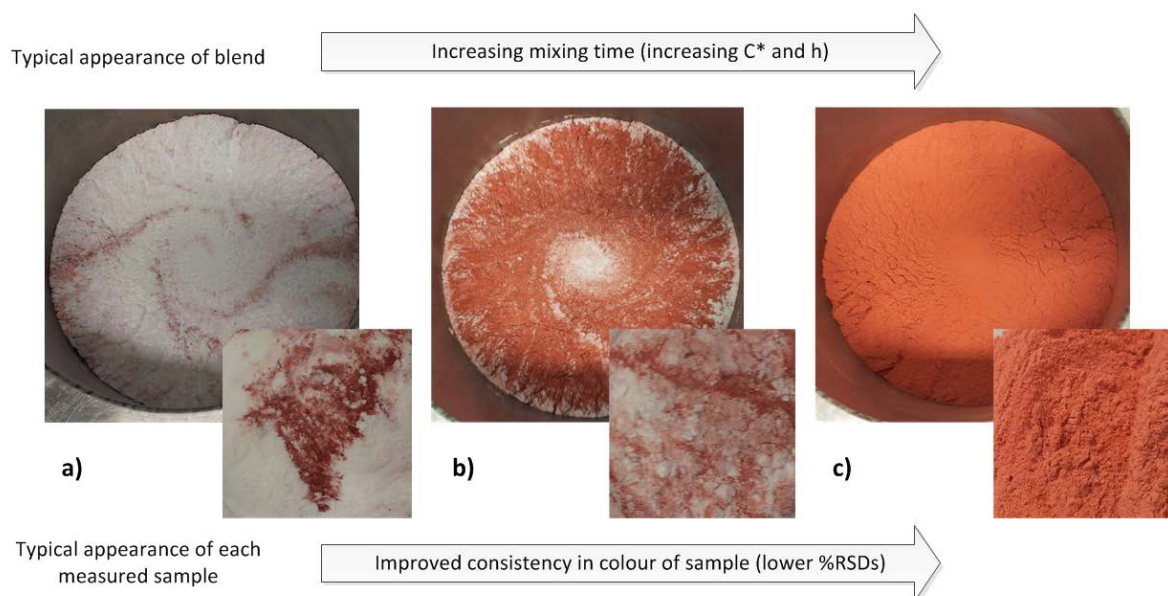


Figure 6.10: Typical appearance of overall blend and collected samples for low (a), moderate (b) and high (c) mixing times. Intensity or colour and consistency between samples improved with increasing mixing time.

### 6.3.2.1 Shape of formulation curves in CIE colour space

As with previous studies, the degree of tracer dispersion and de-agglomeration can be quantified through assessment of the blend's hue intensity (Chroma,  $C^*$ ) and hue (hue angle,  $h$ ) respectively. By taking the average degrees of dispersion and de-agglomeration across all sixteen samples at each time point, a series of blend curves can be constructed (Figure 6.11).

All blend curves appear to fall onto a common line, meeting up with one another at large degrees of dispersion and de-agglomeration. Unlike the blend curves in Chapter 4 which overlapped for a given formulation, the blend curves in this study deviate from one another at low degrees of dispersion and de-agglomeration, which is caused by discrepancies between individual measurements at a given time point. Standard deviations for the average colour values have been left out for clarity, but are discussed in the following subsection (Section 6.3.2.2). Quite often for low mixing times, and in particular with low impeller speeds, blends are observed to not be uniform and thus have high standard deviations in the mean values of the blend. As blending progresses, the uniformity of the

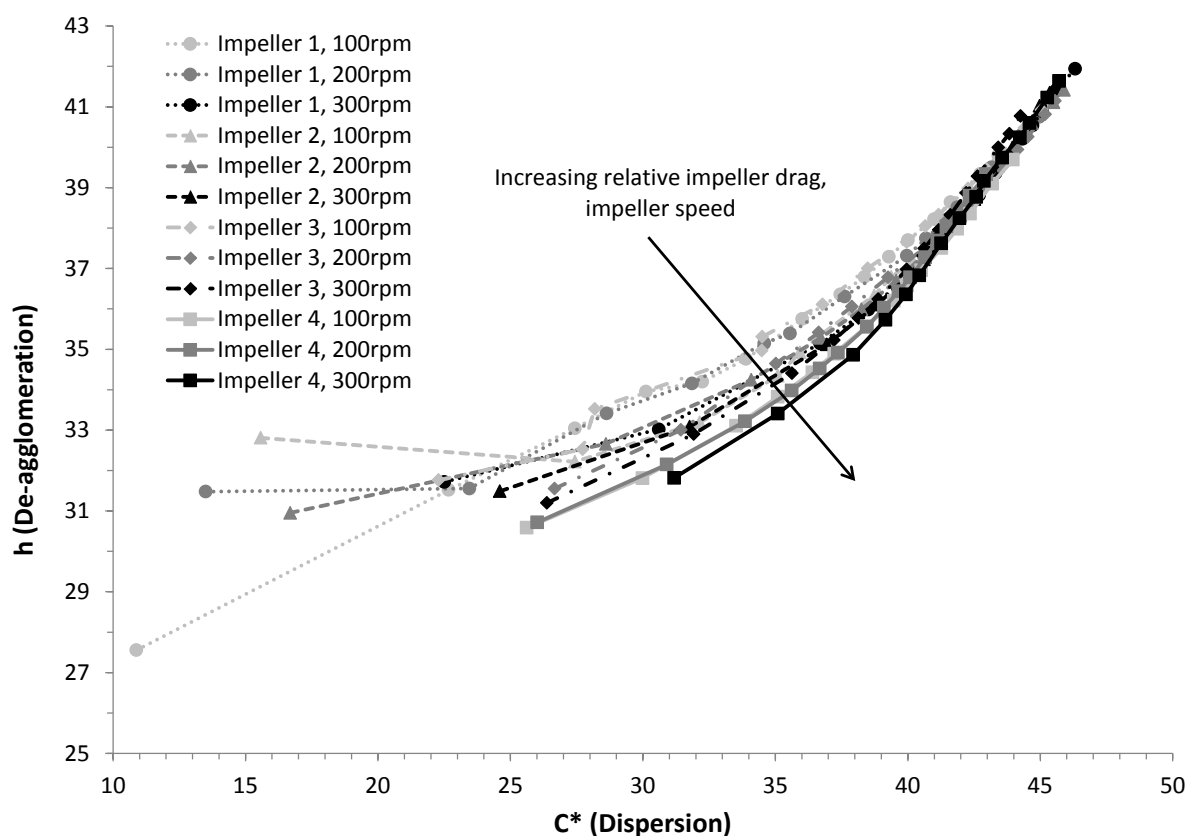


Figure 6.11: Progression of mean degree of dispersion ( $C^*$ ) and de-agglomeration ( $h$ ) for each impeller and operating speed.

blend increases and thus the blend curves overlap as observed in Chapters 4 and 5. For values of  $C^*$  less than  $\sim 42$ , process curves deviate further from one another with decreasing levels of 'relative impeller drag'. For instance, a dual-blade impeller imparts less energy to the system than a geometrically similar tri-blade impeller, and that more energy is imparted on a system with increasing 'front face area' of the blade in relation to the powder.

Colour curves generated exhibit the same shape as those from previous studies, with no obvious deviations between curves at high de-agglomeration and dispersion. This suggests that no milling or segregation occurred during the mixing process. Each blend curve deviates from the blend curve for Impeller 4 at 300 rpm (Figure 6.11), which represents the system with the highest relative impeller drag and highest blend progression. This curve aligns with the formulation curve results in Chapter 4, and is discussed and compared in Section 6.4.1. The deviation of blend curves from one another at low  $C^*$  and  $h$  are within the standard deviation of the mean values displayed, and serve as an

indicator of uniformity for a given formulation, with standard deviations decreasing at higher values of  $C^*$  and  $h$ . As the curves generated by Impeller 4 are the closest to those generated in previous work, the deviation of other curves can be used to represent their relative deviation in content uniformity in both dispersion and de-agglomeration. In the  $C^*$ - $h$  plane, it would appear that content uniformity can be improved by increasing the relative impeller drag and/or operating speed.

The assumption of no milling is further backed by the  $L^*$ - $C^*$  plane, which shows no sharp increase in blend lightness at a high degree of dispersion (Figure 6.12), which were previously observed in Chapter 4.

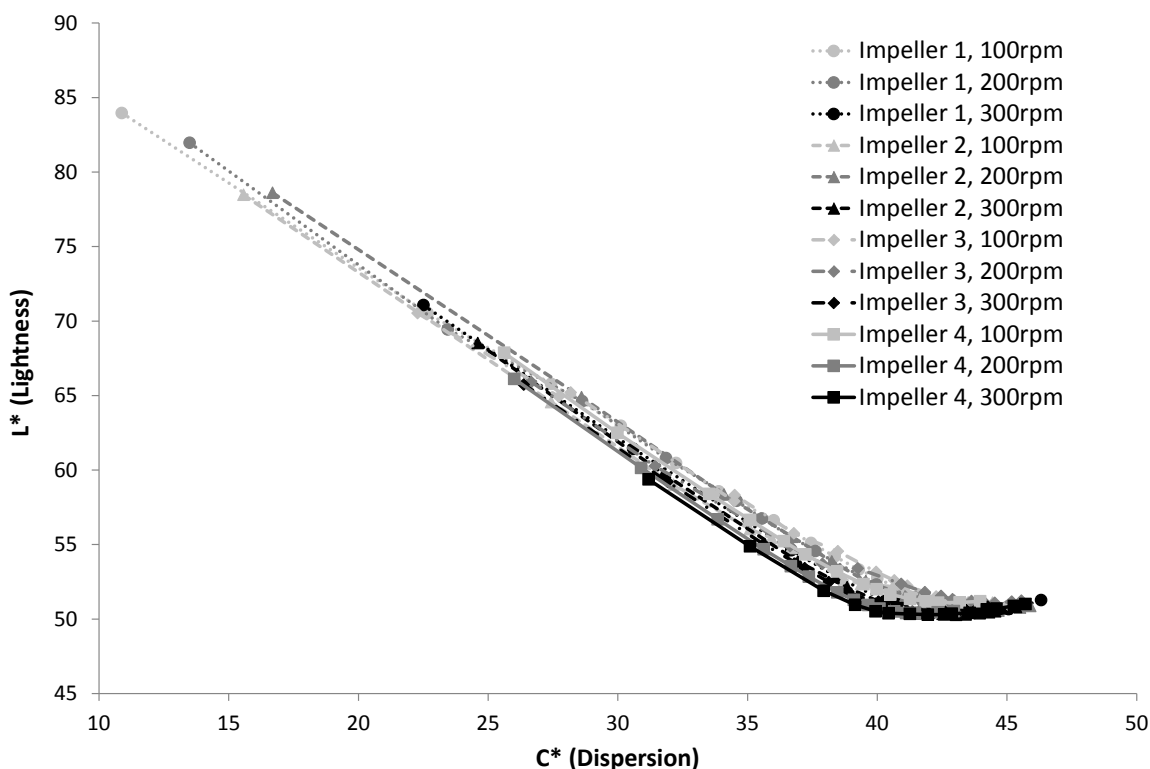


Figure 6.12: Comparison of mean blend lightness ( $L^*$ ) and the degree of dispersion ( $C^*$ ) for each mixing condition. Blend curves suggest no change in formulation due to milling/particle damage.

The deviation of blend curves from one another is identical in the  $L^*$ - $C^*$  plane to the  $C^*$ - $h$  plane, however the disparity between blend curves is less visible. Blend curves hold the same shape as those in previous chapters, suggesting dispersion-dominant and de-agglomeration/dispersion mixing.

### 6.3.2.2 Errors in formulation curves

The deviation between each of the sixteen colour samples at each time point decreases as the hue and hue intensity increase. It is important to note that the sensitivity of the spectrophotometer allows for analysis of %RSDs down to 0.4% (conservatively and in respect to  $C^*$ ). Below this, values cannot be significantly distinguished from the background of measurements (which occurs at 0.1 %RSD) and are considered to be uniform. Therefore, values below the limit of analysis (LoA, 0.4% RSD) are considered to have maximum measurable uniformity and actual values are disregarded. This can be seen in the case of Impeller 4 in respect to the relative standard deviation in  $C^*$  (Figure 6.13).

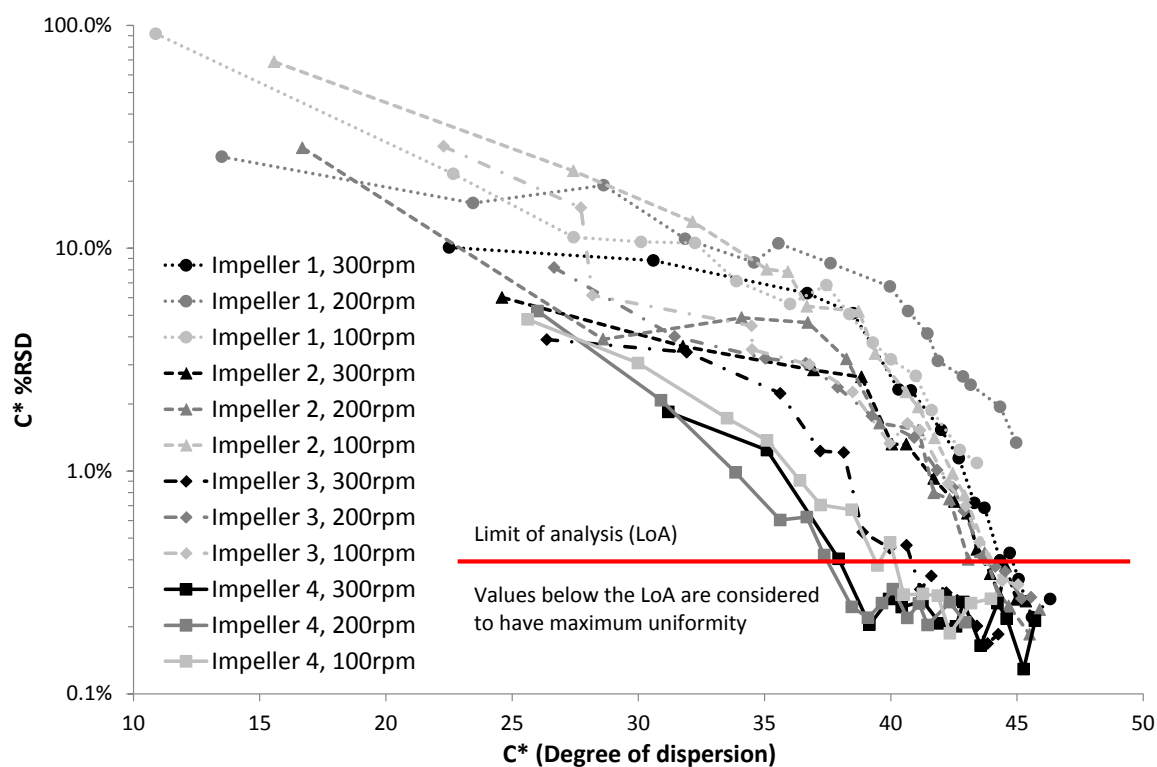


Figure 6.13: Comparison of Relative Standard Deviation (RSD) to mean value for degree of dispersion ( $C^*$ ). %RSD decreases as mean degree of dispersion increases.

Indeed, with increasing hue intensity, the relative standard deviation between samples for a given time point decreases. Impeller 4 blends are observed to reach uniformity at values of  $C^*$  greater than  $\sim 38$ , with blend curves of Impellers 2 and 3 following suit at values of  $C^*$  greater than 45. At high  $C^*$  however, Impeller 1 blends at speeds below 300 rpm (i.e. at 100 and 200 rpm) do not reach

uniformity. This is most likely due to the lack of intensity from having only 2 blades on the impeller. These results indicate that  $C^*\%RSD$  is sensitive enough to be used to quantify uniformity and differentiate between blends, and that there is a loose correlation between  $C^*$  and content uniformity. Analysis of content uniformity is provided in Section 6.3.2.3.

Similarly to hue intensity, there is a limit to the measurement of the relative standard deviation of the hue and blend lightness beyond the background of the spectrophotometer. In the case of the blend's hue, any  $\%RSD$  below 0.2% is considered to not have significant resolution above the background (which is 0.05% for hue) (Figure 6.14). For blend lightness the limit of analysis is similar to hue intensity at approximately 0.4%.

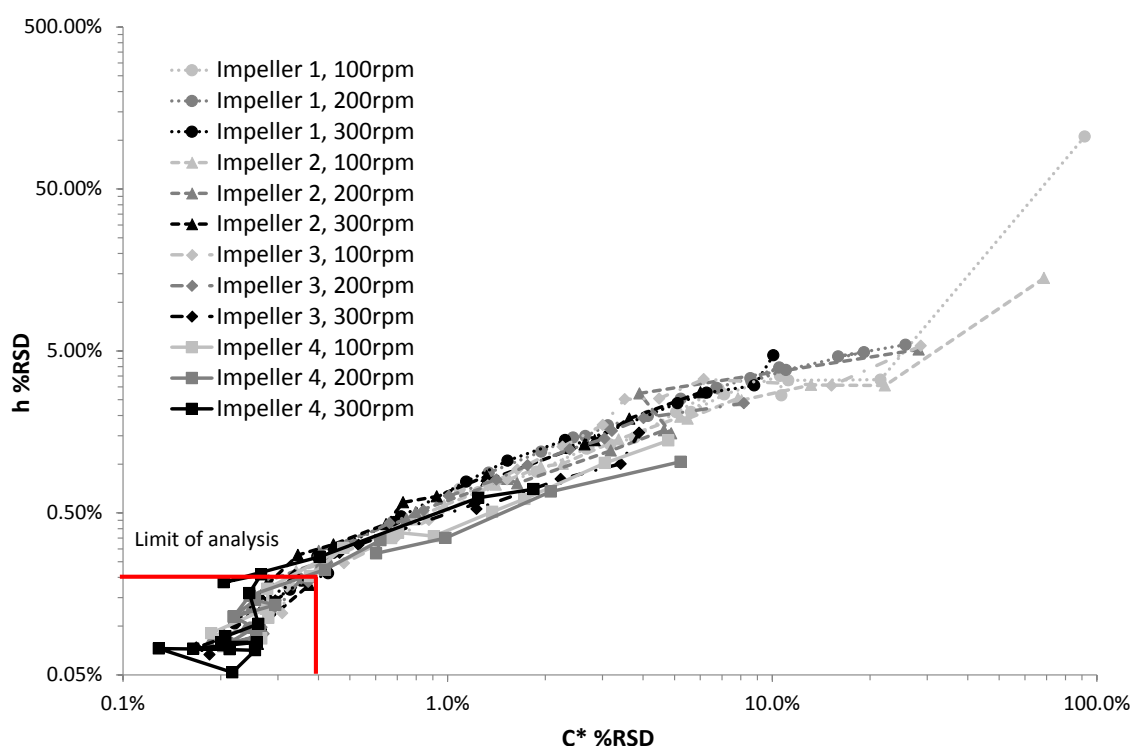


Figure 6.14: Correlation between the relative standard deviation of hue and hue intensity.

The  $\%RSD$  of all values in the CIELCH colour space decrease with increased mixing, and are understandably linked to the uniformity of the blend, as poor uniformity leads to high deviation between sample measurements. For instance, the  $\%RSD$  of hue and hue intensity can be seen to be linked with one another and hence the blend uniformity.

### 6.3.2.3 Measurement of content uniformity and rate of mixing

As mentioned in Section 6.1.2, content uniformity is typically assessed by measuring the deviation of powder composition between samples. In the case of a coloured tracer, where blend homogeneity is defined by the spread (dispersion) of tracer and not its breakup (de-agglomeration), this can be achieved by calculating the relative standard deviation (%RSD) of tracer dispersion (i.e. %RSD of  $C^*$ ).

To better quantify content uniformity and enable thorough blend analysis, RSDs of dispersion were analysed as a function of blend time (Figure 6.15).

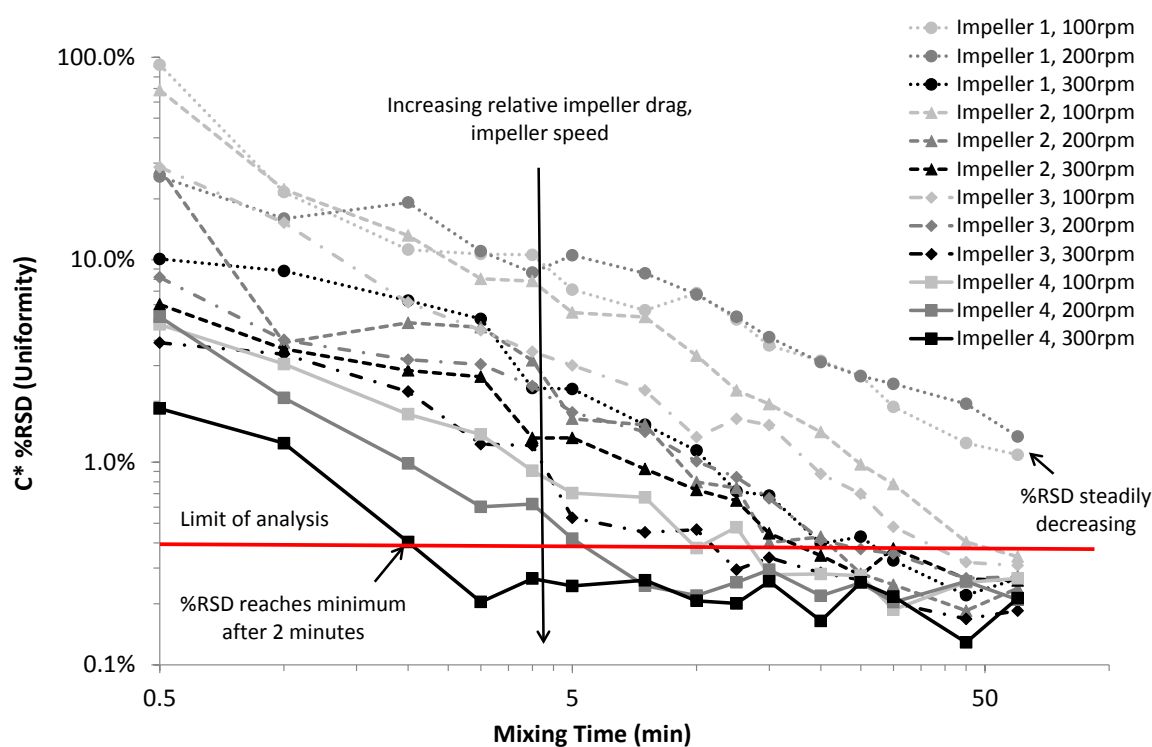


Figure 6.15: Content uniformity of blends ( $C^*$  %RSD) over time.

As expected, the uniformity of the blend improves over time, with all but two of the blends reaching a maximum uniformity (i.e.  $\leq 0.4$  %RSD) over the 60 minutes of mixing. At a given mixing time, blend uniformity increases with increasing relative impeller drag and impeller speed. It is also evident that some configurations (particularly those with low relative impeller drag and impeller speed) are incapable of reaching uniformities that can be achieved by other configurations. This highlights the importance in selecting the right mixing system to achieve the desired blend properties.

The rate of mixing (*RoM*) can be analysed through the rate of change in the content uniformity of the blend with respect to time. In this study, the instantaneous *RoM* at each time point has been approximated to the change in blend uniformity with each change in total mixing time (Eqn. 6.14).

$$RoM = \frac{\partial(C^* \%RSD)}{\partial t} \approx \frac{\Delta(C^* \%RSD)}{\Delta t} = \frac{[(C^* \%RSD)_2 - (C^* \%RSD)_1]}{[t_2 - t_1]} \quad (\text{Equation 6.14})$$

Using this method, the rate of mixing is plotted against mixing time to compare impeller types and operating conditions (Figure 6.16).

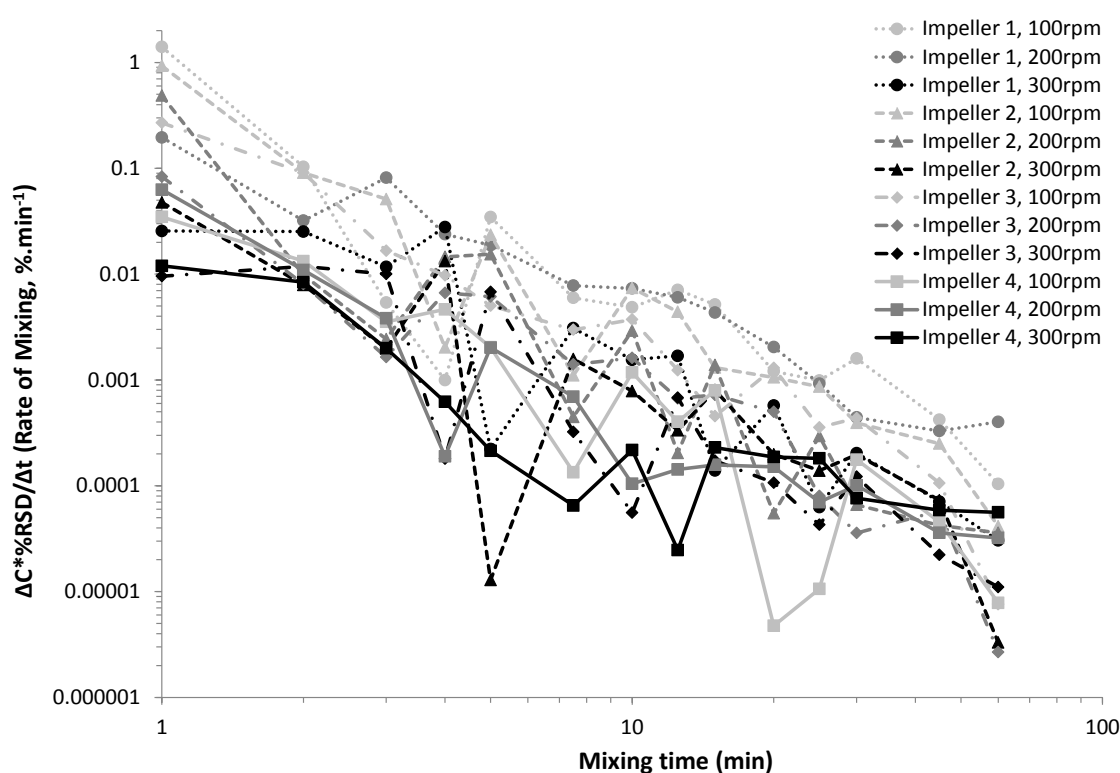


Figure 6.16: Rate of Mixing (*RoM*) for all blends compared to mixing time.

The rate of mixing is different for each system, decreasing over time as blends reach the maximum limit of measurable content uniformity. The initial and time-specific rates of mixing vary between blends, with systems with a higher relative impeller drag and impeller speed typically showing a smaller initial rate of mixing. This is to be expected given that these systems reach a greater uniformity after a given period of mixing and are inherently closer to their maximum limit. Whilst rates are different between blends at each mixing time, the proportional change in the rate of

mixing (i.e. the slope of each curve in Figure 6.16 on the log-log plot) appears to be fairly constant between blends, suggesting that the same fundamental mechanisms for the spread and breakup of tracer are prevalent for the particular parameters used in this study (e.g. speed, impeller type, etc.).

This notion of similar fundamental tracer mixing mechanisms can also be seen in the degree of de-agglomeration over mixing time (Figure 6.17), as indicated by the change in hue ( $h$ ).

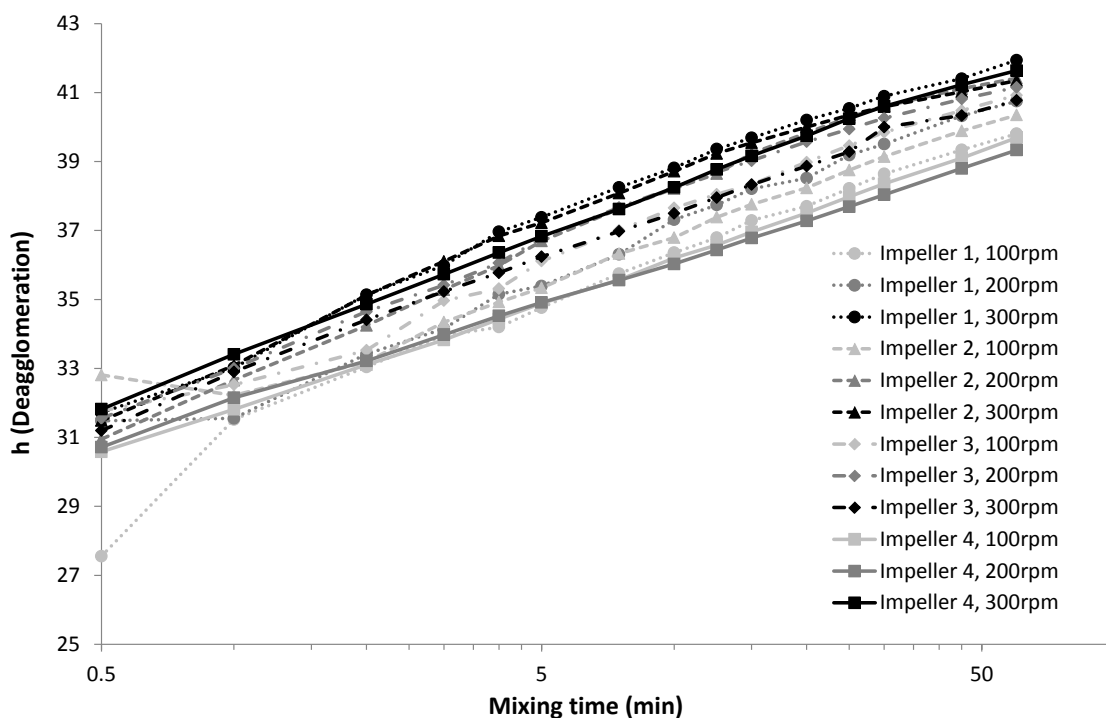


Figure 6.17: Degree of tracer de-agglomeration for all blends versus mixing time.

Each blend shows a logarithmic increase in de-agglomeration over time (shown as a straight line in Figure 6.17), with the degree of de-agglomeration increasing with increased relative impeller drag and impeller speed. This suggests that with a higher mixing intensity, a larger amount of tracer is de-agglomerated. Whilst the degree of de-agglomeration achieved varies at each mixing time, the rate of de-agglomeration (i.e. the slope of each curve in Figure 6.17) is virtually identical between blends, exponentially decreasing over time (Figure 6.18).

As shown in Figure 6.18, the rate of de-agglomeration is higher during the initial stages of mixing, and decreases sharply within the first minute as the formulation consolidates to a rate of

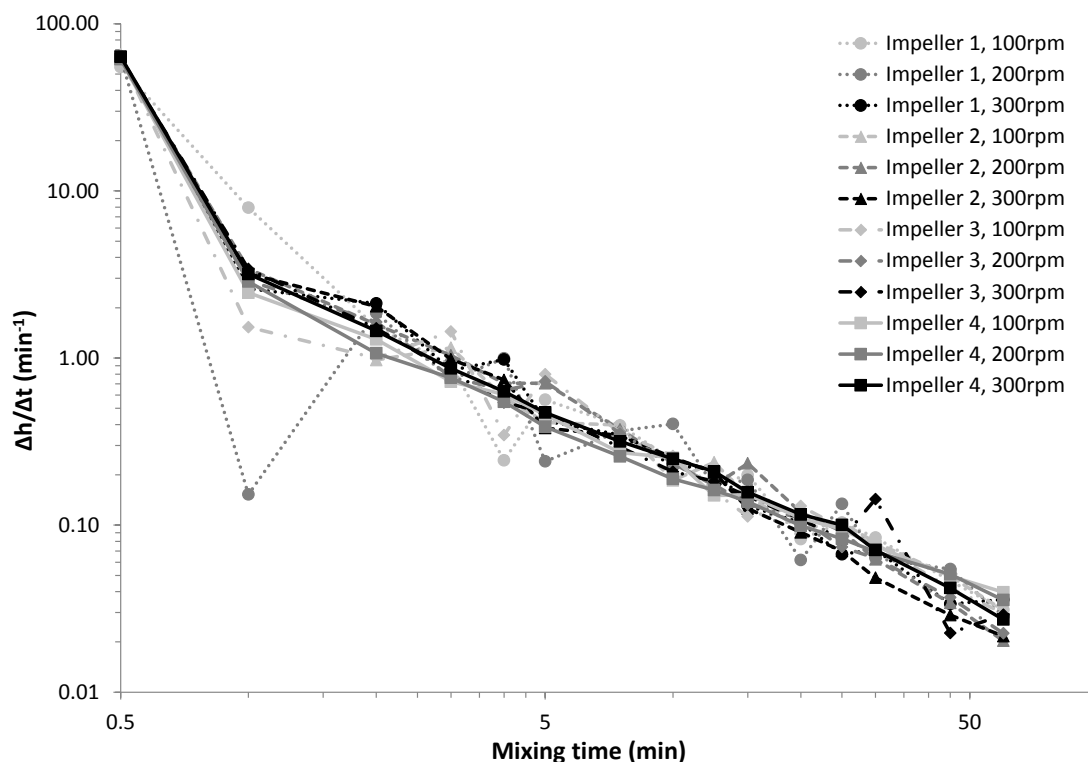


Figure 6.18: Rate of de-agglomeration for each blend over mixing time

deceleration that is independent of both impeller type and speed. As there appears to be no influence of mixing intensity or powder flow regime on the rate of de-agglomeration (unlike with the rate of mixing), it can only be assumed that the de-agglomeration mechanism is dependent on the powder properties themselves. As a single formulation was used in this study, this may account for the identical rates of de-agglomeration across all impeller types and speeds. This theory is further tested against different formulations from other chapters in Chapter 8.

#### 6.3.2.4 Regional changes with different flow regimes

Whilst analysis of the average colour values for each blend can provide insight into content uniformity and rates of mixing, predictions about flow behaviour can be made from analysis of all sixteen sampled regions at each time point. Figures 6.19-6.26 show the progression of blend hue and hue intensity for each cross-sectional region in the blend at each mixing time point. Due to the scale of scrutiny in colour measurements it is difficult to show the unevenness in colour within a single sample. Flow classes from Section 6.3.1 have also been included to assist comparison of colour curves to powder flow.

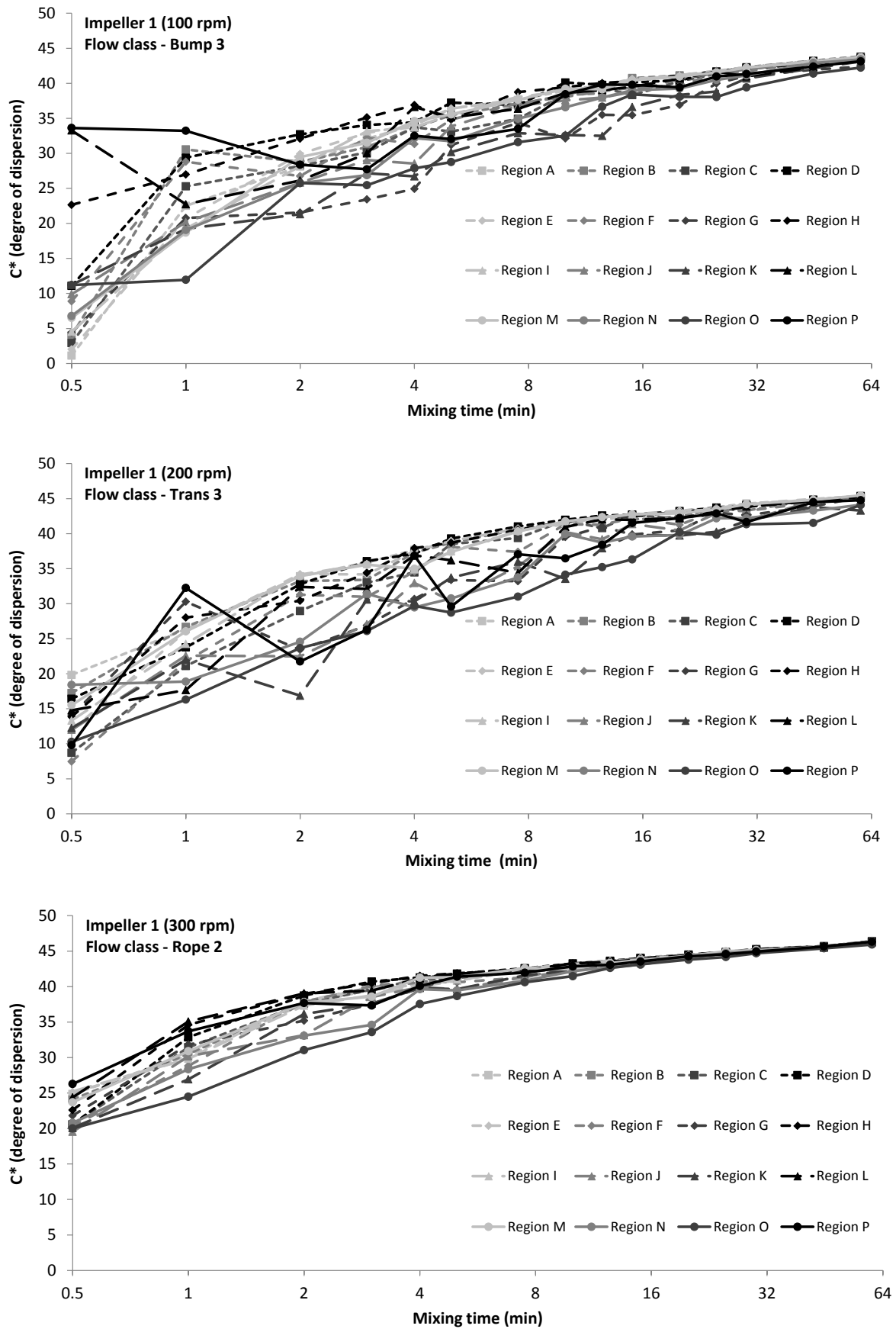


Figure 6.19: Regional blend hue intensities for Impeller 1 at 100, 200 and 300 rpm, showing disparity of the amount and spread of tracer through the powder bed at low mixing times.

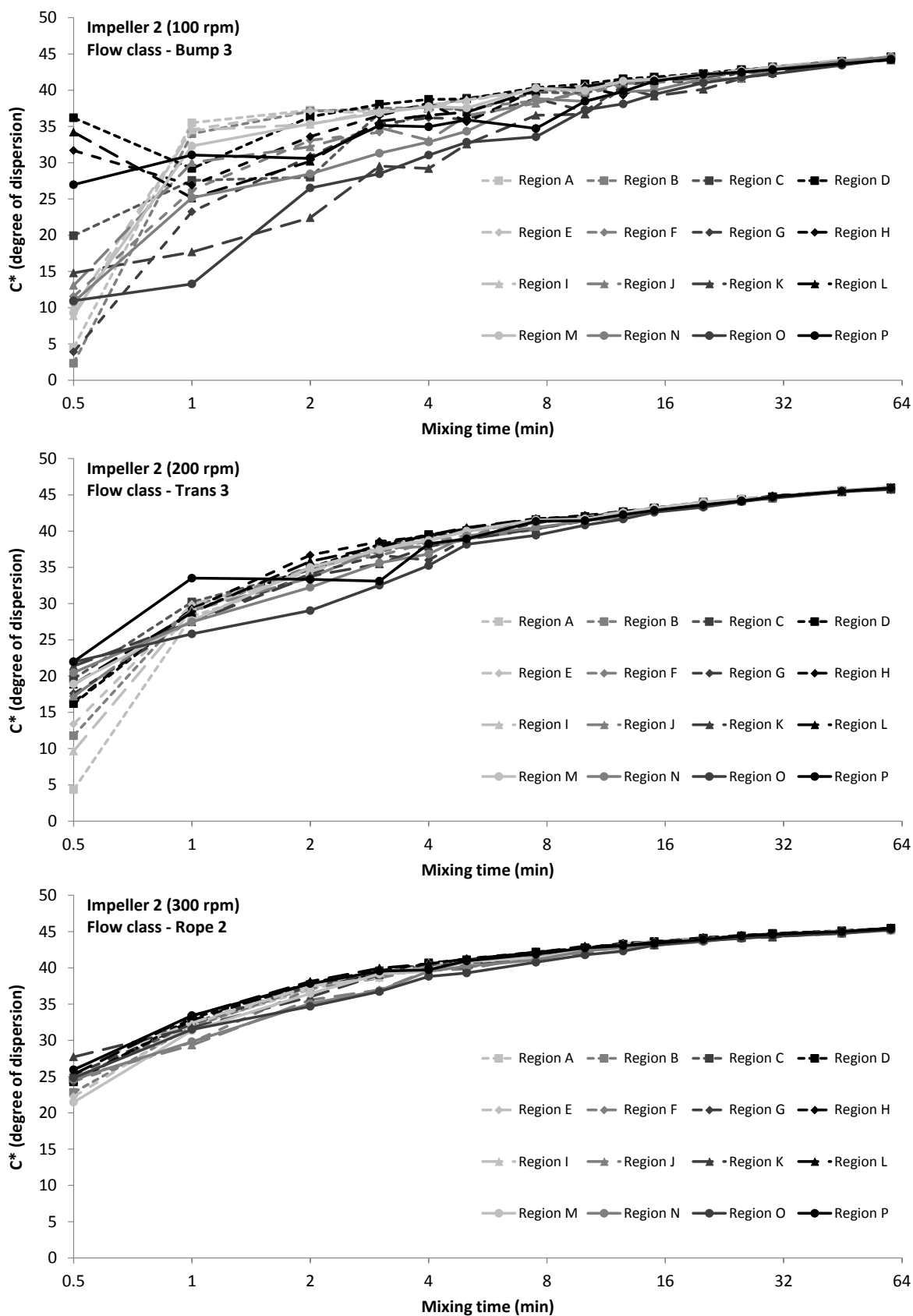


Figure 6.20: Regional blend hue intensities for Impeller 2 at 100, 200 and 300 rpm, showing disparity of the amount and spread of tracer through the powder bed at low mixing times.

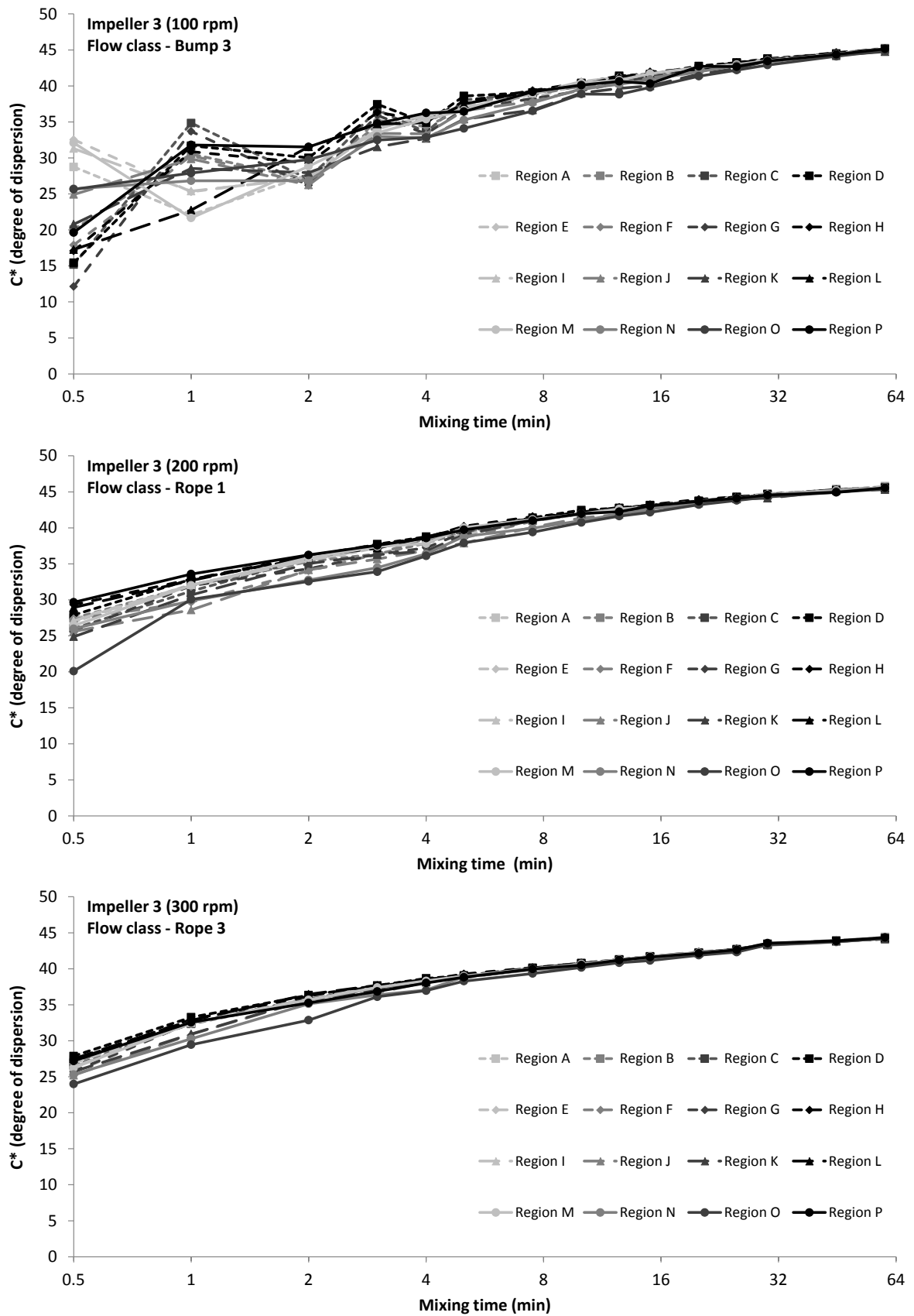


Figure 6.21: Regional blend hue intensities for Impeller 3 at 100, 200 and 300 rpm, showing disparity of the amount and spread of tracer through the powder bed at low mixing times.

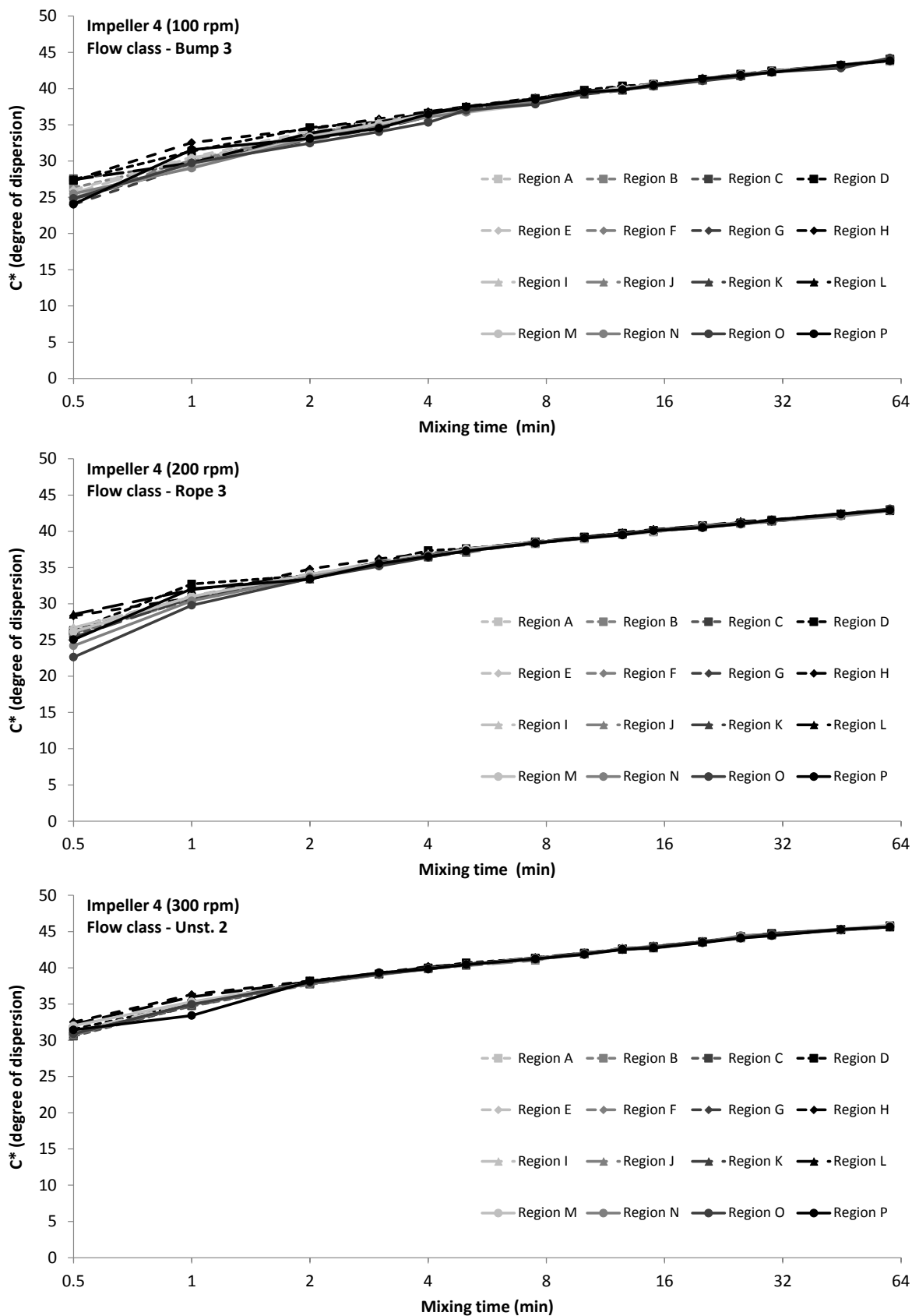


Figure 6.22: Regional blend hue intensities for Impeller 4 at 100, 200 and 300 rpm, showing disparity of the amount and spread of tracer through the powder bed at low mixing times.

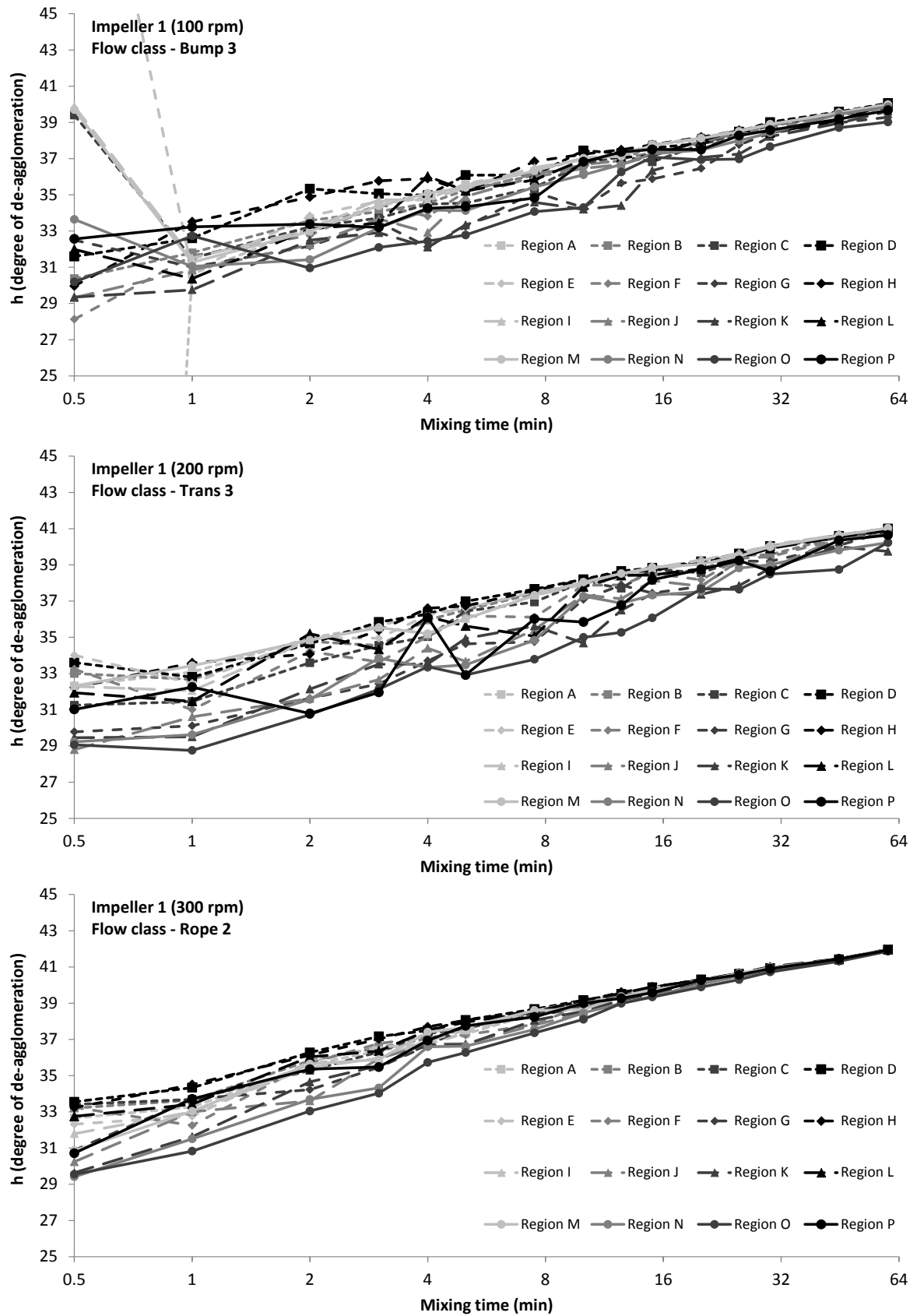


Figure 6.23: Regional blend hue for Impeller 1 at 100, 200 and 300 rpm showing disparity in tracer de-agglomeration and spread throughout the powder bed at low mixing times.

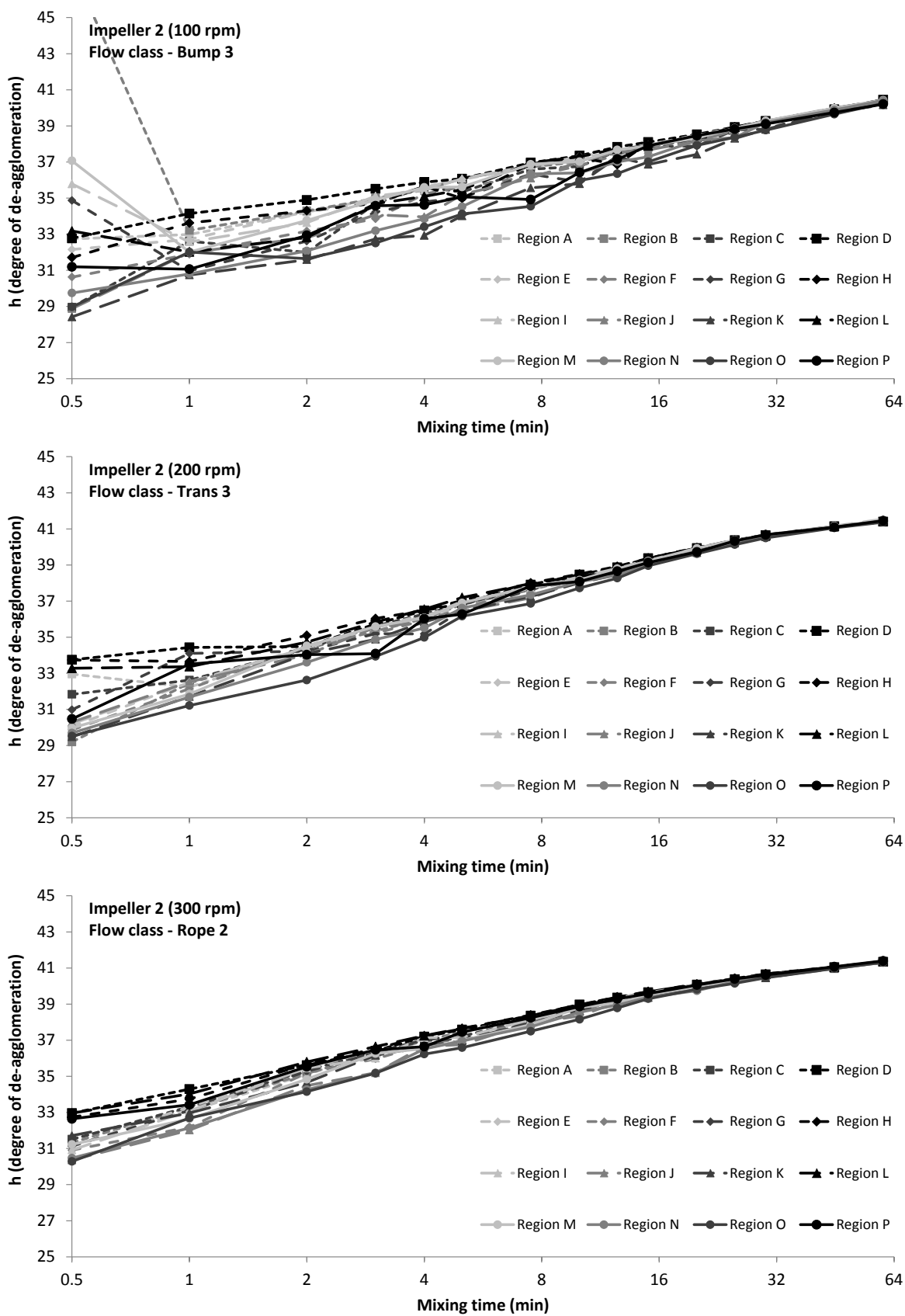


Figure 6.24: Regional blend hue for Impeller 2 at 100, 200 and 300 rpm showing disparity in tracer de-agglomeration and spread throughout the powder bed at low mixing times.

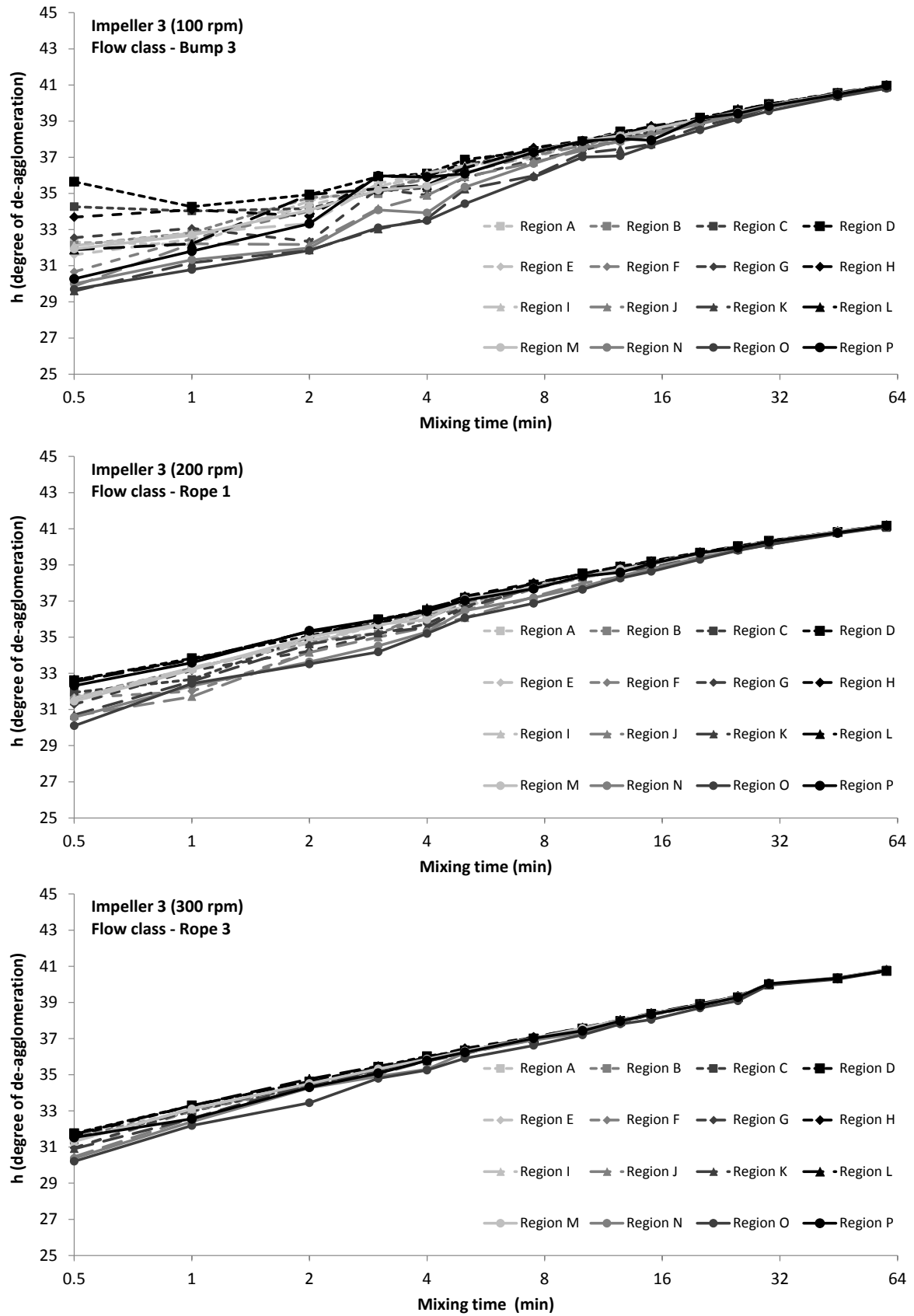


Figure 6.25: Regional blend hue for Impeller 3 at 100, 200 and 300 rpm showing disparity in tracer de-agglomeration and spread throughout the powder bed at low mixing times.

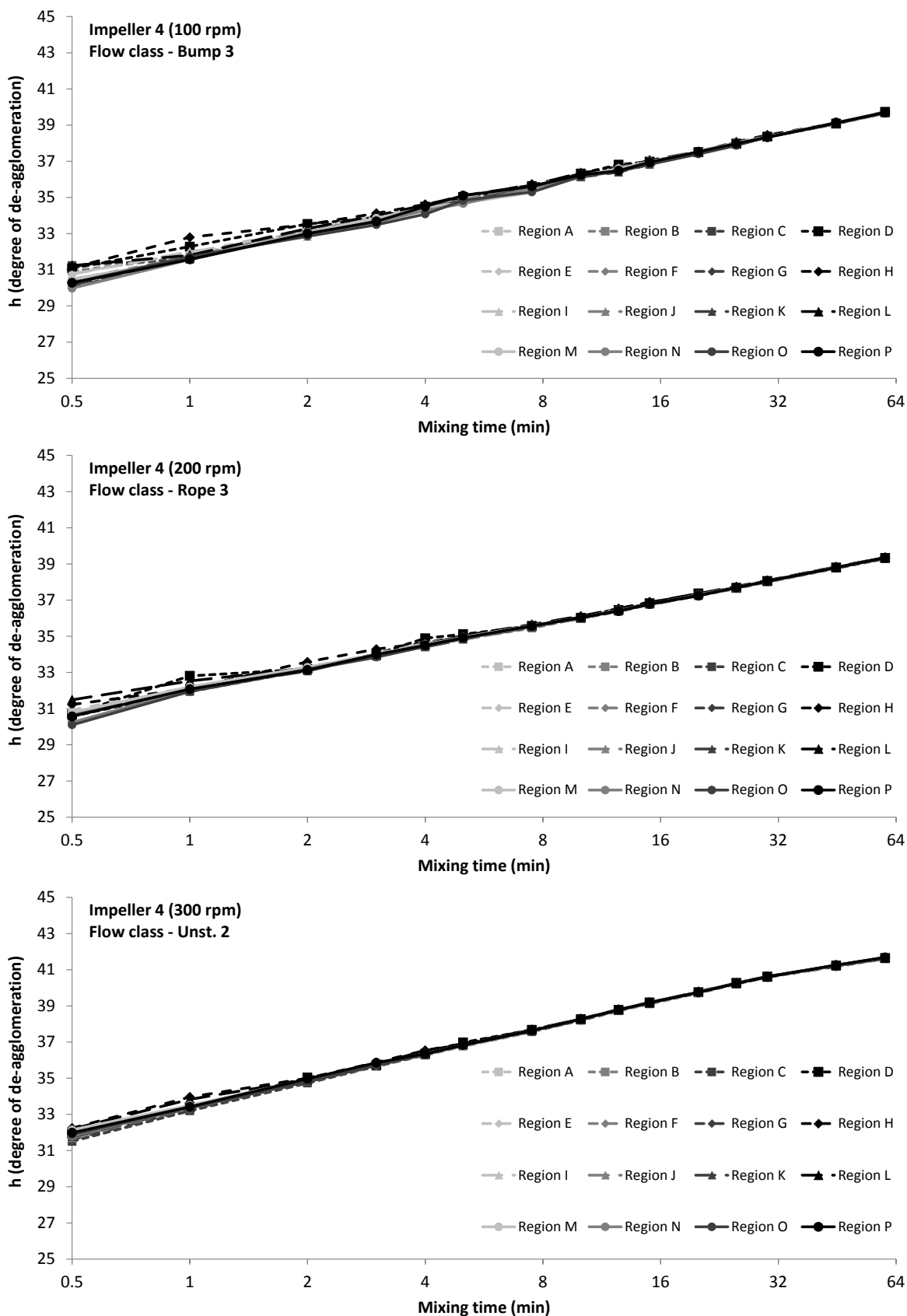


Figure 6.26: Regional blend hue for Impeller 4 at 100, 200 and 300 rpm showing disparity in tracer de-agglomeration and spread throughout the powder bed at low mixing times.

When analysing the regions of blend separately, particularly at low mixing times, they cannot be explicitly described as the degrees of dispersion and de-agglomeration. Instead when blend uniformity is poor (i.e. when region colour curves are separated from one another) the hue intensity ( $C^*$ ), which normally relates to the degree of tracer dispersion, becomes a function of both tracer dispersion and the amount of tracer in the local region. Similarly, hue ( $h$ ), which normally relates to the degree of tracer de-agglomeration, not only assesses the local degree of tracer de-agglomeration but can also show migration patterns of de-agglomerated material away from the source of shear (such as from an impeller at the base of the mixer). Therefore, both hue and hue intensity can be used to assess blending mechanics and flow patterns in different and complimentary aspects. When assessing the regions of sampling (as shown in *Figure 6.8*) they are both discussed as Regions A-P and also in rows and columns (i.e. Rows 1-4 and Columns 1-4).

At low mixing times it is expected that the hue intensity would be higher in the middle of the powder bed (i.e. through Rows 2 and 3) as the tracer was sandwiched between equal masses of lactose prior to blending. Without being given sufficient time to disperse, a higher than average amount of tracer would be expected in the centre of the powder bed where it was placed initially.

The hue intensity profiles ( $C^*$ , *Figures 6.19-6.22*) show that:

- For a given impeller type, the degree of separation between region curves decreases with increasing mixing time and impeller speed. It can also be generally said that the separation of curves decreases with increasing flow class. These findings are linked to content uniformities in Section 6.3.2.3.
- After the initial mixing where tracer has migrated from the centre of the powder mass, the powder at the centre of the mixer (Column 1) typically shows higher than average hue intensity. This suggests that this region shows superior mixing, and is indicative of circulating flow such as in the roping regime, where all the impacted material that rises up the vessel walls converges to a small volume at the centre of the mixer.

- The hierarchy of region curves in less intense mixing conditions (such as with Impeller 1 at 100 and 200 rpm, and Impellers 2 and 3 at 100 rpm) changes dramatically as mixing time progresses. This is thought to be a product of poor powder circulation and the slow migration of rich pockets of tracer to different regions. This 'zig-zagging' of region curves is most likely an indicator of poor powder flow, such as in the bumping flow regime (outlined in Section 6.1.3).
- Regions D and H, located closest to the surface along the vessel wall, almost always show better than average hue intensity. This suggests that strong convective mixing caused by inertial effects at the vessel wall and sufficient clearance above the impeller, create uninterrupted bulk motion and an ideal environment for strong inter-particle collisions. This allows for effective transfer of tracer clumps between lactose surfaces.
- There is no correlation between the hue intensity and vertical depth of the sample in the powder bed. This is most likely due caused by the circulation of powder during mixing.

Similar trends to hue intensity curves are found in the hue region curves (*Figures 6.23-6.26*):

- Blends that exhibit fluctuations in the hierarchy of hue intensity also fluctuate in hue.
- Regions D and H both show higher than average degrees of de-agglomeration which is believed to be attributed to powder that has not only recently migrated from the impeller but also undergoes high intensity inter-particle interactions due to inertial effects at the vessel walls. Unsurprisingly there are also high levels of de-agglomeration along the base of the powder bed, where high levels of shear dispersion are applied directly to the powder by the impeller.
- For blends which are predicted to have poor powder circulation (such as Impellers 1 and 2 at 100 rpm) many of the regions that exhibit lower than average hue intensity show higher than average hue. This indicates that these regions have a below average amount of tracer.

Because of this the tracer is easily dispersed and any additional energy goes into its de-agglomeration.

In summary, both the hue and hue intensity profiles are believed to be able to provide additional insights beyond quantifying content uniformity. The profiles show qualitatively whether there is good circulation of powder during mixing. Blends that exhibit fluctuations in hue and hue intensity indicate poor powder circulation, which is synonymous with bumping or transitional flow. Further discussion on flow analysis from colour values is provided in Section 6.4.3.

### 6.3.3 Power and energy input measurements

From the readings provided by the torque arm of the mixer (*Figure 6.9*), the energy input (calculated from *Equation 6.13*) can be plotted for each impeller type and speed as a function of time (*Figure 6.27*).

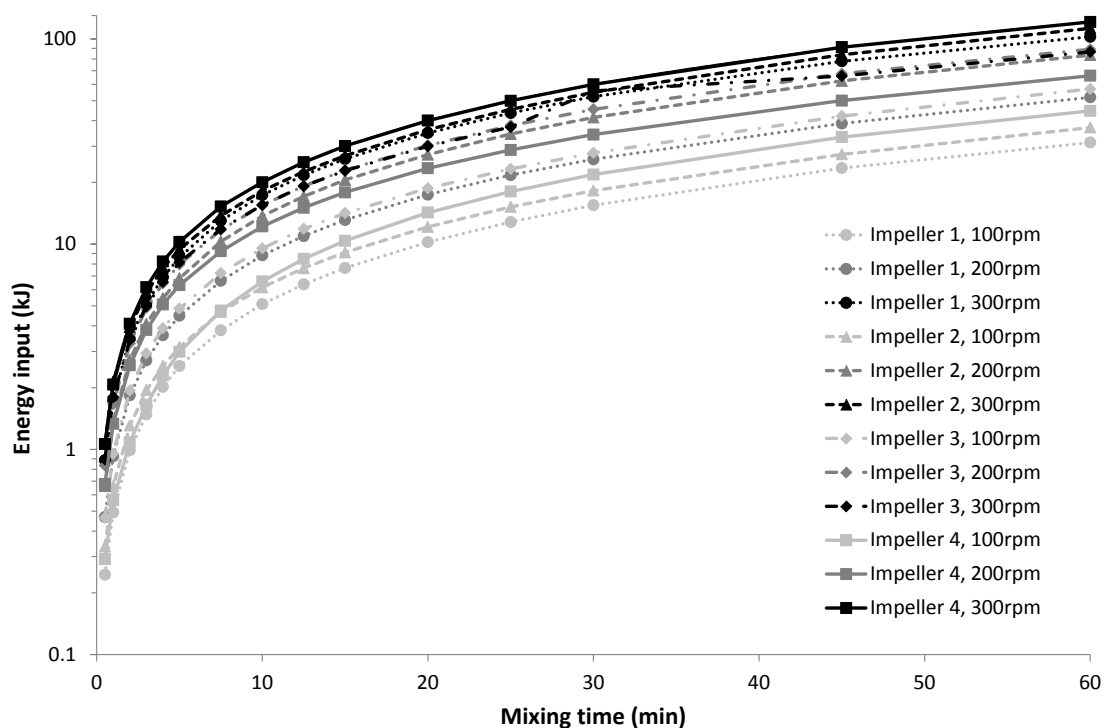


Figure 6.27: Cumulative energy input to the blend over duration of mixing for each impeller type and speed.

Energy inputs in Figure 6.27 are cumulative over the entire mixing time and account for variations in the measured force on the transducer over time. The gain of the transducer altered, particularly in the early stages of mixing; hence altering the calculated power and energy input.

Whilst some blends show dramatic changes in measured power, the majority of blends change only slightly over the duration of mixing. Blend with large shifts in the measured power inherently have large errors in the average power input across the 60 minutes of mixing (Figure 6.28).

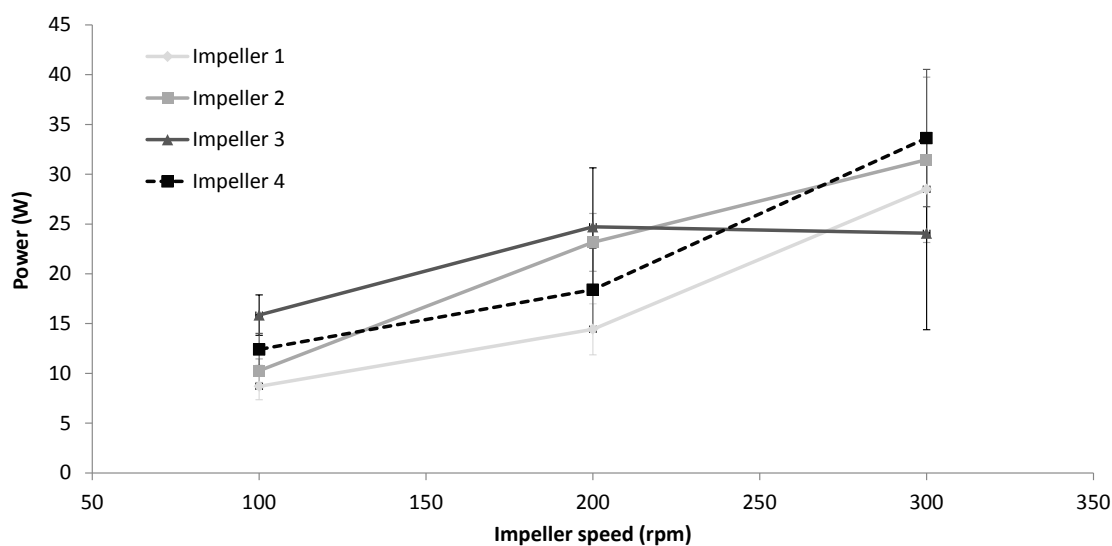


Figure 6.28: Weighted average power input over 60 minutes of mixing for each impeller type and speed.

Due to the uncertainty associated with calculating the power input to the blend, it is difficult to draw conclusions about the full effect of power input on colour changes and blend attributes.

Despite limitations in drawing conclusions from the power input, there appear to be further conclusions that can be drawn from the total energy input to the blend. Blend curves for each impeller type and speed align when the total energy input (calculated from Equation 6.13) is plotted against the degrees of dispersion (Figure 6.29) and de-agglomeration (Figure 6.30).

The values in the above correlations are the average values for hue and hue intensity at each time point. Errors have not been included for clarity but are provided in Figure 6.14. Blend curves within each correlation follow a straight line on a semi-log plot, suggesting a power-law relationship. Below

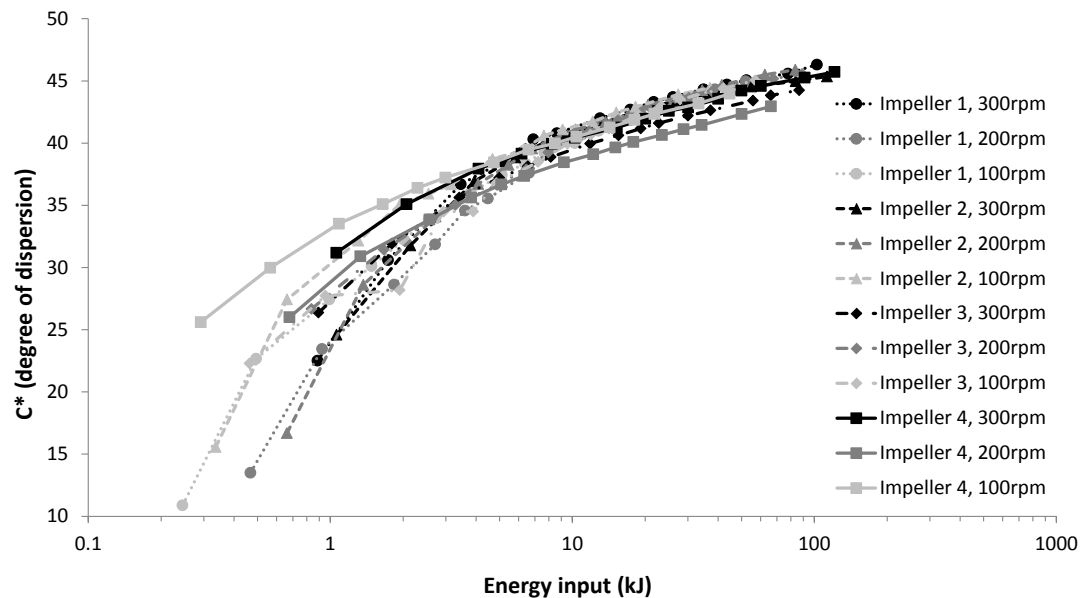


Figure 6.29: Relationship between calculated energy input and the average measured degree of dispersion ( $C^*$ ) for all impeller types and speeds.

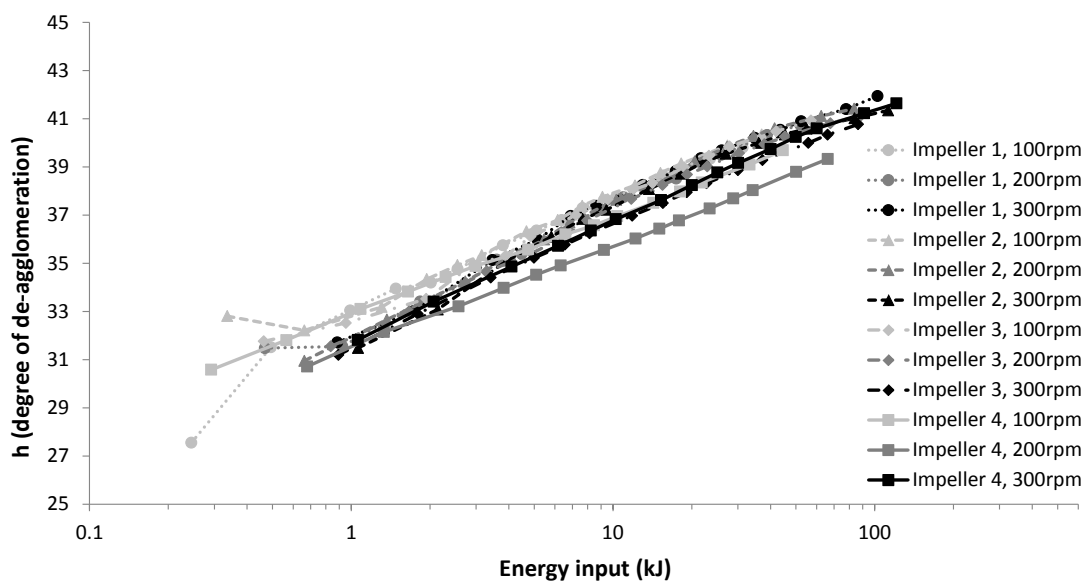


Figure 6.30: Relationship between calculated energy input and the average measured degree of de-agglomeration ( $h$ ) for all impeller types and speeds.

~3kJ however, results do not align well for either correlation and are most likely attributed to poor content uniformity with low mixing time. The deviation of the blend curve for Impeller 4 at 200 rpm may be attributed to errors in the measurement of the mixer torque. Errors may have arisen from a variety of factors including the powder flow, or problems with the transducer such as a shift in the gain during mixing. There is potential for the total energy input to be quantifiable based on knowing

the hue and hue intensity. Discussion on the use of colour changes to measure energy input is given in Section 6.4.2.

### 6.3.4 PEPT flow analysis

To further assess the ability of the colour tracer to provide information on powder flow, tracer blends were analysed using PEPT. Whilst PEPT has been used to assess powder mixing in a high-shear mixer during wet granulation (such as changes in particle speed over time). The results do not directly apply to the assessment of powder flow during dry powder mixing as the properties of the blend are not changing with liquid binder addition. In this study the tracker occupancy, short-term flight and short term velocities are used to assess different aspects of the bulk powder motion, and linked back to the colour data detailed in Section 6.3.2. This section looks at further justifying the colour observations, while Section 6.4.3 investigates the use of colour data to infer powder flow.

The tracker particle is represented in terms of its relative occupancy (or residence time) at a particular location within the powder bed during mixing. The side and plan cross-sectional occupancy plots attached (*Figure 6.31* and *Figure 6.32* respectively) include all recorded tracker particle locations within the mixer over the designated 120 minutes of mixing and as such represent flow in 'steady state' mixing. Powder flow classes obtained from visual observations of the surface flow patterns in Section 6.3.1 are also included for comparison. The small black regions of high occupancy, which can be found in some plots and show the location of the radioactive tracker particle in the powder bed during recording but prior to mixing, can be disregarded for flow analysis.

The side (*Figure 6.31*) and plan (*Figure 6.32*) occupancy plots largely agree with the observations of powder flow in Section 6.3.1, and clearly show distinct and characterisable types of flow (which are believed to be associated with the bumping, transitional, roping and unstable flow regimes). There is a clear progression in flow regime with higher mixing intensity (either through increased impeller drag or speed). The powder flow classes largely agree with the PEPT occupancy data. However, there are some differences as the powder flow on the surface only provides a component of the overall

information. From PEPT occupancy plots, four distinct types of flow are observed, which link to each of the flow regimes.

Impellers 1 (at 100 and 200 rpm) and 2 (at 100 rpm) show pockets with poor tracker occupancy away from the walls and centre of the mixer, suggesting they are regions of poor mixing. The tracker particle in these blends is believed to predominantly migrate upwards close to the vessel walls, and flow back down to the impeller from the surface through a vortex in the centre. This is confirmed from the plan views, where the tracker particle is shown to spend a lot of time along the vessel wall and in a wide circle at the centre of the mixer. As no vortex is clearly visible by eye in these systems, as mentioned by Litster *et al.* (2002), the upwards and downwards migration of powder in the vessel is considered to be too slow to detect. Occupancy profiles of this nature are believed to indicate *bumping* flow.

Impellers 1 (at 300 rpm), 2 (at 200 rpm) 3 and 4 (both at 100 rpm) show fairly even occupancy of the tracker particle through the powder bed, with slightly higher occupancy at the top and centre of the bed. As the areas of low occupancy have disappeared and the darker region in the top and centre of the bed suggest the beginning of a strong vortex forming (both in the side and plan views), these plots can be regarded to be in the *transitional* regime.

Impeller 2 (300 rpm) and Impeller 3 (200 rpm) show a solid vortex in the powder with small regions of low occupancy, suggesting good *roping* flow. This can be seen in the plan views through the return of the darker rings at the vessel walls and in the centre; however the centre ring is smaller than in the bumping regime. Also, the region that the impeller occupies (i.e. the sweeping area) can be seen as a bar of poor occupancy at the base of the mixer. This suggests that when the tracker particle is in the vicinity of the impeller, it is quickly shifted by direct impeller impacts or through strong powder convection.

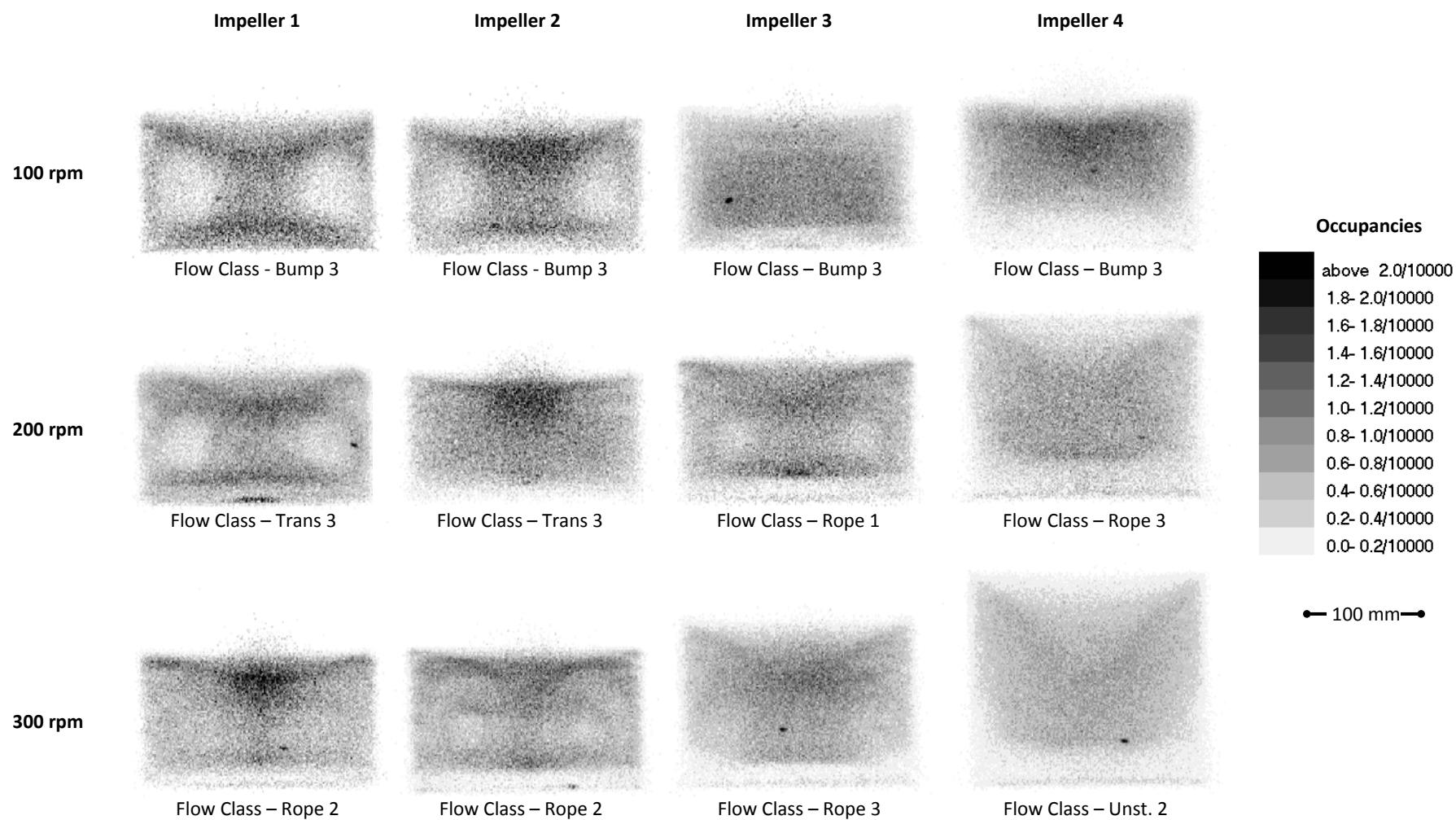


Figure 6.31: Side PEPT tracker occupancy plots within powder mass during mixing for each impeller type at 100, 200 and 300 rpm with observed Flow Classes from Section 6.3.1. All occupancy plots are to scale with one another and show bed dilation with different impeller types and speeds.

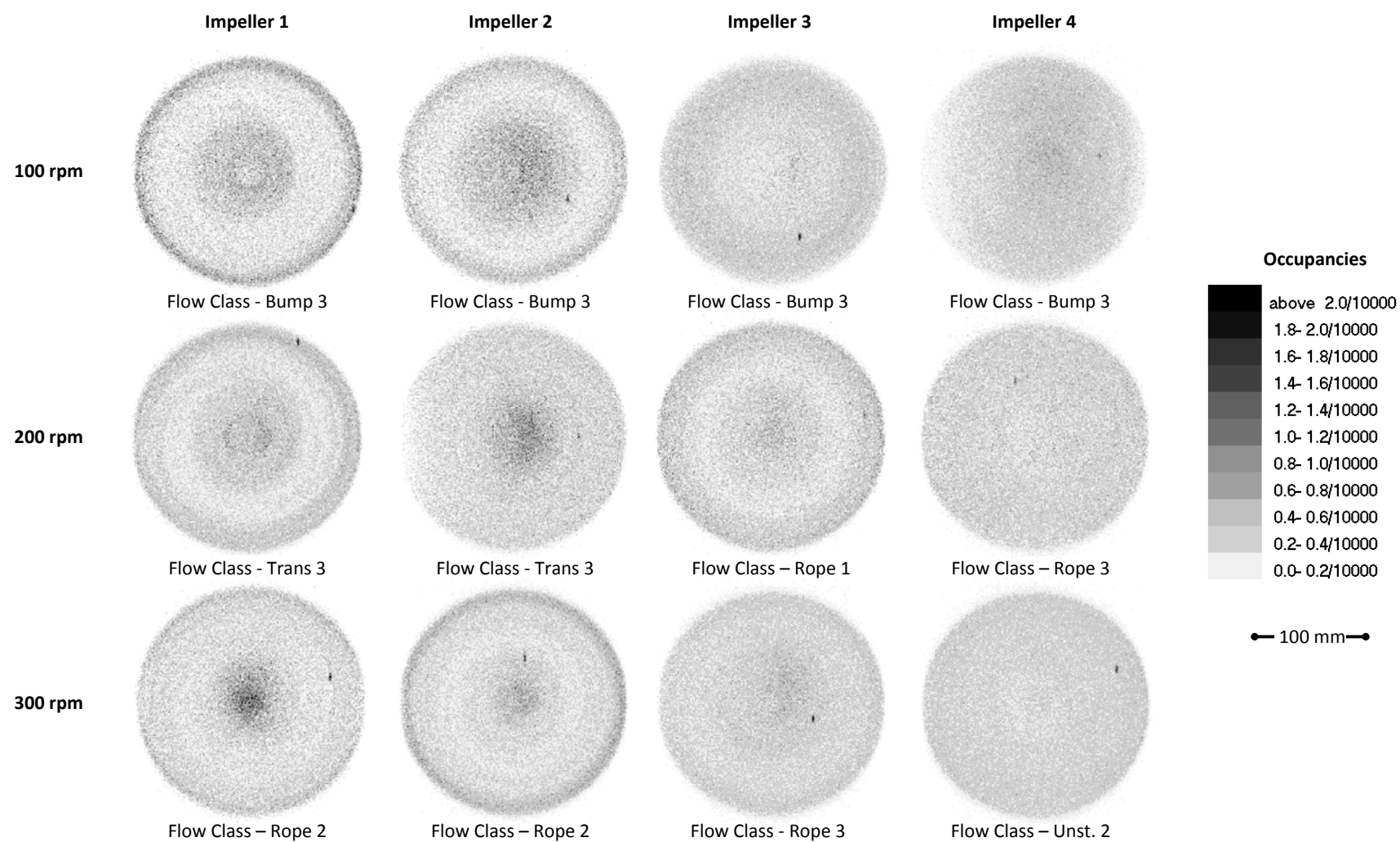


Figure 6.32: Plan PEPT tracker occupancy plots within powder mass during mixing for each impeller type at 100, 200 and 300 rpm with observed Flow Classes from Section 6.3.1.

The other blends (Impeller 3 at 300 rpm and Impeller 4 at 200, 300 rpm) indicate the presence of a very strong vortex in the centre of the bed with the powder at the walls climbing considerably higher than the centre of the bed. Also, the occupancy of the tracker is quite even throughout the bed in both the side and plan occupancy plots. This indicates very strong and possibly turbulent mixing and is consistent with the observations of *unstable* flow in Section 6.3.1.

Whilst PEPT data is able to create particle velocity profiles through the powder mass, they were unable to compare or distinguish between the flow types. Instead, the flight of the tracker particle through the powder over a small period of mixing is assessed to gain a stronger grasp of the powder flow during mixing. To show the short-term behaviour of mixing with each impeller type and speed, side (*Figure 6.33*) and plan (*Figure 6.34*) views of the tracker flight over 60 seconds of mixing are shown. The respective speed profiles for mixing in *Figure 6.33* and *Figure 6.34* are also included (*Figure 6.35*), which are calculated from the tracker velocity using the 6-point method (*Eqn. 6.4*). These are used to assess the types of interactions that the tracker particle has with the impeller in different powder flow regimes.

Again, four general types of tracker flight are observed over the 60 seconds of mixing, and correlate to the four flow regimes. The types of tracker flight at each impeller type and speed coincide with and help to further explain the types of occupancy plots that were observed. A couple of settings (such as Impeller 3 at 300 rpm and Impeller 4 and 100 rpm) again show properties of two flow regimes.

Across all tracker flight plots, a general observation about the relative speed of the tracker can be made in relation to its location. When the tracker has energy imparted to it, either through convection or direct impact with an impeller blade, it accelerates in the vicinity of the impeller. Inertial effects then force it to the vessel wall. Conservation of energy then forces the tracker upwards near the vessel wall until it reaches the surface of the powder mass, and then tumbles back down towards the impeller through the centre of the mixer. Due to a dissipation of energy through

inter-particulate interactions and gravitational resistance when climbing upwards, the tracker particle travels down towards the impeller at a relatively lower speed than when it is climbing. Large jumps can be seen in the short term flight of the tracker, which are shown as straight lines. The combination of short migrations and large leaps are indicative of Levy flights (Kaye, 1997b), which are used to describe and model particle motion (as discussed in Section 6.1.3).

Occupancy plots linked to *bumping* flow show flights that take multiple rotations to climb along the vessel wall from the impeller region to the powder surface, and then spiral back down through the centre of the mixer. The downwards spiral also occurs over several rotations. From the speed profiles over the 60 seconds there appears to be no distinct imparting of energy to the tracker particle which is typical of a direct interaction with the impeller. Slight rounded bumps can be seen however, which suggest weak acceleration of the tracker in the vicinity of the impeller, most likely through powder convection.

The *transitional* regime shows flow characteristics that are distinctly different. The centre vortex of these systems appears to widen from those in the bumping regime. Also, the flow does not show smooth climbing and falling of the tracker, but rather various combinations of fast climbing and/or fast falling. In the corresponding speed profiles, there appear to be more distinct bumps than in those under bumping flow, suggesting that more energy is being imparted on the particle. Many show the smooth bumps indicative of convective acceleration of the tracker, however some of the systems also show sharp peaks which are believed to indicate direct impaction of the particle by the impeller itself. Impeller 4 at 100 rpm is the most interesting of the systems observed to be in transitional flow, and shows 'chaotic' trajectories as the particle is bounced around the mixer in straight lines without spiralling. The speed profile is also very different to the others in this regime, and shows a large amount of interactions with the impeller with different amounts of energy imparted on it on each occasion.

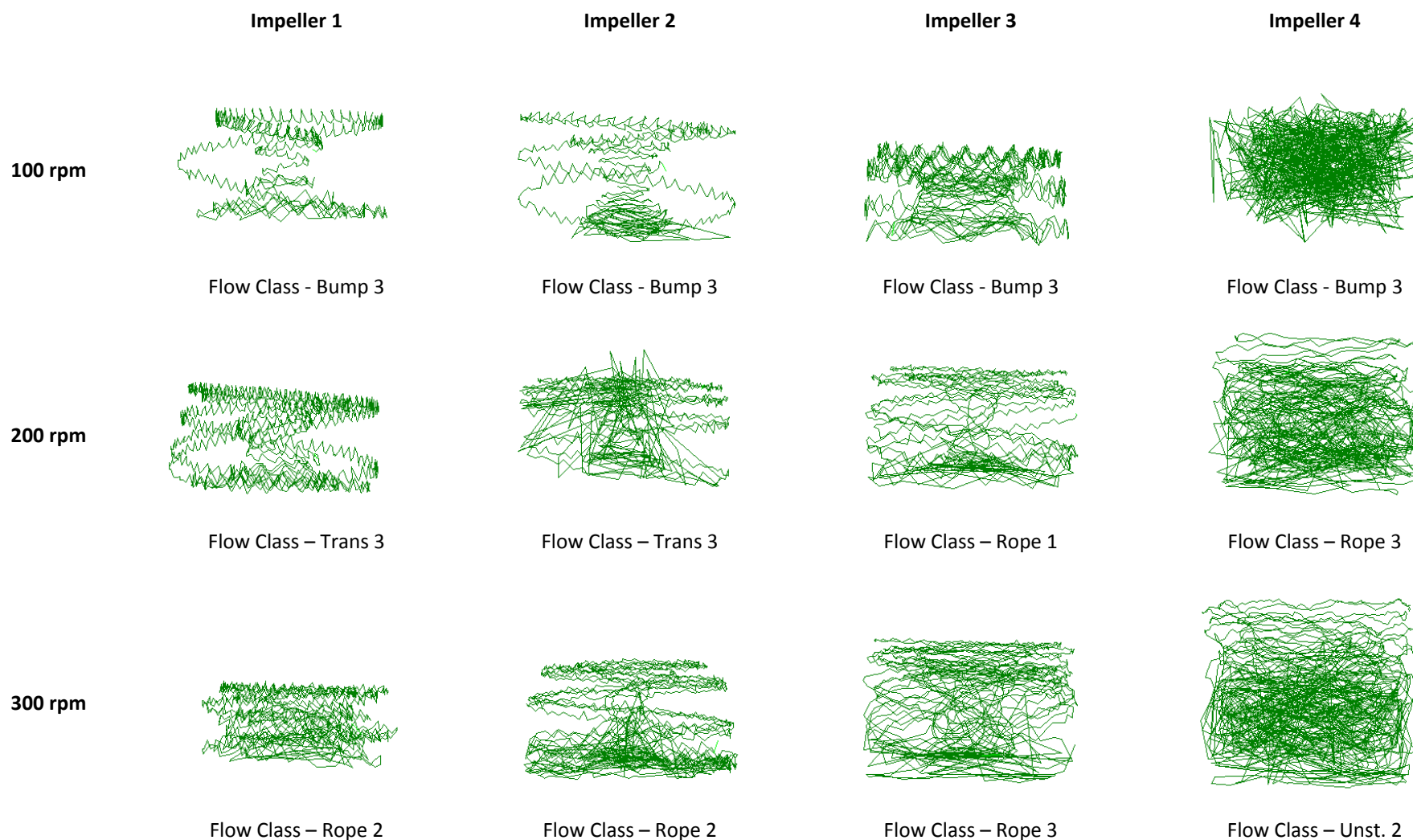


Figure 6.33: Tracker particle cross-sectional trajectory through the powder bed over 60 seconds of mixing for all impeller types and speeds, with associated flow classes from Section 6.3.1

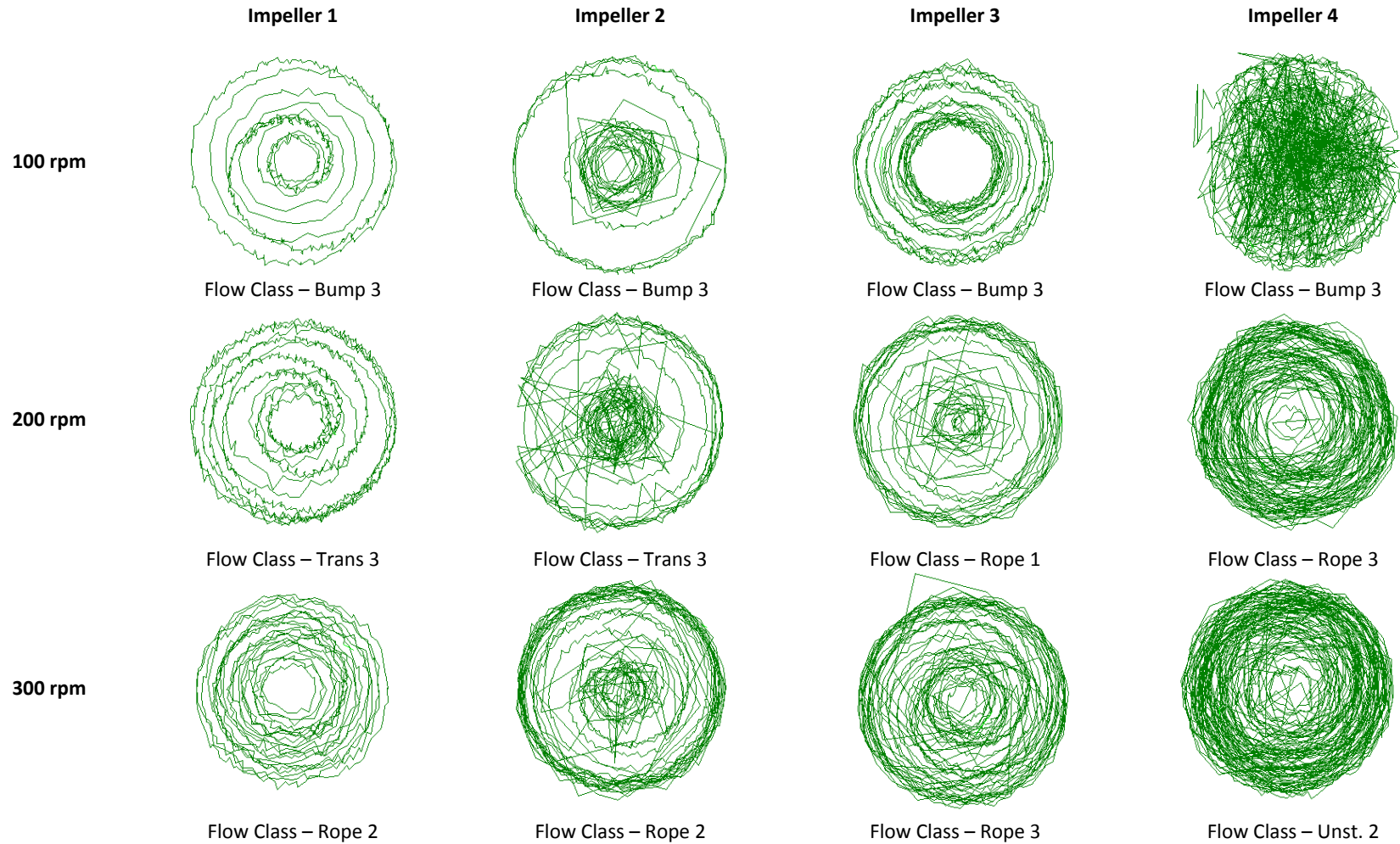


Figure 6.34: Tracker particle plan-view trajectory through the powder bed over 60 seconds of mixing for all impeller types and speeds, with associated flow classes from Section 6.3.1.

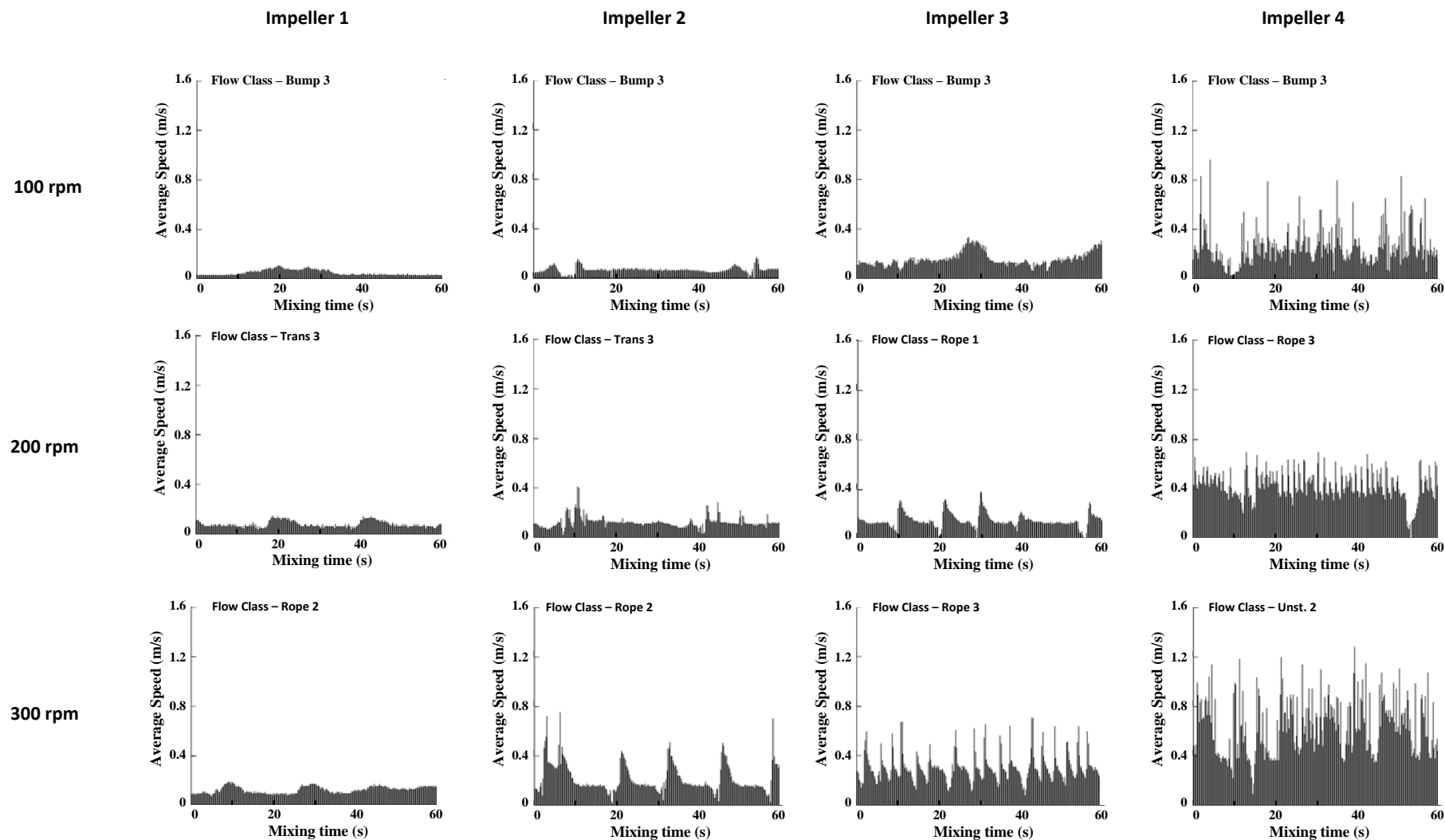


Figure 6.35: Tracker particle velocity during the sixty seconds of mixing in Figure 6.33 and 6.34 showing interaction with impeller for each impeller type and speed.

Occupancy plots that indicated *roping* flow have the outwards climbing and inwards downwards spiralling of the tracker which is present in bumping flow. However the centre spiralling occurs considerably quicker and within a tighter volume, and appears to spend more time close to the vessel walls than in the bumping regime. Both of these effects are believed to be caused by the particles having more energy imparted by the impeller during the 60 seconds of mixing, which can be seen in the corresponding speed profiles. Speed profiles show clear impacts with the impeller at a fairly consistent frequency, with distinct dissipation of the tracker velocity as it climbs upwards along the vessel walls. The consistent frequency and profile of interactions with the impeller indicate stable and steady-state flow.

*Unstable* flow shows very 'chaotic' mixing with a large number of tracker particle rotations at the vessel walls, which occupy the vessel evenly over the 60 seconds of mixing. Speed profiles show very frequent and irregular impacts with the impeller or surrounding powder in the vicinity of the impeller, with the frequency of interactions less predictable than in roping flow. The speed profiles and flight path of the tracker in Impeller 3 at 300 rpm (which was classed as unstable flow in the occupancy plots) are more likely to be in the roping regime than the unstable regime.

With increasing intensity over the 60 seconds of mixing, Figures 6.33 and 6.34 show that the distance covered by the tracker particle increases with increasing process intensity (i.e. either through increased relative impeller drag or impeller speed), which is related to the tracker speed. It is also worth noting that the tracker never reaches the same speed as the blade tip, which at 100, 200 and 300 rpm is 1.1, 2.2 and 3.3 m/s respectively, regardless of the blade design used. This is most likely due to the tracker entering the impeller region from the centre of the mixer, which makes it highly unlikely to be accelerated by the impeller tip itself. When assessing the overall flow within each system, the most meaningful velocities in the context of a high-shear mixer are those associated with cylindrical flow (i.e. axial, radial and angular). Histograms for each of these *velocities*, as well as a histogram for the tracker *speed* over the 120 minutes of mixing are attached for all

impeller types and speeds (*Figure 6.36 and Figure 6.37*). These can be used to obtain further information about the steady state behaviour of the powder during mixing.

As the axial, radial and angular velocity profiles are symmetrical around zero due to the circular and upwards/downwards movement of the tracker, negative velocities in the distributions have been removed for clarity in *Figure 6.36 and Figure 6.37*, and are compared through their respective standard deviations. Tracker speeds however, which are scalar, are compared through their average values as well as their standard deviation. From the velocity and speed histograms, some general trends can be taken:

- The standard deviation of velocity profiles increases with increasing relative impeller drag (i.e. impeller type) and also with increasing impeller speed.
- The average and standard deviation of the tracker speed increases with increasing impeller speed.

Many of these observations are driven by an increase in the velocity differential across the mixer between the base and the powder surface. This increases with increasing relative impeller drag and/or speed, which increases with the amount and intensity of particle interactions with the impeller. The tracker particle never reaches the tip speed of any system. The average tracker particle speed is always less than 25% of the impeller tip speed, and typically under 10 percent. This is consistent with the previous observations in high-shear mixers (*Hosikian et al., 2010, Knight et al., 2001, Plank et al., 2003*).

*Darelius et al. (2007a)* suggests that if the axial velocity component is high in the near wall region then the powder should be in the roping flow regime. Unfortunately, no such correlations are observed in this study between types of powder flow and tracker velocity or speed.

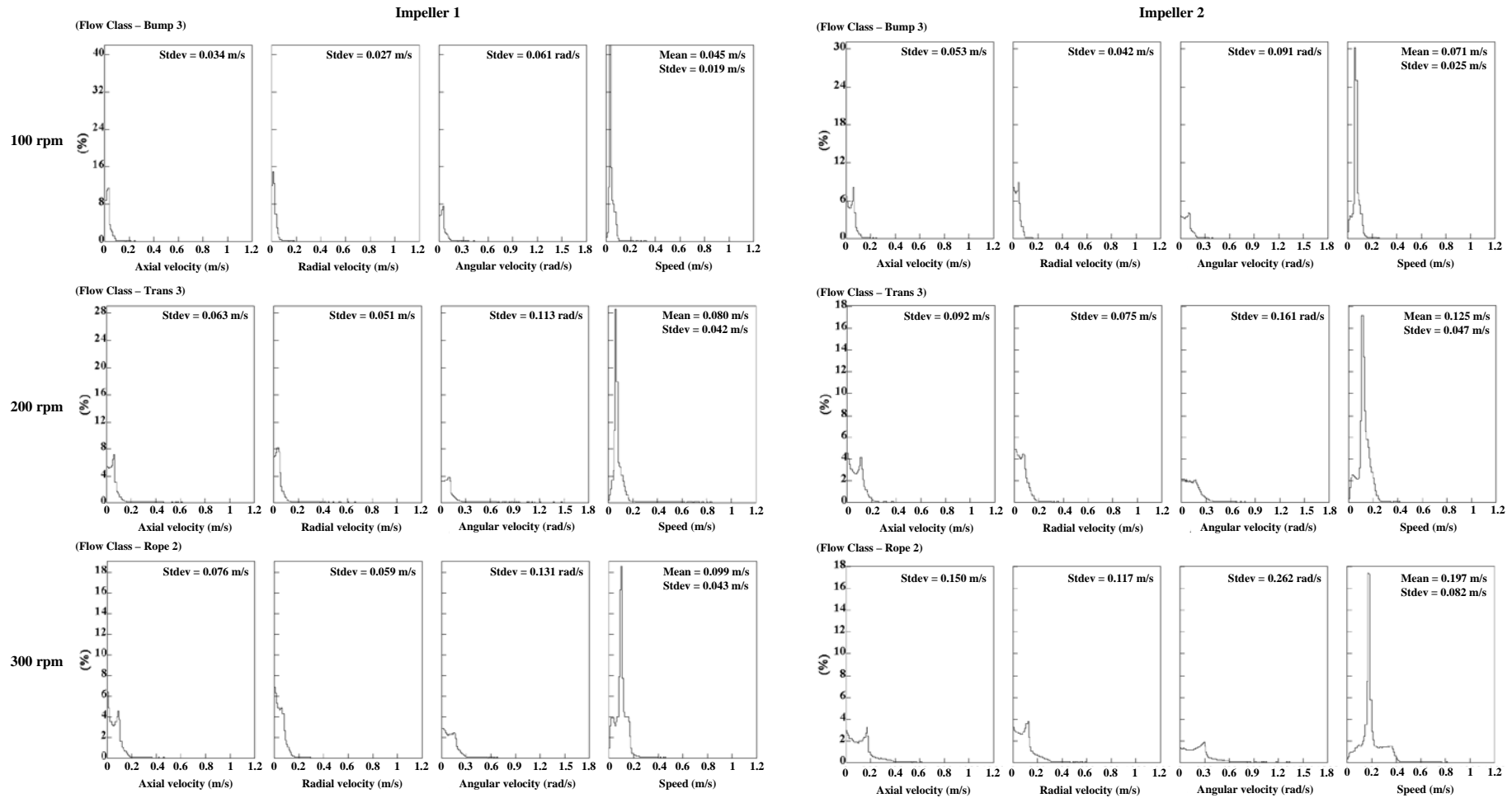


Figure 6.36: Velocity histograms obtained from PEPT for Impellers 1 and 2 at 100, 200 and 300 rpm with associated flow classes

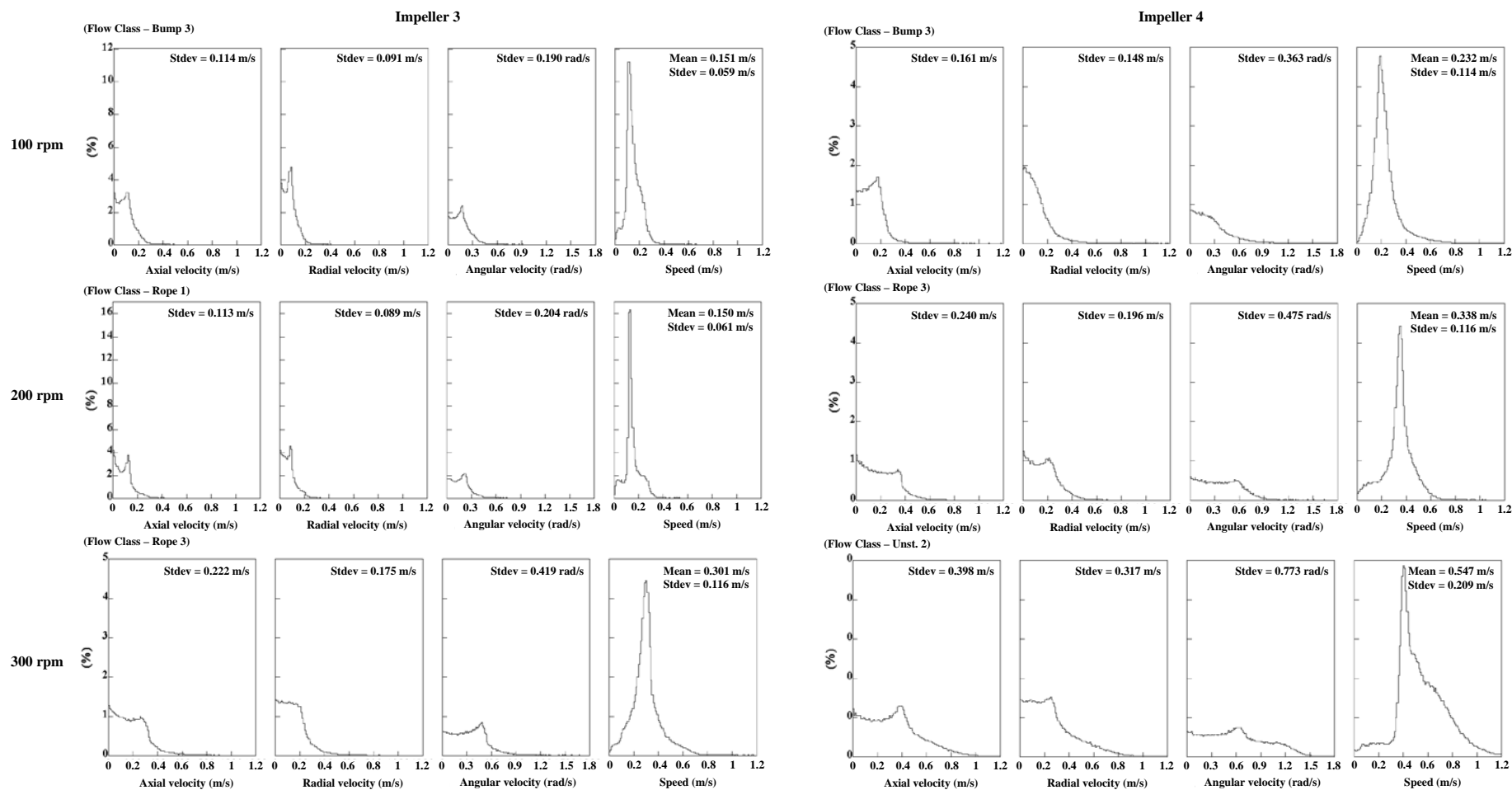


Figure 6.37: Velocity histograms obtained from PEPT for Impellers 3 and 4 at 100, 200 and 300 rpm with associated flow classes.

## 6.4 Discussion

In this section the use of the colour tracer to quantitatively assess content uniformity and energy input are tested, as well as the ability for the tracer to provide information on powder flow within the mixer. Also the colour, energy and PEPT data are combined to provide a brief discussion on the effects of impeller type and speed on the type of mixing achieved, and the benefits and limitations of the tracer method outlined.

### 6.4.1 Analysing uniformity from the shape of blend curves

The colour curve for Impeller 4 at 300 rpm was used in this study as the basis for best mixing. It is important to see how this fits to previously gathered standard formulation data from Chapter 4 (i.e. for lactose LH200 with 1 wt% coloured tracer) to test its validity (Figure 6.38).

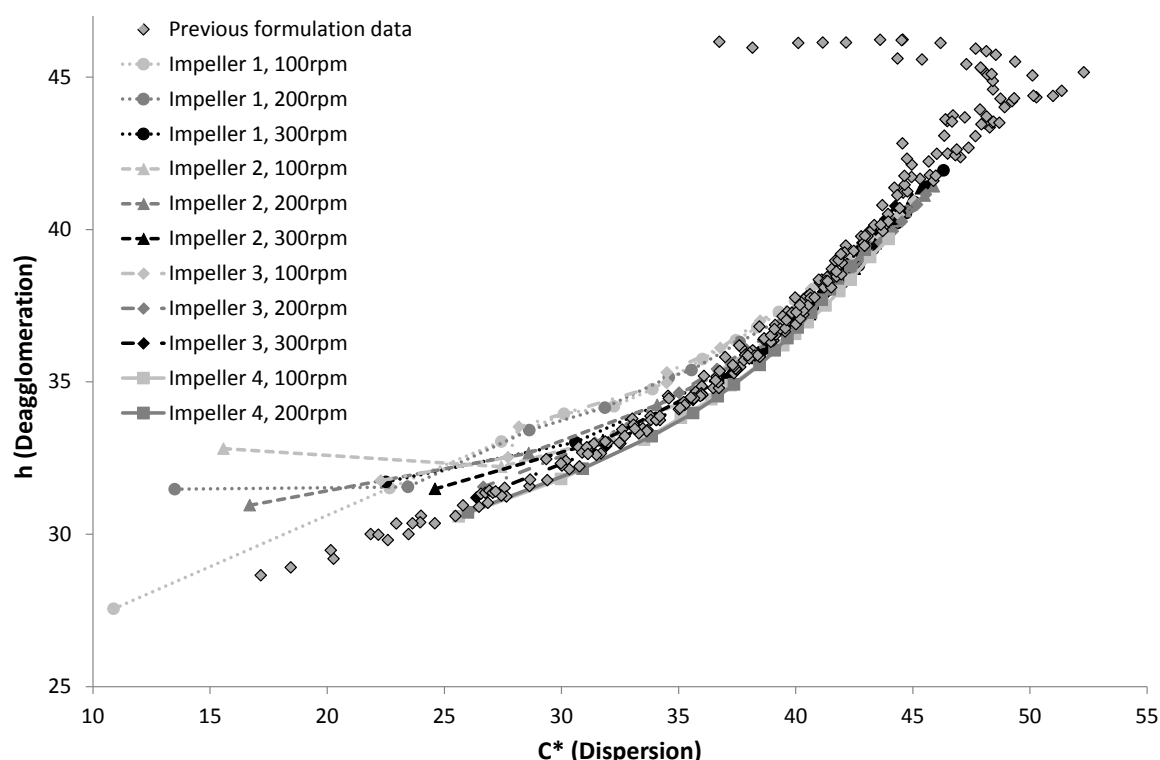


Figure 6.38: Comparison of formulation curves in the CIE  $C^*$ - $h$  plane obtained in this study and in Chapter 4.

When comparing blend curves it can be seen that not only does the base curve (i.e. Impeller 4 at 300 rpm) fit the previous data points at low degrees of dispersion ( $C^*$ ), but also appears to correct for deviations caused by mechanofusion phenomena at high values of  $C^*$ . This substantiates and

justifies the use of the Impeller 4 curve as a baseline for best mixing in this study as it aligns with those of Chapter 4.

Section 6.3.2 showed that the relative standard deviation of hue intensity ( $C^*$ ) across samples at a given time point allow quantification and comparison of uniformity, and that curves deviate from one another with increasingly poor content uniformity. Whilst this deviation is certainly an indicator of deviation in content uniformity, no quantifiable correlation was found between deviations between blend curves in the CIELCH colour space and deviations in content uniformity. There is also no correlation between energy input and the level of content uniformity. As energy input is calculated from power input and is a function of time, the relationship between energy input and content uniformity is identical in form to Figure 6.15.

#### 6.4.2 Quantification of energy input with colour change

Section 6.3.3 showed there is a relationship between the total energy input and the degree of tracer dispersion and de-agglomeration. Both profiles show the shape of a classic 2<sup>nd</sup>-order power-law relationship, with a clear upper limit that can be reached at high energy inputs and a rate constant that describes the decaying step increase in values with a given step increase in energy input (Eqn. 6.17).

$$[Q] = a[E]^b + c \quad \text{for } E < 130 \text{ kJ} \quad (\text{Equation 6.17})$$

Where  $Q$  is the quantity of interest (either degree of dispersion or de-agglomeration),  $E$  is the energy input (in kJ) and  $a$ ,  $b$  and  $c$  are coefficients of the correlation. Applying this to Figure 6.29 and Figure 6.30, the following curves of best fit are found by minimising the root mean standard error (RMSE) with bisquare robustness (Figure 6.39 and Figure 6.40).

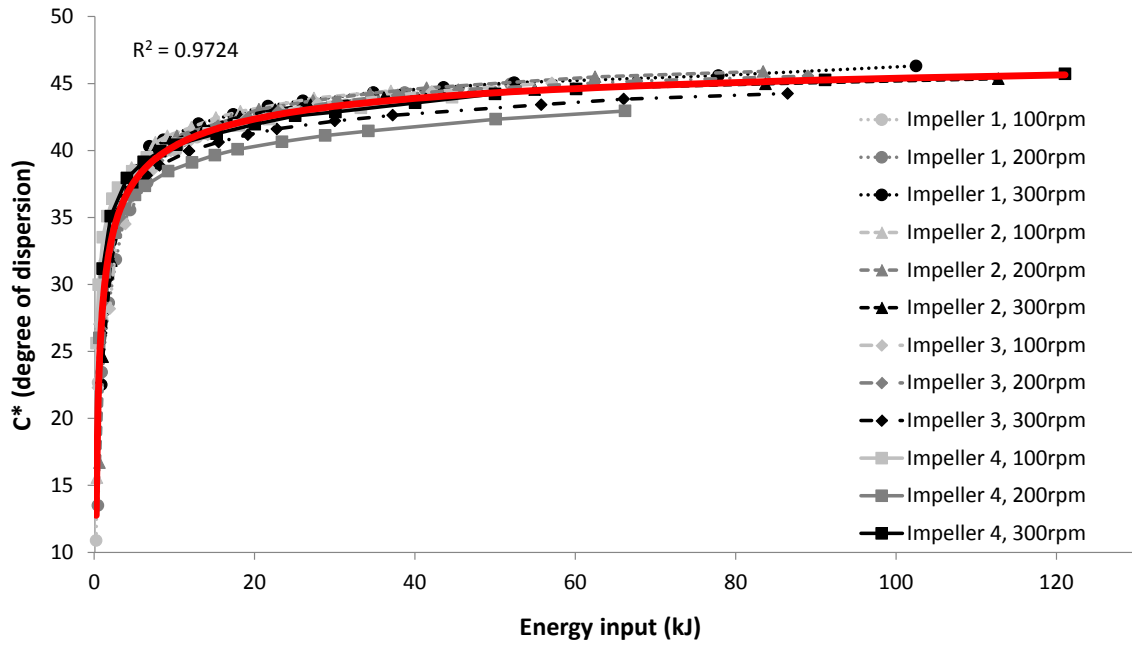


Figure 6.39: Best fit for correlation between energy input and degree of dispersion (C\*)

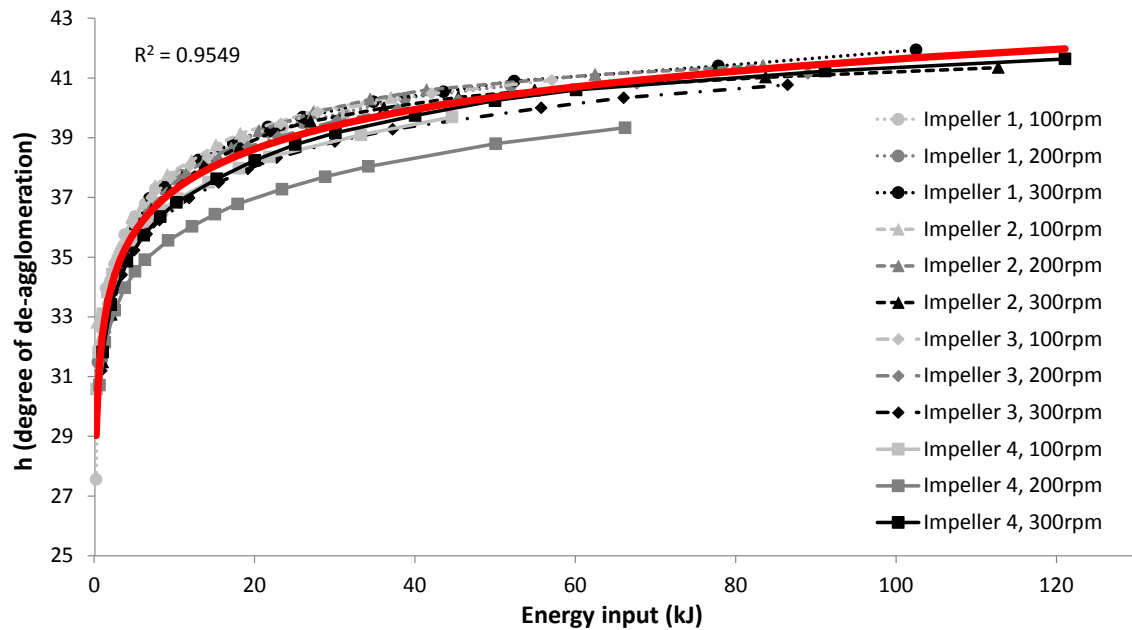


Figure 6.40: Best fit for correlation between energy input and degree of de-agglomeration (h)

The 2<sup>nd</sup>-order power law curves of best fit can be expressed for the degrees of dispersion and de-agglomeration as Equations 6.18 and 6.19 respectively.

$$C^* = 48.9 - 20.9E^{-0.388} \quad (\text{Equation 6.18})$$

$$h = 77.6 - 45.3E^{-0.050} \quad (\text{Equation 6.19})$$

These two equations indicate that the energy input to the powder can indeed be quantified from colour values alone. As blend lightness ( $L^*$ ) is a function of both the degree of dispersion and de-agglomeration, the energy input can be quantified within the dispersion-dominant and dispersion/de-agglomeration regions using  $L^*$ ,  $C^*$  or  $h$ . It is recommended however that energy input be calculated from the hue intensity (using Eqn. 6.18) to minimise error.

It can also be seen from Equations 6.18 and 6.19 that the rate constant ( $b$ ) for dispersion is greater than that for de-agglomeration. This suggests that the mixing of tracer through the lactose is driven by dispersion, with agglomerates only being able to break up once dispersed. This makes tracer dispersion the rate-limiting step and fits well with the mechanism for tracer mixing in the dispersion-dominant and dispersion/de-agglomeration regions as proposed in Chapter 4.

### 6.4.3 Coupling of flow analysis and colour data

It would be beneficial to be able to infer powder flow properties from colour data, particularly in industrial dry-powder mixing systems, where mixing is difficult to characterise often cannot be observed by eye. Some information about powder flow may enable better comparison of 'equivalent' operating conditions and can provide insight into the causes of poor blend attributes (such as content uniformity). Whilst there is no direct correlation between flow types and a single quantity (such as the rate of mixing, hue, content uniformity, or the maximum hue that can be reached within the mixer), flow assessment can be made by studying all regional colour data collectively as a function of time. By comparing regional colour changes within the mixer (Figure 6.19-Figure 6.26) and the occupancy and short term tracker flight data obtained from PEPT (Figure 6.31-Figure 6.35), the following relationships are found between colour changes and flow in this study (Figure 6.41).

To summarise the findings of Section 6.2.2:

- Powder mixing in the bumping regime (Figure 6.41a) shows fluctuations in the regional hierarchy (i.e. 'zig-zagging') in respect to both their degree of hue and hue saturation.

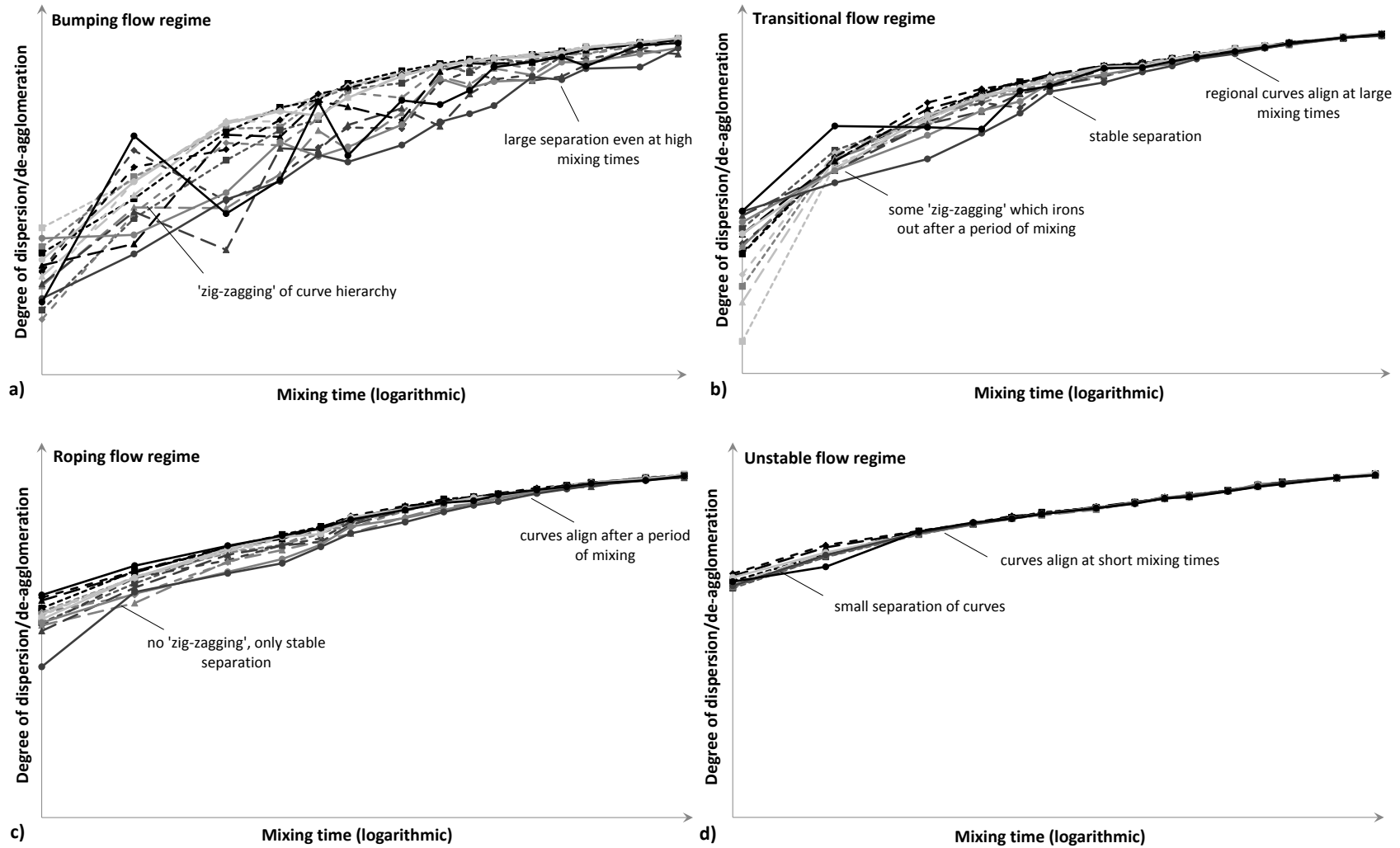


Figure 6.41: Schematic of typical regional colour curves over time for bumping (a), transitional (b), roping (c), and unstable (d) powder flow.

There is also a relatively high separation of region colour curves from one another even at large mixing times.

- Powder mixing in the roping regime (*Figure 6.41c*) shows regional curve separation with both hue and hue saturation; however the hierarchy remains fairly constant at each time point until the point where all regions align with one another at high mixing times.
- Transitional flows (*Figure 6.41b*) appear to show varying amounts of 'zig-zagging' and constant regional hierarchy at low mixing times, depending on its respective similarities to bumping and roping regimes. 'Zig-zagging' irons out at high mixing times.
- Unstable or chaotic flow (*Figure 6.41d*) shows small separation between colour values between regions at low mixing times, which align with one another, even at low mixing times.

In essence, this study shows that by taking multiple colour samples through the blend at each time point and assessing sub-regional fluctuations and their relative separation from one another, information about the type of powder flow can be achieved. Whilst this study only shows its use in predicting flow regimes within high-shear mixers, it is believed that it can easily be transferred to other mixing technologies. This adds another benefit and dimension to the use of the iron oxide colour tracer in assessment of mixers and operating conditions.

#### **6.4.4 Comments on the effect of impeller types on formulation curves**

Whilst this study serves to validate the use of the iron oxide colour tracer in assessing blend uniformity, energy input and predicting flow, the results can also show the effect of changing the impeller type and speed on the type of mixing that occurs. Results indicate that the content uniformity and the time-specific rate of mixing all depend on the impeller speed selected and the impeller type, with higher impeller speeds and impellers with a larger relative drag giving greater content uniformity for a given mixing time.

The results of this study imply that with increasing kinetic energy applied to the powder through an increase in the number of blades to an impeller, the impeller speed, sweeping area or the degree of direct frontal area of the impeller, content uniformity can be achieved more quickly. Also, a higher degree of de-agglomeration can be achieved for the same uniformity. Also, the type of impeller and impeller speed selected impact the flow of powder within the mixer, changing the bulk powder kinetics and inherently affecting content uniformity and the ability for tracer particles to undergo sufficient shearing to ensure their de-agglomeration. Some impellers and speeds were also found to be able to create flexible formulations, with excellent uniformity and ‘tuneable’ degrees of tracer de-agglomeration. Impeller 4 at all tested speeds and Impeller 3 at 300 rpm were found to have this ability, with Impeller 4’s ability attributed to the chaotic mixing that occurs with its use. Each type of impeller was found to create different powder flow regimes at the selected impeller speeds and related to their relative drags. Those with a high drag created flows in more developed flow regimes. In summary a large number of factors come into play when trying to optimise the mixing within a high-shear mixer, and consideration needs to be given to the type of impeller employed, its operating speed and mixing time to ensure the final blend meets desired specifications.

#### **6.4.5 Benefits and limitations in use of iron oxide tracer**

Results from this study agreed with previous findings for the attributes of using iron oxide. Through analysis of the CIE colour space there appeared to be no changes in the particle size distribution between blends, and curves generated were able to be distinguished at different impeller speeds. Several additional benefits were identified, including the ability to quantify content uniformity and energy input, distinguish the degree of mixing between different impeller types, and detect regions of poor and no mixing. In addition, the measurement of multiple regions within the powder allowed for the colour data to be used to assess, predict and compare powder flow types between different sets of operating conditions. Whilst the sampling of sixteen different regions of the powder bed was sufficient for this study, it is anticipated that more accurate insight into blend uniformity and effects of bulk powder motion can be obtained through a larger number of samples. Also, the uses of the

colour tracer method outlined in this chapter are believed to be applicable to other mixing technologies beyond high-shear mixers. This requires further validation work, beyond the scope of this thesis.

## 6.5 Conclusion

In this study lactose and iron oxide colour tracer were blended in a vertical-axis high-shear mixer using different impeller types and impeller speeds to assess the ability of the tracer to measure several key attributes such as homogeneity and rate of mixing. From the CIELCH colour space analysis of several samples through the powder bed at different mixing times, content uniformity, and the rate of mixing could be measured and compared, even when using different impeller types and speeds. These findings were consistent with previous chapters in the analysis and use of colour curves, and added further knowledge to their versatility and application. Formulation curves were also determined to be able to quantify the total energy input to the blend (through complimentary torque measurements), and predict the flow regime under which powder mixing was occurring. The ability to be able to measure and compare content uniformity (which is calculated from the relative standard deviation of blend hue intensity at through the blend at a given mixing time) shows the greatest significance. Impeller types with large sweeping volume and front facing regions (i.e. having greater drag force) were able to reach higher content uniformities in a reduced mixing time, with a larger flexibility in the degree of dispersion for a given uniformity. These added attributes to the colour tracer method enable it to be even more effective in determining appropriate mixing conditions during process optimisation, validation and scale-up, and allow for more robust process development prior to drug blend manufacturing.



## The effect of fines on the shape of formulation curves in nominal and extreme blending conditions

**T**he level of fines and product stability are important attributes for pharmaceutical dry powder formulations, and can be influenced by several factors including the nature of the powder blending process with which they are manufactured. The high intensity forces required during blending to ensure sufficient product uniformity and de-agglomeration of highly cohesive drug particles often cause excipient particle surface modification and damage. This can increase the rate of atmospheric moisture uptake within the formulation and decrease its storage lifespan and aerosol performance in the case of dry powder inhalation formulations. Abilities to detect and assess unintentional particle damage and milling during blending are very limited and often require post-blending techniques. In addition, batch-to-batch variations in fines can affect performance. In this chapter, the colour tracer is used to assess its viability as a tool to not only detect, but also quantify the extent of milling in a formulation, and identify batch-to-batch variations. Using a range of formulations, the method's sensitivity to variations in the amount of fines is investigated.

## 7.1 Introduction

The level of fines in formulation can have a profound impact on the inhalation performance of DPI formulations (Shur *et al.*, 2008), and in many cases is used as a tool to manipulate fine particle fraction and emitted dose (Andreou *et al.*, 2009, Jones and Price, 2006). In some cases, performance and storage stability can even be swayed by batch-to-batch variation of the level of fines in excipient from the suppliers (Guenette *et al.*, 2009). As DPI formulation performance is sensitive to the level of fines, it is desirable and reproducible to ensure that no further fines are generated during the blending of active and excipient, which also affects product stability.

The stability of a pharmaceutical formulation is vital to many factors, including shelf-life, long term performance, methods of transportation, storage and ultimately the cost and accessibility of the final product (Bridson *et al.*, 2007). It can be affected by particle damage and attrition, which are an inevitable consequence of the processing of particles (Bridgwater *et al.*, 2003), and the conditions that lead to it are not well understood (Neil and Bridgwater, 1994). Many pharmaceutical actives, especially those of a DPI formulation which have a desired particle size of the order of 1-5  $\mu\text{m}$ , are typically highly cohesive and therefore form cohesive clumps which are difficult to break up and disperse within the bulk material. As mentioned in Chapter 2, to ensure that this occurs and that the entire blend can achieve sufficient homogeneity to the scale of a unit dose, an excess of energy during mixing (typically high intensity) is used. This excess of energy can lead to undesirable side effects such as cracking and milling (attrition) of the large excipient particles.

Many terms exist to describe the damage and breakage of particles. In this study, the term *attrition* is used to denote both particle surface modification (abrasion) and fracture into fine particles (milling). The abrasion incorporates effects which include the removal of surface layers of particles, edges or corners. The term *milling* is used to denote particle fragmentation into two or more parts with at least two of the parts of similar order to the parent particle (as opposed to chipping). Other smaller particles may also be formed during milling.

### 7.1.1 Milling and milling mechanisms

The milling of a material relies on the generation and propagation of cracks in the surface (*Rhodes, 2008*). To achieve crack propagation it has been proposed that the strain energy applied to the material must overcome its surface energy (to create plastic deformation) and that there must also be a mechanism available in the material for the crack to propagate (*Griffith, 1921*). In brittle materials, such as lactose, multiple cracks can form before the first crack brings material failure.

Small particles are inherently more difficult to break. With smaller particles, the length of a crack is limited and there is less room for stress distribution patterns to develop. Therefore, a higher mean stress needs to be applied to cause failure (*Rhodes, 2008*). As particle size decreases, the required strength to fracture the particle increases until a critical size is reached where crack propagation becomes impossible (*Kendall, 1978*). There are two mechanisms in powder blending which can result in particle milling (*Rhodes, 2008*):

- Crushing, where a stress is applied on two surfaces of a particle or collection of particles
- Impact fracture, where a moving particle impacts on a surface or other particle

A third mechanism exists for wet milling systems, where the medium can apply stress on the particles. This is not significant in the dry blending of DPI formulations however it plays a key role in the aerolisation of the product when inhaled (as outlined in *Chapter 2*).

The rate of particle attrition for a given material is determined by both the physical process and the internal/external morphology of the particles (*Bridgwater et al., 2003*). The types of attrition caused by shearing in moving beds of powder are well documented (*Couroyer et al., 2000*). Several experimental studies in the past have used annular shear cells to assess the breakage and deformation behaviour of different materials, morphologies and particle sizes (*Bridgwater et al., 2003, Ghadiri et al., 2005*). An annular shear cell study (*Bridgwater et al., 2003*) found that in a mixture of particles that varied in shape and size, there was a rounding of corners due to local abrasion in systems with low strain and high stress.

Numerical simulations based on annular shear cell studies also exist (*Jones and Price, 2006, Potapov and Campbell, 1997*), and have found the degree of milling to be proportional to the work done on the particles.

During the flow of bulk solids under consolidation, particle motion occurs through the motion of discrete 'pockets' of the powder mass, each with low shear strain. Between each discrete pocket of powder is a high shear strain failure zone, which has been reported to be around ten particle diameters in width (*Bridgwater et al., 2003, Hare et al., 2011, Stephens and Bridgwater, 1978*). In such a system the packing of the particles is restructured to create sufficient free space for one block of powder to slip past another (*Neil and Bridgwater, 1994*).

### 7.1.2 Issues associated with milling during blending

The above processing mechanisms that lead to particle attrition can occur at several steps along the production route. It can occur during the initial manufacturing of the excipient (i.e. primary processing), where the powder may experience some form of milling or sieving, particularly when intrinsic fines are generated for ternary DPI formulations (as opposed to binary formulations, which contain only coarse carrier and drug). It may also occur unintentionally during the excipient's secondary blending with the pharmaceutical active due to the nature of mixing required to disperse and de-agglomerate the drug particles. A number of studies have previously reported the effect of mechanical processing on the surface modification of powder in high intensity processes, in particular following milling (*Briggner et al., 1994, Brodka-Pfeiffer et al., 2003, Elamin et al., 1994, Newell et al., 2001*). It is well documented that the processing of crystalline materials using high-energy processes will induce damage to the crystalline lattice (*Ward and Schultz, 1995*), resulting in long-range disorder of molecules in the crystalline structure (i.e. generate amorphous regions), electrostatic charge build-up or change in bipolar charging, particulate rearrangement (including agglomeration) or chemical contamination (*Andreou et al., 2009*). Such induced changes can lead to uncertainty and inconsistency in product behaviour, namely its aerolisation and degradation

characteristics. Little is reported on the effects of secondary blending on solid dosage forms (Bridson *et al.*, 2007). The unintentional milling of formulations during secondary mixing has been observed previously in high-shear blenders (Shur *et al.*, 2008), which are frequently employed in the manufacturing of DPI formulations. It was found that the *in situ* (from the Latin for 'in position') milling of excipient in the blend may provide immediate improvement to the product by increasing the level of fines, however the added benefit is short-lived as the surface modifications readily absorb atmospheric moisture, creating solid bridges between drug and excipient particles and eventually hindering the de-agglomeration of the formulation upon inhalation (Guenette *et al.*, 2009). This can also have negative effects to downstream processes, making it more difficult to meter doses and fill capsules or boluses.

When discussing the stability of an ordered mixture there are two types (Guenette *et al.*, 2009);

- Physical stability (i.e. the propensity for ordered structures to disorder through agitation).
- Chemical stability (i.e. the chemical degradation of the powder due to atmospheric moisture absorption).

Whilst high intensity processes that are likely to cause milling may also affect the physical stability of a formulation by embedding fine particles on to the carrier particle surfaces, stability in this chapter refers to their chemical degradation through attrition. The amorphous state of a material is thermodynamically unstable by nature, and over time is driven to the more stable crystalline state. When sufficient molecular motion is provided (i.e. when the amorphous material temperature is greater than or equal to the glass transition temperature,  $T_g$ ), molecules have the freedom to re-arrange into a crystalline form. Typically, the  $T_g$  of pharmaceutical actives in their amorphous state is greater than atmospheric temperature, giving them stability in normal conditions. In the presence of moisture however, the effective  $T_g$  is significantly lowered and many materials can revert to their crystalline form at ambient temperature. This is caused by the ability for water to increase molecular mobility through plasticisation. For example, the  $T_g$  of lactose is 108°C, however at elevated relative

humidity (56% RH), the effective  $T_g$  can be lowered to 25°C (*Price and Young, 2005*). Therefore, when using lactose in a formulation, the amount of material in an amorphous state has a significant effect on product stability.

The kinetics of degradation are dependent on many factors including the dimensions of the amorphous region (surface area, depth, pore dimensions, etc.), the surrounding structure and environmental conditions (*Price and Young, 2005*). The dimensions of amorphous regions and their surrounding structure are affected by the nature of the blending process and the intensity and type of inter-particle interactions. The industrial remedy for instability caused by high intensity blending is to 'condition' the powder post-blending, whereby the powder is handled in a passive manner (often relaxed or rested for a period of time) so as to minimise the problems associated with blending such as the dissipation of static electricity that builds up within the powder (*Andreou et al., 2009*). To complicate matters, the presence of lactose in formulation can also promote or increase the rate of chemical degradation in certain pharmaceutical actives (*Wirth et al., 1998*), as certain drug and lactose DPI formulations are susceptible to increased adhesion forces with exposure to elevated relative humidities (*Podczek et al., 1997*). With an increase in fines in formulation, the propensity for the degradation of the pharmaceutical active increases as the rate of moisture uptake increases (*Guenette et al., 2009*). Due to the multitude of effects that fine lactose can have on the final product, or means of ensuring consistent fine levels is vital.

### 7.1.3 Current methods of detection

Current technologies for the measurement of fines, both initially and during blending, particularly for batch processes, are limited (*Andreou et al., 2009*). The most commonly used technique is laser diffraction (*Pitchayajittipong et al., 2010*), whereby a powder sample is fluidised and conveyed past a laser beam which passes through the stream perpendicularly. The degree of resulting obscuration of the laser beam on a series of detectors on the other side of the fluidised powder stream gives an indication of a particle's equivalent volume sphere diameter. Changes in the level of fines in

formulation can also be detected through the use of BET analysis, which measures the surface area of the powder based on its gas adsorption/desorption profile. Other techniques such as Atomic Force Microscopy (AFM) and Scanning Electron Microscopy (SEM) can show whether any surface modification of the sample has occurred.

Beyond measuring the level of fines in formulation, tests are also required to measure the chemical stability of the formulation. The current tests for the stability of a DPI formulation rely on storing the powder for a predetermined length of time at a particular relative humidity and retesting the inhalation performance of the product. Predictions of the particle behaviour can be initially assessed through dynamic vapour sorption (DVS), whereby the rate of moisture uptake by the particles gives information on their surface energy and hence their chemical stability. Other initial testing tools include the measurement of electrostatic charge on the powder after blending, which can provide an indication of the level and intensity of impacts that particles have undergone, and can be related to any potential surface modifications in the formulation (*Jones and Price, 2006*).

#### **7.1.4 Effect of level of fines on DPI performance**

As mentioned previously, one means of increasing the de-agglomeration efficiency of the DPI formulation upon inhalation, and hence, the therapeutic efficiency is via the addition of ternary agents such as fines (*Louey and Stewart, 2002, Tee et al., 2000*). For such preparations, a small quantity of fine excipient (which is of similar size to the active pharmaceutical ingredient) is used. As mentioned in Chapter 2, fines can be either co-added with the API and coarse carrier during the blending process, or generated intrinsically during the primary processing of the excipient (*Tee et al., 2000*). The improved performance in the inhaler device from the addition of fines may be related to an increase in the tensile strength of the powder bulk, which significantly increases the minimum fluidisation velocity of the powder and thereby increases the aerodynamic drag on the formulation (*Shur et al., 2008*). The increase in drag may improve the detachment of drug particles from carrier active sites and improve aerosol performance. The associated risk of instability in formulation from

the presence of fines can be lowered by their manufacture prior to (and not during) secondary processing.

As described in Chapter 2, the fluidisation of the DPI formulation is largely a function of the relationship between the pressure differential across the device and the tensile strength of the DPI formulation, as well as the types and intensity of capsule impacts (in a capsule based system). Therefore, processes which influence the tensile strength of a powder blend may be able to significantly influence the fluidisation and aerolisation behaviour of the DPI formulation (*Shur et al., 2008*). The tensile strength of a formulation increases with increasing consolidation stress and free volume (*Watson et al., 2001*), and the bulk physicochemical properties of binary and ternary DPI formulations are critical in determining their fluidisation and entrainment behaviour (*Stephenson and Thiel, 1980*). Powder flow properties are an important consideration and have been shown to be a key factor in predicting the *in vitro* and *in vivo* performance of passive DPI systems (*Concessio et al., 1999*).

The sensitivity of product fluidisation behaviour to the level of fines may even be affected by batch-to-batch variations caused by their production, particularly in industrial scale equipment (*Gamble et al., 2010, Guenette et al., 2009, Steckel et al., 2006*). Batch-to-batch variations can come from a single supplier or between multiple suppliers and are caused by differences in raw materials, manufacturing processes, storage conditions and modes and lengths of transportation (*Moreton, 2009*). Such variations that may lead to unusual characteristics and formulation behaviour during blending and in downstream processing, and can go undetected initially due to relaxed regulatory testing guidelines. The regulatory requirements for excipients (such as respective Pharmacopoeias), are often based on the verification of a material's identity (such as purity and chemical stability) and not necessarily the size and physical properties of the powder (*Gamble et al., 2010*). As such, there are cases where an excipient meets the Pharmacopoeial tests but provides surprising characteristics during processing or in its final form.

### 7.1.5 Previous work in level of fines on DPIs

Extensive studies have been conducted on the effect of fines and their characteristics on formulation (Shur *et al.*, 2008). As mentioned in Chapter 2, drug delivery can be enhanced by adding a larger amount of fines to the formulation. A number of mechanisms are proposed to be behind this phenomenon, including corrosion (i.e. the filling of active sites (Hersey, 1975)) and the formation of drug/fine agglomerates (Lucas *et al.*, 1998a). The validity of each mechanism has been questioned however as the body of evidence in support of both mechanisms is limited (Jones and Price, 2006). Several studies have found that the carrier materials that contain the highest proportion of intrinsic fines gave greater performance (de Boer *et al.*, 2003, Lahrib *et al.*, 1999, Lambregts *et al.*, 2004, Steckel *et al.*, 2006, Tee *et al.*, 2000), which can also be decreased by their removal. The addition of lactose or other types of fines to formulation increases performance however literature suggest that it results in increased drug retention in the device (Jones and Price, 2006). The optimum size range of fines has been debated in literature (Adi *et al.*, 2007, Stewart *et al.*, 2005, Zeng *et al.*, 1999, Zeng *et al.*, 1998), and the optimum median aerodynamic particle size appears to be approximately 5-8  $\mu\text{m}$  (Jones and Price, 2006). It has also been suggested that the optimum concentration of fines in ternary formulations occurs when the ratio of drug particles to fine excipient particles is 1:1 (Islam *et al.*, 2004, Stewart *et al.*, 2003). The fine particle fraction (FPF) decreases as this ratio increases. A correlation between powder packing efficiency and flow-ability has been previously reported (Watson *et al.*, 2001), in which it has been suggested that uniform powder packing creates good flow properties upon inhalation. Whilst this can be influenced by shape, for systems where the shape of particles are similar this is governed by the adhesion/cohesion properties of the powders, good packing can be achieved with low tensile strengths (Valverde *et al.*, 1998). Flow agents can also be added to improve flow (Zhou *et al.*, 2010, Zhou and Morton, 2012). A comprehensive review of literature on the influence of fines on DPI performance can be found in Jones and Price (2006).

### 7.1.6 Use of iron oxide to detect milling and batch variation

As proposed in Chapter 4, the 3-dimensional colour space can be used to measure and potentially quantify the level of fines in formulation, both initially and with standard blending, and also from *in situ* milling of particles. The milling of lactose particles in a colour tracer formulation provides a unique and measureable shift of colour in the 3-dimensional colour space. In Figure 3.13 the colour change from the attrition of lactose carrier particles results in a sharp increase in blend lightness ( $L^*$ ) and a decrease in hue intensity ( $C^*$ ) at constant hue ( $h$ ). This is caused by the fracture of coated carrier particles, which generate fresh white surfaces and ‘pastel down’ the observed colour. As described in Chapter 5, if the tracer concentration is in the optimal range and does not allow saturated coverage of the lactose, any white surfaces generated after coating will remain uncoated as all tracer particles are already fully de-agglomerated and fixed to the initially available sites on the carrier surfaces. This colour change was observed in the work of Chapter 4 and classed as the ‘milling’ region of the formulation curve. Due to the nature of the viability study in Chapter 4, insufficient results were gathered to fully investigate the milling region or the transitional point with the de-agglomeration/dispersion region. It was also unclear from the study as to whether the length of progression of formulation curves into the milling region could be used to quantify the level of milling in formulation. In the same study, the initial level of lactose fines in formulation was found to dictate the position of a formulation curve along the common plane. It was unclear however whether the shift in the plane could be predicted and/or measured.

In this study, further investigation of the shape and nature of the milling region of formulation curves is conducted to determine whether the degree of milling can be quantified, as well as the effects of the level of fines on the position of formulation curves along the common plane (described in Chapter 4). This will add benefit to the use of the tracer method and allow for effective determination of the appropriate design space for different mixers to prevent stability issues in formulation, and mitigate against the negative effects of batch-to-batch variations.

## 7.2 Materials and Method

### 7.2.1 Powder selection and powder properties

Formulations with different levels of fine material and cohesivity were created with combinations of fine grade lactose (Lactohale LH230) and standard lactose (Lactohale LH200). Five formulations were made from 0, 10, 20, 40 and 99 wt% fine grade lactose in final formulation (with 1 wt% tracer). These formulations differed greatly in their particle size distributions (*Figure 7.1*) and volume of ultrafines and fines as determined by laser diffraction (*Table 4.1*). Further information on lactoses and lactose blends beyond what is required for this study are provided in Chapter 8.

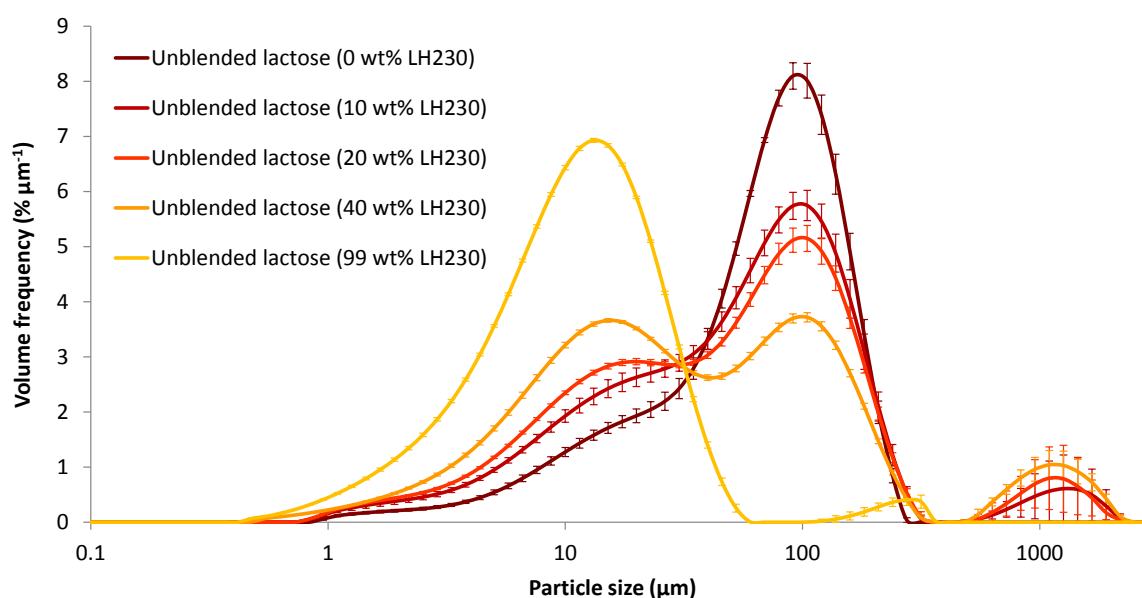


Figure 7.1: Particle size distributions for lactose blends used in this study.

Table 7.1: Fine particle properties of lactose mixtures selected for this study. Lactose mixtures are expressed in weight percentages of Lactohale LH230 in final pigmented formulation containing 1 wt% iron oxide tracer.

Label	Lactose in formulation	vol.% < 4 μm	vol.% < 15 μm
0 wt% LH230	LH200	2.77 ± 0.31	12.83 ± 0.97
10 wt% LH230	LH200 + 10% LH230	5.13 ± 0.56	20.51 ± 1.44
20 wt% LH230	LH200 + 20% LH230	6.09 ± 0.17	24.72 ± 0.45
40 wt% LH230	LH200 + 40% LH230	8.48 ± 0.24	33.96 ± 0.64
99 wt% LH230	LH230	17.98 ± 0.27	68.73 ± 0.37

### 7.2.2 Experimental scheme

To gain a broad amount of information on the milling region and the transition from the de-agglomeration/dispersion region for each formulation curve, a set of 20 blending experiments was created by mixing each formulation in the mechanofusion mixer (outlined in *Section 4.2.2*) at four different impeller speeds (600, 1000, 2000 and 3000 rpm). A further five blends (one of each formulation) were manufactured in the tumbler mixer at 72 rpm to generate full formulation curves in the CIELCH colour space (*Table 7.2*). Colour results were collected as specified in *Section 3.2.2* using the standard time points up to 60 min. Particle size distributions were obtained from dry powder laser diffraction as per *Section 4.2.1*.

**Table 7.2: Experimental matrix for fines study showing blend labels for all 20 mechanofusion (ultra-high shear) blends and 5 tumbler blends.**

Blend labels	0 wt% LH230 (1)	10 wt% LH230 (2)	20 wt% LH230 (3)	40 wt% LH230 (4)	99 wt% LH230 (5)	
Unblended (A)	1A	2A	3A	4A	5A	
Tumbler 72 rpm (B)	1B	2B	3B	4B	5B	
Mechanofusion	600 rpm (C)	1C	2C	3C	4C	5C
	1000 rpm (D)	1D	2D	3D	4D	5D
	2000 rpm (E)	1E	2E	3E	4E	5E
	3000 rpm (F)	1F	2F*	3F	4F	5F

\*Mixed for 45 minutes only (limited by physical properties of formulation in system at 3000 rpm)

## 7.3 Results

To thoroughly study the effects of fines on the shape and position of formulation curves, both colour and particle size distribution data was collected. The colour data gave insight into the mixing behaviour of each blend and formulation, and the particle size data reinforced any hypotheses about mixing mechanics and milling that arose from the colour data.

### 7.3.1 CIELCH formulation curves

As per previous studies, the colour values for each blend were found to overlap and generate formulation-specific colour curves in the CIELCH colour space (Figure 7.2).

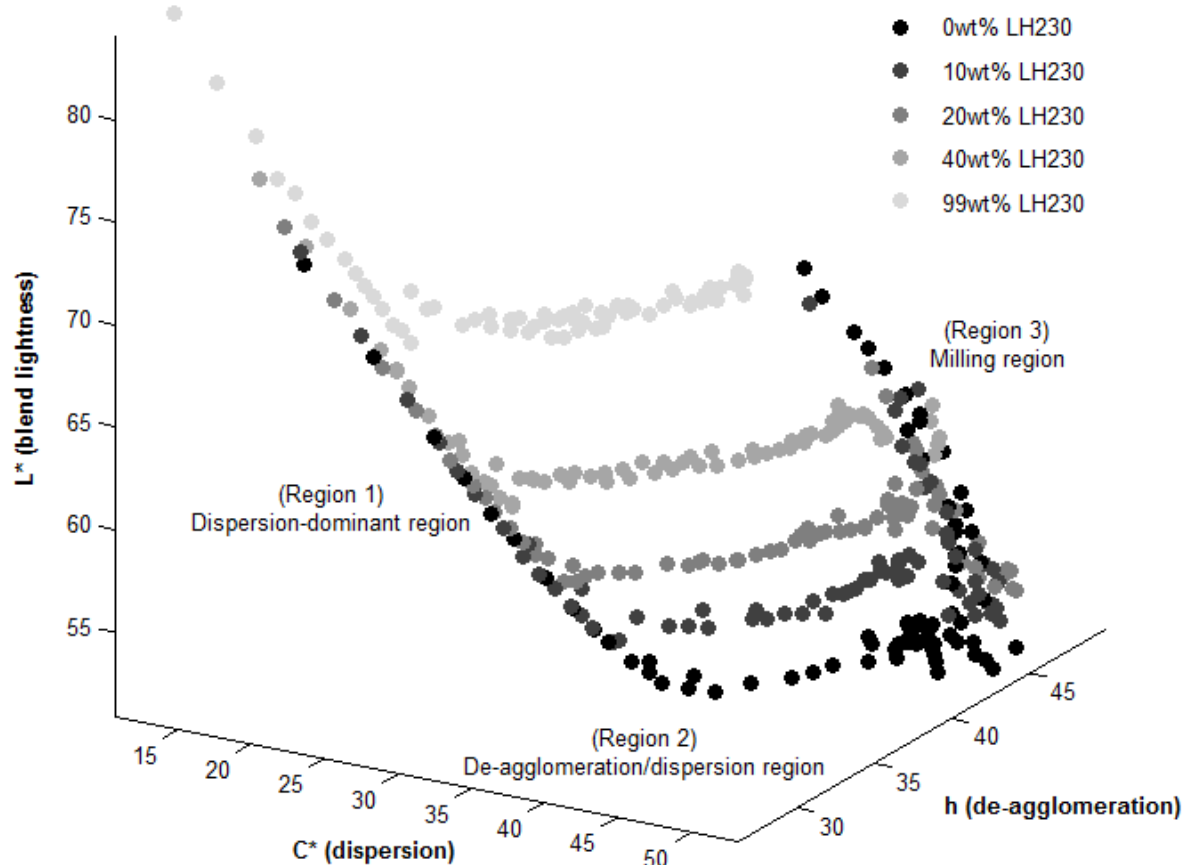


Figure 7.2: CIELCH colour data collected for each blend and time point. Values overlap to create formulation-specific colour curves.

These formulation-specific curves have the same position and shape to those obtained in previous chapters, with the three previously discussed distinct regions of mixing (dispersion-dominant, de-agglomeration/dispersion and milling regions, *Chapter 4*). Again in the dispersion-dominant region, formulation curves all align on a straight line with decreasing  $L^*$ , which indicates dispersion-dominant mixing. Formulation curves lie in this region at low mixing times and/or low process intensities. At the limits of the dispersion-dominant region, formulation curves then deviate into a transitional region. This transitional region is curved and indicates the limit of tracer dispersion-dominant mixing and the beginning of tracer de-agglomeration/dispersion mixing. The de-

agglomeration/dispersion region follows a straight line with constant  $L^*$  and is the product of iterative tracer de-agglomeration and dispersion as outlined in Chapter 3. At the limits of the de-agglomeration/dispersion region, some formulation curves appear to dip in blend lightness to a common vicinity and then progress along another straight line with increasing  $L^*$  (the milling region). This region indicates the milling of lactose particles and appears to only occur for certain mixing conditions and formulations. All formulation curves again align on a common plane as per Chapter 4. The level of initial fines in formulation appears to dictate the position of the formulation curve along the common plane, as well as its shape. Formulations comprising of low levels of fines enter the milling region and sit relatively low along the common plane. As the level of initial fines in the formulation increases, the formulation curves shift vertically upwards along the common plane and the length of progression into the milling region either decreases or ceases.

The start and end points for each blend along a given formulation curve also vary with process intensity and/or mixing time in the same manner as in previous work; with more intense processes/larger mixing times finishing further along the formulation curves. This can be viewed in the  $C^*-h$  plane, which also provides direct information on the degrees of tracer dispersion and de-agglomeration (Figure 7.3).

In Figure 7.3, the hollow points depict tumbled blends whilst solid shapes show mechanofused blends. These can be seen to overlap in the dispersion-dominant and de-agglomeration/dispersion regions.

One addition to previous studies is the extra data points obtained for the milling region, where each formulation exhibits different behaviour. Formulations with 0-20 wt% LH230 (which are classed as having a low level of fines) appear to exhibit a large decrease in hue intensity ( $C^*$ ) in this region, suggesting milling has occurred. Formulations with greater than 20 wt% LH230, which contain the largest amount of fine particles by mass, do not extend into the milling region and therefore are assumed to not mill (from the colour data).

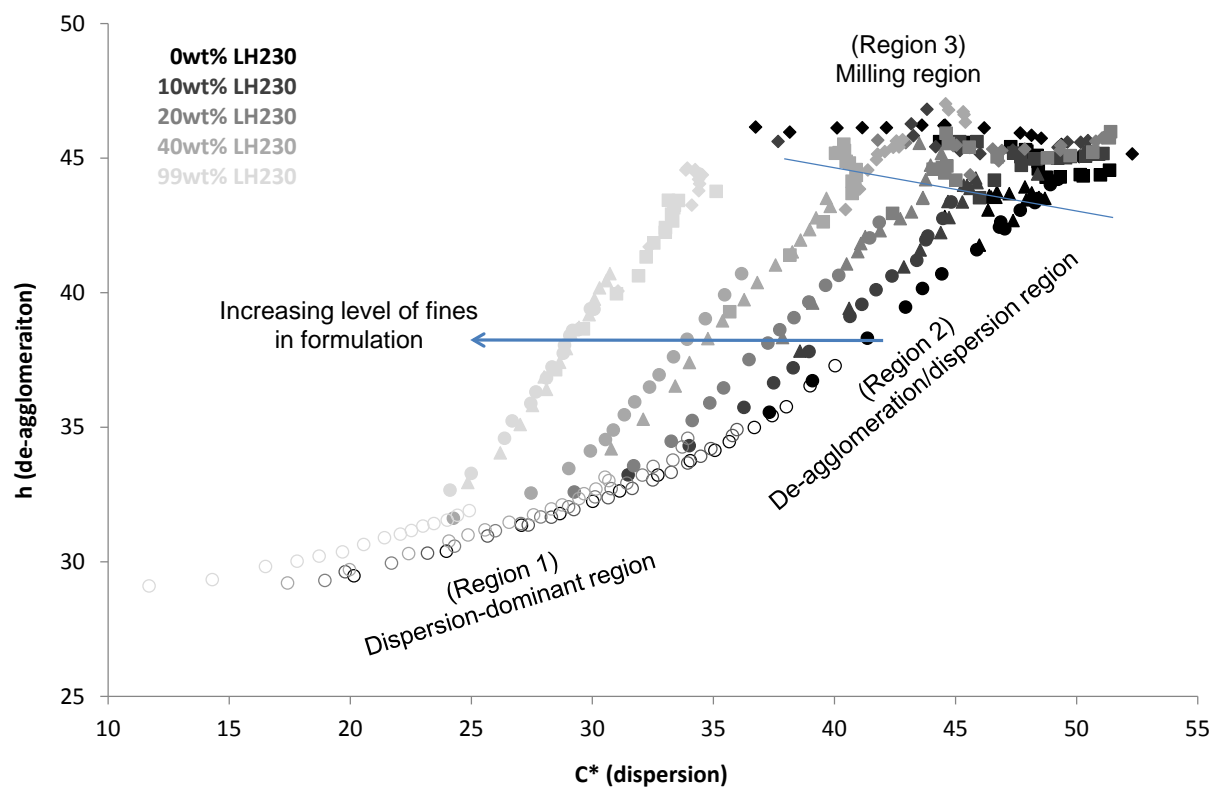


Figure 7.3: Blend curves in the  $C^*$ - $h$  plane showing overlap and the separation based on level of fine lactose.

Using an expression analogous with  $\Delta E^*$  (outlined in Section 2.4.2), but in respect to the CIELCH space and not the CIELAB space, the length between two values ( $A$  and  $B$ ) in the 3-dimensional colour space can be quantified from their respective  $L^*C^*h$  values (Eqn. 7.1):

$$\Delta E_{AB(LCH)}^* = \sqrt{(L_B^* - L_A^*)^2 + (C_B^* - C_A^*)^2 + (h_B - h_A)^2} \quad (\text{Equation 7.1})$$

The shift of formulation curves in the milling region in respect to hue intensity ( $C^*$ ) or 3-dimensional position in the CIELCH colour space ( $\Delta E^*(LCH)$ ) appear to be similarly dependent on the amount of initial fines in formulation (Figure 7.4).

As data points in the milling region for the 10 wt% LH230 formulation (at 3000 rpm) is taken up to 45 minutes of mixing and not 60 minutes like the other formulations, it is assumed that the colour of the blend would be

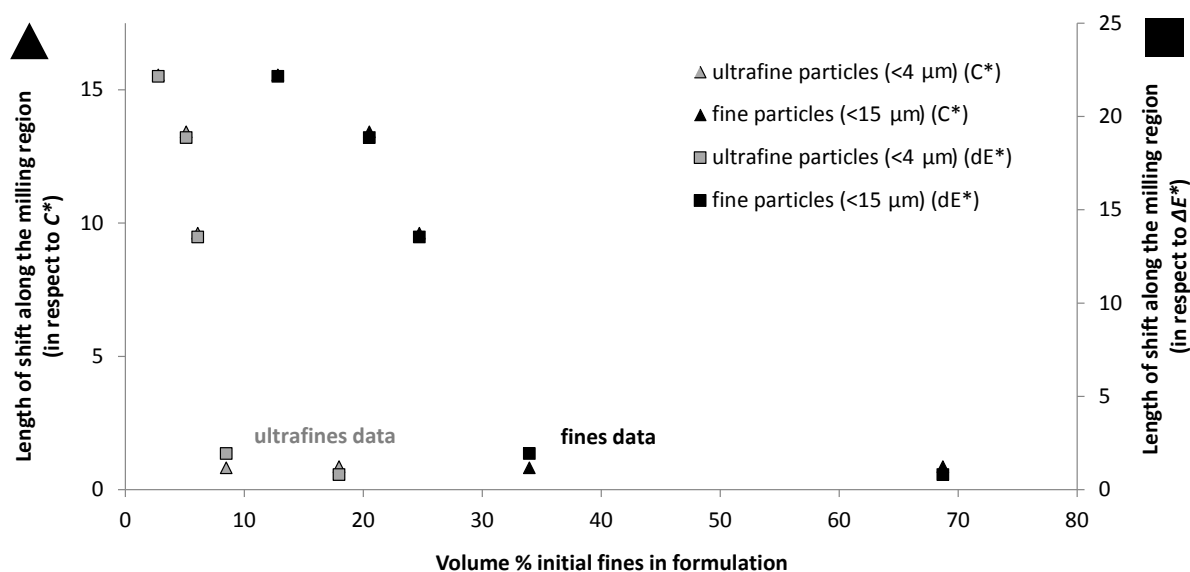


Figure 7.4: The length of the milling region (at 3000 rpm) in respect to change in  $C^*$  and  $\Delta E^*$  (LCH) with changing initial level of fines in formulation.

the same after 60 minutes of mixing. With this assumption for the 10 wt% LH230 blend, the shift of formulation curves in the milling region is calculated from the difference between the lowest value of  $C^*$  in the milling region (at 3000 rpm) compared with the maximum value of  $C^*$  along the formulation curve (which occurs at the beginning of the milling region). A similar trend can be seen when comparing the shift along the common plane (in respect to  $\Delta E^*$ ) with the initial amount of fines in formulation. Results suggest that all formulations but the pure fine lactose (99 wt% LH230) show some degree of milling. The degree of milling decreases with increasing fines, and appears to be negligible beyond a certain critical value of fines in formulation, which is estimated to be around 7 vol% for ultrafines and 30 vol% for fines. This critical concentration of initial fines in formulation is likely to be process dependant, and would likely increase with a more intense process than the ones used in this study.

As not all formulations mill with mechanofusion and the nature of milling is chaotic, the transition between mixing and milling (i.e. from the de-agglomeration/dispersion to milling region) is more complex than the transition from dispersion-dominant mixing to de-agglomeration/dispersion mixing. The transition between the de-agglomeration/dispersion and milling regions appears to occur very rapidly at a given set of mixing conditions. Most data jumps from the constant- $L^*$  section

of the de-agglomeration/dispersion within one or two data points, suggesting that the mechanism behind this pre-milling phenomenon is quite rapid.

All process curves that exhibit these transition ‘kinks’ also progress into the milling region. The decrease in  $C^*$  as mixing time increases in the milling region is consistent with the proposed theory of colour changes outlined in Chapter 3; whereby the fracture of large lactose particles creates a larger specific surface area of white and thereby ‘dulls’ the intensity of a given hue. Other aspects of the different regions, transitions and ‘kink’ can also be viewed in respect to the  $L^*$ -axis (Figure 7.5).

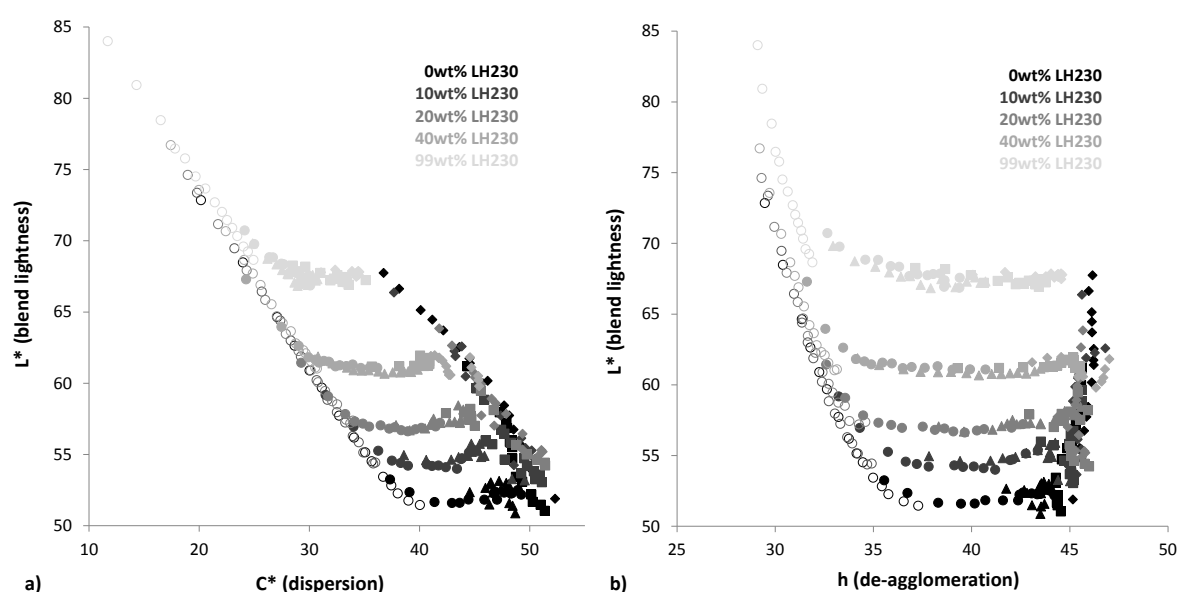


Figure 7.5: Comparison of degree of blend lightness ( $L^*$ ) with degree of dispersion ( $C^*$ ) (a), and degree of de-agglomeration ( $h$ ) (b) for different levels of fine lactose.

Results suggest that there is a common and predictable location in the CIELCH colour space in which formulation curves enter (or ‘kink’ to) prior to milling, regardless of the initial level of fines in formulation. This may indicate a common agglomerate size of fine and coarse lactose that leads to milling, or may be attributed to other unknown effects. This is further investigated in Section 7.4.

### 7.3.2 Particle size data

To provide better insight into the mechanistic behaviour behind colour data, particle size distributions were taken for each blend after 60 minutes of mixing (Figures 7.6-10).

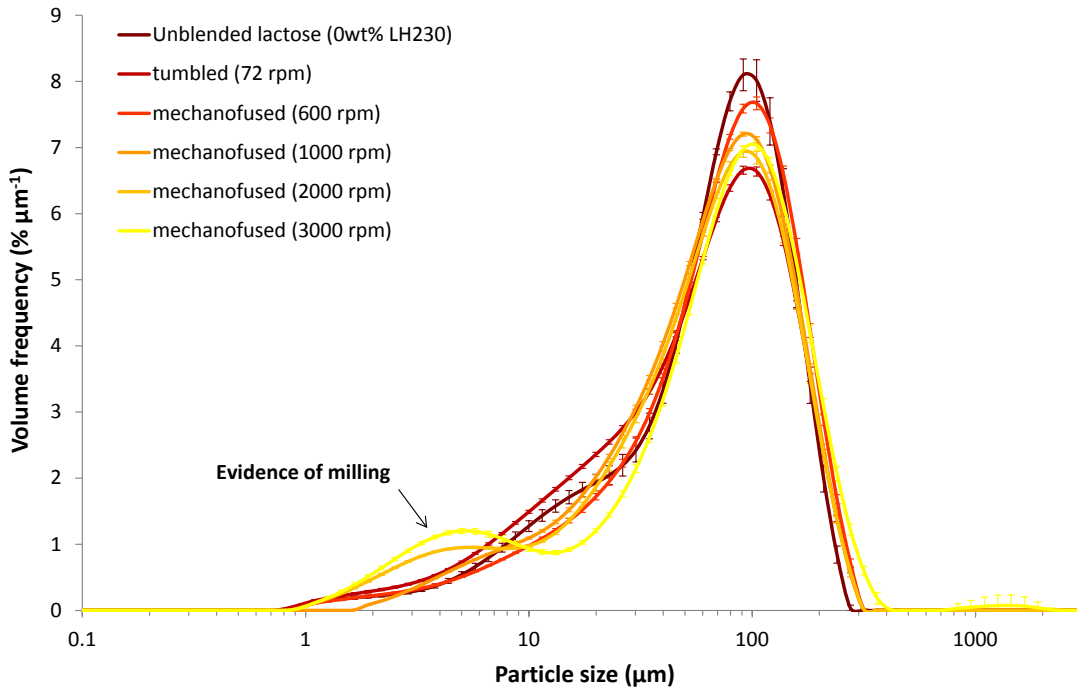


Figure 7.6: Particle size distribution for 0 wt% fine grade lactose (Lactohale LH230), showing shift in distribution for each blend due to different mixing conditions.

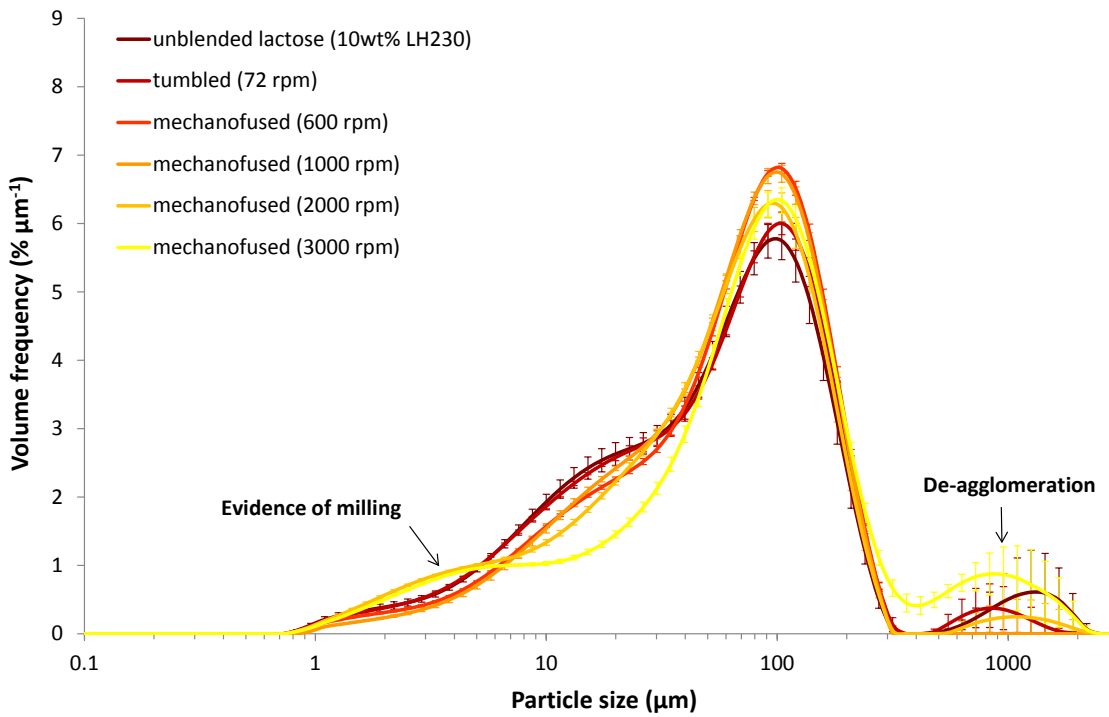


Figure 7.7: Particle size distribution for 10 wt% fine grade lactose (Lactohale LH230), showing shift in distribution for each blend due to different mixing conditions.

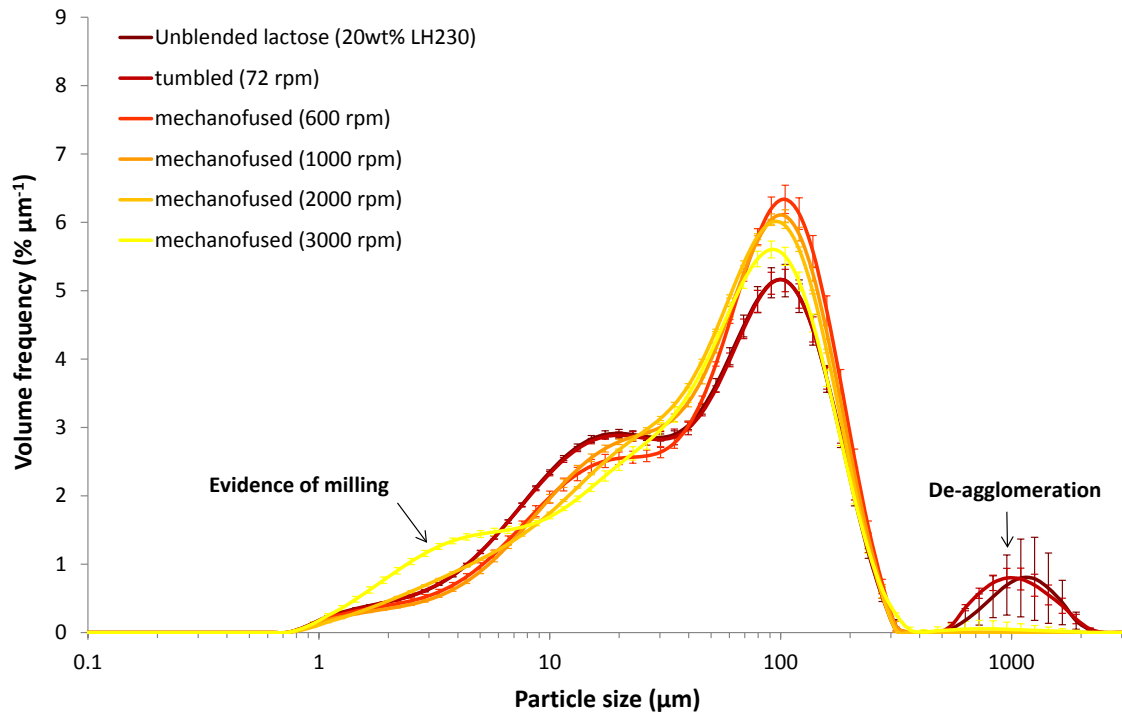


Figure 7.8: Particle size distribution for 20 wt% fine grade lactose (Lactohale LH230), showing shift in distribution for each blend due to different mixing conditions.

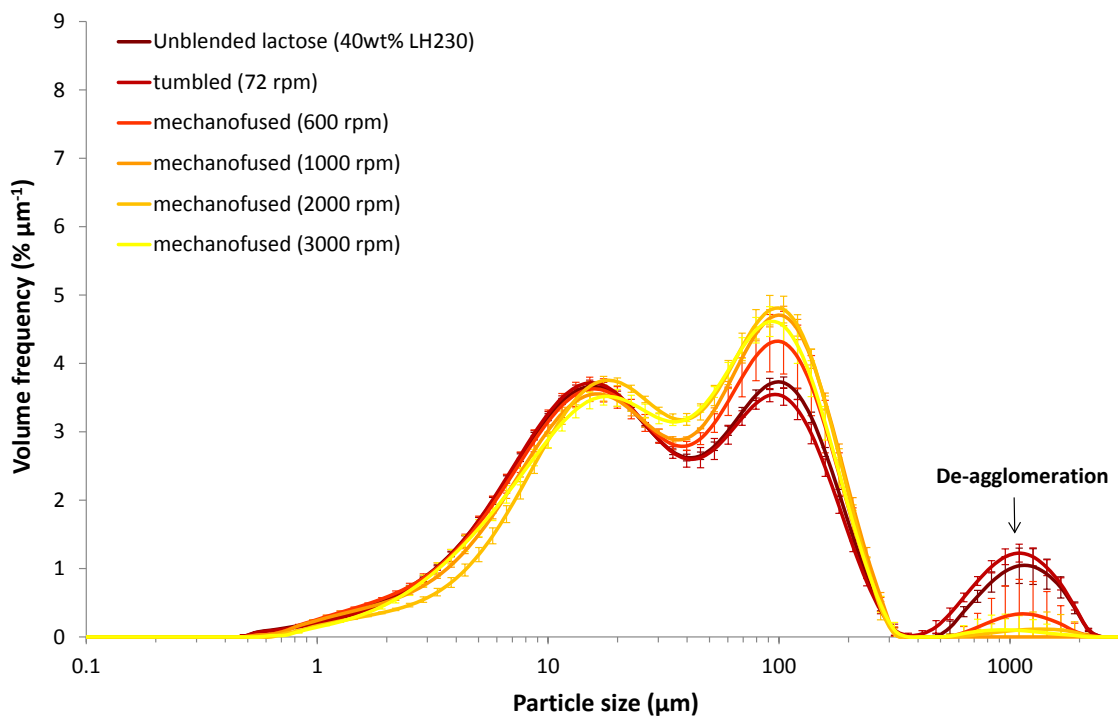


Figure 7.9: Particle size distribution for 40 wt% fine grade lactose (Lactohale LH230), showing shift in distribution for each blend due to different mixing conditions.

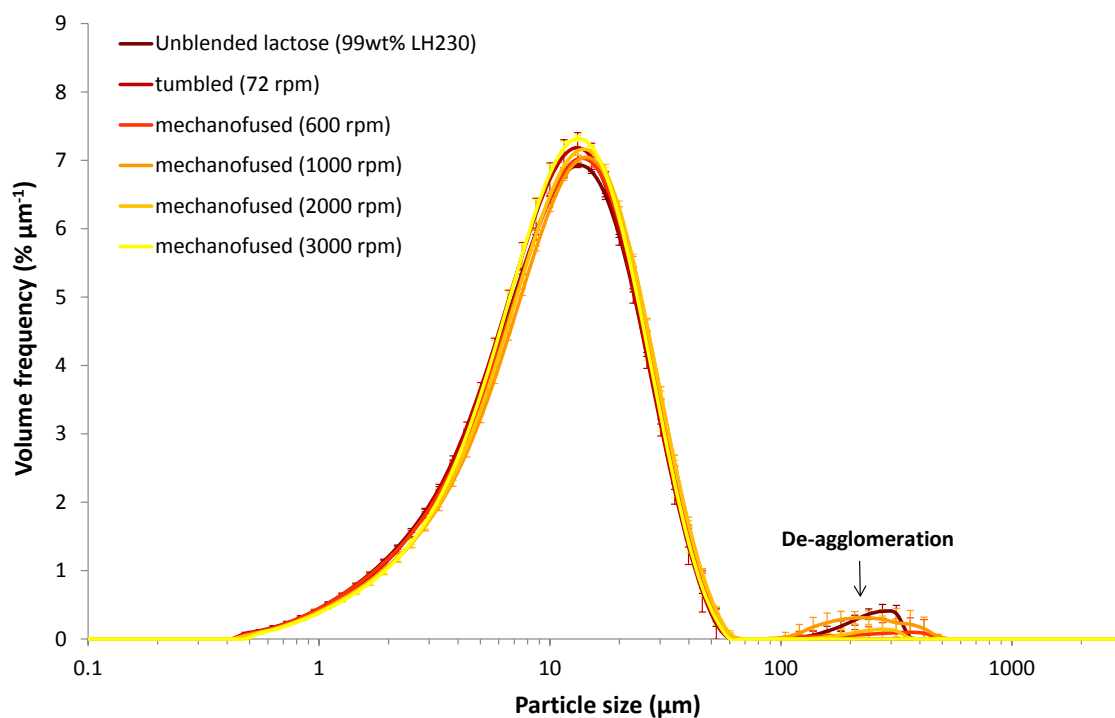


Figure 7.10: Particle size distribution for 99 wt% fine grade lactose (Lactohale LH230), showing shift in distribution for each blend due to different mixing conditions.

These particle size distributions show general trends which are common for all formulations with increasing process intensity:

- i. There is little difference in size distributions between the unblended and tumbled material.
- ii. When mechanofused, even at low rpm (i.e. 600 or 1000 rpm), peaks greater than 300  $\mu\text{m}$  are reduced or eliminated and the peak around 100  $\mu\text{m}$  increases.
- iii. When mechanofused at low and moderate rpm (i.e. less than 2000 rpm), depending on the formulation, the volume percentage of fine and ultrafine particles decreases with increasing intensity.
- iv. At a certain high intensity (rpm) of mechanofusion, and only for formulations that mill, the peak around 100  $\mu\text{m}$  decreases and the level of ultrafines and/or fines increases. This is observed in some aspect of all formulations, with the exception of 99 wt% LH230.

The effect of mechanical processing of the particle size distribution is different for each formulation. For the formulation containing low amounts of fine grade LH230 lactose (i.e. 0 and 10 wt%), there is little difference between particle size distributions for the unblended and tumbled blend. When mechanofused at low speeds (i.e. 600 and 1000 rpm) it would appear that fine particles attach to the larger carrier particles. At higher speeds (2000 and 3000 rpm), ultrafine particles are generated (< 4 µm), with the amount increasing with increasing rpm. A similar trend is observed at 20 wt% LH230, however ultrafines appear to only be generated at 3000 rpm. With 40 wt% LH230, the level of ultrafines decreases up to 2000 rpm, and is then restored at 3000 rpm, perhaps explaining why there is a small and measureable amount of milling occurring, but little change in the CIE formulation curve. The LH230 formulation shows no change with processing, save for the breakup of agglomerates with increasing process intensity.

The particle size distributions for the 0, 10 and 20 wt% LH230 formulations confirm milling during mechanofusion, as predicted from the shift of formulation curves into the milling region. The level of ultrafines and fines after 60 minutes of blending in each process can be compared to see what mixing intensities lead to milling with each formulation, or if in fact milling has occurred (*Table 7.3*). The onset of milling is taken to be the points at which the level of fines/ultrafines significantly *increases* (and where standard deviations do not overlap) and are highlighted in grey.

All formulations show an increase in fines and/or ultrafines when mechanofused, often at 2000 or 3000 rpm. The initial increase in fines for the 0 wt% LH230 formulation when tumbled is attributed to the de-agglomeration of lactose and not due to milling. This is also observed for the 99 wt% LH230 formulation when mechanofused at 3000 rpm. The levels of fines and ultrafines in blend 2F, whilst lower than that of 2E, is likely to have been higher if it was allowed to be further mechanofused to the standard time of 60 minutes (and not 45 minutes).

The mixing intensity at which in-process milling occurs appears to also increase with increasing initial fines, which can be seen more clearly by plotting the level of ultrafines (which are more selective

Table 7.3: Volume percentages of ultrafine and fine particles (below 4 and 15 µm respectively) for each blend as determined by laser diffraction.

Blend label (As per Table 7.2)	Unblended material	Tumbled 72 rpm 60 min	Mechanofused			
	A	B	600 rpm 60 min C	1000 rpm 60 min D	2000 rpm 60 min E	3000 rpm 60 min F
<b>Vol.% particles ≤ 4 µm (ultrafines)</b>						
1	2.77 ± 0.31	3.87 ± 0.18	2.83 ± 0.12	2.20 ± 0.04	5.93 ± 0.12	7.14 ± 0.22
2	5.13 ± 0.56	5.09 ± 0.02	4.11 ± 0.13	3.28 ± 0.23	6.80 ± 0.20	6.22 ± 0.14*
3	6.09 ± 0.17	6.06 ± 0.14	5.23 ± 0.42	4.66 ± 0.19	6.01 ± 0.12	9.78 ± 0.47
4	8.48 ± 0.24	8.12 ± 0.31	8.52 ± 0.51	7.60 ± 0.20	5.49 ± 0.33	7.30 ± 0.69
5	17.98 ± 0.27	17.82 ± 0.68	17.57 ± 0.52	15.98 ± 0.65	16.07 ± 0.48	16.33 ± 0.44
<b>Vol.% particles ≤ 15 µm (fines)</b>						
1	12.83 ± 0.97	15.94 ± 0.35	10.88 ± 0.23	11.60 ± 0.18	15.21 ± 0.17	16.39 ± 0.41
2	20.51 ± 1.44	20.12 ± 0.17	16.69 ± 0.27	15.67 ± 0.80	18.58 ± 0.44	15.58 ± 0.33*
3	24.72 ± 0.45	24.56 ± 0.38	20.94 ± 1.10	20.22 ± 0.63	20.68 ± 0.22	24.93 ± 0.64
4	33.96 ± 0.64	33.93 ± 0.59	33.48 ± 1.89	31.36 ± 0.73	27.85 ± 1.25	30.58 ± 1.71
5	68.73 ± 0.37	70.59 ± 1.00	68.29 ± 1.12	65.23 ± 0.94	66.86 ± 0.81	69.45 ± 1.43

\*mechanofused for 45 mins (and not 60 min) due to process limitations.

than the level of fines in showing milling and not material de-agglomeration) against process intensity (Figure 7.11). An increased vol% of ultrafines indicates that milling has occurred. For simplicity, the number of mixing revolutions has been used to account for both process intensity and the shorter mixing time in blend 2F (Table 7.3).

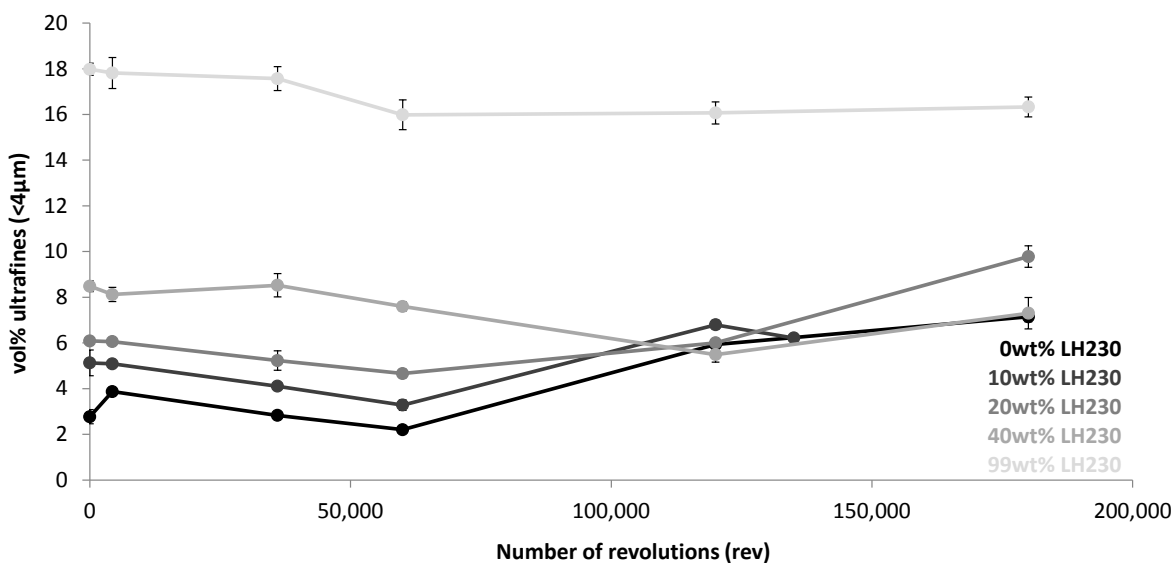


Figure 7.11: Level (vol%) of ultrafines in each formulation at different process intensities and times (expressed as mixing revolutions).

As previously observed, mechanofusion at 2000 rpm has sufficient intensity to mill large lactose particles in formulations comprising of 20 wt% LH230 or less. Milling can also be seen in the 40 wt% LH230 formulation at 3000 rpm, which was difficult to detect with colour information. Again, the lack of milling in the 99 wt% LH230 formulation is evident in the constant slope between processing at 1000 and 3000 rpm. The increase in the level of fines and ultrafines for formulations containing 20 wt% LH230 or less supports the theory that the milling region is associated with particle attrition. When highlighting the level of fines and ultrafines for each blend in the  $C^*$ - $h$  colour plane, increases in fines from de-aggregation of *in situ* milling (shown in bold) can be seen (Figure 7.12).

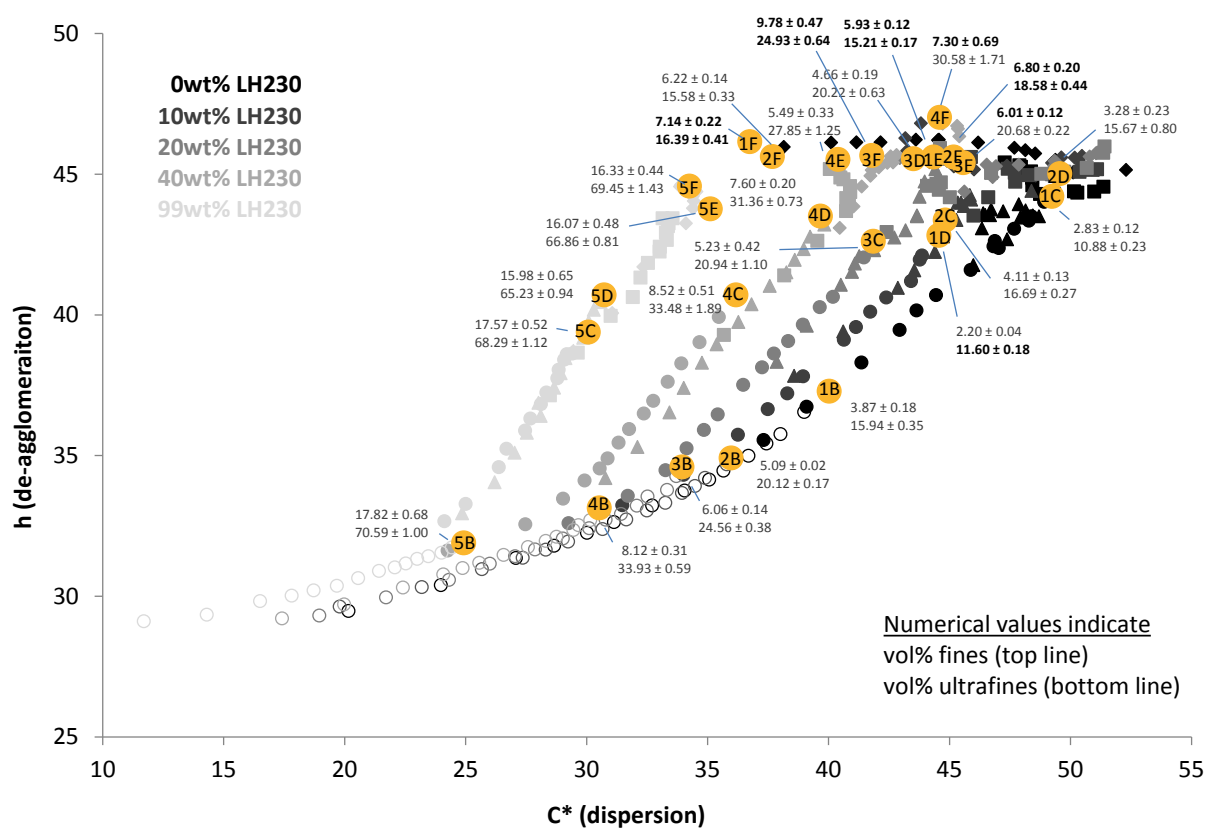


Figure 7.12: Levels of fines and ultrafines for different blend samples and their respective corresponding position in the CIE colour space. Black values indicate level of fines or ultrafines has increased from the previous blend in Table 7.3.

Discounting increases in fines/ultrafines that come from powder de-aggregation, points that correspond to increases in fines/ultrafines all lie in the milling region. This confirms that the milling region does indeed indicate the milling of lactose particles within the formulation. This link between colour and particle size distribution data may also provide valuable insights into the mixing

mechanisms both in the transitional period between the de-agglomeration/dispersion and milling regions, and within the milling region itself.

## 7.4 Discussion

With the confirmation that the milling region indeed relates to the milling of lactose particles, the colour and particle size data are more thoroughly compared with one another to assess the viability of using the colour plane to quantify the level of fines in formulation; both in terms of initial fines and generated fines from unintentional milling. Additional mechanisms to those of Chapter 4 are also proposed based on the findings in this study, which will allow a stronger interpretation of the entire formulation curve.

### 7.4.1 Correlation of level of fines and position in CIE colour space

To determine whether colour data can be used to assess variations in fines between different formulations or milling conditions, correlations need to be found. One simple means of assessing correlations between particle size and colour data is to view the level of ultrafines against their corresponding positions in the  $C^*-h$  plane (*Figure 7.13*).

The shape of this plot is similar in shape to the common plane in the CIELCH colour space, with higher levels of ultrafines (analogous with high  $L^*$ ) occurring at low levels of  $C^*$  and  $h$ . An identically shaped plot is observed when plotting the level of fines. Whilst not immediately apparent, there are two well-fitting correlations within this data; one for standard blending conditions (within the dispersion-dominant and de-agglomeration/dispersion regions), and the other for formulations within the milling region. No one correlation exists across all regions of the formulation curve.

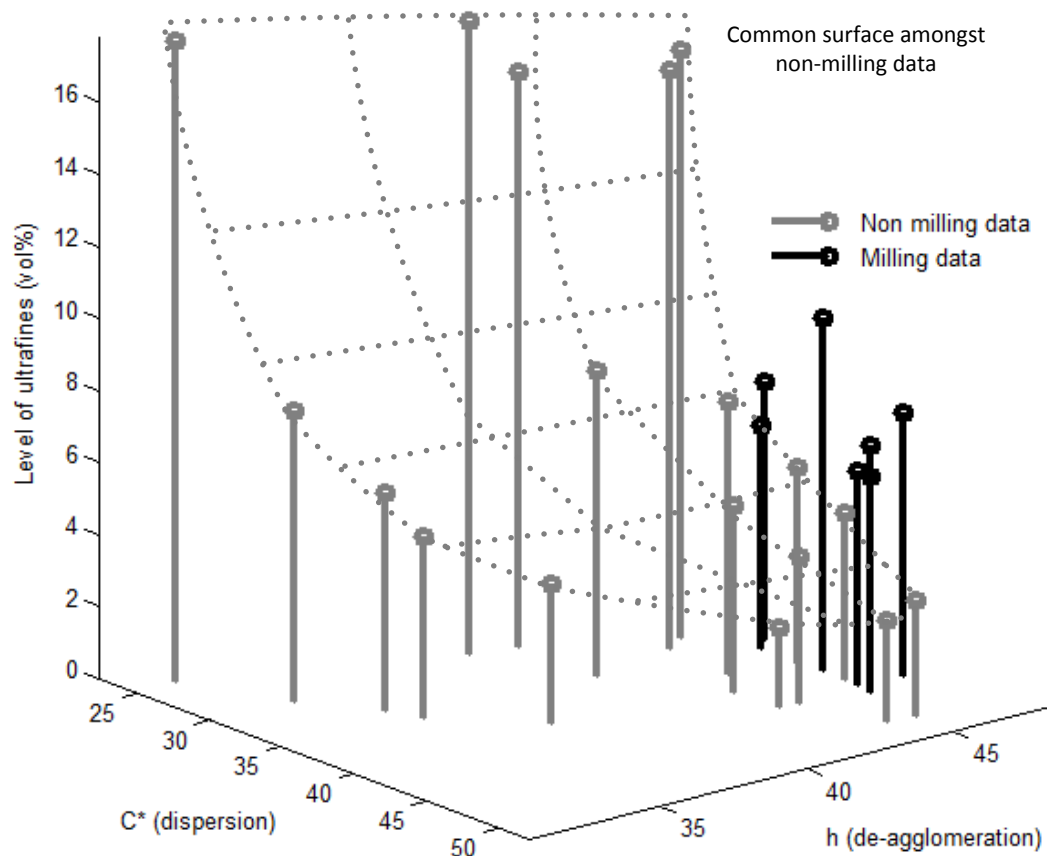


Figure 7.13: 3-dimensional plot of the correlation between the level of ultrafines and position in colour space for all formulations.

As the increase in fines/ultrafines relates to an increase in  $L^*$  along the common plane, it is unsurprising that a correlation exists between the two within the dispersion-dominant and de-agglomeration/dispersion regions. This can be plotted to show the direct correlation between the two (Figure 7.14).

There is no direct correlation between the level of fines/ultrafines and  $C^*$  or  $h$ , however there is with  $L^*$ , which is a function of the two (as described in Section 4.4.2). An exponential correlation within the dispersion-dominant and de-agglomeration/dispersion regions, with good fit, exists for both fines and ultrafines. This suggests that blend lightness can be used to detect variations in formulation under standard blending conditions, and this creates a third means of utilising the CIELCH colour space as it is independent of  $C^*$  and  $h$ , which relate to the extent of mixing.

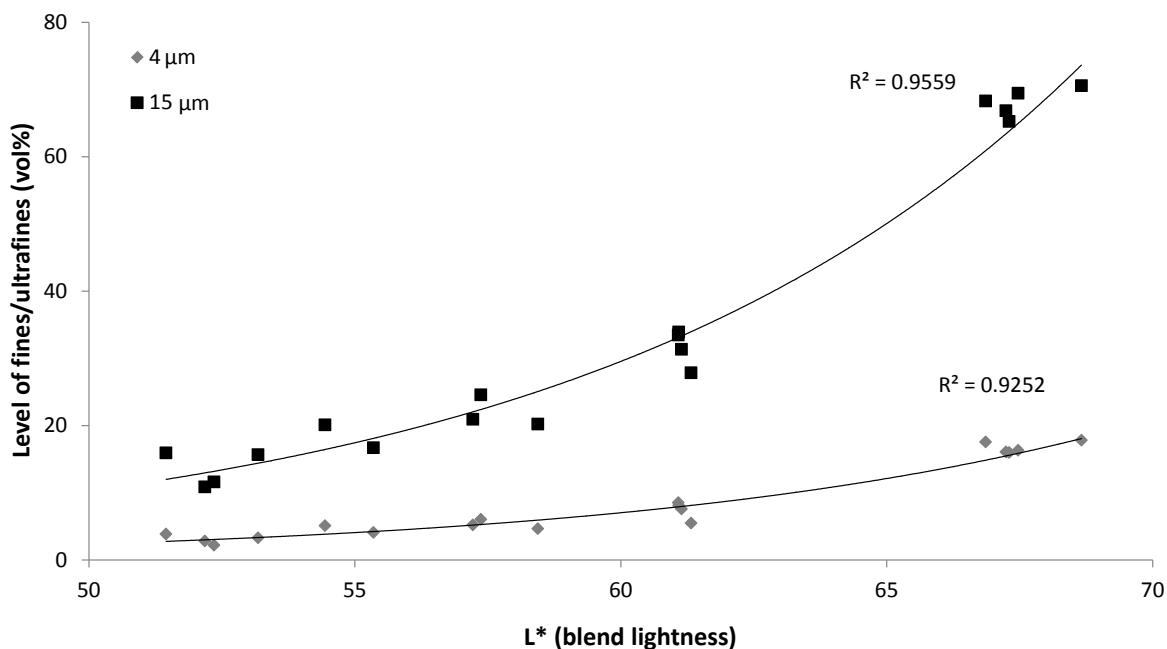


Figure 7.14: Correlation between the level of fines and ultrafines for all formulation curves at data points at which no milling occurred.

As discussed in Section 7.3, formulation curves shift upwards in the common plane (with respect to  $L^*$ ) with increasing levels of initial fines. To determine whether the vertical position on the common plane can be used to quantify the level of fine material in formulation, the measure of  $L^*$  from the constant- $L^*$  section of the de-agglomeration/dispersion region ( $L_c^*$ ) can be compared to the initial level of fines in formulation (Figure 7.15).

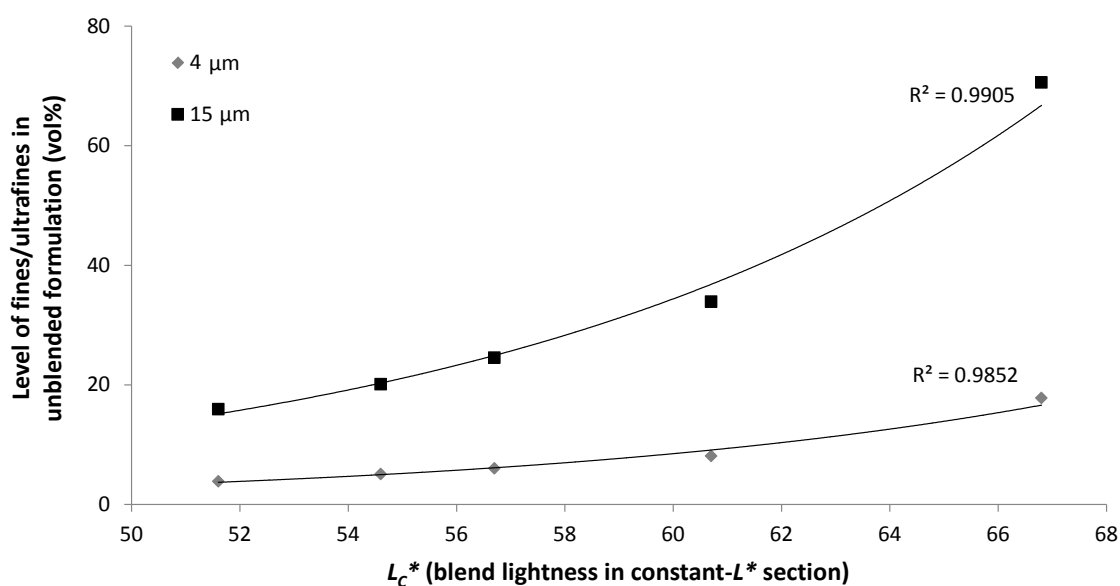


Figure 7.15: Correlation between the initial level of fines/ultrafines with blend lightness in the constant- $L^*$  section of the de-agglomeration/dispersion region.

This assumption is valid as no milling is observed outside of the de-agglomeration/dispersion region. Again, an exponential correlation is found between blend lightness and the level of fine material in the formulation. However, Figure 7.15 indicates that if the initial level of fines and/or ultrafines is known, that the position of the formulation curve in the CIELCH colour space can be predicted. Further discussion on the prediction of the shape and position of formulation curves is provided in Chapter 8.

#### 7.4.2 Quantification of milling

Whilst the non-milling data shows that the position of formulation curves in the CIE colour space can be predicted from knowing the initial level of fines, the correlation between the level of fines and position in the milling region of the formulation curve is less straight forward, and relies on a more complex relationship. It was shown in Figure 7.4 that a relationship exists between the length of the milling region (in terms of  $C^*$  or  $\Delta E^*(LCH)$ ) and the initial level of fines/ultrafines in the formulation. This however was related to the maximum intensity process of the study, which was constant across all formulations but does not allow for a general study and the use of more intense processes. No correlation can be found in the data between the length of the milling region and the level of fines or ultrafines, however there is a correlation between the *change* in  $L^*$  (from the constant- $L^*$  value in the de-agglomeration/dispersion region) and the *change* in ultrafines (from the initial unblended amount) (Figure 7.16).

Data points for this correlation were taken for all blends at which milling was observed in Table 7.3 (i.e. those shown in grey in columns *E* and *F*), with three formulations giving points when mechanofused at 2000 and 3000 rpm. The outlier (shown as a diamond) relates to the 10 wt% LH230 formulation blended at 3000 rpm. As mentioned in Section 7.3.1, the blend exhibited unusual blending behaviour and required termination after only 45 minutes of blending.

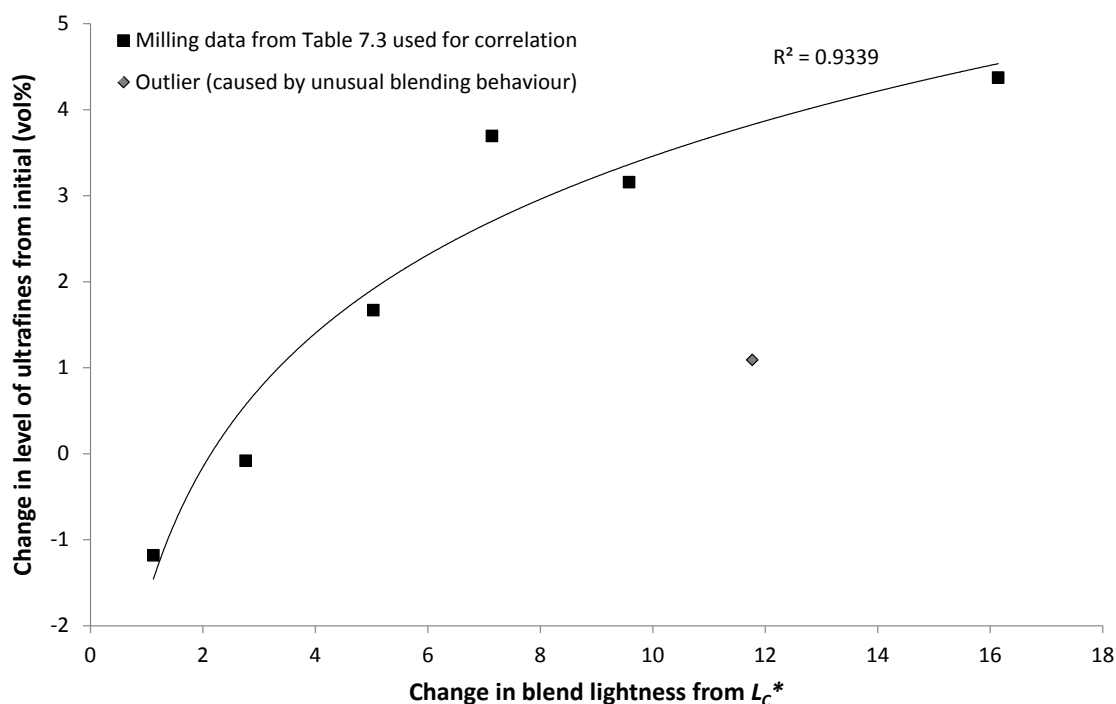


Figure 7.16: Correlation between the shift in blend lightness from  $L_c^*$  and the shift in ultrafines from initial in the milling region.

When assembled, and ignoring the outlier, the other data points follow a logarithmic regression with good fit ( $R^2 = 0.9339$ ) (Eqn.7.2):

$$\Delta uf = uf - uf_i = 2.246 \ln[L^* - L_c^*] - 1.711 \quad (\text{Equation 7.2})$$

Where  $L_c^*$  is the constant- $L^*$  value in the de-agglomeration/dispersion region and  $uf$  and  $uf_i$  relate to the final and initial level of ultrafines respectively. These findings suggest that the milling region does indeed relate to the degree of milling, and that the degree of milling in any formulation can be quantified. It is also suggested that the kink between the de-agglomeration/dispersion and milling regions relates only to pre-milling kinetics, and has no consequence on the quantification of the degree of milling. This finding is reassuring to the applicability of the tracer method for industrial analysis as measurements do not rely on particle size knowledge and formulation curve colour data in the pre-milling region; which may be difficult to obtain.

Whilst beyond the scope of this work, there may also be a means of determining the amount of loose fines adhered to carrier particles from its shift below constant- $L^*$  in the de-

agglomeration/dispersion region along the milling region. A good idea of the extent of loose fines absorption can be made by comparing the initial level of fines and ultrafines with the level prior to milling (from Table 7.3) (Figure 7.17).

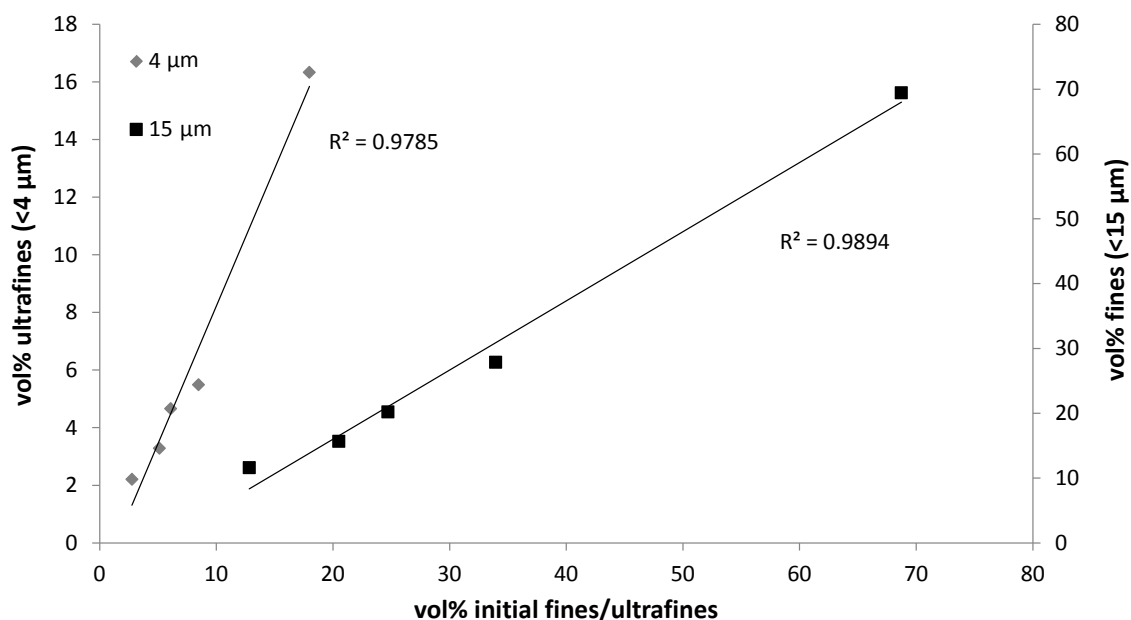


Figure 7.17: Relationship between the initial level of fines/ultrafines and the corresponding level prior to milling when loose powder fines are absorbed.

This correlation goes some of the way to finding a relationship between the extent of loose fine absorption and the initial properties of the formulation. No correlation was found however that would relate to the degree of loose fine absorption and the shift in  $L^*$  along the milling region below constant- $L^*$ . Despite not finding a correlation for the pre-milling absorption of loose fines, the milling region still provides a powerful tool for the identification and quantification of milling.

#### 7.4.3 Proposed tool for calculation of fines in milled formulation based on colour values

Although particle size distributions can be easily measured by laser diffraction, they require sample preparation time and offline analysis. The colour method proposed in this work can be used online and in real time as a process analytical technology (PAT) tool to obtain some information on whether milling is occurring and to what extent.

As there is a correlation between the shift in  $L^*$  above  $L_c^*$  and the degree of milling, and a correlation between the initial level of ultrafines and the value of  $L_c^*$ , a general equation can be constructed to predict the level of ultrafines in the formulation given its initial content and location in the milling region.

The correlation between the initial level of ultrafines and the value of  $L_c^*$  takes the form of Equation 7.3:

$$uf_i = Ae^{B L_c^*} \quad (\text{Equation 7.3})$$

Where  $A$  and  $B$  are constants. Similarly, the correlation between the shift in  $L^*$  from  $L_c^*$  and the change in ultrafines takes the following form (Eqn. 7.4):

$$\Delta uf = uf - uf_i = C \ln[L^* - L_c^*] + D \quad (\text{Equation 7.4})$$

Where  $C$  and  $D$  are constants. Re-arranging Equation 7.3 to be in terms of  $L_c^*$  (Eqn. 7.5), and substituting it into Equation 7.4, a general expression for the level of ultrafines in a milled sample can be created (Eqn. 7.6):

$$L_c^* = \frac{1}{B} (\ln[uf_i] - \ln[A]) \quad (\text{Equation 7.5})$$

$$uf = uf_i + C \ln \left[ L^* - \frac{\ln[uf_i]}{B} + \frac{\ln[A]}{B} \right] + D \quad (\text{Equation 7.6})$$

In the case of this study, the general equation can be specified by substituting values for all the constants in Equation 7.6 based on the regressions in Figures 7.16 and 7.17 (Eqn. 7.7):

$$A = 0.023 \quad B = 0.0985 \quad C = 2.246 \quad D = -1.711$$

$$uf = uf_i + 2.246 \ln[L^* - 10.152 \ln[uf_i] - 38.297] - 1.711 \quad (\text{Equation 7.7})$$

This provides a result within  $\pm 10\%$  of the measured values of ultrafines in this study. Equations 7.6 and 7.7 provide a tool with which the amount of ultrafines (vol%) can be calculated from the  $L^*$ -

value along the milling region by knowing only the level of ultrafines in unblended formulation (which can be obtained from the manufacturer). The equations above, specifically Equation 7.7, relate to the use of 1 wt% of the iron oxide tracer used in this thesis. It would be anticipated that other tracer concentrations, types of colour tracer and the use of bulk materials that mill differently to lactose would all affect the coefficients and even the nature of correlations that underpin these expressions. This equation is also limited to the analysis of the section of the milling region that lies at a higher  $L^*$  than within the de-agglomeration/dispersion region. Despite its current limitations, this provides a tool for real time PAT analysis and the prediction of milling without the use of laser diffraction. It also shows that perhaps other correlations and expressions are possible for different systems. It is important to note that the current method also only works with iron oxide present in formulation, and is therefore limited to preliminary process development and not DPI formulation manufacturing.

#### 7.4.4 Comments on pre-milling behaviour and proposed mechanisms

It was observed in the CIE colour space that for formulations with relatively low levels of fines (i.e. 20 wt% LH230 or less, which equates to < 6 vol% ultrafines and < 25% fines), the formulation curves would dip (or 'kink') from the de-agglomeration/dispersion region prior to entering the milling region. These kinks are proposed to be a part of the milling initiation process as each formulations curve that kinked also entered the milling region. Curves that kinked all converged to a single area of the CIE colour space, termed the 'critical point', which appears to be independent of the level of fines present in the blend. It is thought based on the associated dramatic increase in hue intensity and decrease in the level of fines in formulation that these kinks relate to the densification of powder as fines are adhered to the large lactose surfaces. This densification process appears to be part of a pre-milling mechanism by which all free fines need to be fixed prior to milling.

Results indicate that the mechanofusion process used in this study is only capable of milling the larger carrier lactose (from the presence of Lactohale LH200) and not the fine grade lactose

(Lactohale LH230). This would explain the decrease in milling as the weight percentage of the coarse grade lactose was decreased. There are therefore two proposed causes for the different degrees of milling in each formulation:

- The decrease in milling with formulation is purely a reflection of the amount of large carrier lactose particles (from LH200) in formulation.
- The added fines in formulation help to insulate and 'shield' the larger carrier lactose from inter-particle collisions and subsequent attrition. The greater the level of fines in formulation, the more insulated the carrier particles become and the less milling occurs (*Figure 7.18*).

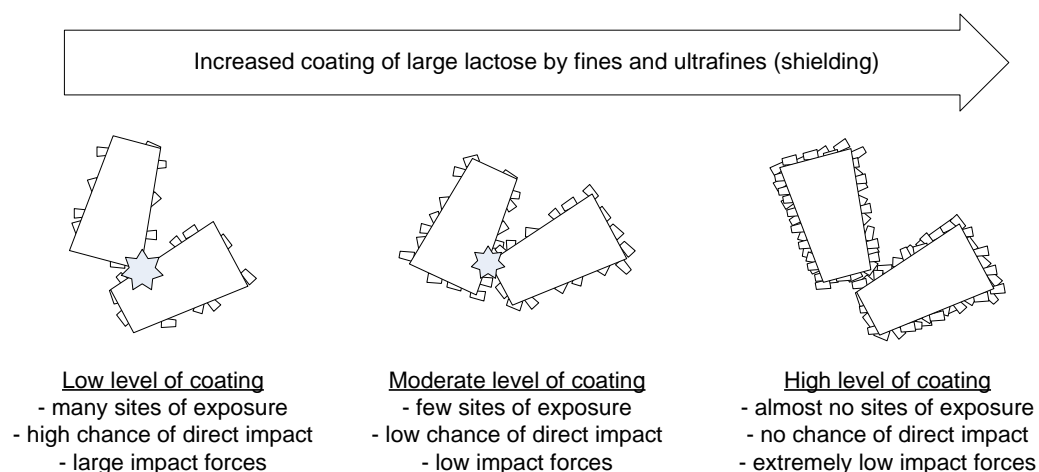


Figure 7.18: Schematic of proposed 'shielding' of large lactose particles by fine lactose particles. This is believed to help protect large particles from direct impact and subsequent attrition.

As fine particles are adhered to the large lactose surfaces, they become insulated from direct impact with one another. With increased coating, the force experienced on the large particle from impact with other large particles is decreased by either partial or full absorption by the fine lactose. In this way the development of tensile stresses in the particle are suppressed, decreasing the amount of deviatoric stress and increasing the amount of isotropic stress. Coated particles are even more likely to deflect or shear across each other as their momentum is redirected by the rough surface, and can change the friction mechanism from sliding to rolling. At a certain degree of coating, the large particles would be fully 'shielded' from direct impact, which would minimise the force they experience and the chance of attrition/damage. Carrier shielding would account for the observed

kink in formulation curves from the de-agglomeration/dispersion region into the milling region. As fines are adhered to the coarse particles the effective surface area of the formulation decreases, thereby increasing the potency of the tracer coating. This would explain the sharp spike in the hue intensity ( $C^*$ ) prior to milling. The particle size distribution data also supports this theory. As mentioned in Chapter 2, the mechanofusion system is an excellent particle coating tool. The PSDs from unmilled mechanofusion blends in this study show the loss of fine and ultrafines, with an increase in large carrier particles (*Figures 7.6-10*), supporting this theory of large particle coating.

In Chapter 4 a series of blending mechanisms was proposed for tracer coverage on the lactose particles:

- a) Tracer aggregates disperse through the bulk lactose and adhere to lactose surfaces in their immediate vicinity (*dispersion-dominant region mechanism*).
- b) Inter-particle collisions between lactose particles occur, causing de-agglomeration (*transitional region between dispersion-dominant and de-agglomeration/dispersion regions*).
- c) Tracer is de-agglomerated and dispersed across the surface of carrier particles through friction and collisions between particles (*de-agglomeration/dispersion region mechanism*).
- d) If there is sufficient intensity in the process, coated lactose particles are fractured, exposing new uncoated surfaces and lowering the hue intensity of the sample (*milling region mechanism*).

Based on the particle size distributions and colour curve results in this study, further distinct mechanisms can be added to those of Chapter 4 after mechanism c) and in place of d) (*Figure 7.19*):

- i. With sufficient intensity, fines and ultrafine lactose are adhered to the surface of large lactose particles (*transitional region between the de-agglomeration/dispersion and milling regions*). Inter-particle collisions result in both the detachment and attachment of fine particles. The ratio between the rate of detachment/attachment of fine particles decreases with increasing process intensity.

- ii. At a sufficient intensity of mixing, fine particles are rigidly adhered to the large lactose particle surfaces and are not easily removed, dramatically increasing the surface roughness of the large particles. Once a certain level of fines are adhered to the large lactose, inter-particle collisions result in shearing and 'chipping' of the large lactose particles which exposes new uncoated surfaces and lowers the hue intensity of the sample (*milling region mechanism*).

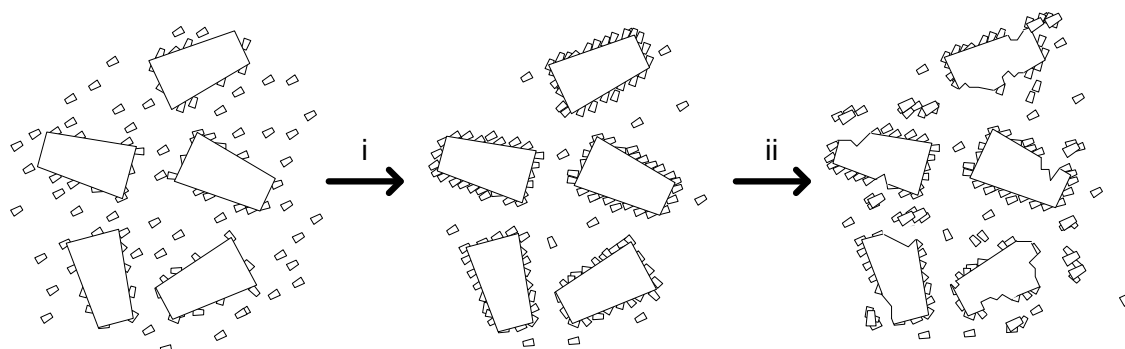


Figure 7.19: Proposed pre-milling mechanism in which fines adhere to the large lactose surfaces (i) and facilitate milling (ii).

This mechanism accounts for the adherence of loose fines onto coarse carrier particles prior to milling and also explains the phenomenon of 'shielding' at high levels of fines.

#### 7.4.5 Ability of method to detect batch-to-batch variation in formulation

In Chapter 6 the sensitivities of each colour value were defined to establish the limits of meaningful assessment of the content uniformity of tracer throughout the blended powder mass. Through the collection of a sizeable amount of data, the limits of analysis were found to be 0.40%, 0.40% and 0.20% relative standard deviation (*RSD*) for  $L^*$ ,  $C^*$  and  $h$  respectively.

In Section 7.4.1 it was shown that a correlation exists between the blend lightness in the constant- $L^*$  section (in the *de-agglomeration/dispersion region*) and the level of fines in formulation. Under the assumption that batch-to-batch variation would be tested in the well-mixed range to avoid uncertainties caused by content uniformity (i.e. in the constant- $L^*$  section of the de-agglomeration/dispersion region), it is calculated that this method would be able to theoretically detect deviations in fines and ultrafines between batches at approximately 3% (variation between

two samples and not to be confused with a difference of 3 vol%). Based on the results obtained in Figure 7.14 however, this is more realistically expected to be closer to 10% variation for fines and almost meaningless with ultrafines alone (i.e. if the variation in the level of fines between two separate batches is greater than 10% then the formulation curves will be noticeably separate in the CIELCH colour space). This is further investigated, and tested against the data from other chapters in Chapter 8.

The use of this method to detect batch-to-batch variation is limited to the de-agglomeration/dispersion region as variations in uniformity would drown-out any changes due to formulation variance.

## 7.5 Conclusion

In this study, formulations which varied in the level of fine lactose were blended in the high intensity mechanofusion mixer at a range of impeller speeds. This was done to deliberately mill material and gain further information about the use of the iron oxide tracer in detecting and possibly quantifying unintentional milling during mixing as well as batch-to-batch variations in formulation. Through the additional data collected in this study beyond that of previous chapters, it was shown that the milling region of colour curves could be used to quantify the level of ultrafines (i.e. vol% particles < 4  $\mu\text{m}$ ) in formulation. An expression was also found that could be used to estimate the level of ultrafines in any lactose formulation from its  $L^*$ -value in the milling region and the knowledge of the level of ultrafines in unblended formulation. An additional 'kink' in formulation curves between the de-agglomeration/dispersion and milling regions was also further defined and additional mechanisms were proposed to add to those of Chapter 4. The ability of the method to detect batch-to-batch variation in formulation was also investigated. It was found that theoretically the method would be able to detect batch-to-batch variation in formulation with differences in the level of fines by 3%, however this is more likely to be closer to 10% in practice, and hence deemed not sensitive enough for the detection of typical deviations in formulation.





## Review and application of colour tracer method in industrial blend analysis

**S**everal advantages and benefits have been shown in this thesis for the use of the iron oxide colour tracer in preliminary formulation development. These include its simplicity, cost-effectiveness, and breadth of information it provides about the nature and extent of mixing in a given mixer and set of operating conditions. Over the previous chapters, the colour tracer has been found to analyse and quantify the degree of tracer dispersion and de-agglomeration, energy input to the blend, blend uniformity and the degree of milling (in systems where milling occurs). In this chapter, the results of previous chapters are culminated to discuss common aspects and trends, potential extensions of the method to other powders and colour tracers, and suggestions for future work in this area. A step-by-step tutorial is also provided for the industrial application of the method and interpretation of results.

## 8.1 Introduction

The previous chapters of this thesis have outlined the potential benefits of the use of iron oxide tracer blending as a preliminary step in process development and/or optimisation. From these studies, several capabilities of the submicronised hematite colour tracer have been identified; with each one providing useful information about the type and extent of powder blending:

1. The **degree of tracer dispersion and de-agglomeration can be quantified** independently and simultaneously through a single colour measurement. Values over mixing time can be assembled to create formulation-specific curves in the CIELCH colour space.
2. The **type of mixing can be identified** from the sample's position along these formulation curves, and predictions of blend structure under the same conditions can be made.
3. Inferences about **mixing kinetics** can be made by analysing the rate of tracer dispersion and de-agglomeration.
4. Colour values for a given formulation that occur at the same position along the colour curve are believed to **demonstrate equivalent mixing**.
5. **Unintentional particle damage and milling can be identified** from the sample's colour, and the degree of milling can be quantified based on the blend lightness of the sample when in the milling region of the formulation curve.
6. **Batch-to-batch variations** in the level of lactose fines can be identified providing that the variation in fines (i.e. particles < 15  $\mu\text{m}$ ) between batches exceeds 10%.
7. An estimate of the **energy input** to the blend by the mixer can be provided through measurement of the degree of tracer dispersion.
8. When taking multiple samples through the powder mass at a single time point, the blend's **content uniformity can be quantified**.
9. Multiple sampling can be used to provide **insight into powder flow regimes** in high-shear mixers.

Each of these attributes can be used to compare different mixers and operating conditions, and when coupled with drug data can form a basis for efficient blend optimisation. As the iron oxide method is simple to use and relatively cost effective (when compared to drug blending in product development), it provides an attractive alternative for preliminary blend studies when developing a new formulation, optimising the blending of an existing product or up-scaling equipment.

Whilst the results from each chapter have stand-alone conclusions, there are common traits between them which deserve further discussion. This chapter not only serves a review chapter for the findings of this thesis, but also explores more deeply some topics briefly mentioned in previous chapters. This chapter also provides discussion on future directions for this work, and gives a procedure for its implementation in pharmaceutical blending development.

## 8.2 Review of formulations used in this thesis

Common trends between studies in this thesis relate to the formulations themselves, both in respect to tracer concentration and the size distribution of the lactose or lactose mixture used. Therefore, some key properties of each formulation need to be highlighted to enable effective comparisons and analysis, particularly in relation to the surface area, level of fines and mean particle size (*Table 8.1*). Particle size distributions of each formulation are also included (*Figure 8.1*).

For this review, formulations are numbered in order of increasing level of fines (i.e. vol% of particles < 15  $\mu\text{m}$ ), which vary from 13% to 69% on a volume basis. The five commercially available lactoses used in this thesis are supplied by DFE Pharma (*Germany*) and have no unusual shapes arising from novel manufacturing techniques such as spray drying.

Table 8.1: Properties of lactoses sources for studies in this thesis

Lactose type	Supplier	Method of production	Mean particle diameter ( $\mu\text{m}$ )
Lactohale LH200	DFE Pharma, Germany	Milled	$67.51 \pm 3.10$
Lactohale LH230		Milled	$10.38 \pm 0.07$
Respitose SV003		Sieved	$59.44 \pm 1.83$
Pharmatose 200M		Milled	$34.06 \pm 0.62$
Pharmatose 450M		Milled	$20.76 \pm 0.47$

Table 8.2: Table of key powder properties in assessing trends between formulation curves. Formulations are numbered in order of increasing lactose fines.

Formulation	Lactose type	Specific surface area ( $\hat{\text{A}}\text{s}$ ) ( $\text{m}^2/\text{kg}$ )	Mean particle diameter ( $\mu\text{m}$ )	Level of ultrafines (vol% < 4 $\mu\text{m}$ )	Level of fines (vol% < 15 $\mu\text{m}$ )
1-5	Lactohale LH200	$240.0 \pm 1.8^{\#}$	$67.51 \pm 3.10$	$2.8 \pm 0.3$	$12.8 \pm 1.0$
6	Respitose SV003 + 19wt% Pharmatose 450M	$287.0 \pm 0.3^{\#}$	$47.36 \pm 0.44$	$3.2 \pm 0.1$	$13.9 \pm 0.2$
7	Lactohale LH200 + 10wt% Lactohale LH230	$347.0 \pm 2.8^{\#}$	$55.64 \pm 4.77$	$5.1 \pm 0.6$	$20.5 \pm 1.4$
8	Respitose SV003 + 19wt% Lactohale LH230	$366.0 \pm 0.5^{\#}$	$44.74 \pm 0.49$	$5.0 \pm 0.1$	$21.3 \pm 0.4$
9	Lactohale LH200 + 20wt% Lactohale LH230	$394.0 \pm 0.9^{\#}$	$48.78 \pm 1.64$	$6.1 \pm 0.2$	$24.7 \pm 0.5$
10	Pharmatose 200M	$396.4 \pm 0.7^{\#}$	$34.06 \pm 0.62$	$5.3 \pm 0.2$	$25.6 \pm 0.4$
11	Lactohale LH200 + 40wt% Lactohale LH230	$526.0 \pm 1.0^{\#}$	$29.57 \pm 1.11$	$8.5 \pm 0.2$	$34.0 \pm 0.36$
12	Lactohale LH230	$990.0 \pm 0.7^{\#}$	$10.38 \pm 0.07$	$18.0 \pm 0.3$	$68.7 \pm 0.4$

<sup>#</sup>Obtained from laser diffraction size distribution based on volume percentages and equivalent sphere diameters

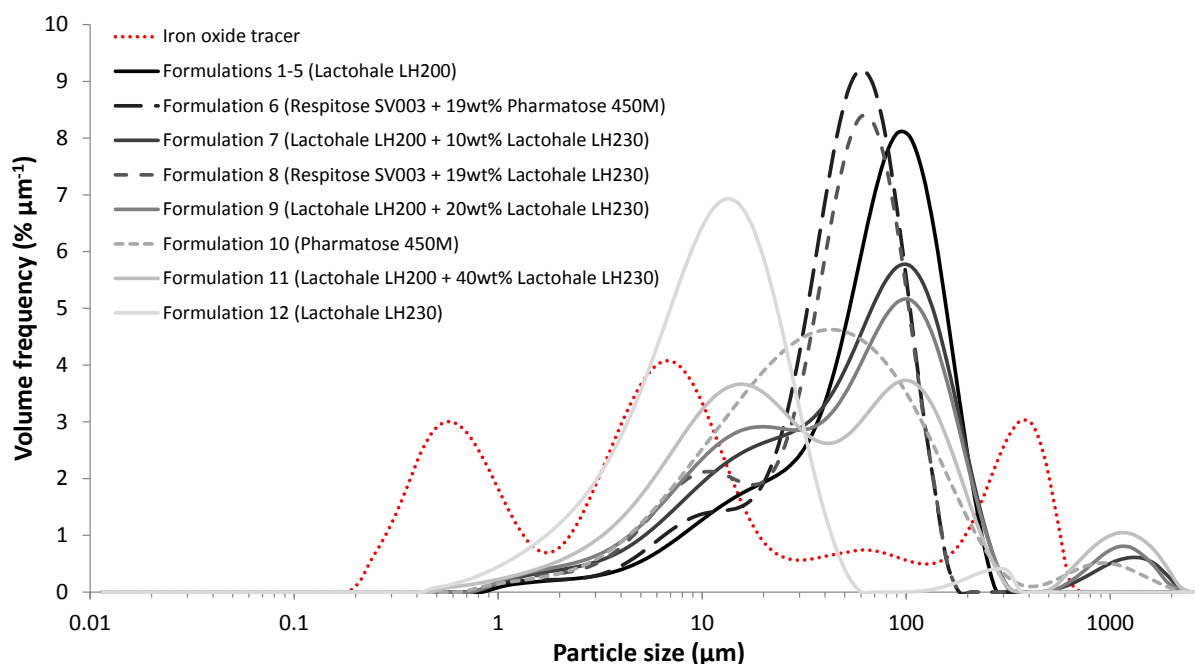


Figure 8.1: Particle size distributions for raw iron oxide colour tracer and lactoses used in each formulation.

Throughout this thesis, the blend's  $L^*C^*h$  values were recorded and used for analysis. For studies where different lactose types were compared by their  $L^*C^*h$  values, an assumption was made that they all had the same baseline (i.e. that the colour values of the lactoses themselves were similar enough to ignore). Colour values and a sample for each lactose type are shown in Table 8.3. The colour samples in Table 8.3 are set to the exact colour values recorded for each lactose type. Printing variations may cause minor changes but the contrasts will be unchanged.

Table 8.3: Baseline measured colour values for each formulation based on the type or combination of lactoses used.

Formulation	Lactose type	Baseline colour			Sample
		L	C*	h	
1-5	Lactohale LH200	97.11	1.84	-88.13	
6	Respitose SV003 + 19 wt% Pharmatose 450M	96.53	3.47	-88.35	
7	Lactohale LH200 + 10 wt% Lactohale LH230	97.06	1.77	-86.44	
8	Respitose SV003 + 19 wt% Lactohale LH230	96.32	3.89	89.71	
9	Lactohale LH200 + 20 wt% Lactohale LH230	96.69	1.76	-87.40	
10	Pharmatose 200M	97.34	1.75	-86.73	
11	Lactohale LH200 + 40 wt% Lactohale LH230	96.89	1.89	89.39	
12	Lactohale LH230	97.61	1.68	0.00	

Strictly speaking, for a true comparison it is more apt to present the difference between baseline and measured colour changes (i.e.  $\Delta L^*$ ,  $\Delta C^*$  and  $\Delta h$ ), particularly in systems where the bulk powder varies greatly in colour (such as comparing white with non-white powders). As the lactose colours were very similar, this convention was ignored in this thesis and colours were instead reported by their  $L^*C^*h$  values for simplicity.

### 8.2.1 Flooding fractions for each formulation

In Chapter 5 a term called the flooding fraction was introduced. Flooding fraction relates to the maximum fraction of total substrate surface that can be covered by the tracer (*Eqn. 5.10*).

$$f = \frac{\beta w}{\eta(100 - w)}; \beta = \frac{3}{2\rho_{tp}D_{tp}\hat{A}_s} \quad (\text{Equation 5.10})$$

Where  $\eta$  is a coefficient relating to the type of packing of tracer particles on the substrate surface (which is given as 0.547 for random packing, *Chapter 5*),  $w$  is the weight percentage of tracer in formulation,  $\hat{A}_s$  is the specific surface area of the substrate and  $\rho_{tp}$  and  $D_{tp}$  relate to the true density and the mean diameter of the tracer particles respectively. A value of 1 represents complete coverage of the substrate. Equation 5.10 relies on measurement of the specific surface area of the substrate and assumes mono-sized spherical tracer particles. As not all the lactose and lactose mixture surface areas were measured with BET, surface areas from laser diffraction are used in their place. These surface areas are calculated from equivalent sphere diameters across all size fractions measured, and have sufficient accuracy for calculations. An example of this is provided for Lactohale LH200, which was measured using BET. It was found to have a surface area of 240 m<sup>2</sup>/kg with laser diffraction, and 250 m<sup>2</sup>/kg with BET analysis (a difference of only 4.2%).

Using the lactose data from Table 8.1 and Equation 5.10, the flooding fractions are calculated for each formulation (*Table 8.4*). In Chapter 5 it was recommended for meaningful colour readings, the flooding fraction should be between 0.05 and 0.4. All formulations with 1 wt% tracer are within this range, and only the 2-10 wt% tracer formulations exceeding the recommended maximum flooding

fraction. No formulations in this thesis fall below the minimum recommended flooding fraction of 0.05.

Table 8.4: Calculated flooding fractions for each formulation in this thesis

Formulation	Lactose type	Tracer concentration (wt%)	Specific surface area ( $\hat{A}_s$ ) ( $m^2/kg$ )	Flooding fraction (f)
1	Lactohale LH200	1	240.0 $\pm$ 1.8	0.22
2	Lactohale LH200	0.3	240.0 $\pm$ 1.8	0.07
3	Lactohale LH200	2	240.0 $\pm$ 1.8	0.45
4	Lactohale LH200	5	240.0 $\pm$ 1.8	1.15
5	Lactohale LH200	10	240.0 $\pm$ 1.8	2.42
6	Respitose SV003 + 19 wt% Pharmatose 450M	1	287.0 $\pm$ 0.3	0.18
7	Lactohale LH200 + 10 wt% Lactohale LH230	1	347.0 $\pm$ 2.8	0.15
8	Respitose SV003 + 19 wt% Lactohale LH230	1	366.0 $\pm$ 0.5	0.14
9	Lactohale LH200 + 20 wt% Lactohale LH230	1	394.0 $\pm$ 0.9	0.13
10	Pharmatose 200M	1	396.4 $\pm$ 0.7	0.13
11	Lactohale LH200 + 40 wt% Lactohale LH230	1	526.0 $\pm$ 1.0	0.10
12	Lactohale LH230	1	990.0 $\pm$ 0.7	0.05

### 8.2.2 Similarity in mechanism between formulations

In Chapter 6 (*Section 6.3.2.3*) it was found from analysis of the 12 different high-shear blends that the second derivative of de-agglomeration with respect to time (i.e. the acceleration of tracer de-agglomeration or slope of  $\Delta h/\Delta t$  plot) was independent of impeller type and speed. This suggested that there was an underlying property of the powder itself which governed the tracer de-agglomeration mechanism, and the mixer and mixing conditions simply govern the final state of de-agglomeration. This theory can be tested against other mixers and formulations by plotting the rate of de-agglomeration against time for each blend in this thesis and excluding those that enter the milling region (*Figure 8.2*). All formulations follow a straight line on the log-log plot, with some outliers relating to the tumbler mixer. It would appear from results that the 'acceleration of de-agglomeration' (i.e. the slope of the lines) is also independent of formulation and mixer type. *Figure*

8.2 suggests that the second derivative provides information on the adhesion/cohesion properties of the system, particularly in regards to the likelihood of the tracer to bind to itself and the lactose. Different tracers and substrates may create different slopes.

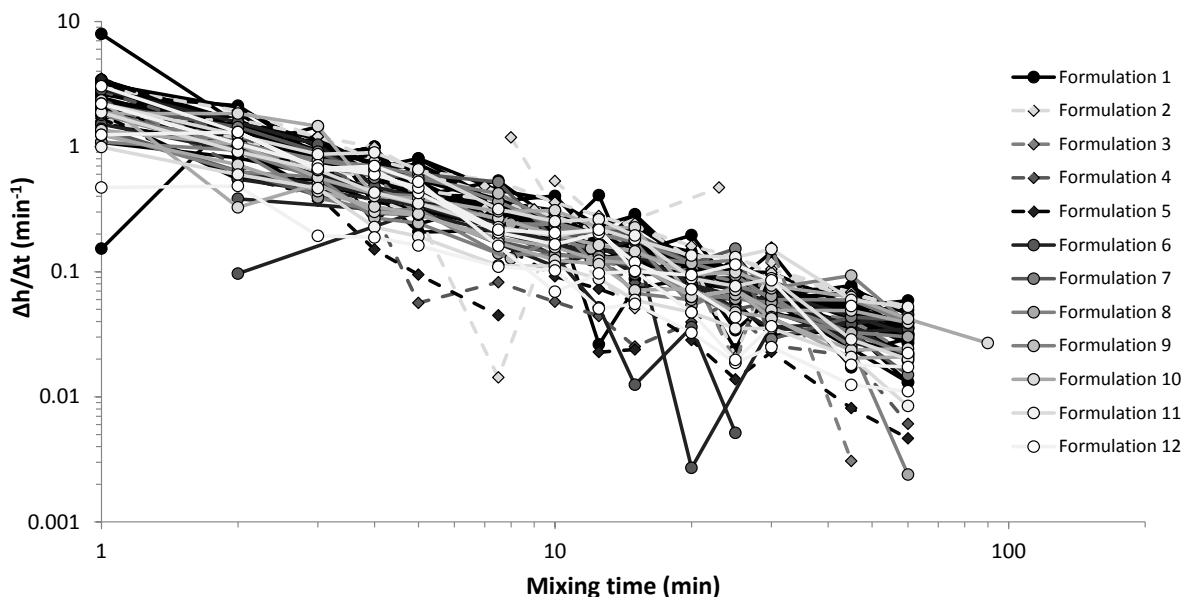


Figure 8.2: Rate of tracer de-agglomeration for each formulation over mixing time.

### 8.3 Review of colour tracer method results

#### 8.3.1 Analysis of common plane/surface in colour space

In Chapter 4 a common surface was described in the 3-dimensional CIELCH colour space on which all blend curves lie, regardless of lactose type that was used and mixing conditions. It was proposed that the surface was a function of the type of colour tracer used, and would therefore change with a different colour tracer. When all blend curves from this thesis are assembled together, they can be seen to share a common plane with the exception of those found to have an excess of tracer (i.e. Formulations 3-5) (Figure 8.3). From this plot, all the properties previously discussed in the previous chapters can be seen:

- Formulation curves that align on the common plane exhibit three distinct regions relating to the type of mixing the colour tracer is undergoing in a given mixing process.
- The formulation curves maintain their shape and shift along the common plane to a higher blend lightness ( $L^*$ ) with increasing lactose fines. Similarly, formulation curves shift downwards along the common plane with increasing tracer concentration.
- Formulations with an excess of tracer deviate from the common plane and enter the saturated region.

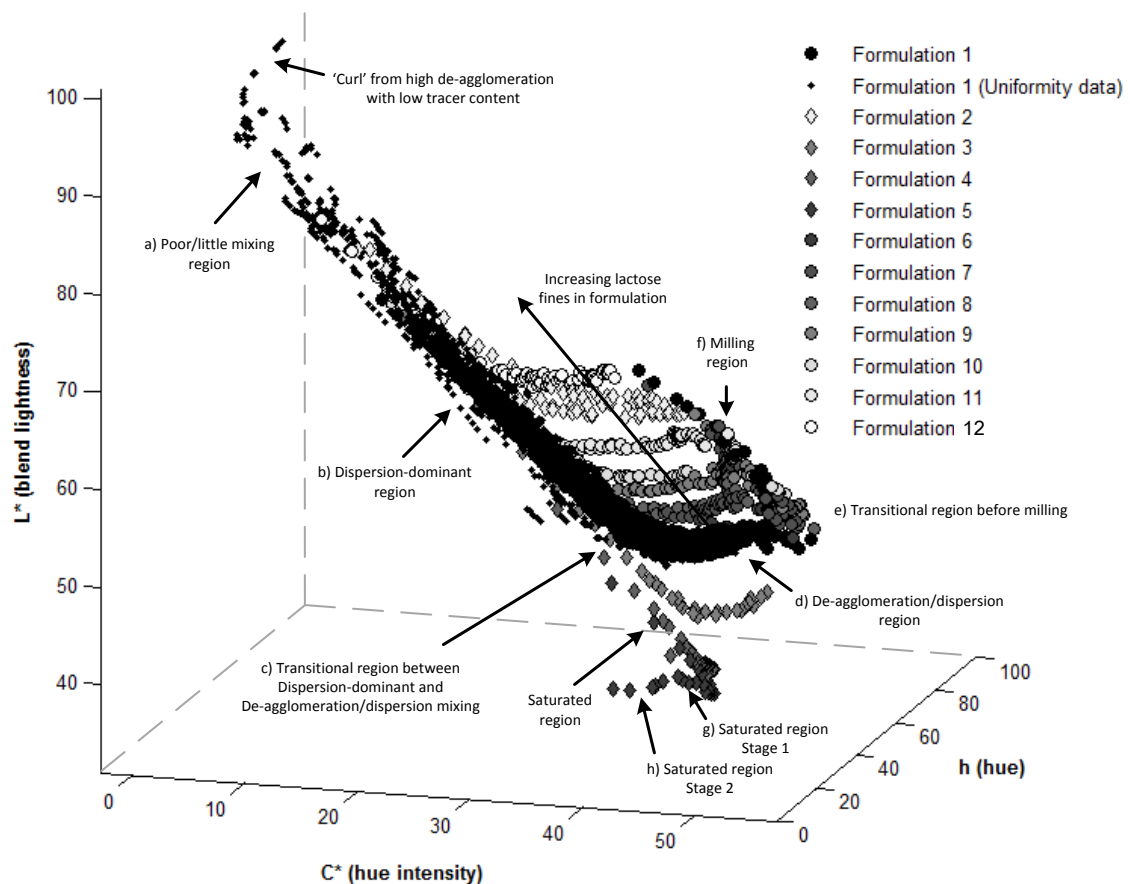


Figure 8.3: All formulation curves in the CIELCH colour space showing the different mixing regions and common surface. In addition to the regions previously identified in other chapters, the average values for each region of the content uniformity blends in Chapter 6 can be compiled to show an additional region - the low/poor mixing region. This region of the formulation curve consists of colour measurements taken from different locations within the powder bed at low mixing times and impeller speeds. These

colour values represent near-white samples where either a small amount of tracer is present or a low degree of dispersion has occurred. Colour values in the low/poor mixing region which deviate from the dispersion-dominant region (at  $L^*$ -values close to 100) represent good tracer deagglomeration with a low tracer amount in the sample (Figure 8.3). These points correspond to samples taken near the impeller at low mixing times. Colour values in the low/poor mixing region are indicative of poor sampling points and would only expect to be seen when multiple samples are taken from the blend at a given time point, and not for single-sample analysis.

For formulation data that sits within the recommended flooding fraction range (i.e. between 0.05 and 0.4), a cubic surface can be fitted with good accuracy ( $R^2 = 0.9929$ ,  $RMSE = 0.5693$ ) (Figure 8.4).

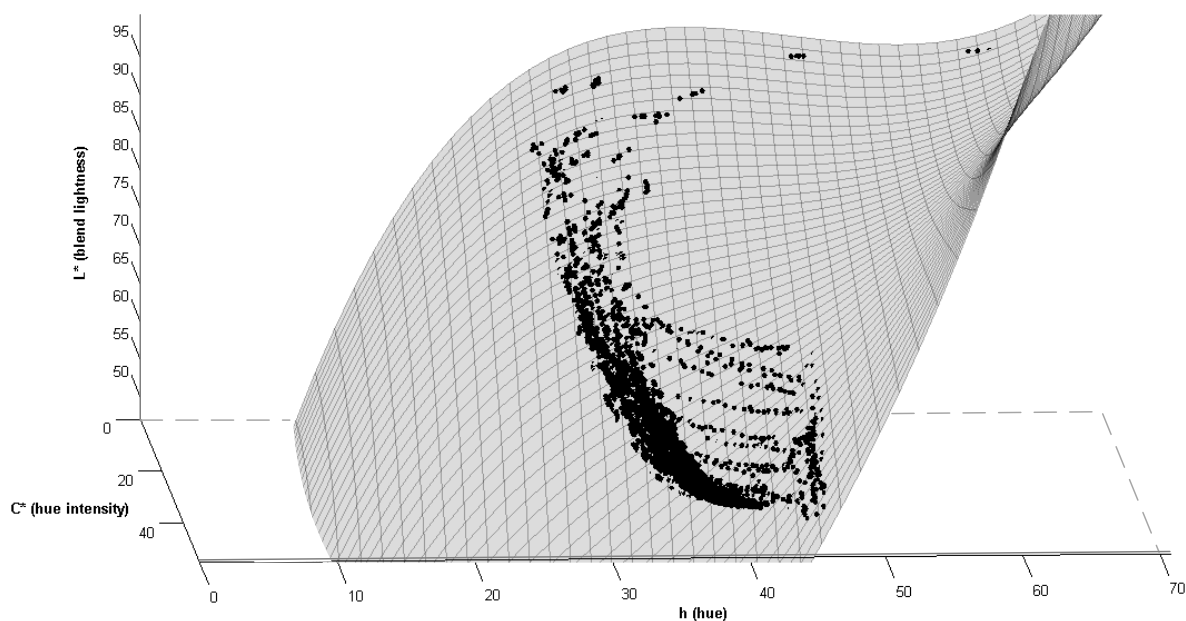


Figure 8.4: Cubic surface plot modelled to all colour data using *MATLAB*.

The surface above is cubic in respect to both  $C^*$  and  $h$  and takes the form:

$$L^* = f(C^{*3}, h^3) \quad (\text{Equation 8.1})$$

For the specific surface fitted in Figure 8.4, the following equation was found through bisquare robustness testing and minimisation of the root mean standard error (RMSE) (Eqn. 8.2):

$$L^* = 54.37 - 10.31C^* + 4.088h - 0.7499C^{*2} + 1.56C^*h - 0.04309h^2 - 0.05557C^{*3} + 0.165C^{*2}h + 0.06139C^*h^2 + 0.03893h^3 \quad (\text{Equation 8.2})$$

Again, as in Chapter 4, a simple plane can also be fitted to the data reasonably well ( $R^2 = 0.9872$ ,  $RMSE = 0.7642$ ) (Figure 8.5).

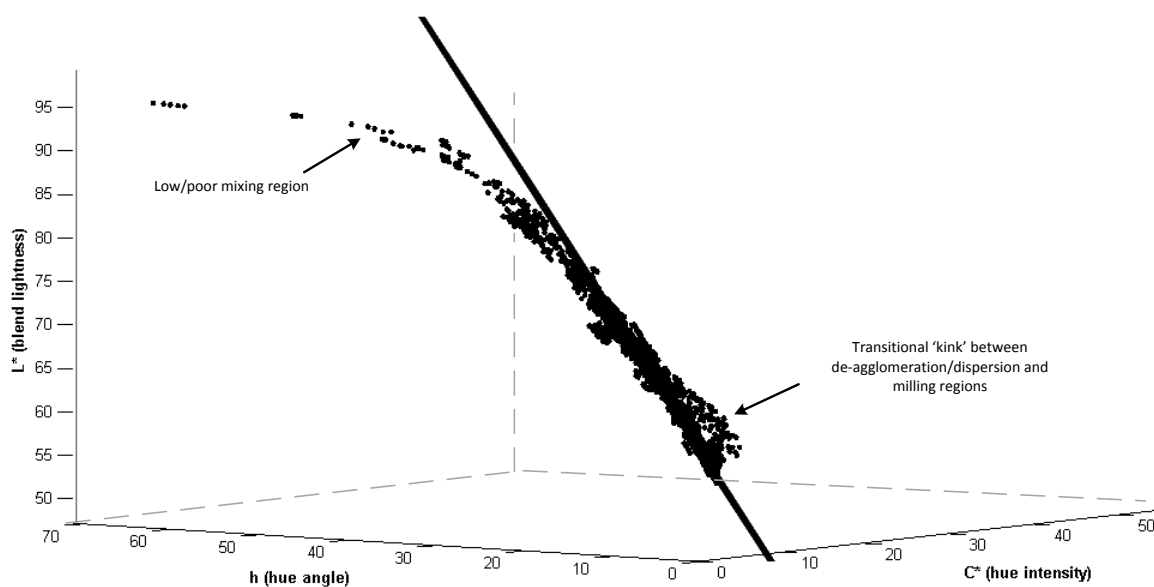


Figure 8.5: Plane of best fit for all colour data obtained in this thesis using *MATLAB*.

This plane fits along the critical sections of each formulation curve (i.e. all of the de-agglomeration/dispersion region and most of the dispersion-dominant and milling regions). The deviations from the plane shown in Figure 8.5 relate to the low/poor mixing region and the transitional 'kink' which leads into the milling region (discussed in Chapter 7), which are not pivotal to blending analysis. The plane above can be expressed by Equation 8.3.

$$L^* = 54.9 - 10.98C^* + 4.793h \quad (\text{Equation 8.3})$$

Both of these approximations show potential in being able to predict the location of other formulation curves in the CIELCH colour space.

### 8.3.2 Predicting the location and shape of formulation curves in CIELCH colour space

The ability to predict the shape and location of a formulation curve prior to obtaining blend information would certainly reduce the amount of experiments required to obtain full information on a given process. By knowing the full shape of a formulation curve in the CIELCH colour space, a reference can be made for single colour measurements. In doing so, a single measurement could provide information about what region of mixing the system is in, and could also indicate poor uniformity if it deviates significantly from the predicted curve.

To be able to predict the position and shape of formulation curves, two of the three colour parameters need to be defined. As outlined in Chapter 3, blend lightness ( $L^*$ ) is a function of both the hue ( $h$ ) and hue intensity ( $C^*$ ). Because of this, it is best practice to define  $C^*$  and  $h$  when predicting the position of a formulation curve, and ideally there should be some means of distinguishing formulations in the  $C^*$ - $h$  plane from one another.

In Figure 8.3 different formulation curves can be distinguished by their level of fines or tracer concentration. As both of these properties play a part in a formulation's flooding fraction, it is not surprising that they can also be distinguished with flooding fraction (*Figure 8.6*).

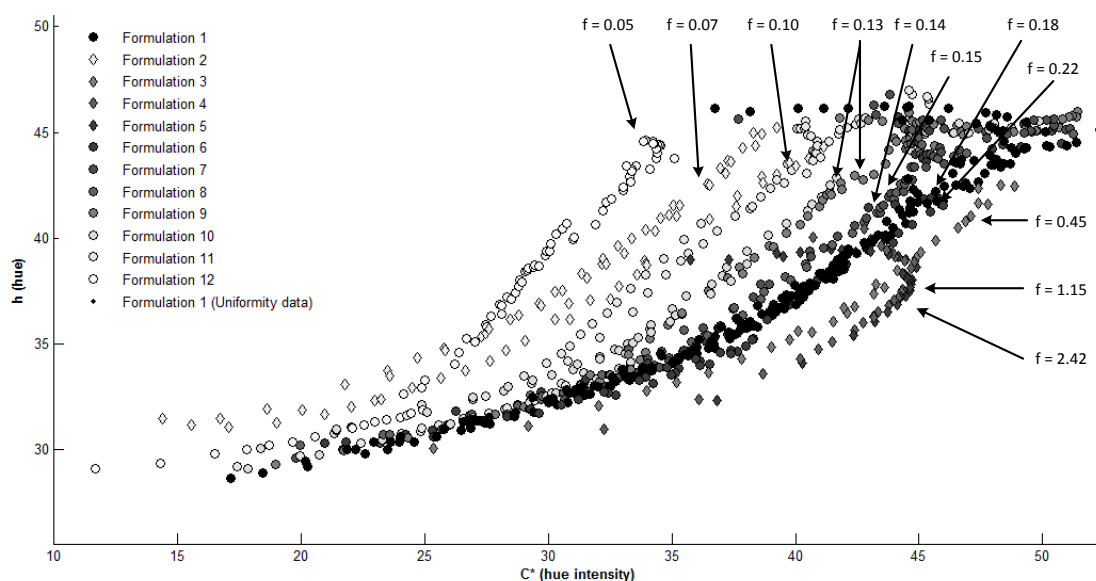


Figure 8.6: Flooding fractions for all formulation curves in this thesis and their positions in the 2-dimensional  $C^*$ - $h$  plane.

Formulations with flooding fractions in the recommended range, shift along the  $C^*-h$  plane to increasing  $C^*$  with increasing flooding fraction. This therefore shows potential as a means of determining the location of formulation curves along the common surface, and can be used for both the level of bulk fines or tracer in formulation. Further testing is required however for its validation.

### 8.3.3 Description of all colour space regions

From all the formulation colour data throughout this thesis, several regions were observed which relate to different types of tracer blending. The following describes each type of mixing region that was identified, as well as the fundamental principles which are believed to lead to the observed colour changes (*Figure 8.3*):

- a) *Low/ poor mixing region.* Tracer is barely or very poorly mixed throughout the bulk lactose. Because of this, blends appear to be very light pink or white, depending on the amount of tracer in the sample collected.
- b) *Dispersion-dominant mixing region.* Tracer aggregates and agglomerates disperse through the bulk lactose and adhere to lactose surfaces in their immediate vicinity. De-aggregation (i.e. the breakup of clumps of tracer into small agglomerates) also occurs which has no influence on the measured hue.
- c) *Transitional region between dispersion-dominant and de-agglomeration/dispersion regions.* Inter-particle collisions between lactose particles occur, forcing those with tracer aggregates and agglomerates to share tracer with non-coated particles, inherently causing de-agglomeration. Initially the population of aggregates adhered to the lactose is large and the rate of de-agglomeration is low due to the size-driven preferential de-aggregation of tracer with inter-particle collisions.
- d) *De-agglomeration/dispersion region.* As the population of aggregates decreases, the rate of de-agglomeration increases and eventually becomes greater than that of de-aggregation.

Tracer agglomerates are de-agglomerated and dispersed across the surface of carrier particles through friction and collisions between particles (*mechanism*).

- e) *Transitional region between the de-agglomeration/dispersion and milling regions.* With sufficient intensity, fines and ultrafine lactose are adhered to the surface of large lactose particles. Inter-particle collisions result in both the detachment and attachment of fine particles. The ratio between the rate of detachment/attachment of fine particles decreases with increasing process intensity.
- f) *Milling region.* At a sufficient intensity of mixing, fine particles are rigidly adhered to the large lactose particle surfaces and are not easily removed. Once a certain level of fines are adhered to the large lactose, inter-particle collisions result in shearing and 'chipping' of the large lactose particles which exposes new uncoated surfaces and lowers the hue intensity of the sample. Formulations with a high level of fines do not have a milling region to their formulation curves due to particle 'shielding', where the fines insulate the coarse particles from chipping and fracture.

In a saturated system, the formulation curves deviate at step b) into the saturated mixing region. This region has two stages, which relate to the degree of saturation of tracer (i.e. the flooding fraction):

- g) *Saturated region, Stage 1.* Agglomerates of tracer are de-agglomerated and dispersed across the surface of carrier particles through friction and collisions between particles. Surfaces become completely covered in de-agglomerated tracer, and are also covered in agglomerates. Additional loose tracer aggregates and agglomerates in the formulation drown out the change in hue. This is observed for formulations where the flooding fraction is approximately 1.
- h) The packing of tracer primary particles on the lactose surface is consolidated as agglomerates on saturated lactose particles collide with one-another

- i) *Saturated region, Stage 2.* Once consolidated packing is achieved on the lactose surface, multi-layering of tracer on lactose particles occurs, driven by inertial effects of the lactose particles which are able to overcome inter-particle adhesion between tracer particles. The multi-layering causes tracer particles to no longer be isolated from one another and thus the hue reverts slightly. This stage occurs for formulations with a flooding fraction considerably higher than 1.

Saturated regions of the formulation curve are easy to identify as they deviate from the common plane as outlined in Section 8.3.1.

## 8.4 Proposed method for industrial application

As outlined in Section 8.1, there are a multitude of benefits to the integration of the iron oxide colour tracer in powder blending development, particularly prior to the manufacturing of drug blends. This section provides a step-by-step method for its application in industry including the interpretation of colour results. It is important to note that this method has only been tested with white powders and the Ferroside 212P iron oxide tracer. However, we expect it to be applicable to a wider range of powders and tracers, as discussed further in Section 8.5.

### 8.4.1 Pre-blending procedures

#### *Step 1 - Determine bulk powder properties*

To enable effective analysis of the colour data points, some properties of the bulk powder need to be obtained. These include:

- True density of the colour tracer material ( $\rho_{tp}$ ).
- Mean diameter of the tracer particles ( $D_{tp}$ )
- Volume percentage of bulk powder less than 4  $\mu\text{m}$  (level of ultrafines)
- Volume percentage of bulk powder less than 15  $\mu\text{m}$  (level of fines)

- Colour (CIELCH) values for the tracer and bulk powder
- Surface area of the bulk material/s ( $\hat{A}_s$ ) (from manufacturer, BET analysis or calculated from size distribution data)

It is also recommended for analysis to have:

- Knowledge of particle shape and morphology (through optical microscopy)
- Particle size distribution data for the tracer and bulk powder

### *Step 2 - Calculate the desired tracer concentration to give good colour measurements*

Knowing the above properties of the tracer and substrate powders, the optimum weight percentage of tracer to enable good colour analysis can be calculated (Eqn. 5.15). This helps to create a formulation which will provide good sensitivity to measurement of colour changes, and also prevent the masking of specific changes due to a saturation of tracer.

$$w_{optimal} \approx \frac{1}{(0.14/\rho_{tp}D_{tp}\hat{A}_s) + 0.01} \quad (\text{Equation 5.15})$$

It is recommended that the flooding fraction (or fraction of substrate surface that can be theoretically covered by tracer) should be kept between 0.05 and 0.4 to prevent issues with low sensitivity or tracer oversaturation. If a non-optimum weight percentage of tracer is used, the flooding fraction can be calculated to check it is within the recommended range (Eqn. 5.10).

$$f = \frac{\beta w}{\eta(100 - w)}; \beta = \frac{3}{2\rho_{tp}D_{tp}\hat{A}_s} \quad (\text{Equation 5.10})$$

If different formulations are being tested that vary in the bulk powder surface area, it is recommended that the optimum weight percentage of tracer be calculated for the substrate or substrate mixture with the lowest specific surface area, and that the same weight percentage of tracer is applied to all formulations. This allows for better comparison *between* formulations.

### Step 3 - Select desired mixers and operating conditions for blending

Once the composition of the tracer formulation is determined, the mixers and operating conditions for testing (such as fill weight and impeller speed) should be set. The selected conditions should be based on realistic conditions in the manufacturing of drug blends. To enable effective process optimisation, a series of drug blends need to be manufactured in identical mixing conditions and linked to the colour data.

## 8.4.2 Colour blending procedures and analysis

### Step 4 - Blend tracer formulation and sample colour

With the fill weight and impeller speed selected for each mixer, the tracer blends can now be blended, and the colour of the blend assessed at selected time points of mixing. Ideally, the pigment should be sandwiched in the middle of the powder bed during loading to allow for best initial mixing and minimise tracer migration to dead zones within the mixer. When blending commences, the colour tracer will spread through the bulk powder and over time, will create a homogenous blend (Figure 6.9).

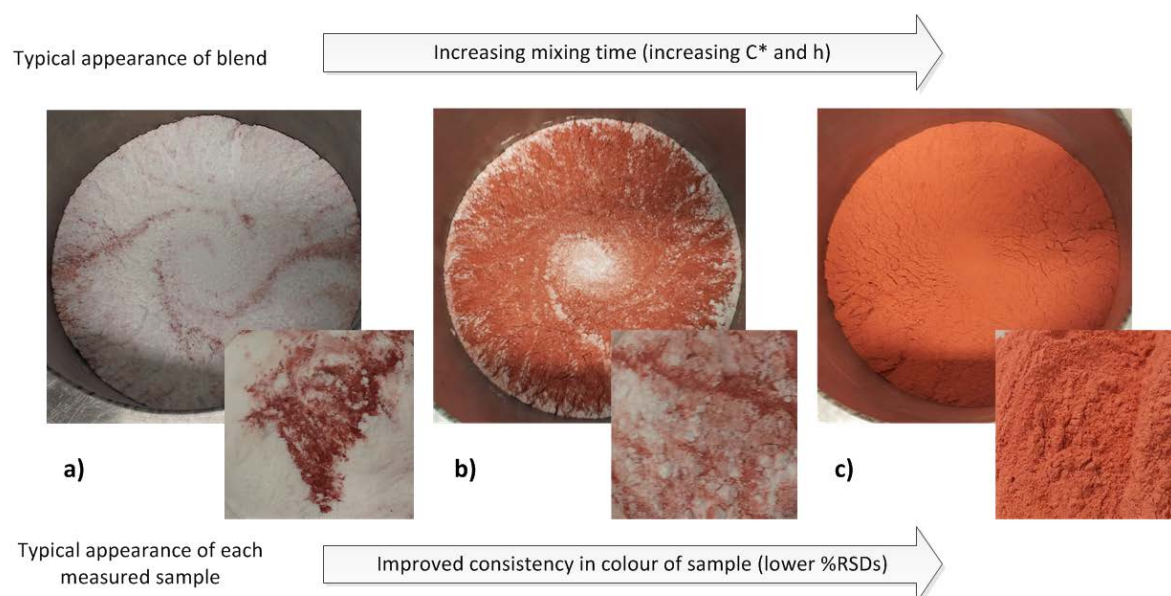


Figure 6.9: Typical appearance of overall blend and collected samples for low (a), moderate (b) and high (c) mixing times. Intensity or colour and consistency between samples improved with increasing mixing time.

The blend colour can be measured through various means, however interpretation of the data is best conducted in the CIELCH (1976) colour space. If the sampling equipment records in other colour spaces, algorithms are readily accessible to convert those values to the CIELCH space (*Easy RGB*, 2014). Either single or multiple samples can be taken at each time point of mixing, depending on the level of information desired. For information on content uniformity of the blend, multiple samples (at least 10) should be taken at set and spread locations within the mixer. To obtain robust results for analysis, and to maximise information obtained about a mixer's behaviour from colour analysis, it is recommended to 'over mix' the powder beyond standard pharmaceutical blending times. Blends in this thesis were mixed for a total of 60 minutes, and sampled at 0.5, 1, 2, 3, 4, 5, 7.5, 10, 12.5, 15, 20, 25, 30, 45 and 60 minutes. This provided a broad mixing profile for the particular mixer and gave insight into mixing kinetics (such as the rate of mixing). Additional time points, particularly at low mixing times can be added to give more information about specific mixing in the practical region that is likely to be used for drug blend manufacturing.

Whilst the method of recording colour values (i.e. the instrument used) is not particular, it must be consistent between measurements to prevent errors and allow effective comparisons to be made. To ensure reproducibility, the light source, background light (if system not encased), angle of light source and detector, as well as the preparation of the sample should all be exactly the same as one another. The simplest way to do this is to use an off-the-shelf spectrophotometer with shielding from other light sources.

#### *Step 5 - Assemble formulation curve in the CIELCH colour space*

Taking the colour values from each time point (or the average if multiple samples are collected) and assembling them in the CIELCH colour space, 3-dimensional 'blend curves' are created which overlap with one another for a given formulation (*Figure 4.7*).

A single blending experiment will not span the entire formulation curve, but will start and finish along it. Therefore, to generate an entire formulation curve in the CIELCH colour space, the results of

industrial scale blending runs can be complimented by separate blending in smaller lab-scale mixers with low and high intensity. Generation of the entire formulation curve is not required in industry for blend optimisation and/or demonstrating equivalent mixing. It can however be used to fully define the design space for a given mixer and provide information on the mixing mechanics. If taking single samples from a mixer, having a pre-populated formulation curve can enable identification of poor content uniformity.

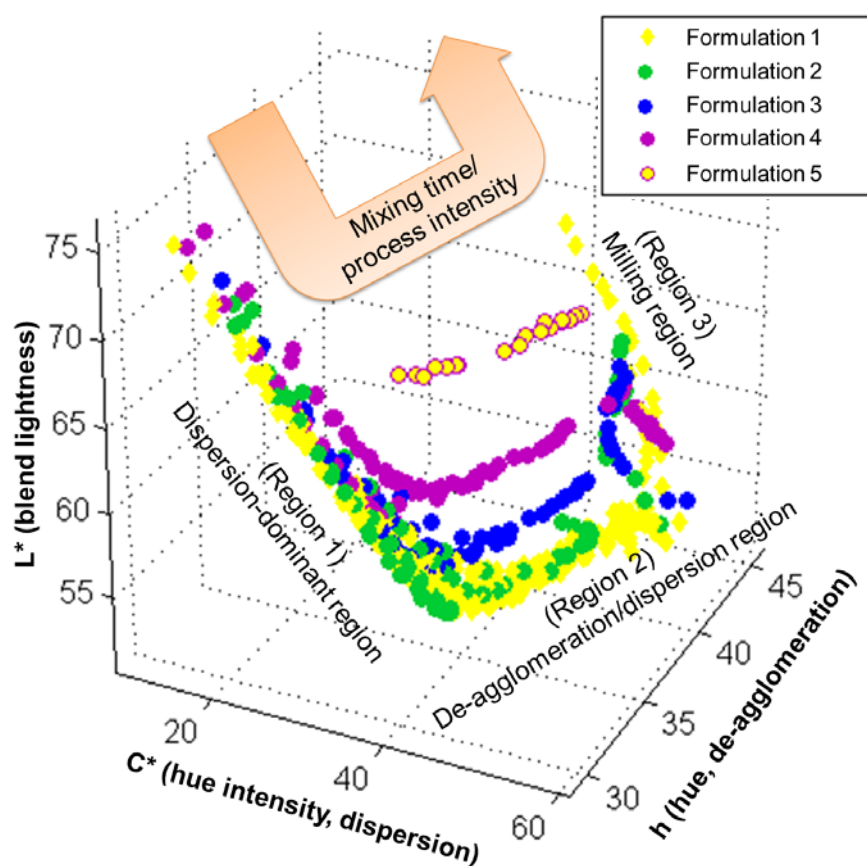


Figure 4.7: Colour curves generated for each formulation in the CIELCH colour space.

### Step 6 – Analyse blending conditions from the generated blend curve/s

The crux of industrial analysis relies on generating blend curves with the mixers on hand. Blend curves overlap with one another along their respective formulation curves, with their start and end points varying with process intensity (as shown in a section of a formulation curve, *Figure 4.6*).

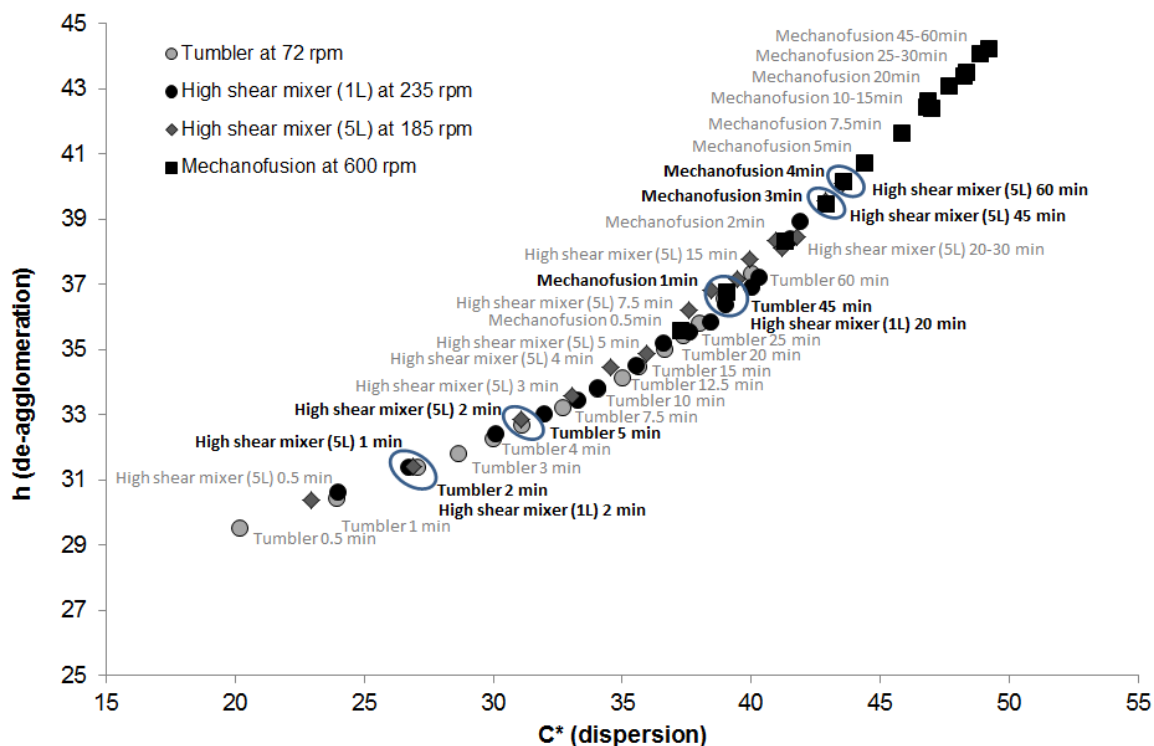


Figure 4.6: Section of the colour curve for Formulation 1 in the  $C^*$ - $h$  plane showing the overlap of blend curves in different mixers and scales.

Points at which colour data align are often easy to collect and represent equivalent mixing. The circled points in Figure 4.6 indicate that blend equivalence is achievable. For instance, the circle at lowest  $C^*$  ( $C^* = 31.4$ ,  $h = 26.9$ ) shows the blend colour achieved in a 5L high-shear mixer after 1 minute of mixing at 185 rpm can also be achieved in a 1L high-shear mixer after 2 minutes of mixing at 235rpm, or by using a tumbling mixer for 2 minutes at 72 rpm. Similarly at higher values on the formulation curve ( $C^* = 39.1$ ,  $h = 36.7$ ), mechanofusion, tumbler and high-shear mixer blends all show the same colour. This point also represents equivalent mixing.

From these blend curves, key information on the blend and blending kinetics can be taken. The following headings outline different information that can be extracted from the CIELCH data for a given mixer and set of operating conditions.

#### Quantifying the degrees of tracer dispersion and de-agglomeration

The novel attribute of using this tracer is its multiple dimensions in colour change beyond blend lightness alone. Due to the primary particle size causing a shift in the blend hue from red to orange,

two dimensions to the colour change of the blend can be simultaneously and independently quantified and evaluated; the increase in hue intensity ( $C^*$ ) caused by the spread (dispersion) of tracer and the change in hue ( $h$ ) due to its de-agglomeration (Figure 3.5).

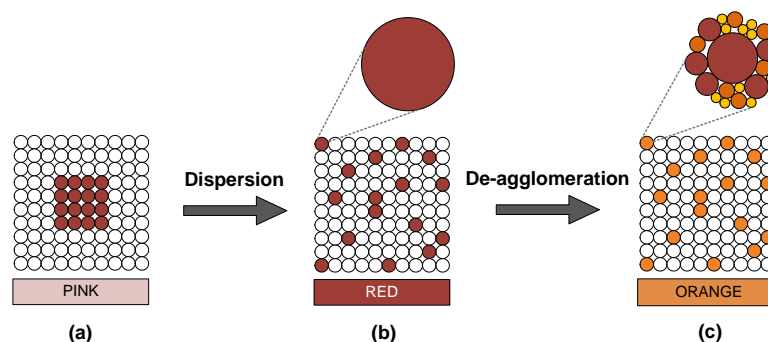


Figure 3.5: Schematic of sub-micronised hematite tracer dispersion (a-b) and de-agglomeration (b-c).

Units for both the hue and hue intensity are arbitrary, but allow for various comparisons and calculations to be made. With increasing hue and hue intensity, the degree of tracer dispersion and de-agglomeration increase.

#### *Identifying mechanisms of powder blending*

Along the 'u-shaped' formulation curve different types of tracer mixing can be seen based on the different directions the curve takes in the CIELCH colour space (Figure 4.3). These regions relate to different mixing mechanisms, and colour values which lie in each region indicate the type of mixing the powder is undergoing. Mixing regions are outlined in Section 8.3.3.

Over large mixing times, blend curves are observed to span across more than one mixing region. By knowing which region/s the blend lies within and coupling this with the degree of tracer dispersion and de-agglomeration, mixing end points can be targeted and unintentional milling can be mitigated.

#### *Detecting and quantifying milling and unintentional particle damage*

For formulations that enter the milling region of the formulation curves, the degree of milling (in respect to the volume percentage of ultrafines,  $uf$ ) can be quantified based on the measured blend lightness (Eqn. 7.7).

$$uf = uf_i + 2.246 \ln[L^* - 10.152 \ln[uf_i] - 38.297] - 1.711 \quad (\text{Equation 7.7})$$

Where  $uf_i$  is the initial volume percentage of ultrafines (i.e. particles  $< 4 \mu\text{m}$ ) and  $L^*$  is the recorded blend lightness in the milling region. This provides a result within  $\pm 10\%$  of the measured values of ultrafines in this study. Whilst the above equation relates to the use of one weight percent submicronised hematite tracer in lactose, other correlations of the same form are likely to exist with different types of tracer and/or bulk powder.

#### *Detecting batch-to-batch variation*

Detection of batch-to-batch variations in the level of fines is dependent on the sensitivity of the spectrophotometer used. With a typical bench-top spectrophotometer, it is expected that variations in fines (i.e. particles  $< 15\mu\text{m}$ ) can be detected if their volume percentages of fines differ by 10 percent from one another.

The use of this method to detect batch-to-batch variation is limited to analysis within the de-agglomeration/dispersion region, as variations in uniformity would drown-out any changes due to formulation variance.

#### *Demonstrating equivalent mixing*

The measured hue intensity of the formulation is linked to the energy input to the blend during mixing. For a given formulation, most likely linked to a particular flooding fraction, the energy input can be quantified (Eqn. 6.18).

$$C^* = 48.9 - 20.9E^{-0.388} \quad (\text{Equation 6.18})$$

This particular correlation was found for one weight percent hematite tracer in 2kg of Lactohale LH200. Different formulations would have a correlation of the same form with different values for the coefficients. As the hue intensity is linked to energy input, the energy input and power can also be used to determine mixing times to achieve equivalent mixing between two mixers or sets of operating conditions.

## Quantification of content uniformity (multiple sampling)

For large scale mixers where multiple samples can be taken at each time point, the content uniformity of the blend can be assessed. When taking the average hue ( $h$ ) and hue intensity ( $C^*$ ) values at each time point, blend curves can deviate from the typical formulation curve at low values of  $C^*$  and  $h$  with decreasing uniformity (Figure 6.10). This can be used as a preliminary means of identifying poor uniformity.

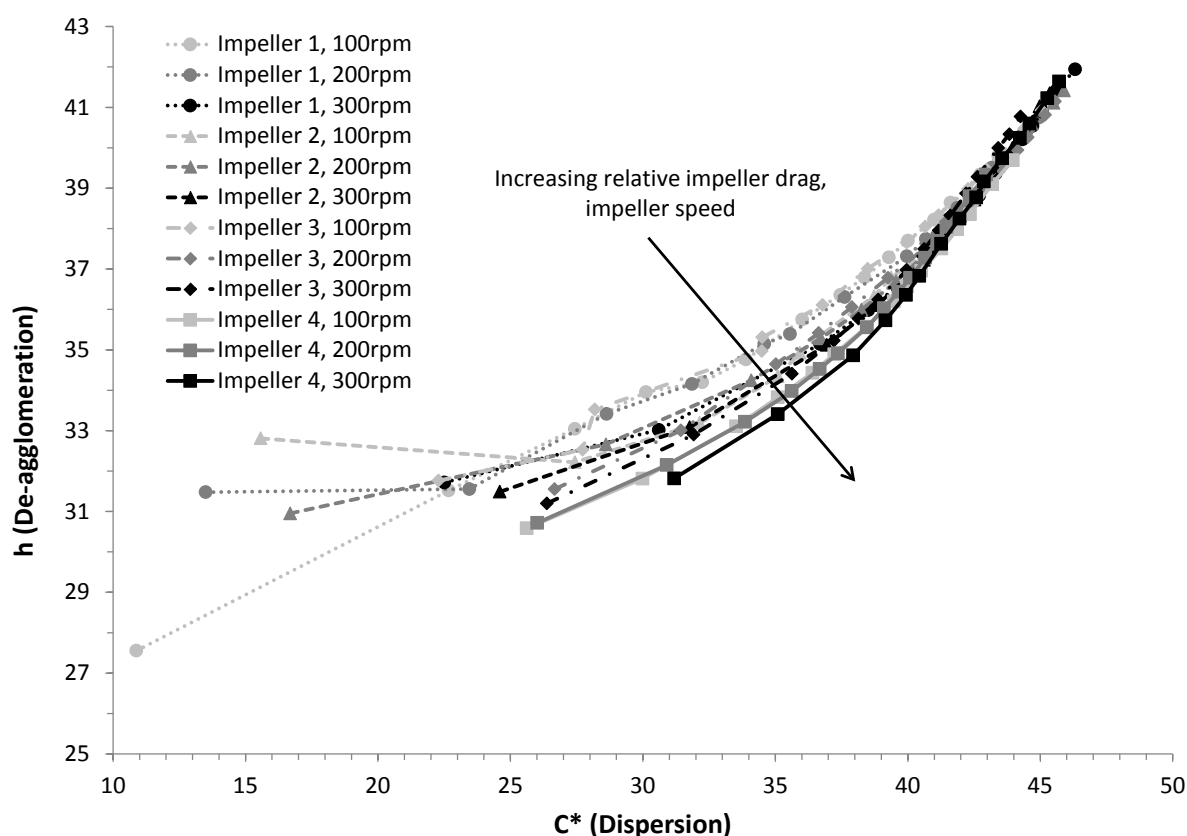


Figure 6.10: Progression of mean degree of dispersion ( $C^*$ ) and de-agglomeration ( $h$ ) for each impeller and operating speed.

The standard content uniformity test is to take several small masses of drug blend and measure the relative standard deviation of drug content across the samples. An analogous calculation is used with the colour tracer blends by taking the relative standard deviation of dispersion ( $C^*\%RSD$ ) at each time point (Eqn. 6.1).

$$\%RSD = \frac{\text{st. deviation}}{\text{average}} \times 100 \quad (\text{Equation 6.1})$$

The relative standard deviations can be plotted against mixing time to compare uniformities between systems, and also give insight into the relative rates of mixing (Figure 6.14).

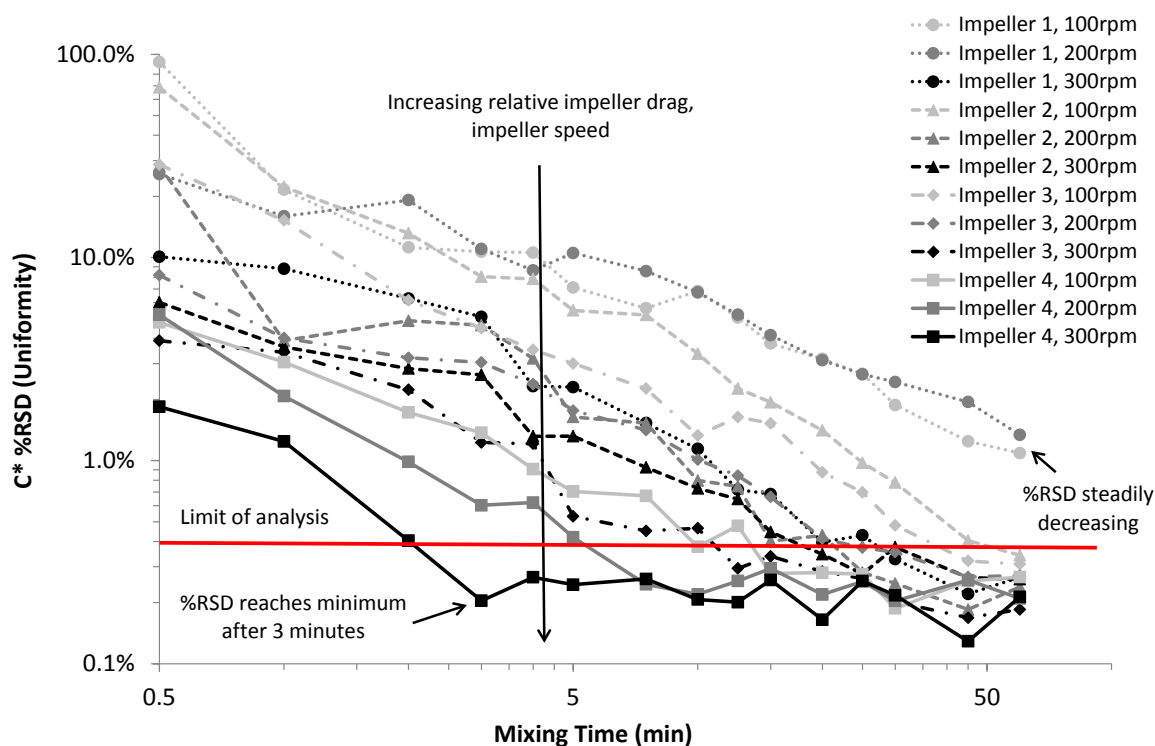


Figure 6.14: Content uniformity of blends ( $C^*$  %RSD) over time.

With any analytical process there will be a certain level of background noise associated with measurements. With spectrophotometric analysis of powders this noise is considerably higher than for chromatographic methods in drug analysis. Because of this, blends will assume a maximum level of uniformity with colour data long before uniformity may be reached with drug blends. This should be factored in to mixing time calculations if new drug blends are to be blended with no existing data from current mixers (even on a lab-scale).

Measurements for content uniformity have been shown to be sensitive enough to make meaningful comparison between different mixing speeds, times and mixer internal configurations. It would be no surprise if the method could also be used to compare different mixers.

*Identifying powder flow regimes in high-shear mixing (multiple sampling)*

An additional benefit of taking multiple samples at each time point is that powder flow types can be predicted. In a high-shear mixer, comparison of the hierarchies of hue intensity for each specific sampling location can give insights into powder flow regimes (*Figure 6.45*). This information can help in providing a better comparison of 'equivalent' operating conditions and the causes of poor blend attributes (such as content uniformity).

- Powder mixing in the bumping regime (*Figure 6.45a*) shows fluctuations in the regional hierarchy (i.e. 'zig-zagging') in respect to both their degree of hue and hue saturation. There is also a relatively high separation of regional curves from one another even at large mixing times.
- Powder mixing in the roping regime (*Figure 6.45c*) shows regional curve separation with both hue and hue saturation; however the hierarchy remains fairly constant at each time point until the point where all regions align with one another at high mixing times.
- Transitional flows (*Figure 6.45b*) appear to show varying amounts of 'zig-zagging' and constant regional hierarchy at low mixing times, depending on its respective similarities to bumping and roping regimes. 'Zig-zagging' irons out at high mixing times.
- Unstable or chaotic flow (*Figure 6.45d*) shows small separation between colour values between regions at low mixing times, which align with one another, even at low mixing times.

Whilst the work in this thesis only confirms the ability of the colour method to predict flow types in high-shear mixers, it is believed that it can easily be transferred to other mixing technologies, but is heavily dependent on the location of samples within the tracer blend.

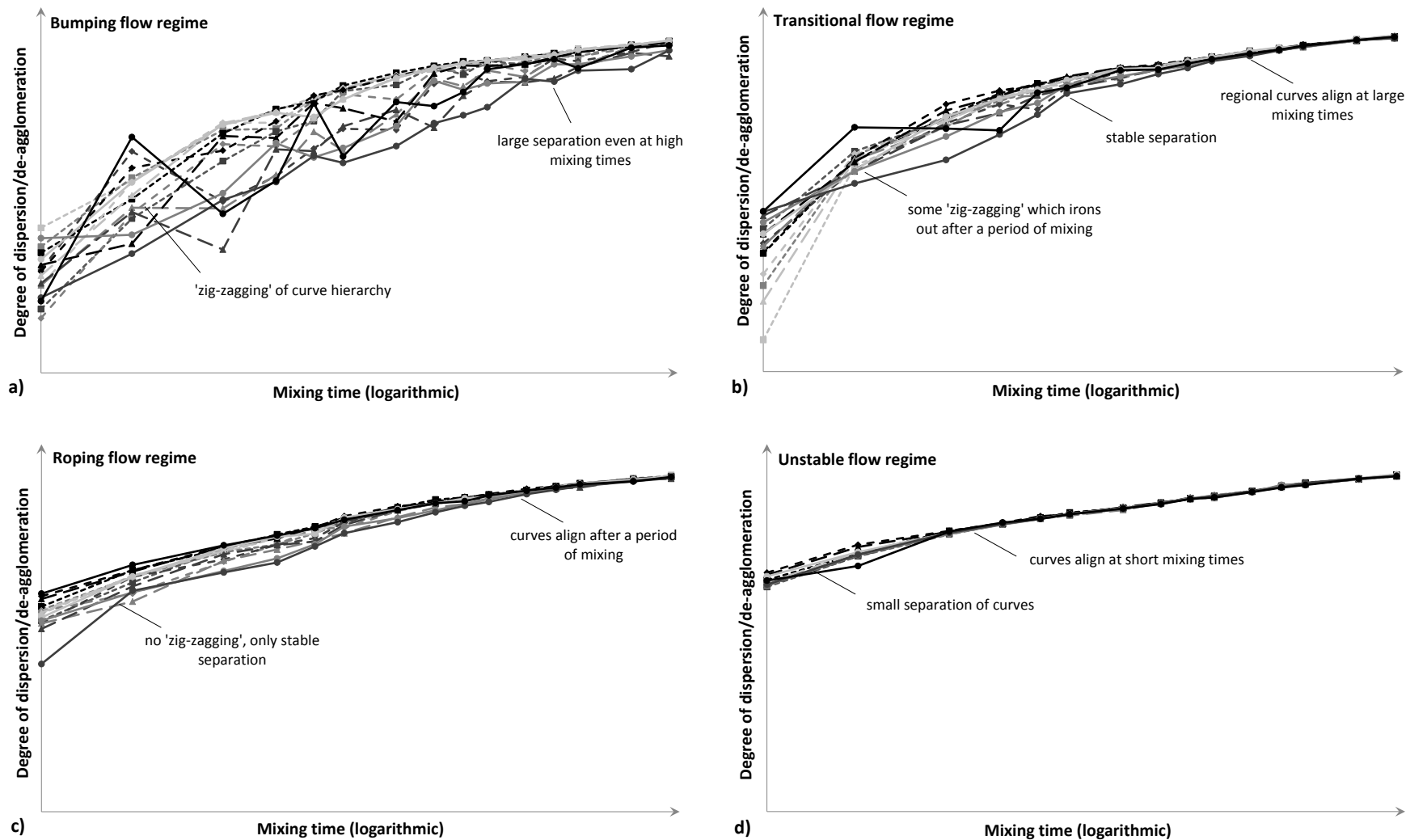


Figure 6.45: Schematic of typical regional colour curves over time for bumping (a), transitional (b), roping (c), and unstable (d) powder flow.

### 8.4.3 Comments on drug blending

#### *Step 7 – Linking colour information to drug blending data*

Colour data alone only demonstrates equivalent mixing between different sets of operating conditions or mixers. It does not provide information on the blending behaviour of any drug and because of this, requires complimentary drug data in confirming equivalence in process upscale and for process optimisation.

By linking product performance data to specific locations along the CIELCH formulation curve, design spaces can be defined and specific colour points selected as desirable mixing end points. In doing so, other mixers and operating conditions can be quickly tested with colour data alone to be able to predict their design spaces and optimal operating conditions. For systems where there is no initial reference for blending, operating conditions for drug blending can be selected from conditions that give good content uniformity in tracer blends.

## 8.5 Application of colour tracer method to previous work

One simple means of testing the colour tracer method with other powders and colour tracers is to test it against the previous work. Only one paper provides full CIELAB colour data to test the method against rather than  $L^*$ -values alone (Satoh *et al.*, 1993). The CIELAB data from Satoh's paper is converted to CIELCH data using the equations in Section 2.4 and compared to colour curves generated in this thesis.

The formulation used in their study comprises of 5 wt% iron oxide tracer in calcium carbonate, with an order of magnitude difference between the mean particle size of calcium carbonate and iron oxide tracer (Figure 8.7). The iron oxide again shows a red hue and the bulk powder is white.

Whilst the work does not specify which type of iron oxide was used as a tracer, the red-purple colour of the tracer is consistent with that of hematite given its particle size distribution in Figure 8.7b

(Cornell and Schwertmann, 1996). Whilst the tracer of Satoh’s study and the one used in this thesis are both hematite, the one used in this thesis has a yellow shade due to its primary particle size being less than 100 μm (as described in Chapter 3).

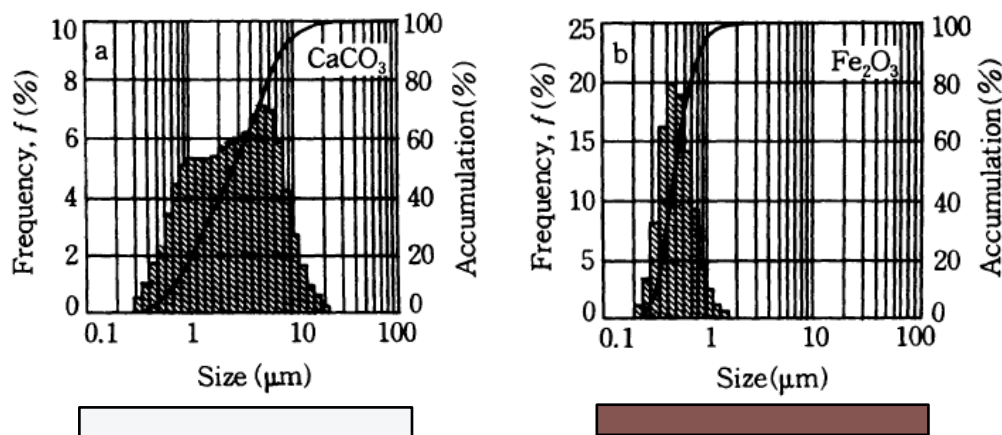


Figure 8.7: Particle size distributions of a) calcium carbonate and b) iron oxide tracer from Satoh et al. (1993) with colour swatches based on recorded CIELAB values of each material.

Before analysing the colour values from Satoh’s study the flooding fraction, which is outlined in Section 8.2.1, should be calculated (Eqn. 5.10). This determines whether the system is too weak or too saturated to give meaningful colour readings.

$$f = \frac{\beta w}{\eta(100 - w)}; \beta = \frac{3}{2\rho_{tp}D_{tp}\hat{A}_s} \quad (\text{Equation 5.10})$$

Many of the powder properties for calculating the flooding fraction are provided in the paper by Satoh et al. (1993) (Table 8.5).

Table 8.5: Properties of the calcium carbonate and iron oxide powders from Satoh et al. (1993).

$\rho_{tp} (\text{Fe}_2\text{O}_3)$	5200 kg/m <sup>3</sup>	$\rho_{sp} (\text{CaCO}_3)$	2600 kg/m <sup>3</sup>
$D_{tp} (\text{Fe}_2\text{O}_3)$	$0.47 \times 10^{-6} \text{ m}$	$D_{sp} (\text{CaCO}_3)$	$2.66 \times 10^{-6} \text{ m}$

$\rho_{sp}$  and  $D_{sp}$  are the true density and particle diameter of the substrate material respectively. One that is not provided directly however is the specific surface area of the substrate (i.e. calcium carbonate). On the assumption of mono-sized, spherical particles, the specific surface area can be calculated based on the substrate’s mean particle diameter (Eqn. 8.4).

$$\hat{A}_s = \frac{6}{\rho_{sp} D_{sp}} \quad (\text{Equation 8.4})$$

Substitution of this surrogate term into Equation 5.10 gives an adjusted equation for calculating the flooding fraction, which now assumes mono-sized, spherical particles for both the substrate and tracer (Eqn. 8.5).

$$f = \frac{\rho_{sp} D_{sp} w}{4\eta\rho_{tp} D_{tp} (100 - w)} \quad (\text{Equation 8.5})$$

Populating Equation 8.5 with values provided by Satoh *et al.* (Table 8.5) and the assumption of random tracer coverage ( $\eta=0.547$ , Chapter 5) the flooding fraction of the 5 wt% tracer formulation can be calculated (Eqn. 8.6).

$$f = \frac{2600 \times 2.66 \times 10^{-6} \times 5}{4 \times 0.547 \times 5200 \times 0.47 \times 10^{-6} \times (100 - 5)} = 0.068 \quad (\text{Equation 8.6})$$

This flooding fraction is low but within the recommended range for providing meaningful colour data (i.e. between 0.05 and 0.4). Because of this, the colour data can be extracted from the paper and compared to the work of this thesis.

As previously mentioned, the work by Satoh *et al.* (1993) provides  $L^*a^*b^*$  data for a component of their mixing (Figure 8.8).

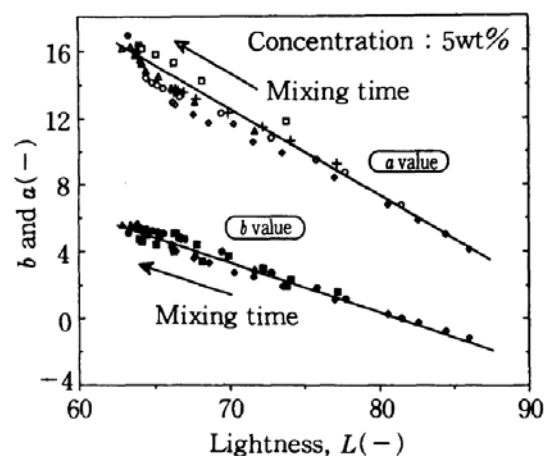


Figure 8.8:  $L^*$ ,  $a^*$  and  $b^*$  values from calcium carbonate and iron oxide blending (Satoh *et al.*, 1993).

Using *ImageJ* software to collect data points from Figure 8.8, they are replotted in the CIELCH space and compared to the data from Figure 8.3 (Figure 8.9).

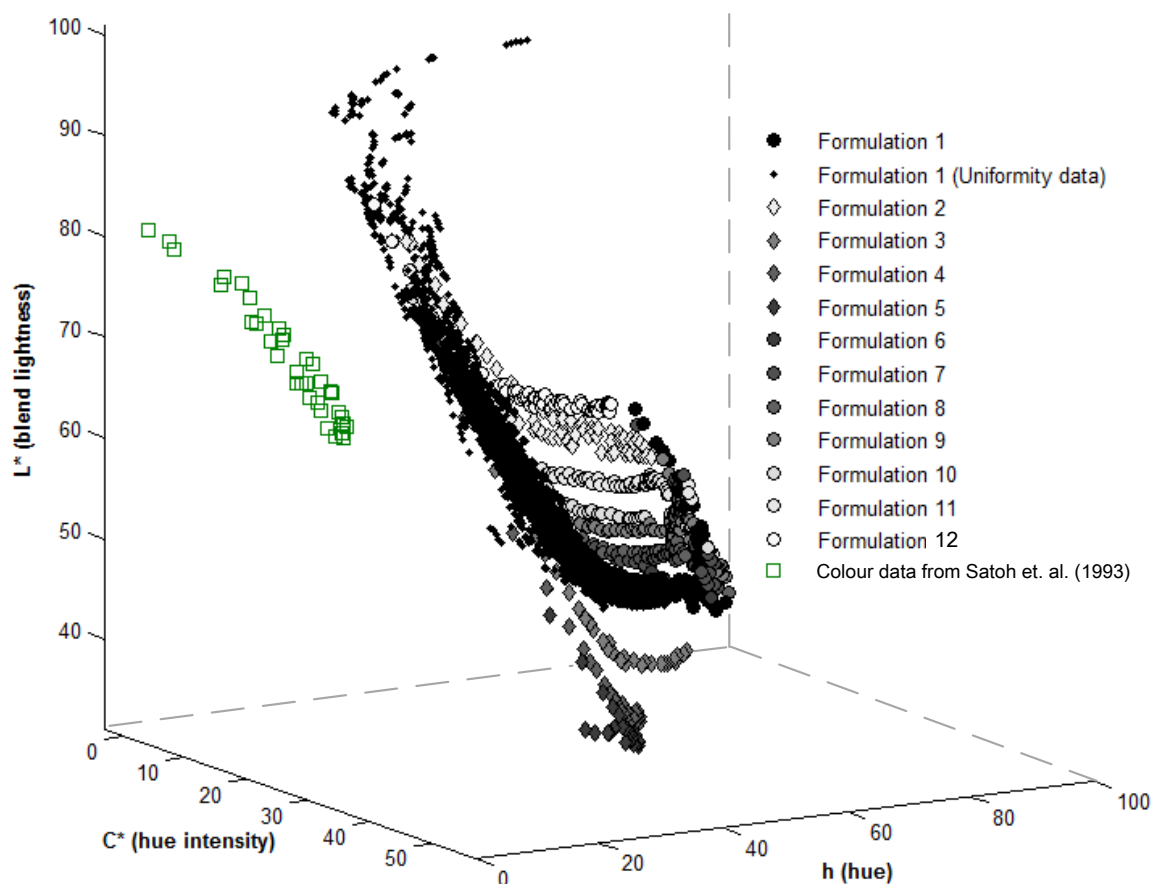


Figure 8.9: CIELCH data from Satoh *et al.* (1993) compared to colour curve data from Figure 8.3.

Because of the different hue that is generated in the tracers (based on particle size), Satoh's colour curve sits at a lower hue than the data obtained in this thesis. The colour data also falls on a curve in the colour space, suggesting that a formulation curve could be formed with more data points. The high blend lightness in the Satoh data obtained suggests that the powder is poorly mixed, possibly by hand. This would explain why the data also sits higher in the CIELCH space than expected. The shape of the 'blend curve' is similar to those in the low/poor mixing region. Unfortunately, Satoh *et al.* (1993) do not specify what method of mixing was used to achieve these values (i.e. hand mixed, high-shear mixed or milled; which were all used in the study). Given their very high position along the formulation curve the data most likely comes from hand stirring. This would also explain the lack

of conformity between data points. The Satoh curve also does not curl at high blend lightness, suggesting that there is no change in hue when mixed.

Whilst not definitive, this comparison suggests that other powders and tracers could potentially be used to assess blending in the CIELCH colour space, and that different tracers may indeed generate different surfaces in the colour space. Further comparisons are required however, particularly with powder blending in mixers, for robust conclusions. One of the benefits of the colour tracer in this thesis is that it has multiple dimensions to its colour change, which may not necessarily exist in other colour tracers. For tracers that do not change colour when they de-agglomerate and simply increase in colour intensity due to tracer spread throughout the bulk powder, it may suffice to simply assess blending through blend lightness ( $L^*$ ) alone. This may be the case for the tracer used in the work of Satoh *et al.*

## 8.6 Limitations of method and recommendations for future work

Naturally, several questions arise in regards to the robustness, scope and significance of the use of iron oxide as an analytical tool for powder blending – in particular its ability to mimic a drug formulation's blending and the reproducibility, and reliability of colour data collected. It is important to note that the agglomeration strength and cohesion/adhesion properties of the tracer will almost certainly never perfectly match those of any particular drug. The method outlined in this work does not provide direct information about how a drug would spread and de-aggregate in a mixing system, but rather can be used as a cost and time effective preliminary tool for showing equivalent blending between two systems or enabling process optimisation. In addition the flow behaviour of the tracer blend is almost certainly different to that of any drug blend due to the different adhesion/cohesion properties of the tracer and APIs. Also, the tracer used in these studies is spherical and smaller than DPI drugs, which are often shard-like due to their pre-blending micronisation.

The studies described in this work are based on a pre-manufacturing process, in which the mechanics of the *bulk excipient* are assessed in a quick and simple manner. It is not intended in

these works for the tracer to be included in future drug blends to assess the quality of each batch. Such a system would create a multitude of complexities to the formulation, with the tracer having an influence on drug delivery and blending, as well as the associated regulatory concerns and revisions with altering the formulation. It should also be stressed that this method is a bulk analysis method. The scale of scrutiny in this method is not of the order of a pharmaceutical dose (i.e. milligrams) but considerably larger (i.e. in the order of grams). In addition, the method does not indicate whether tracer has coated the fine or coarse lactose in a given sample, which for a drug in a DPI formulation dictates the inhalation performance. These factors make the use of a colour tracer a purely preliminary method for process optimisation, and simply suggest its use in cutting time and costs in process development. Ideally, pre-manufacturing colour data would be coupled with drug blend data under the same mixing conditions and compared to enable for educated estimates of drug performance for a certain colour blend, particularly where specific powder structures are desired.

Based on these remarks, several avenues are recommended for future work to strengthen the findings in this thesis, and also validate and extend the method:

- **Testing the colour tracer method against drug blends.** The next stage of the colour tracer method development would be to link drug data with the formulation curves to show that equivalency in colour relates to equivalency of content uniformity (for example in drug blending), and also that colour curves could be used to optimise drug blending. This would validate the use of colour tracers in process development. Whilst not substantial enough to include in this thesis, preliminary drug tests have been conducted between lab and industrial scale mixers which suggest that process up-scaling is possible with the colour method.
- **Developing a model for predicting the shape and location of formulation curves.** This would create a means of assessing blending for a single or small amount of colour measurements by providing information about mixing mechanisms and content uniformity.

Such a study would also require validation of the use of the formulation's flooding fraction in generating the formulation curve in the CIELCH colour space.

- **Determining a means of measuring tracer adhesion to fine or coarse substrate.** A study of this nature would certainly allow for more robust analysis of mixing in relation to ensuring good DPI formulation blending. By knowing whether the tracer is preferentially adhering to fine or coarse bulk material, and the associated effects on the measured colour, formulation curves could potentially be used to not only indicate design spaces for effective drug dispersion and de-agglomeration, but also for effective drug-carrier adhesion. This could provide benefit to process optimisation and ultimately enable fine tuning of drug formulations to give different drug release profiles.
- **Testing with different types of colour tracer.** Part of the success of the method relies in the multiple dimensions of colour change in the submicronised iron oxide tracer, which are unlikely to occur in many other coloured tracers. It would be beneficial however, to investigate the use of other multi-dimensional colour tracers in powder blending, as well as the types of assessment that could be applied to colour tracers that only changed in hue intensity over time.
- **Testing the method for different types and colours of bulk powder.** Whilst this work has focussed on the blending of pharmaceutical lactose formulations, there is no foreseeable reason why it cannot be applied to a wider range of powders in other manufacturing processes. Previous work into the use of colour tracers has shown that colour changes can be used to assess dry powder blending with calcium carbonate (*Satoh et al., 1993*) and microcrystalline cellulose (*Alonso et al., 1989a*), and it is believed that the use of this iron oxide tracer would be no different. The only limitation of its use with other powders would be that a colour change still needs to be visible, and may not be possible with dark coloured powders.

Additional aspects which are not essential to strengthening the method but would also be beneficial to investigate are as follows:

- **Testing the method against other mixers and flow regimes.** It was highlighted in Chapter 6 that the fluctuations in colour readings for specific regions within a high-shear mixer could be used to infer the powder flow regime that mixing occurred in. It would be an interesting study, but not essential to the success of the method, to determine whether other powder flow regimes in other mixers (such as avalanching in a drum mixer) could also be predicted from colour results.
- **Testing the effect of milling at different flooding fractions.** In Chapter 7 it was demonstrated that the level of ultrafines (i.e. volume percentage of particles  $< 4 \mu\text{m}$ ) caused by milling could be quantified. This however was only tested at a specific tracer concentration, and it is not clear whether the level of ultrafines could also be quantified at different tracer concentrations. By determining the relationship between tracer concentration and the change in blend curves in the milling region, a more flexible correlation could be found for quantification of the degree of milling.

Whilst there are other areas of the method to explore to realise its full potential, they should by no means detract from the significance of the findings within this thesis. Overall and so far, this blend tracer approach appears to provide a robust and simple means of blend analysis and provides information about multiple aspects of blending, allowing for simpler and cost effective process optimisation as well as technology transfer and scale-up.



## Conclusion

**T**he current state of pharmaceutical powder blend process development and optimisation relies heavily on problematic trial-and-error approaches and costly and repetitive drug blend manufacturing. These can lead to a non-optimal selection of operating conditions for the manufacturing of Dry Powder Inhalation (DPI) formulations (as well as other types of powder mixtures), and create processes that are often sensitive to failure due to a lack of understanding of the mixer and formulation. The focus of the work in this thesis was therefore centred on improving process development for DPI formulation manufacturing, and outlined in Chapter 1 as determining whether;

***“[there is] a means of making blend analysis simpler and cheaper to improve process optimisation and/or scale-up.”***

A method has been developed in this thesis that is simple and cost effective to implement and can be used to improve process development and optimisation. By blending the bulk excipient with a small quantity (in the order of approximately one percent by mass) of submicronised iron oxide

tracer in place of the pharmaceutical active, information about the type and extent of powder blending can be obtained. In doing so, a vast amount of information can be gathered for a given mixer, formulation and set of operating conditions, which can improve the means of selecting drug blending conditions, and interpreting results. The key factors for assessing the quality of DPI blending were defined in the Introduction as:

- ***The degree of drug breakup and spread during mixing***
- ***The homogeneity of the blend/controlled total blend energy input***
- ***The degree of particle damage during blending (due to unintentional milling)***

The method developed in this thesis is shown to assess all of these key factors, and is also able to detect batch-to-batch variation in powders. It can give insight into powder flow within the mixer, which also affect blending and ultimately product performance. These factors can be used to demonstrate equivalence between two different mixing conditions, and ultimately allow for process optimisation by identifying undesirable mixing conditions.

The method outlined in this thesis relies on measuring the colour change of the tracer blend over mixing time. Measuring the change in hue and intensity of sub-micronized iron oxide (specifically hematite, with a particle size of ca. 0.1  $\mu\text{m}$ ) in a lactose bulk enables the analysis of two distinct mixing behaviours. These behaviours are the de-agglomeration of the tracer (transition from red to orange) and the dispersion of a given sized aggregate through the bulk material (increase in the intensity of the blend's hue). From analysis of the blend colour values over mixing time, formulation-specific curves are generated in the CIELCH (1976) colour space which are independent of process type, intensity and scale. Different processes lie on different regions of the curve. These formulation curves can identify and quantify both the degree of tracer dispersion and de-agglomeration.

Blending kinetics can also be inferred from the three distinct regions of formulation curves in the CIELCH colour space, which relate to different types of mixing. For low intensity processes or short mixing times, blend curves lie in the dispersion-dominant mixing region. Moderate intensity mixing

or large mixing times result in blend curves entering the de-agglomeration/dispersion region. The third region, termed the milling region, exists for intense mixing systems and can be used to detect and quantify the degree of unintentional milling during mixing. Equivalent mixing can also be demonstrated through two systems aligning at the same location along a formulation curve, and it was shown in this thesis that the location along the formulation curve also relates to the energy input to the powder.

In addition, when sampling a blend at multiple locations for each time point, information about the blend's homogeneity and powder kinetics can be made. By taking the relative standard deviation (RSD) of the hue intensity between samples at a single time point, the content uniformity can be quantified and compared to other systems and time points. Also, by plotting the hue intensity for each specific location over mixing time, the oscillation in hierarchy between different regions can be used to infer the powder flow regime for a given mixer.

The method outlined in this thesis is designed to be implemented in preliminary process development to develop a robust understanding of a given mixer or set of operating conditions, and enable better selection of test points for drug blend manufacture. In doing so, significant time and costs can be saved. It can allow reduction in the amount of drug blends manufactured and ensuring that an appropriate design space is constructed first time. As the colour tracer method is a bulk analysis method and does not give information as to whether tracer particles are adhered to the fine or coarse bulk material, it is difficult to know how well it can predict drug blending behaviour and product performance. Because of this, further validation is required in relation to using the colour tracer method to predict drug blending behaviour. As it stands however, the colour tracer method of this thesis shows great promise and adds value when integrated into current process development. This method may also be applicable to other colour tracers and bulk materials, and could be transferred to other powder mixing processes, for other dosage forms and powder blends beyond pharmaceutical manufacturing.



## Nomenclature and glossary of abbreviations

$a$	Coefficient in energy input correlation	-
$a^*$	Degree of red (positive) or green (negative)	-
$A$	Power calculation coefficient relating to force transducer	N.m.unit <sup>-1</sup>
$A$	Coefficient in regression fits	-
$\hat{A}_{ftc}$	Total area of tracer coverage per unit mass of formulation	m <sup>2</sup> .kg <sup>-1</sup>
$\hat{A}_{fs}$	Total surface area of substrate per unit mass of formulation	m <sup>2</sup> .kg <sup>-1</sup>
$\hat{A}_s$	Specific surface area of substrate	m <sup>2</sup> .kg <sup>-1</sup>
$\hat{A}_{tc}$	Area of tracer coverage per unit mass	m <sup>2</sup> .kg <sup>-1</sup>
$A_{tpc}$	Area of tracer particle coverage	m <sup>2</sup>
$A_{ttpc}$	Area of total tracer coverage (per particle)	m <sup>2</sup>
$b$	Coefficient in energy input correlation	-
$b^*$	Degree of yellow (positive) or blue (negative)	-
$B$	Coefficient in regression fits	-
ACI	Anderson Cascade Impactor	-
AFM	Atomic Force Microscopy	-
API	Active Pharmaceutical Ingredient	-
APSD	Aerodynamic Particle Size distribution	-

---

BET	Brunauer Emmet Teller Analysis	-
C	Coefficient in regression fits	-
C*	Hue intensity, Chroma	-
CAT	Computerised Axial Tomography	-
CFCs	Chlorofluorocarbons	-
CFD	Computational Fluid Dynamics	-
Ci	Curies, SI unit for radioactivity	-
CI	Cascade Impactor	-
CIE (1976)	Colour space created by the International Commission on Illumination	-
CIELAB	CIE (1976) colour space expressed in Cartesian L*a*b* coordinates	-
CIELCH	CIE (1976) colour space expressed in Cylindrical L*C*h coordinates	-
COPD	Chronic Obstructive Pulmonary Disease	-
CPMA	Colour Pigments Manufacturers Association	-
CQA	Critical Quality Attribute	-
$D$	Impeller diameter	m
$D$	Coefficient in regression fits	-
$d_{50}$	Median particle diameter (equivalent sphere basis)	$\mu\text{m}$
$d_{ae}$	Aerodynamic diameter	-
$D_{sp}$	Substrate particle diameter	m

---

---

$D_{tp}$	Tracer particle diameter	m
DD	Delivered Dose	$\mu\text{g}$
$\%dm/dt$	Change in mass over time as a percentage of total mass	$\%.\text{min}^{-1}$
DPI	Dry powder inhalation	-
DoD	Degree of Dispersion	-
dt	Differential in respect to time	-
DVS	Dynamic Vapour Sorption	-
ED	Emitted Dose	$\mu\text{g}$
D65	CIE standard illuminants, corresponding to daylight	-
DEM	Discrete Element Modelling	-
$E$	Energy input to the powder during mixing	J
$e^+$	Electron	-
$\Delta E^*$	Distance between two measurements in the CIELAB colour space	-
$\Delta E^*_{(LCH)}$	Distance between two measurements in the CIELCH colour space	-
$f$	Flooding fraction relating to tracer coverage of a substrate	-
$F$	Force or torque of mixer	N
$F_m$	Measured force by transducer	N
FDA	Food and Drug Administration, U.S.A.	-
FPF	Fine Particle Fraction	%

---

FPM	Fine Particle Mass	$\mu\text{g}$
G	Gain of force transducer	$\text{N}\cdot\text{unit}^{-1}$
GDS	Geometric Standard Deviation	
<i>h</i>	hue, hue angle	$^{\circ}$
HPLC	High performance Liquid Chromatography	-
HSM	High-shear mixer	
<i>I</i>	Blend intimacy	$\%^{-1}$
ICH	International Conference on Harmonisation of Technical Requirements for Registration of Pharmaceuticals for Human Use	-
IR	Infrared	-
keV	kiloelectron volts, unit of energy	
$L^*$	Blend lightness, ranges from white (100) to black (0)	-
$L_C^*$	Blend lightness from the constant- $L^*$ section of the de-agglomeration/dispersion region of formulation curves	-
$L_{eq}$	Equilibrium (or minimum) blend lightness	-
$L_{max}$	Maximum blend lightness (baseline)	-
$L_{sample}$	Measured blend lightness of a sample	-
LoA	Limit of Analysis	
$m_{tp}$	Mass of single tracer particle	kg

---

---

MDI	Metered Dose Inhaler	-
MFV	Minimum Fluidisation Velocity	m.s <sup>-1</sup>
MMAD	Mass Median Aerodynamic Diameter	-
$N$	Impeller speed	rev.min <sup>-1</sup>
$N_p$	Newton or Power number	-
NGI	Next Generation Impactor	-
P	Power applied to the powder during mixing	W
$p_n$	Tracker particle's Cartesian location at time point $n$	m
PAT	Process Analytical Technology	-
PEPT	Positron Emission Particle Tracking	-
PIV	Particle Image Velocimetry	-
PSD	Particle Size Distribution	-
$q$	Blend quality	-
$Q$	Quantity of interest in energy input correlation (either $C^*$ or $h$ )	-
QbD	Quality by Design	-
$R$	Radius of mixing vessel	m
$R^2$	Quality of fit for regression	-
RH	Relative Humidity	%
RMSE	Root Mean Standard Error	-

---

---

<i>RoM</i>	Rate of Mixing, change in uniformity over time	$\%.\text{min}^{-1}$
<i>rpm</i>	Revolutions per minute	$\text{min}^{-1}$
<i>%RSD</i>	Relative standard deviation	%
SEM	Scanning Electron Microscopy	-
$t_n$	Tracking time point $n$	s
$T_g$	Glass transition temperature	$^{\circ}\text{C}$
TI	Twin Impinger	-
$\Delta uf$	Change in the level of ultrafines in formulation (volume basis)	%
$uf$	Level of ultrafines in formulation (volume basis)	%
$uf_i$	Initial level of ultrafines in formulation (volume basis)	%
USD	Currency of the United States of America (U.S. Dollars)	
UV	Ultraviolet	-
UV/Vis	Ultraviolet/Visible light spectroscopy	-
$v_{\theta}$	Tracker tangential particle velocity	$\text{m}.\text{s}^{-1}$
$v_e$	Electron neutrino	-
$v_n$	Tracker particle velocity at time $n$	$\text{m}.\text{s}^{-1}$
$V_{eq}$	Equilibrium (or minimum) voltage during analysis	V
$V_{max}$	Maximum voltage (baseline)	V
$V_{sample}$	Measured voltage for a sample	V

---

---

$V_{tp}$	Volume of a single tracer particle	$m^3$
$v_x$	x-directional component of tracker particle velocity	$m.s^{-1}$
$v_y$	y-directional component of tracker particle velocity	$m.s^{-1}$
$v_z$	z-directional component of tracker particle velocity	$m.s^{-1}$
vol%	Volume percentage	%
$w$	Weight percentage of tracer in formulation	%
$w_{flooding}$	Weight percentage of tracer that causes flooding	%
$w_{optimal}$	Optimum weight percentage of tracer for good colour measurements	%
wt%	Weight percentage of a specified component	%
XRD	X-ray diffraction	-
$\beta$	Coefficient in the calculation of flooding factor	$kg^{-1}$
$\gamma$	Reading of force transducer	unit
$\gamma_0$	Base level of force transducer	unit
$\eta$	particle packing density on substrate surface	-
$\vartheta$	Angle of transducer from tangential to the mixer	$^\circ$
$\rho$	Density of powder bed during mixing	$kg.m^{-3}$
$\rho_{sp}$	True density of substrate material	$kg.m^{-3}$
$\rho_{tp}$	True density of tracer material	$kg.m^{-3}$
$\psi_p$	Angular location of tracer particle	$^\circ$

---



## References

- Abboud, L., Hensley, S. (2003). "New Prescription for Drug Makers: Update the Plants. After Years of Neglect, Industry Focuses on Manufacturing: FDA Acts as a Catalyst". The Wall Street Journal. N.Y., U.S.A. **September 2003**.
- Adam, S., Suzzi, D., Radeke, C., Khinast, J.G. (2011). "An integrated Quality by Design (QbD) approach towards design space definition of a blending unit operation by Discrete Element Method (DEM) simulation." *Eur. J. Pharm. Sci.* **42**: 106-115.
- Adi, H., Larson, I., Chiou, H., Young, P., Traini, D., Stewart, P. (2007). "Agglomerate strength and dispersion of salmeterol xinafoate from powder mixtures for inhalation." *Pharm. Res.* **23**: 2556-2565.
- Al-Chalabi, S.A.M., Jones, A.R., Luckham, P.F. (1990). "A simple method for improving the dispersability of micron-sized solid spheres." *J. Aerosol Sci.* **21**(6): 821-826.
- Allen, T. (1975). Particle size measurement. 2nd Edn. London, Chapman & Hall 12.
- Alonso, M., Satoh, M., Miyamoto, K. (1988). "Powder Coating in a Rotary Mixer with Rocking Motion." *Powder Tech.* **55**: 135-141.
- Alonso, M., Satoh, M., Miyamoto, K. (1989a). "Mechanism of the combined coating-mechanofusion processing of powders." *Powder Tech.* **59**: 45-52.
- Alonso, M., Satoh, M., Miyamoto, K. (1989b). "Influence of Rocking Motion on the Mixing of Powders." *Powder Tech.* **59**: 65-67.
- Andreou, J.G., Stewart, P., Morton, D.A.V. (2009). "Short-term changes in drug agglomeration within interactive mixtures following blending." *Int. J. Pharm.* **372**(102): 1-11.
- Angberg, A. (1995). "Lactose and thermal analysis with special emphasis on microcalorimetry." *Thermochimica Acta* **248**: 161-176.
- Armstrong, B., Seville, J.K., Adams, M.J., Parker, D.J., Fan, X., Page, T., Freeman, R. (2010). Evaluation of dry powder blending using Positron Emission Tomography and the relationship between powder bulk properties and process parameters. Proc. WCPT6 2010.
- Ashton, M.D., Schofield, C., Valentin, F.H.H. (1966). "The use of a light probe for assessing the homogeneity of powder mixtures." *Chem. Eng. Sci.* **21**: 843-849.
- Barigou, M. (2004). "Particle tracking in opaque mixing systems: An overview of the capabilities of PET and PEPT." *Chemical Engineering Research and Design* **82**(A9): 1258-1267.

- Bbosa, L.S., Govender, I., Mainza, A.N., Powell, M.S. (2011). "Power draw estimations in experimental tumbling mills using PEPT." *Minerals Engineering* **24**: 319-324.
- Begat, P., Morton, D.A.V., Staniforth, J.N., Price, R. (2004). "The Cohesive-Adhesive Balances in Dry Powder Inhaler Formulations I: Direct Quantification by Atomic Force Microscopy." *Pharm. Res.* **21**(9): 1591-1597.
- Behara, S.R.B., Kippax, P., McIntosh, M.P., Morton, D., Larson, I., Stewart, P. (2011a). "Structural influence of cohesive mixtures of salbutamol sulphate and lactose on aerolisation and de-agglomeration behaviour under dynamic conditions." *Eu. J. Pharm. Sci.* **42**: 210-219.
- Behara, S.R.B., Larson, I., Kippax, P., Morton, D., Stewart, P. (2011b). "The kinetics of cohesive powder de-agglomeration from three inhaler devices." *Int. J. Pharm.* **421**: 72-81.
- Behara, S.R.B., Larson, I., Kippax, P., Morton, D., Stewart, P. (2011c). "An approach to characterising the cohesive behaviour of powders using a flow titration aerolisation based methodology." *Chem. Eng. Sci.* **66**: 1640-1648.
- Bellamy, L., Nordon, A., Littlejohn, D. (2008). "Real-time monitoring of powder mixing in a convective blender using non-invasive reflectance NIR spectrometry." *The Analyst* **133**: 58-64.
- Berman, J., Schoeneman, A., Shelton, J.T. (1996). "Unit Dose Sampling: A Tale of Two Thieves." *Drug Development and Industrial Pharmacy* **22**(11): 1121-1132.
- Billmeyer, F.W.J. (1987). "Survey of Color Order Systems." *Color Research and Application* **12**(4): 173-186.
- Billmeyer, F.W.J., Alessi, P.J. (1981). "Assessment of Color-Measuring Instruments." *Color Research and Application* **6**(4): 195-202.
- Billmeyer, F.W.J., Saltzman, M. (1981), in: *Principles of Colour Technology. Colour and Colour Difference Measurement*. USA, J. Wiley and Sons. **3**, pp.67-109.
- Bodson, C., Dewe, W., Hubert, P., Delattre, L. (2006). "Comparison of FT-NIR transmission and UV-Vis spectrophotometry to follow the mixing kinetics and to assay low-dose tablets containing riboflavin." *J. Pharm. Biomed. Anal.* **41**: 783-790.
- Borgström, L., Olsson, B., Thorsson, L. (2006). "Degree of throat deposition can explain variability in lung deposition of inhaled drugs." *J. Aerosol Sci.* **19**: 473-483.
- Bridgwater, J., Utsumi, R., Zhang, Z., Tuladhar, T. (2003). "Particle attrition due to shearing - the effects of stress, strain and particle shape." *Chem. Eng. Sci.* **58**: 4649-4665.
- Bridson, R.H., Robbins, P.T., Chen, Y., Westerman, D., Gillham, C.R., Roche, T.C., Seville, J.K.P. (2007). "The effects of high shear blending on alpha-lactose monohydrate." *Int. J. Pharm.* **339**: 84-90.

- Briggner, L., Buxton, G., Bystrom, K., Darcy, P. (1994). "The use of isothermal microcalorimetry in the study of changes in crystallinity induced during hte processing of powders." *Int. J. Pharm.* **105**: 125-135.
- Brittain, H.G. (2002). "Particle-Size Distribution II: The Problem of Sampling Powdered Solids". *Pharmaceutical Technology North America*: 67-73.
- Brodka-Pfeiffer, K., Langguth, P., Grab, P., Häusler, H. (2003). "Influence of mechanical activation on the physical stability of salbutamol sulphate." *Eur. J. Pharm. Biopharm.* **56**: 393-400.
- Bulisk, D. (1950). "Mixing and sampling with special reference to multi-scale granular material." *ASTM Bulletin* **66**(April).
- Bulisk, D. (1973). "A proposed universal homogeneity and mixing index." *Powder Tech.* **7**: 111-116.
- Burcham, C.L., Roginski, R.T. (2009). Correlating powder flowability to particle size distribution using chemometric techniques. Proc. Talk Held at the QbD Topical Conference at the 2009 AIChE Annual Meeting, Nashville, TN.
- Byron, P.R. (1994). Compendial dry powder testing: USP perspectives. Proc. Respiratory Drug Delivery IV, Deerfield, IL, Interpharm Press.
- Byron, P.R., Jashnani, R.N. (1990). "Efficiency of aerolisation from dry powder blends of terbutaline sulfate and lactose NF with different particle size distributions." *Pharmaceutical Research* **7**: 881.
- Byron, P.R., Kelly, E.L., Lovering, M.J., Poochikian, G.K., Sethi, S., Theil, C.G. (1994). "Recommendations of the USP Advisory Panel on the USP general chapters on Aerosols <601> and Uniformity of Dosage Units <905>." *Pharm. Forum* **20**: 7477-7505.
- Cameron, I.T., Wang, F.Y., Immanuel, C.D., Stepanek, F. (2005). "Process systems modelling and application in granulation: a review." *Chem. Eng. Sci.* **60**: 3723-3750.
- Campbell, C.S. (2006). "Granular material flows - an overview." *Powder Tech.* **162**(3): 208-229.
- Campbell, J.J. (2008a), in: Understanding Pharma - The Professional's Guide to How Pharmaceutical and Biotech Companies Really Work. NC, United States of America, Pharmaceutical Institute **Chapter 2**, pp.18-38.
- Campbell, J.J. (2008b), in: Understanding Pharma - The Professional's Guide to How Pharmaceutical and Biotech Companies Really Work. NC, United States of America, Pharmaceutical Institute **Chapter 11**, pp.226-250.
- Capel, J., Huertas, F., Pozzuoli, A., Linares, J. (2006). "Red ochre decorations in Spanish Neolithic ceramics: a mineralogical and technological study." *J. Arch. Sci.* **33**: 1157-1166.
- Carman, P.C. (1937). "Fluid flow through granular beds." *Trans. Inst. Chem. Eng.* **15**: 150.

- Castellanos, A. (2005). "The relationship between attractive interparticle forces and bulk behaviour in dry and uncharged fine powders." *Adv. Phys.* **54**: 263-376.
- Castellanos, A., Valverde, J.M., Perez, A.T., Ramos, A., Watson, P.K. (1999). "Flow regimes in fine cohesive powder." *Phys. Rev. Lett.* **82**: 1156-1159.
- Chan, C.W., Brems, A., Mahmoudi, S., Baeyens, J., Seville, J.K., Parker, D.J., Leadbeater, T., Gargiuli, J. (2010). "PEPT study of particle motion for different riser exit geometries." *Particuology* **8**: 623-630.
- Chan, W.Y. (2006). "A novel colour measurement method using tristimulus colourimeter for evaluation of colour coat distribution on pellets". Department of Pharmacy. Singapore, National University of Singapore. **PhD Thesis**.
- Chang, R.-K., Shukla, J., Buehler, J. (1996). "An Evaluation of a Unit-Dose Compacting Sample Thief and a Discussion of Content Uniformity Testing and Blending Validation Issues." *Drug Dev. Ind. Pharm.* **22**(9&10): 1031-1035.
- Chaudhuri, B., Mehrotra, A., Muzzio, F.J., Tomassone, M.S. (2006). "Cohesive effects in powder mixing in a tumbling blender." *Powder Technology* **165**: 105-114.
- Chayes, F. (1956). Petrographic Model Analysis NY, J. Wiley & Sons.
- Cheng, Y., Barr, E.B., Yeh, H.C. (1989). "A Venturi disperser as a dry powder generator for inhalation studies." *Inhal. Toxicol.* **1**: 365-371.
- Chong, T.F. (1988). "Instrumental measurement and control of colour." *Rev. Prog. Color. Relat. Top.* **18**: 47-55.
- CISCRP. (2014). "Total cost to Develop a Single Approved Drug (Direct plus Capitalized Costs)." Clinical Trial Facts and Figures, from [http://www.ciscrp.org/patient/facts\\_graphs.html](http://www.ciscrp.org/patient/facts_graphs.html).
- Ciurczac, E.W. (1991). "Pharmaceutical mixing studies using near infrared spectroscopy." *Pharm. Tech.* **15**(9): 140-145.
- Cliff, M.J., Parker, M.D. (1990). Scale-up of mixer granulators. Proc. 12th Interphex Conference, NEC, Birmingham.
- Concessio, N.M., VanOort, M.M., Knowles, M., Hickey, A.J. (1999). "Pharmaceutical dry powder aerosols: Correlation of powder properties with dose delivery and implications for pharmacodynamic effect." *Pharmaceutical Research* **16**(6): 828-834.
- Conway, S.L., Lekhal, A., Khinast, J.G., Glasser, B.J. (2005). "Granular flow and segregation in a four-bladed mixer." *Chem. Eng. Sci.* **60**(24): 7091-7107.
- Copley (2010). "Quality Solutions for Inhaler Testing". C. S. Ltd. UK.
- Copley, M., McDonald, J. (2009). "Cascade impactor flow control". *Inhalation*. **3**: 14-17.

- Cornell, R.M., Schwertmann, U. (1996). The Iron Oxides - Structure, Properties, Reaction, Occurrence and Uses D-69451 Weinheim, VCH Verlagsgesellschaft mbH.
- Couroyer, C., Ghadiri, M., Laval, P., Brunard, N., Kolenda, F. (2000). "Methodology for investigating the mechanical strength of reforming catalyst beads." *Oil and Gas Science and Technology* **55**(1): 67-85.
- Crompton, G.K. (1982). "Problems patients have using pressurised aerosol inhalers." *European Respiratory Disease* **119**: 101-104.
- Crompton, G.K., Barnes, P.J., Broeders, M., Corrigan, C., Corbetta, L., Dekhuijzen, R., Dubus, J.C., Magnan, A., Massone, F., Sanchis, J., Viejo, J.L., Voshaar, T. (2006). "The need to improve inhalation technique in Europe: A report from the Aerosol Drug Management Improvement Team." *Respir. Med.* **100**: 1479-1494.
- Crowder, T.M., Louey, M.D., Sethuraman, V.V., Smyth, H.C., Hickey, A.J. (2001). "An odyssey in inhaler formulation and design." *Pharm. Tech.* **25**(7): 99-113.
- Curry, S.H., Taylor, A.J., Evans, S., Godfrey, S., Zeidifard, E. (1974). "Disposition of disodium cromoglycate administered in three particle sizes." *J. Pharm. Pharmacol* **26**: 79P-80P.
- Dalby, R.N., Tiano, S.L., Hickey, A.J. (2007), in: A. J. Hickey (Eds.). *Medical Devices for the Delivery of Therapeutic Aerosols to the Lung. Inhalation Aerosols - Physical and Biological Basis for Therapy*. N.Y., Informa Healthcare **Chapter 15**, pp.417-444.
- Darelius, A., Lennartsson, E., Rasmuson, A., Bjorn, I.N., Folestad, S. (2007a). "Measurement of the velocity field and frictional properties of wet masses in a high shear mixer." *Chem. Eng. Sci.* **62**: 2366-2374.
- Darelius, A., Rasmuson, A., Bjorn, I.N., Folestad, S. (2007b). "LDA measurements of near wall powder velocities in a high shear mixer." *Chem. Eng. Sci.* **62**(5770-5776).
- de Boer, A.H., Hagedoom, P., Gjaltema, D., Goede, J., Kussendrager, K.D., Frijlink, H.W. (2003). "Air classifier technology (ACT) in dry powder inhalation Part II. The effect of lactose carrier surface properties on the drug-to-carrier interaction in adhesive mixtures for inhalation." *International Journal of Pharmaceutics* **260**: 201-216.
- de Boer, J.H., Bolhuis, G.K., Doornbus, D.A. (1991). "Comparitive evaluation of multi-criteria decision making and combined contour plots in optimization of directly compressed tablets." *Eu. J. Pharm. and Biopharm.* **37**(3): 159-165.
- de Villers, M.M. (1997). "Description of the kinetics of the de-agglomeration of drug agglomerates during powder mixing." *Int. J. Pharm.* **151**: 1-6.
- Devore, J.L. (1982). Probability and Statistics for Engineering and the Sciences Monterey, CA, Brooks/Cole 640.
- Ding, Y.L., Forster, R.G., Seville, J.K., Parker, D.J. (2002). "Segregation of granular flow in the transverse plane of a rolling mode rotating drum." *International Journal of Multiphase Flow* **28**: 635-663.

- Ding, Y.L., Seville, J.K., Forster, R.G., Parker, D.J. (2001). "Solids motion in rolling mode rotating drums operated at low to medium rotational speeds." *Chem. Eng. Sci.* **56**: 1769-1780.
- Donovan, M.J., Smyth, H.C. (2010). "Influence of size and surface roughness of large lactose carrier particles in dry powder inhaler formulations." *International Journal of Pharmaceutics* **402**: 1-9.
- Drugs.com. (2014). "U.S. Pharmaceutical Sales - Q4 2013: Top 100 Drugs for Q4 2013 by Sales." Retrieved March 2014, from <http://www.drugs.com/stats/top100/sales>.
- Dunbar, C.A., Hickey, A.J. (2000). "Evaluation of probability density functions to approximate particle size distribution of representative pharmaceutical aerosols." *J. Aerosol Sci.* **31**: 813-831.
- Easy RGB. (2014). "Colour conversion calculator." from <http://www.easyrgb.com/index.php?X=CALC>.
- El-Hagrasy, A.S., Morris, H., D'Amico, F., Lodder, R., Drennen, J.K. (2001). "Near-infrared spectroscopy and imaging for the monitoring of powder blend homogeneity." *J. Pharm. Sci.* **90**: 1298-1307.
- Elamin, A.A., Ahlneck, C., Alderborn, G., Nyström, C. (1994). "Increased metastable solubility of milled griseofulvin, depending on the formation of a disordered surface structure." *Int. J. Pharm.* **111**: 159-170.
- Epple, R., Englisch, A. (1975). *Congr. FATIPEC XII*. Weinheim, Verlag Chemie: 241-248.
- Fan, L.T., Chen, Y.-M., Lai, F.S. (1990). "Recent developments in solid mixing." *Powder Tech.* **61**: 255-287.
- Faure, A., Grimsey, I.M., Rowe, R.C., York, P., Cliff, M.J. (1998). "Importance of wet mass consistency in the control of wet granulation by mechanical agitation: a demonstration." *J. Pharm. Pharmacol.* **50**(12): 1431-1432.
- Faure, A., York, P., Rowe, R.C. (2001). "Process control and scale-up of pharmaceutical wet granulation processes: a review." *European Journal of Pharmaceutics and Biopharmaceutics* **52**: 269-277.
- FDA (2003), in: (Eds.). *Guidance for Industry. Powder Blends and Finished Dosage Units - Stratified In-Process Dosage Unit Sampling and Assessment. Draft Guidance. Pharmaceutical cGMPs*.
- FDA (2004). "Guidance for industry PAT - a framework for innovative pharmaceutical development, manufacturing and quality assurance".
- Forrest, S., Bridgwater, J., Mort, P.R., Litster, J., Parker, D.J. (2003). "Flow patterns in granulating systems." *Powder Technology* **130**: 91-96.
- Forster, R.N., Seville, J.K., Parker, D.J., Ding, Y. (2000). "Tracking single particles in process equipment or probing processes using positrons." *KONA Powder and Particle Journal* **18**: 139-148.

- Freeman, T. (2012) "Fundamentals of Particle Interactions and Powder Flow - Measurement and Understanding for Better Product and Process Development."
- Frijlink, H.W., de Boer, A.H. (2004). "Dry powder inhalers for pulmonary drug delivery." *Expert. Opin. Drug. Del.* **1**: 67-86.
- Fults, K.A., Miller, I.F., Hickey, A.J. (1997). "Effect of particle morphology on emitted dose of fatty acid-treated disodium cromoglycate powder aerosols." *Pharm. Dev. Tech.* **2**(1): 67-79.
- Gall, L. (1975). *Farbe und Lack* **81**: 1015-1024.
- Gamble, J.F., Chiu, W.-S., Gray, V., Toale, H., Tobby, M.J., Wu, Y.-M. (2010). "Investigation into the Degree of Variability in the Solid-State Properties of Common Pharmaceutical Excipients - Anhydrous Lactose." *AAPS PharmSciTech* **11**(4): 1552-1557.
- Ganderton, D. (1992). "The generation of respirable clouds from coarse powder aggregates." *Journal of Biopharmaceutical Science* **3**: 101-105.
- Ganderton, D. (1997). "General factors influencing drug delivery to the lung." *Respir. Med.* **91**: 13-16.
- Garcia-Munoz, S., Gierer, D. (2009). Film coating end-point determination for coloured immediate release tablets using multivariable image analysis. Proc. Talk Held at the QbD Topical Conference at the 2009 AIChE Annual Meeting, Nashville, TN.
- Garetto, F. (2012). "Process for producing red iron oxide". Rockwood Italia SpA (IT),
- Geldart, D., Abdullah, E.C., Verlinden, A. (2009). "Characterisation of dry powders." *Powder Tech.* **190**: 70-74.
- Geldart, D., Harnby, N., Wong, A.C. (1984). "Fluidization of cohesive powders." *Powder Tech.* **37**(1): 25-37.
- Ghadiri, M., Moreno-Atanasio, R., Hassanpour, A., Antony, S.J. (2005), in: (Eds.). *Analysis of Agglomerate Breakage. Handbook of Powder Technology*, Elsevier. **12 19**, pp.837-872.
- Gonda, I. (1990). "Aerosols for delivery of therapeutic and diagnostic agents to the respiratory tract." *Crit. Rev. Ther. Drug Carrier Syst.* **6**: 273-313.
- Gottfries, J., Depui, H., Fransson, M., Jongeneelen, M., Josefson, M., Langkilde, F.W., Witte, D.T. (1996). "Vibrational spectrometry for the assessment of active substance in metoprolol tablets: a comparison between transmission and diffusive reflectance near-infrared spectrometry." *J. Pharm. Biomed. Anal.* **14**: 1495-1503.
- Govender, I., Mangesana, N., Mainza, A.N., Franzidis, J.-P. (2011). "Measurement of shear rates in a laboratory tumbling mill." *Minerals Engineering* **24**: 225-229.
- Gray, J.B. (1957). "Dry solids mixing equipment." *Chem. Eng. Prog.* **53**(1): 25-32.

- Griffith, A.A. (1921). "The phenomena of Rupture and Flow in Solids." *Phil. Trans. R. Soc.* **221**: 163-198.
- Guenette, E., Barrett, A., Kraus, D., Brody, R., Harding, L., G., M. (2009). "Understanding the effect of lactose particle size on the properties of DPI formulations using experimental design." *Int. J. Pharm.* **380**(1): 80-88.
- Hare, C., Ghadiri, M., Dennehy, R. (2011). "Prediction of attrition in agitated particle beds." *Chem. Eng. Sci.* **66**(20): 4757–4770.
- Harmer, Q., Morton, D.A.V., Newton, M., Staniforth, J.N., Toby, M.J. (2004). "Active and intelligent inhaler device development." *International Journal of Pharmaceutics* **277**: 31-37.
- Heng, P., Chan, L.W., Lim, L.T. (2000). "Quantification of the surface morphologies of lactose carriers and their effect on the *in vitro* deposition of salbutamol sulphate." *Chem. Pharm. Bull.* **48**: 393-398.
- Hersey, J.A. (1975). "Ordered mixing: a new concept in powder mixing practice." *Powder Technology* **11**: 41-44.
- Hersey, J.A. (1981). "Determination of interparticulate forces in ordered powder mixes." *Journal of Pharmacy and Pharmacology* **33**: 485.
- Hersey, J.A., Cook, P.C. (1974). "Homogeneity of pharmaceutical dispersed systems." *Journal of Pharmacy and Pharmacology* **26**: 126-133.
- Hersey, J.A., Cook, P.C., Smyth, M., Bishop, E.A., Clarke, E.A. (1974). "Homogeneity of multicomponent powder mixtures." *J. Pharm. Sci.* **63**: 408-411.
- Heyder, J., Svartengren, M.U. (2001), in: H. Bisgaard, C. O'Callaghan and G. Smalderone (Eds.). *Basic Principles of Particle Behavior in the Human Respiratory Tract. Drug Delivery to the Lung*, Hoboken : Marcel Dekker Inc. **2**.
- Hickey, A.J. (1988). "Particle aspects of aerosol characterisation in an environment of controlled temperature and relative humidity." *Drug Dev. Ind. Pharm.* **14**: 337-352.
- Hickey, A.J. (1993). "Targeting of pharmaceutical aerosols to the lung: what can be learned from inhalation technology and industrial hygiene?" *Sci. Technol.* **18**: 290-304.
- Hickey, A.J. (2004), in: A. J. Hickey (Eds.). *Methods of aerosol particle size characterisation. Pharmaceutical Inhalation Aerosol Technology*. New York, Marcel Dekker, Inc., pp.345-384.
- Hickey, A.J., Connessio, N.M. (1994). "Aerodynamic behaviour of micronized powders dispersed as aerosols." *Pharm. Tech.* **18**: 88-98.
- Hickey, A.J., Connessio, N.M., Van Oort, M.M., Platz, R.M. (1994). "Factors influencing the dispersion of dry powders as aerosols." *Pharmaceutical Technology* **18**: 58-64, 82.

- Hickey, A.J., Crowder, T.M. (2007), in: A. J. Hickey (Eds.). Next Generation Dry Powder Inhalation Delivery Systems. Inhalation Aerosols - Physical and Biological Basis for Therapy. N.Y., informa healthcare **Chapter 16**, pp.445-460.
- Hindle, M., Byron, P.R. (1993). "Measurement of the unit dose emitted from dry powder inhalers." *Pharm. Res.* **10**: 532.
- Hinrichsen, E.L., Feder, J., Jossang, T. (1986). "Geometry of Random Sequential Adsorption." *J. Stat. Phys.* **44**(5/6): 793-827.
- Hogan, S.E., Buckton, G. (2001). "The application of near infrared spectroscopy and dynamic vapour sorption to quantify low amorphous contents of crystalline lactose." *Pharmaceutical Research* **18**: 112-116.
- Holm, P., Bonde, M., Wigmore, T. (1996). "Pelletization by granulation in a roto-processor RP-2. Part I: Effects of process and product variables on granule growth." *Pharm. Tech. Eur.* **8**: 22-36.
- Honingmann, B., Stabenow, J. (1962). Proc. Cong. FATIPEC VI, Weinheim, Verlag Chemie.
- Horsthuis, G.J.B., van Laarhoven, J.A.H., van Rooij, R.C.B.M., Vromans, H. (1993). "Studies on upscaling parameters of the Gral high shear granulation process." *Int. J. Pharm.* **92**: 143.
- Hosikian, A., Zhang, P., Hapgood, K.P. (2010). "Powder Velocity in High Shear Granulator". Melbourne, Monash University Department of Chemical Engineering: 62.
- Hosokawa Micron Ltd. "Integrated Powder Processing and Containment Systems". H. M. Ltd. Cheshire, UK.
- Howard, J.R. (1989). Fluidized Bed Technology: Principles & Application Bristol, U.K. 25-32.
- Hunter, R.S., Harold, R.W. (1987a), in: R. S. Hunter and R. W. Harold (Eds.). Uniform Colour Scales. The Measurement of Appearance. USA, J. Wiley and Sons **8**, pp.143-153.
- Hunter, R.S., Harold, R.W. (1987b), in: R. S. Hunter and R. W. Harold (Eds.). Instruments for the chromatic attributes of object appearance. The Measurement of Appearance. USA, J. Wiley and Sons. **14**, pp.296-302.
- Hunterlab (2014) "Specifications ColorFlex EZ." <http://www.hunterlab.com/loose-powders.html>, Accessed 4-Nov-2013.
- Ingram, A., Seville, J.K., Parker, D.J., Fan, X., Forster, R.G. (2005). "Axial and radial dispersion in rolling mode rotating drums." *Powder Technology* **158**(1-3): 76-91.
- Islam, N., Stewart, P.J., Larson, I., Hartley, P. (2004). "Effect of carrier size on the dispersion of salmeterol xinafoate from interactive mixtures." *J. Pharm. Sci.* **93**: 1030-1038.
- Iwasaki, T., Kim, J.H., Satoh, M. (2006). "Characterisation of media mills based on mechanical energy applied to particles." *Chem. Eng. Sci.* **61**: 1065-1073.

- Iwasaki, T., Satoh, M. (2002). "Characterization of powder mixers based on mechanical energy using soft dye granules." *Adv. Powder Technol.* **13**(4): 395-409.
- Iwasaki, T., Satoh, M., Ichio, S. (2003). "Preparation of a UV-attenuating agent using a mechanochemical reaction." *Journal of Materials Processing Technology* **142**: 131-138.
- Jashnani, R.N., Byron, P.R., Dalby, R.N. (1995). "Testing of dry powder aerosol formulations in different environmental conditions." *Int. J. Pharm.* **113**: 123-130.
- Jones, J.R., Parker, D.J., Bridgwater, J. (2007). "Axial mixing in a ploughshare mixer." *Powder Technology* **178**: 73-86.
- Jones, M., Santo, J., Yakub, B., Dennison, M., Master, H., Buckton, G. (2010). "The relationship between drug concentration, mixing time, blending order and ternary dry powder inhalation performance." *Int. J. Pharm.* **391**: 137-147.
- Jones, M.D., Price, R. (2006). "The influence of fine excipient particles on the performance of carrier-based dry powder inhalation formulations." *Pharmaceutical Research.* **23**: 1665-1674.
- Kallon, D.V.V., Govender, I., Mainza, A.N. (2011). "Circulation rate modelling of mill charge using positron emission particle tracking." *Minerals Engineering* **24**: 282-289.
- Kampf, G., Papenroth, W. (1977). *Farbe und Lack* **83**: 18-29.
- Kaye, B.H. (1993). "Improvements in/or relations to a method and apparatus for handling particles". B. P. Applications, **38871-63, October**
- Kaye, B.H. (1997a), *Mixing Technology. Powder mixing.* London, Chapman & Hall **Chapter 1**, pp.1-76.
- Kaye, B.H. (1997b), *Monitoring mixers and mixtures. Powder mixing.* London, Chapman & Hall **Chapter 5**, pp.147-206.
- Kaye, B.H. (1997c), *The impact of chaos theory and experimental mathematics on powder mixing theory and practice. Powder mixing.* London, Chapman & Hall **Chapter 6**, pp.207-217.
- Kaye, B.H. (1997d), *Active Mixing Machines. Powder mixing.* London, Chapman & Hall **Chapter 7**, pp.218-231.
- Kaye, B.H., Sparrow, D.B. (1964). "Role of surface diffusion as a mixing mechanism in a barrel mixer. Part I and II." *Industrial Chemist* **40**: 200-205.
- Kendall, K. (1978). "The impossibility of comminuting small particles by compression." *Nature* **272**: 710.
- Kendall, K., Stainton, C. (2001). "Adhesion and aggregation of fine powders." *Powder Technology* **121**: 223-229.

- Klinzing, J.R., Zavaliangos, A., Cunningham, J., Mascaro, T., Winstead, D. (2009). Modelling density and temperature distributions in powder die compacts. Proc. Talk Held at the QbD Topical Conference at the 2009 AIChE Annual Meeting, Nashville, TN.
- Knight, P. (2004). "Challenges in granulation technology." Powder Tech. **140**(3): 156-162.
- Knight, P.C., Seville, J.K., Wellm, A.B., Instone, T. (2001). "Prediction of impeller torque in high shear powder mixers." Chem. Eng. Sci. **56**: 4457-4471.
- Kobo Products Inc. (2014) "Dispersion Technology for Pigments and Physical Sunscreen."
- Kontny, M.J., Conners, J.J., Graham, E.T. (1994). "Moisture distribution and packaging of dry powder systems". Respiratory Drug Delivery IV: 125-136.
- Kosmas, C.S., Franzmeier, D.P., Schulze, D.G. (1986). "Relationship among derivative spectroscopy, colour, crystallite dimensions and Al substitution of synthetic goethites and hematites." Clays and Clay Minerals **34**: 625-634.
- Kresse, P. (1977). Proc. Congr. FATIPEC XIII, Paris, EREC.
- Kuo, H.P., Knight, J.B., Parker, D.J., Burbidge, A.S., Adams, M.J., Seville, J.K. (2003). "Non-equilibrium particle motion in the vicinity of a single blade." Powder Technology **132**: 1-9.
- Kuo, H.P., Knight, P.C., Parker, D.J., Adams, M.J., Seville, J.K. (2004). "Discrete element simulations of a high-shear mixer." Adv. Powder Technol. **15**(3): 297-309.
- Kuo, H.P., Knight, P.C., Parker, D.J., Seville, J.K. (2005). "Solids circulation and axial dispersion of cohesionless particles in a V-mixer." Powder Technology **152**(1-3): 133-140.
- Lahrib, H., Zeng, X.M., Martin, G.P., Marriott, C., Pritchard, J. (1999). "The use of different grades of lactose as a carrier for aerolised salbutamol sulphate." Int. J. Pharm. **191**: 1-14.
- Lambregts, D., Gruben, K., Boer, A.H. (2004). Importance of the choice of lactose in combination with dry powder inhalers. Proc. Drug Delivery to the Lungs 15, London, The Aerosol Society.
- Landin, M., York, P., Cliff, M.J., Rowe, R.C. (1999). "Scaleup of a Pharmaceutical Granulation in Planetary Mixers." Pharm. Dev. Tech. **4**(2): 145-150.
- Landin, M., York, P., Cliff, M.J., Rowe, R.C., Wigmore, A.J. (1996a). "The effect of batch size on scale-up of a pharmaceutical granulation in a fixed bowl mixer granulator." Int. J. Pharm. **134**: 243-246.
- Landin, M., York, P., Cliff, M.J., Rowe, R.C., Wigmore, A.J. (1996b). "Scale-up of a pharmaceutical granulation in fixed bowl mixer-granulators." Int. J. Pharm. **133**(1-2): 127-131.  
<http://www.sciencedirect.com/science/article/pii/0378517395044272>

- Langston, P.A., Al-Awamleh, M.A., Fraige, F.Y., Asmar, B.N. (2004). "Distinct element modelling of non-spherical frictionless particle flow." *Chem. Eng. Sci.* **59**: 425-435.
- Laurent, B. (2006). "Scaling factors in granular flow - analysis of experimental and simulation results." *Chem. Eng. Sci.* **61**: 4138-4146.
- Laurent, B., Bridgwater, J. (2000). "Continuous mixing of solids." *Chem. Eng. Tech.* **22**(1): 16-18 (Communications).
- Laurent, B.F.C., Bridgwater, J. (2002a). "Dispersive granular flow in a horizontal drum stirred by a single blade." *AIChE Journal* **48**(1): 50-58.
- Laurent, B.F.C., Bridgwater, J. (2002b). "Performance of single and six-bladed powder mixers." *Chem. Eng. Sci.* **57**: 1695-1709.
- Laurent, B.F.C., Bridgwater, J. (2002c). "Influence of agitator design on powder flow." *Chem. Eng. Sci.* **57**: 3781-3793.
- Laurent, B.F.C., Bridgwater, J., Parker, D.J. (2002d). "Convection and segregation in a horizontal mixer." *Powder Technology* **123**: 9-18.
- Lavorini, F., Magnan, A., Dubus, J.C., Voshaar, T., Corbetta, L., Broeders, M., Dekhuijzen, R., Sanchis, J., Viejo, J.L., Barnes, P., Corrigan, C., Levy, M., Crompton, G.K. (2008). "Effect of incorrect use of dry powder inhalers on management of patients with asthma and COPD." *Respir. Med.* **102**: 593-604.
- Lee, T., Lee, J. (2003). "Particle attrition by particle-surface friction in dryers." *Pharm. Tech.* **27**(5): 64-72.
- Lekhal, A., Girard, K.P., Brown, M.A., Kiang, S., Glasser, B.J., Khinast, J.G. (2003). "Impact of agitated drying on crystal morphology: KCl-water system." *Powder Tech.* **132**: 119-130.
- Lekhal, A., Girard, K.P., Brown, M.A., Kiang, S., Khinast, J.G., Glasser, B.J. (2004). "The effect of agitated drying on the morphology of L-threonine (needle-like) crystals." *Int. J. Pharm.* **270**: 263-277.
- Levin, M. (2007), in: (Eds.). *Wet Granulation: End-Point Determination and Scale-Up. Encyclopedia of Pharmaceutical Technology*. USA, Informa Healthcare USA, Inc., pp.4078-4098.
- Lewis, P.A. (1998), in: K. Nassau (Eds.). *Colourants: Organic and Inorganic Pigments. Colour for Science, Art and Technology*, Elsevier Science B.V.
- Lim, L.T. (2003). "Surface topography of lactose carrier and its influence on drug delivery of dry powder inhaler". *Department of Pharmacy*. Singapore, National University of Singapore. **PhD Thesis**.
- Lim, S.Y., Davidson, J.F., Forster, R.N., Parker, D.J., Scott, D.M., Seville, J.K. (2003). "Avalanching of granular material in a horizontally slowly rotating cylinder: PEPT studies." *Powder Technology* **138**(1): 25-30.
- Litster, J.D. (2003). "Scaleup of wet granulation processes: science not art." *Powder Tech.* **130**(1-3): 35-40.

- Litster, J.D., Hapgood, K.P., Michaels, J.N., Sims, A., Roberts, M., Kameneni, S.K. (2002). "Scale-up of mixer granulators for effective liquid distribution." *Powder Tech.* **124**(3): 272-280.
- Louey, M.D., Razia, S., Stewart, P. (2003). "Influence of physico-chemical carrier properties on the in vitro aerosol deposition from interactive mixtures." *Int. J. Pharm.* **252**: 87-98.
- Louey, M.D., Stewart, P.J. (2002). "Particle interactions involved in aerosol dispersion of ternary interactive mixtures." *Pharmaceutical Research* **19**(10): 1524-1531.
- Louey, M.D., Van Oort, M., Hickey, A.J. (2006). "Standardized entrainment tubes for the evaluation of pharmaceutical dry powder dispersion." *Aerosol Science* **37**: 1520-1531.
- Lucas, P., Anderson, K., Staniforth, J.N. (1998a). "Protein deposition from dry powder inhalers: fine particle multiplets as performance modifiers." *Pharm. Res.* **15**: 562-569.
- Lucas, P., Clarke, M.J., Anderson, K., Tobyn, M.J., Staniforth, J.N. (1998b). The role of fines particle excipients in pharmaceutical dry powder aerosols. *Proc. Respir. Drug. Deliv.* VI.
- Luybaert, J., Massart, D.L., Heyden, Y.V.d. (2007). "Near infrared spectroscopy applications in pharmaceutical analysis." *J. Pharm. Biomed. Anal.* **72**: 865-883.
- Mackin, L.A., Rowley, G., Fletcher, E.J. (1997). "An investigation of carrier particle type, electrostatic charge and relative humidity on in-vitro drug deposition from dry powder inhaler formulations." *Pharmaceutical Science* **3**: 583-586.
- Malcolmson, R.J., Embleton, J.K. (1998). "Dry powder formulations for pulmonary delivery." *PSTT* **1**(9): 394-398.
- Malhotra, K., Mujumdar, A.S. (1990). "Particle mixing and solids flowability in granular beds stirred by paddle-type blades." *Powder Technology* **61**: 155-164.
- Malhotra, K., Mujumdar, A.S., Imakoma, H., Okazaki, M. (1988). "Fundamental particle mixing studies in an agitated bed of granular material in a cylindrical vessel." *Powder Technology* **55**: 107-114.
- Malhotra, K., Mujumdar, A.S., Okazaki, M. (1990). "Particle Flow Patterns in a Mechanically Stirred Two-Dimensional Cylindrical Vessel." *Powder Tech.* **60**: 179-189.
- Mandelbrot, B.B. (1977). Fractals: Form, Chance and Dimension San Francisco, U.S.A., Freeman Press.
- Marple, V.A., Roberts, D.L., Romay, F.J., Miller, N.C., Truman, K.G., Holroyd, M.J., Mitchell, J.P., Hochrainer, D. (2003). "Next Generation Pharmaceutical Impactor (A New Impactor for Pharmaceutical Inhaler Testing). Part I: Design." *J. Aerosol Med* **16**(3): 283-299.
- McCarthy, J.J. (2003). "Micro-modeling of cohesive mixing processes." *Powder Technology* **138**: 63-67.

- McCauley, J.L. (1993). Cambridge Nonlinear Science Series 2: Chaos, Dynamics and Fractals, and Algorithmic Approach to Deterministic Chaos Cambridge, U.K., Cambridge University Press.
- Mie, G. (1908). *Ann. Phys.* **25**: 377-444.
- Mitchell, J., Nagel, M.W. (2003). "Cascade impactors for the size characterisation of aerosols from medical." *J. Aerosol Med* **16**(4): 341-377.
- Moreton, C. (2009). "Functionality and performance of excipients in a quality-by-design world: obtaining information on excipient variability for formulation design space." *Am. Pharm. Rev.* **12**(5): 28-33.
- Moroney, M.J. (1953). Facts from Figures. 2nd Edn. Harmondsworth, U.K., Pelican Books.
- Mort, P.R. (2007), in: A. D. Salman, M. J. Hounslow and J. K. Seville (Eds.). Scale-Up of High-Shear Binder-Agglomeration Processes. Granulation, Elsevier B. V.
- Morton, D.A.V., Staniforth, J.N. (Spring 2005). "The Challenge of the New: Device-Formulation Matching in Dry Powder Inhaler Systems." *Pharmaceutical Manufacturing and Packaging Suppliers*.
- Moselmann, D. (1987). "Study of solids motion, mixing and heat transfer in gas fluidised beds." *Particulate Science and Technology* **7**: 335-355.
- Movahedirad, S., Ghafari, M., Dehkordi, A.M. (2014). "A Novel Model for Predicting the Dense Phase Behavior of 3D Gas-Solid Fluidized Beds." *Chem. Eng. Tech.* **37**(1): 103-112.
- Muguruma, Y., Tanaka, T., Tsuji, Y. (2000). "Numerical simulation of particulate flow with liquid bridge between particles (simulation of centrifugal tumbling granulator)." *Powder Tech.* **109**(1-3): 49-57.
- Mullins, M.E., Michaels, L.P., Menon, V., Locke, B., Ranade, M.B. (1992). "Effect of geometry on particle adhesion." *Aerosol Science and Technology* **17**: 105-118.
- Muteki, K., Swaminathan, V., Sekulic, S. (2009). Feed-forward process control strategy for pharmaceutical tablet development. Proc. Talk Held at the QbD Topical Conference at the 2009 AIChE Annual Meeting, Nashville, TN.
- Muzzio, F.J. (2006), in: M. Levin (Eds.). Pharmaceutical process scale-up. Engineering approaches for pharmaceutical process scale-up, validation, optimization, and control in the process and analytical technology (PAT) era, pp.57-69.
- Muzzio, F.J., Alexander, A.W., Goodridge, C.L., Shen, E., Shinbrot, T. (2004), in: V. A. A.-O. Edward, L. Paul and M. S. Kresta (Eds.). Solids mixing, Part A: fundamentals of solids mixing. Handbook of Industrial Mixing: Science and Practice. New York, John Wiley & Sons Inc., pp.887-983.
- Muzzio, F.J., Goodridge, C.L., Alexander, A.W., Arratia, P.E., Yang, H., Sudah, O., Mergen, G. (2003). "Sampling and characterisation of pharmaceutical powders and granular blends." *Int. J. Pharm.* **250**: 51-64.

- Muzzio, F.J., Robinson, P., Wightman, C., Brone, D. (1997). "Sampling practices in powder blending." *Int. J. Pharm.* **155**: 153-178.
- Nassau, K. (1998a), in: K. Nassau (Eds.). *The Fifteen Causes of Colour. Color for Science, Art and Technology*, Elsevier Science B.V. **Chapter 4**, pp.123-168.
- Nassau, K. (1998b), in: K. Nassau (Eds.). *Colour Preservation. Color for Science, Art and Technology*, Elsevier Science B.V. **Chapter 12**, pp.345-352.
- Navrotsky, A., Mazeina, L., Majzlan, J. (2008). "Size-driven Structural and Thermodynamic Complexity in Iron Oxides." *Science* **319**.
- Neil, A.U., Bridgwater, J. (1994). "Attrition of particulate solids under shear." *Powder Tech.* **80**: 207-219.
- Newell, H.E., Buckton, G., Butler, D.A., Thielmann, F., Williams, D.R. (2001). "The use of inverse gas phase chromatography to measure the surface energy of crystalline, amorphous, and recently milled lactose." *Pharm. Res.* **18**: 662-666.
- Newman, S.P., Busse, W.W. (2002). "Evolution of dry powder inhaler design, formulation, and performance." *Respiratory Medicine* **96**: 293-304.
- Newman, S.P., Clarke, S.W. (1983). "Therapeutic aerosols I - physical and practical considerations." *Thorax* **38**: 881-886.
- Ng, B., Ding, Y.L., Ghadiri, M. (2009). "Modelling of dense and complex granular flow in high shear mixer granulator - A CFD approach." *Chem. Eng. Sci.* **64**: 3622-3632.
- Ng, B., Kwan, C.C., Ding, Y.L., Ghadiri, M., Fan, X. (2007a). "Solids motion in a conical frustum-shaped high shear mixer granulator." *Chem. Eng. Sci.* **62**: 756-765.
- Ng, B., Kwan, C.C., Ding, Y.L., Ghadiri, M., Fan, X. (2007b). "Solids motion of calcium carbonate particles in a high shear mixer granulator: A comparison between dry and wet conditions." *Powder Technology* **177**: 1-11.
- Ngai, S.S.H. (2005). "Multi-Scale Analysis of Powder Blending in Pharmaceutical Manufacturing". *Department of Chemical Engineering, Massachusetts Institute of Technology. Doctor of Philosophy*: 256.
- Nichols, S.C., Wynn, E. (2008). New approaches to optimising dispersion in dry powder inhalers - dispersion force mapping and adhesion measurements. *Proc. Respiratory Drug Delivery*
- Niklasson Bjorn, I., Jansson, A., Karlsson, M., Folestad, S., Rasmuson, A. (2005). "Empirical to mechanistic modelling in high shear granulation." *Chem. Eng. Sci.* **60**: 3795-3803.
- Nilpawar, A.M., Reynolds, G.K., Salman, A.D., Hounslow, M.J. (2006). "Surface velocity measurement in a high shear mixer." *Chem. Eng. Sci.* **61**: 4172-4178.

- Nippolainen, E., Ervasti, T., Fauch, L., Miridonov, S.V., Ketolainen, J., Kamshilin, A.A. (2010). "Fast noncontact measurements of tablet dye concentration." *Optics Express* **18**(15): 15624-15634.
- Oehlert, W., Burow, W., Brunn, H., Kunstmann, H. (1997). "Clean colour shade, yellow-tinged red iron oxide pigments, and a process for their manufacture, and their use". Bayer AG, **5,665,157**
- Ogawa, S., Kamijima, T., Miyamoto, Y., Miyajima, M., Sato, H., Takayama, K., Nagai, T. (1994). "A new attempt to solve the scale-up problem for granulation using response surface methodology." *J. Pharm. Sci.* **83**(3): 439-443.
- Orr, N.A. (1974), in: P. B. Deasy and R. F. Timony (Eds.). *Quality control and pharmaceuticals of content uniformity of medicines containing potent drugs with special reference to tablets.* Progress in the Quality Control of Medicines, Elsevier/North Holland Biomedical Press **Chapter 9**.
- Orr, N.A., Shotton, E. (1973). "The mixing of cohesive powders". The Chemical Engineer. **Jan**: 12-18.
- Padmadasastra, Y., Kennedy, R.A., Stewart, P.J. (1994). "Solid bridge formation in sulphonamide-Emdex interactive systems." *Int. J. Pharm.* **112**: 55-63.
- Parker, D.J., Fan, X. (2008). "Positron emission particle tracking - Application and labelling techniques." *Particuology* **6**: 16-23.
- Parker, D.J., Forster, R.N., Fowles, P., Takhar, P.S. (2002). "Positron emission particle tracking using the new Birmingham positron camera." *Nuclear Instruments and Methods in Physical Research A* **477**: 540-545.
- Parker, D.J., Leadbeater, T., Fan, X., Hausard, M.N., Ingram, A., Yang, Z. (2008). "Positron imaging techniques for process engineering: recent developments at Birmingham." *Meas. Sci. Technol.* **19**: 094004 (10pp).
- Patton, T.C. (1973), in: (Eds.). Pigment Handbook. New York, London, pp.333.
- Pedersen, S., Steffenson, G. (1986). "Fenoterol powder inhaler technique in children: influence of inspiratory flow rate and breath holding." *Eur. J. Respir. Dis.* **68**(3): 207-214.
- Pitchayajittipong, C., Price, R., Shur, J., Kaerger, J.S., Edge, S. (2010). "Characterisation and functionality of inhalation anhydrous lactose." *Int. J. Pharm.* **390**: 134-141.
- Plank, R., Diehl, B., Grinstead, H., Zega, J. (2003). "Quantifying liquid coverage and powder flux in high-shear granulators." *Powder Tech.* **134**: 223-234.
- Podczec, F., Newton, J.M., al., e. (1997). "Influence of relative humidity of storage air on the adhesion and autoadhesion of micronised particles to particulate and compacted powder surfaces." *J. Colloid. Interf. Sci.* **187**: 484-491.

- Podczeck, F., Newton, J.M., James, M.B. (1996). "The influence of constant and changing relative humidity of the air on the autoadhesion force between pharmaceutical powder particles." *Int. J. Pharm.* **145**: 221-229.
- Portillo, P.M., Vanarase, A.U., Ingram, A., Seville, J.K., Ierapetritou, M.G., Muzzio, F.J. (2010). "Investigation of the effect of impeller rotation rate, powder flow rate, and cohesion on powder flow behaviour in a continuous blender using PEPT." *Chem. Eng. Sci.* **65**: 5658-5668.
- Potapov, A.V., Campbell, C.S. (1997). "Computer simulation of shear-induced particle attrition." *Powder Tech.* **94**: 109-122.
- Price, R., Young, P.M. (2005). "On the physical transformations of processed pharmaceutical solids." *Micron* **36**: 519-524.
- Radeke, A.C., Radl, S., Khinast, J.G. (2009). Granular flows, showing size effects by using high-performance simulations on GPUs. Proc. Proceedings of the Multi-Scale Modelling Symposium - A CSIRO Cutting Edge Symposium, Melbourne, AUS.
- Ramaker, J.S. (2001). "Possible mechanisms generating the characteristic toroidal flow profile of pellets in a high-shear mixer. Fundamentals of the high-shear palletisation process". Groningen, NED, University of Groningen. **Masters**.
- Ramaker, J.S., Jelgersma, M.A., Vonk, P., Kossen, N.W.F. (1998). "Scale-down of a high shear pelletisation process: Flow profile and growth kinetics." *Int. J. Pharm.* **166**(89-97).
- Rasenack, N., Steckel, H., Muller, B.W. (2003). "Micronisation of anti-inflammatory drugs for pulmonary delivery by a controlled crystallisation process." *Journal of Pharmaceutical Science* **92**: 35-44.
- Rechmann, H., Sutter, G. (1976). *Farbe und Lack* **82**: 793-796.
- Reich, G. (2005). "Near-infrared spectroscopy and imaging: basic principles and pharmaceutical applications." *Advanced Drug Delivery Reviews* **57**: 1109-1143.
- Remy, B., Canty, T.M., Khinast, J.G., Glasser, B.J. (2010a). "Experiments and simulations of cohesionless particles with varying roughness in a bladed mixer." *Chem. Eng. Sci.* **65**: 4557-4571.
- Remy, B., Khinast, J.G., Glasser, B.J. (2010b). "The effect of mixer properties and fill level on granular flow in a bladed mixer." *Powder Tech.* **186**(2): 130-136.
- Rhodes, M. (2008). Introduction to Particle Technology. 2nd Edn. NY, John Wiley & Sons Ltd.
- Rockwood Pigments (2009) "Product Data - Ferroxide High-Purity Synthetic Iron Oxide Red 212P."
- Rowe, R.C., Sheskey, P.J., Weller, P.J. (2003a), in: (Eds.). *Handbook of Pharmaceutical Excipients*, Pharmaceutical Press **Colouring Agents**, pp.165-173.

- Rowe, R.C., Sheskey, P.J., Weller, P.J. (2003b), in: (Eds.). Handbook of Pharmaceutical Excipients, Pharmaceutical Press **Lactose**, pp.323-332.
- Rudolph, G., Gebhart, J., Heyder, J., Scheuch, G., Stahlhofen, W. "Mass deposition from inspired polydisperse aerosols." *Ann. Occup. Hyg.* **196**(32 (suppl. 1)): 919-938.
- Ruegger, C.E., Royce, A.E., Mollan, M.J., Wagner, R.F., Valazza, S.J., Mecadon, M.R. (2006). "Scale-up of solid dose safe forms." *Encyclopedia of Pharmaceutical Technology* **1**(1): 3193-3216.
- Russell, P., Diehl, B., Grinstead, H., Zega, J. (2003). "Quantifying liquid coverage and powder flux in high-shear granulators." *Powder Tech.* **134**(223-234).
- saglikpark.com. (2014). "İNHALER TİPLERİ." *Astım tedavisinde kullanılan ilaçlar* Retrieved Jan 2014, from [http://www.saglikpark.com/yazdir/astim\\_tedavisinde\\_kullanilan\\_ilacilar.htm](http://www.saglikpark.com/yazdir/astim_tedavisinde_kullanilan_ilacilar.htm).
- Saito, Y., Fan, X., Ingram, A., Seville, J.K. (2011a). "PEPT Analysis of Impeller Blade Geometry and Averaged Velocity in a High Shear Mixer." *Journal of Fluid Science and Technology* **6**(2): 169-176.
- Saito, Y., Fan, X., Ingram, A., Seville, J.K. (2011b). "A new approach to high-shear mixer granulation using positron emission particle tracking." *Chem. Eng. Sci.* **66**: 563-569.
- Saito, Y., Ingram, A., Fan, X., Seville, J.K. (2011c). "Effects of Blade Design in Wet Granulation in a High Shear Mixer Determined by Positron Emission Particle Tracking." *Journal of Environment and Engineering* **6**(1): 233-241.
- Saito, Y., Ingram, A., Fan, X., Seville, J.K. (2011d). "Three-Dimensional Visualisation of Powder Motion in a High Shear Mixer." *Materials Transactions* **2**(8): 1693-1696.
- Sarkar, A. (2010). "Continuous blending of cohesive granular material." *Chem. Eng. Sci.* **65**: 5687-5698.
- Sastry, K.V.S., Cooper, H., Hogg, R., Jespen, T.L.P., Knoll, F., Parekh, B., Rajamani, R.K., Sorenson, T., Wechsler, I. (1997), in: Perry (Eds.). *Solid-Solid Operations and Equipment. Perry's Chemical Engineer's Handbook*, McGraw Hill **Section 19**, pp.19-10 to 19-16.
- Satoh, M., Yamashita, T., Yoshida, T., Hasegawa, S., Miyunami, K. (1993). "An evaluation of the mixing characteristics of solid mixers using adhesive fine powders." *J. Soc. Powder Technol., Japan* **30**: 390-396.
- Satoh, M., Yoshida, T., Miyunami, K., Okudaira, Y. (1994). "Evaluation of the performance of a high-speed elliptical-rotor-type powder mixer." *J. Soc. Powder Technol., Japan* **31**: 789-794.
- Satoh, M., Yoshida, T., Yanagida, T., Iwasaki, T., Kimura, H. (1998). "Evaluation of the mixing process based on a disintegrating rate model of the powder agglomerates." *Adv. Powder Technol.* **9**(4): 377-390.
- Schaefer, T. (1988). "Equipment for wet granulation." *Acta Pharm. Seuc.* **25**: 205.

- Schaefer, T., Bak, H.H., Jaegerskou, A., Kristensen, A., Svensson, J.R., Holm, P., Kristensen, H.G. (1986). "Granulation in different types of high speed mixers. Part I: effects of process variables and up-scaling." *Pharm. Ind.* **48**: 1083.
- Schaefer, T., Bak, H.H., Jaegerskou, A., Kristensen, A., Svensson, J.R., Holm, P., Kristensen, H.G. (1987). "Granulation in different types of high speed mixers. Part II: comparison between mixers." *Pharm. Ind.* **49**: 297-304.
- Schaefer, T., Holm, P., Kristensen, H.G. (1992). "Melt granulation in a laboratory scale high shear mixer. I. Effect of process variables and binder." *Acta Pharm. Nord.* **4**(133).
- Schaefer, T., Taagegaard, B., Thomsen, L.J., Kristensen, H.G. (1993). "Melt pelletization in a high shear mixer. V. Effects of apparatus variables." *Eur. J. Pharm. Sci.* **1**: 133-141.
- Scheinost, A.C., Schwertmann, U. (1999). "Colour Identification of Iron Oxides and Hydroxysulfates: Use and Limitations." *Soil Sci. Soc. Am. J.* **63**: 1463-1471.
- Schofield, C. (1976). "The definition and assessment of mixture quality in mixtures of particulate solids." *Powder Technology* **15**(2): 169-180.
- Schultz, M. (2011). "Dye tests for blending scale-up development trials". GlaxoSmithKline Australia, New Product Introduction, Internal Corporate Report: 29.
- Schutyser, M.A.I., Briels, W.J., Rinzema, A., Boom, R.M. (2003). "Numerical Simulation and PEPT measurements of a 3D conical helical-blade mixer: A high potential solids mixer for solid-state fermentation" [www.interscience.wiley.com](http://www.interscience.wiley.com)
- Schwertmann, U., Cornell, R.M. (1991). Iron Oxides in the Laboratory - Preparation and Characterisation D-6940 Weinheim, VCH Verlagsgesellschaft mbH 137.
- Sebhatua, T., Angbergh, M., Ahlneckint, C. (1994). "Assessment of the degree of disorder in crystalline solids by isothermal microcalorimetry." *Int. J. Pharm.* **104**: 135-144.
- Seiler, C., Fryer, P.J., Seville, J.K. (2008). "Statistical modelling of the spouted bed coating process using positron emission particle tracking (PEPT)." *The Canadian Journal of Chemical Engineering* **86**: 571-581.
- Seville, J.K., Ingram, A., Parker, D.J. (2005). "Probing processes using positrons." *Chemical Engineering Research and Design* **83**(A7): 788-793.
- Seville, J.P.K., Tuzun, U., Clift, R. (1997). Processing of Particulate Solids London, Blackie Academic Professional.
- Shinbrot, T., Alexander, A.W., Muzzio, F.J. (1999). "Spontaneous chaotic granular mixing." *Nature* **397**: 675-678.

- Shur, J., Harris, H., Jones, M.D., Kaerger, J.S., Price, R. (2008). "The Role of Fines in the Modification of the Fluidization and Dispersion Mechanism Within Dry Powder Inhaler Formulations." *Pharm. Res.* **25**(7): 1931-1940.
- Sichalwe, K., Govender, I., Mainza, A.N. (2011). "Characterising porosity of multi-component mixtures in rotary mills." *Minerals Engineering* **24**: 276-281.
- Siesler, H.W., Ozaki, Y., Kawata, S., Heise, H.M. (2006). Near Infrared Spectroscopy: Principles, Instruments, Applications Weinheim, WILEY-VCH.
- Sirois, P.J., Craig, G.D. (2000). "Scaleup of a High-Shear Granulation Process Using a Normalised Impeller Work Parameter." *Pharm. Dev. Tech.* **5**(3): 365-374.
- Skoog, D.A., Holler, F.J., Nieman, T.A. (1998). Principles of Instrumental Analysis. 5th Ed., Brooks/Cole.
- Smith, D.K., Bayliss, P., Roberts, A. (1999). "Mineral classification in the mineral powder diffraction file." *JCPDS - International Centre for Diffraction Data*: 606-613.
- Smyth, H.C., Truman, C.R. (2007). "Dry powder inhaler with aerolastic dispersion mechanism", **WO/2007/103152**
- Sou, T., Meeusen, E.N., de Veer, M., Morton, D.A.V., Kaminskas, L.M., McIntosh, M.P. (2011). "New developments in dry powder pulmonary vaccine delivery." *Trends in Biotechnology* **29**(4): 191-198.
- Srichana, T., Martin, G.P., Marriott, C. (1998). "Dry powder inhalers: The influence of device resistance and powder formulation on drug and lactose deposition *in vitro*." *Eur. J. Pharm. Sci.* **7**: 73-80.
- Staniforth, J.N. (1994). The importance of electrostatic measurements in aerosol formulation and preformulation. *Proc. Respiratory Drug Delivery IV*.
- Staniforth, J.N. (1996). Improvement in dry powder inhaler performance: surface passivation effects. *Proc. Drug Delivery to the Lungs VII*, London.
- Staniforth, J.N., Morton, D.A.V. (2005). "Improvements in or relating to formulations for use in inhaler devices", **WO 2001/78696**.
- Steckel, H. (2007), in: K. Bechtold-Peters and H. Luessen (Eds.). *Formulation and production: excipients. Pulmonary Drug Delivery*. Germany, Editio Cantor Verlag, pp.172-173.
- Steckel, H., Markefka, P., teWierik, H., Kammelar, R. (2004). "Functionality testing of inhalation grade lactose." *Eu. J. Pharm. and Biopharm.* **57**: 495-505.
- Steckel, H., Markefka, P., teWierik, H., Kammelar, R. (2006). "Effect of milling and sieving on functionality of dry powder inhalation products." *International Journal of Pharmaceutics* **309**: 51-59.

- Steckel, H., Muller, B.W. (1997). "In vitro evaluation of dry powder inhalers I: drug deposition of commonly used devices." *Int. J. Pharm.* **154**: 19-29.
- Steinhaus, H. (1999). *Mathematical Snapshots*. 3rd Edn. N.Y., Dover 202.
- Stephens, D.J., Bridgwater, J. (1978). "The Mixing and Segregation of Cohesionless Particulate Materials Part 1. Failure Zone Formation." *Powder Tech.* **21**: 17-28.
- Stephenson, P.L., Thiel, W.J. (1980). "The mechanical stability of ordered mixtures when fluidised and their pharmaceutical application." *Powder Tech.* **26**: 225-227.
- Stewart, P.J., Adi, H., Larson, I. (2005). Dry powder inhaler formulations-simple two component powders mixtures or a multi-particulate nightmare. Proc. Drug Delivery to the Lungs 16, Edinburgh, The Aerosol Society.
- Stewart, P.J., Islam, N., Adi, H., Larson, I., Hartley, P. (2003). Key surface characteristics of lactose carriers in the dispersion of salmeterol xinafoate from mixtures for inhalation. Proc. Drug Delivery to the Lungs 14, London, The Aerosol Society.
- Stewart, R.L., Bridgwater, J., Parker, D.J. (2001a). "Granular flow over a flat-bladed stirrer." *Chem. Eng. Sci.* **56**(14): 4257-4271.
- Stewart, R.L., Bridgwater, J., Zhou, Y.C., Yu, A.B. (2001b). "Simulated and measured flow of granules in a bladed mixer--a detailed comparison." *Chemical Engineering Science* **56**(19): 5457-5471. <http://www.sciencedirect.com/science/article/pii/S0009250901001907>
- Subert, J., Cizmarik, J. (2008). "Application of instrumental colour measurement in development and quality control of drugs and pharmaceutical excipients." *Pharmazie* **63**: 331-336.
- Sudah, O.S., Arratia, P.E., Alexander, A.W., Muzzio, F.J. (2005). "Simulations and experiments of mixing and segregation in a tote blender." *AIChE Journal* **51**(3): 836-844.
- Sugai, Y., Satoh, M., Kobayashi, M. (1997). "The Mixing and Deagglomeration Characteristics of an Agitating-type Mixer." *J. Soc. Powder Technol., Japan* **34**: 767-772.
- Susana, L., Canu, P., Santomaso, A.C. (2011). "Development and characterisation of a new thief sampling device for cohesive powders." *Int. J. Pharm.* **416**: 260-267.
- Sutton, H.M. (1976), in: G. D. Parfitt and K. S. W. Sing (Eds.). Characterisation of Powder Surfaces. London, Academic Press, pp.107-158.
- Tardos, G.I., Hapgood, K.P., Ipadeola, O.O., Michaels, J.N. (2004). "Stress measurements in high-shear granulators using calibrated "test" particles: application to scale-up." *Powder Tech.* **140**: 217-227.
- Tee, S.K., Marriott, C., Zeng, X.M., Martin, G.P. (2000). "The use of different sugars as fine and coarse carriers for aerolised salbutamol sulphate." *Int. J. Pharm.* **208**: 111-123.

- Telco, M.J., Hickey, A.J. (2005). "Dry powder inhaler formulation." *Respiratory Care* **50**(9): 1209-1227.
- teWierik, H., Diepenmaat, P. (2002). "Formulation of lactose for inhaled delivery systems." *Pharmaceutical Technology Europe* **11**: 1-5.
- Thalberg, K., Berg, E., Fransson, M. (2012). "Modelling dispersion of dry powders for inhalation. The concepts of total fines, cohesive energy and interaction parameters." *International Journal of Pharmaceutics* **427**: 224-233.
- Ticehurst, M.D., Basford, P.A., Dallman, C.I., Lukas, T.M., Marshall, P.V., Nichols, G., Smith, D. (2000). "Characterisation of the influence of micronisation on the crystallinity and physical stability of revatropate hydrobromide." *International Journal of Pharmaceutics* **193**: 247-259.
- Timko, R.J., Cliff, M.J., Rosenberg, H.A. (1990), in: K. L. Kadam (Eds.). *High intensity mixer granulators. Granulation Technology for Bioproducts*. Boston, CRC Press, pp.119-178.
- Tobyn, M.J., Staniforth, J.N., Morton, D., Harmer, Q., Newton, M.E. (2004). "Active and intelligent inhaler device development." *Int. J. Pharm.* **277**: 31-37.
- Torrent, J., Barron, V. (2002). "Diffuse Reflectance Spectroscopy of Iron Oxides". *Encyclopedia of Surface and Colloid Science*, Marcel Dekker, Inc.: 1438-1446.
- Tran, A.L.H., Litster, J.D., Seville, J.K., Ingram, A., Fan, X. (2006). Dry and cohesive powders in vertical axis high shear mixers using positron emission particle tracking (PEPT). Proc. World Congress on Particle Technology, Orlando, USA.
- Valverde, J.M., Ramos, A., Castellanos, A., Watson, P.K. (1998). "The tensile strength of cohesive powders and its relationship to consolidation, free volume and cohesivity." *Powder Tech.* **97**: 237-245.
- Van de Velden, M., Baeyens, J., Seville, J.K., Fan, X. (2008). "The solids flow in the riser of a circulating fluidised bed (CFB) viewed by positron emission particle tracking (PEPT)." *Powder Technology* **183**(2): 290-296.
- Van den Ban, S. (2007). "Present technical framework process understanding inhaled products", GlaxoSmithKline.
- van der Westhuizen, A.P., Govender, I., Mainza, A.N., Rubenstein, J. (2011). "Tracking the motion of media particles inside an IsaMill™ using PEPT." *Minerals Engineering* **24**: 195-204.
- Vandenbergh, R.E., Barrero, C.A., da Costa, G.M., Van San, E., De Grave, E. (2000). "Mossbauer characterization of iron oxides and (oxy)hydroxides: the present state of the art." *Hyperfine Interactions* **126**: 247-259.
- Visser, J. (1989). "van der Waals and other cohesive forces affecting powder fluidisation." *Powder Technology* **58**: 1-10.

- Volkwyn, T.S., Buffler, A., Govender, I., Franzidis, J.-P., Morrison, A.J., Odo, A., van der Meulen, N.P., Vermeulen, C. (2011). "Studies of the effect of tracer activity on time-averaged positron emission particle tracking measurements on tumbling mills at PEPT Cape Town." *Minerals Engineering* **24**: 261-266.
- Völz, H.G. (1975). *Angew. Chem., Int. Ed. Eng.* **14**: 655.
- Völz, H.G. (2001). *Industrial Colour Testing*. 2. ed. Weinheim, Germany, Wiley-VCH.
- Völz, H.G., Kischkewitz, J., Woditsch, P., Westerhaus, A., Griebler, W.-D., De Liedekerke, M., Buxbaum, G., Printzen, H., Mansmann, M., Råde, D., Trenczek, G., Wilhelm, V., Schwarz, S., Wienand, H., Adel, J., Adrian, G., Brandt, K., Cork, W.B., Winkeler, H., Mayer, W., Schneider, K., Leitner, L., Kathrein, H., Schwab, E., Jakusch, H., Ohlinger, M., Veitch, R., Etzrodt, G., Pfaff, G., Franz, K.-D., Emmert, R., Nitta, K., Besold, R., Gaedcke, H. (2006), in: (Eds.). *Pigments, Inorganic. Ullmann's Encyclopedia of Industrial Chemistry*, John Wiley and Sons, Inc.
- Vromans, H., de Boer, A.H., Bolhuis, G.K., Lerk, C.F., Kussendrager, K.D. (1985). "Studies on tableting properties of lactose. Part I: The effect of initial particle size on binding properties and dehydration characteristics of lactose." *Acta Pharm Suec.* **22**: 163-172.
- Vromans, H., de Boer, A.H., Bolhuis, G.K., Lerk, C.F., Kussendrager, K.D. (1986). "Studies on tableting properties of lactose. Part VI: Consolidation and compaction of spray-dried amorphous lactose." *Acta Pharm Suec.* **23**: 231-240.
- Wade, A. (2003), in: R. C. Rowe, P. J. Sheskey and P. J. Weller (Eds.). *Lactose. Handbook of Pharmaceutical Excipients*. London, Pharmaceutical Press.
- Wagner, D.H., Ramanathan, S., Taylor, M.L., Brown, A.B., Wobker, M.E.S., Prior, M.W. (2009). "The thermodynamics of high shear blending." *Powder Technology* **193**(2): 195-199.
- Wall, D.A. (1995). "Pulmonary absorption of peptides and proteins." *Drug Deliv.* **2**: 1-20.
- Ward, G.H., Schultz, R.K. (1995). "Processed-induced crystallinity changes in albuterol sulphate and its effect on powder physical stability." *Pharm. Res.* **12**: 773-779.
- Watson, P.K., Valverde, J.M., Castellanos, A. (2001). "The tensile strength and free volume of cohesive powders compressed by gas flow." *Powder Tech.* **115**: 45-50.
- Weers, J.G., Bell, J., Chan, H.-K., Cipolla, D., Dunbar, C., Hickey, A.J., Smith, I.J. (2010). "Pulmonary Formulation: What Remains to be Done?" *Journal of Aerosol Medicine and Pulmonary Drug Delivery* **23**(Supplement 2): S5-S23.
- Wellm, A.B. (1997). "Investigation of a high shear mixer/agglomerator". Birmingham, U.K., The University of Birmingham. **Ph.D. Thesis**.
- Wibowo, C., Ng, K.M. (2001). "Operational issues in solids processing plants: systems view." *AIChE Journal* **47**(1): 107-125.

- Wildman, R.D., Huntley, J.M., Hansen, J.-P., Parker, D.J., Allen, D.A. (2000). "Single-particle motion in three dimensional vibrofluidised granular beds." *Phys. Rev. E* **62**(3): 3826-3835.
- Wildman, R.D., Martin, T.W., Huntley, J.M., Jenkins, J.T., Viswanathan, H., Fen, X., Parker, D.J. (2008). "Experimental investigation and kinetic-theory-based model of a rapid granular shear flow." *J. Fluid Mech.* **602**: 63-79.
- Williams, R. (1979), in: (Eds.). Circle Packings, Plane Tessellations, and Networks. The Geometrical Foundation of Natrual Structure: A Source Book of Design. N.Y., Dover **Section 2.3**, pp.34-47.
- Wilson, M.J. (1987). A handbook of determinative methods in clay minerology, Blackie, Glasgow and London 308.
- Winter, G. (1979). "Anorganische Pigmente: Diverse Festkorper mit technisch verwertbaren optischen und magnetischen Eignernschaften." *Fortschr. Miner.* **57**: 172-202.
- Wirth, W.D., Baertschi, S.W., al., e. (1998). "Mailard reaction of lactose and fluoxetine hydrochloride, a secondary amine." *J. Pharm. Sci.* **87**: 31-39.
- Yang, X., Huan, C., Candela, D., Mair, R.W., Walsworth, R.L. (2002). "Measurements of Grain Motion in a Dense, Three-dimensional Granular Fluid." *Phys. Rev. Lett.* **88**(4): 1-4.
- Yip, C.W., Hersey, J.A. (1977). *Powder Tech.* **16**: 189.
- Yokoyama, T., Urayama, K., Naito, M., Kato, M. (1987). "The Angmill Mechanofusion system and its applications." *KONA* **5**: 59-68.
- Yokoyama, T., Urayama, K., Yokoyama, T. (1983). *KONA* **1**: 53.
- Young, P., Edge, S., Traini, D., Jones, M.D., Price, R., El-Sabawi, D., Urry, C., Smith, C. (2005). "The infuence of dose on the performance of dry powder inhalation systems." *Int. J. Pharm.* **296**: 26-33.
- Young, P.M., Price, R., Tobyn, M.J., Buttrum, M., Dey, F. (2003). "Investigation into the effect of humidity on drug-drug interactions using the atomic force microscope." *J. Pharm. Sci.* **92**: 815-822.
- Young, P.M., Tobyn, M.J., Price, R., Buttrum, M., Dey, F. (2006). "The use of colloid probe microscopy to predict aerosolisation performance in dry powder inhalers: AFM and in vitro correlation." *J. Pharm. Sci.* **95**: 1800-1809.
- Zega, J., Lee, D., Shiloach, A., Erb, D. (1995). Scale-up of the wet granulation process for a dicalcium phosphate formulation using impeller power consumption. Proc. AAPS Meeting.
- Zeng, X.M., Martin, G.P., Marriott, C. (2001). Particulate Interaction in Dry Powder Formulations for Inhalation London, U.K., Taylor & Francis 104-114.

- Zeng, X.M., Martin, G.P., Marriott, C., Pritchard, J. (2000). "The influence of carrier morphology on drug delivery by dry powder inhalers." *Int. J. Pharm.* **200**: 93-106.
- Zeng, X.M., Martin, G.P., Tee, S., Ghoush, A.A., Marriott, C. (1999). "Effects of particle size and adding sequence of fine lactose on the deposition of salbutamol sulphate from a dry powder formulation." *International Journal of Pharmaceutics* **182**(2): 133-144.
- Zeng, X.M., Martin, G.P., Tee, S.K., Marriott, C. (1998). "The role of fine particle lactose on the dispersion and deaggregation of salbutamol sulphate in an air stream in vitro." *International Journal of Pharmaceutics* **176**: 99-100.
- Zhou, Q., Armstrong, B., Larson, I., Stewart, P., Morton, D.A.V. (2010). "Understanding the influence of powder flowability, fluidisation and de-agglomeration characteristics on the aerolisation of pharmaceutical model powders." *European Journal of Pharmaceutical Science* **40**: 412-421.
- Zhou, Q., Morton, D.A.V. (2012). "Drug-lactose binding aspects in adhesive mixtures: Controlling performance in dry powder inhaler formulations by altering lactose carrier surfaces." *Advanced Drug Delivery Reviews* **64**: 275-284.
- Zlokarnik, M. (1998). "Problems in the application of dimensional analysis and scale-up of mixing operations." *Chem. Eng. Sci.* **53**(17): 3023-3030.